UNIVERSITY OF SOUTHAMPTON
Faculty of Engineering and Applied Science
Department of Electronics and Computer Science
Southampton SO17 1BJ

Adaptive Modulation and Adaptive Antenna Assisted Wireless TDMA/CDMA Networks

by
Jonathan S. Blogh

A Doctoral thesis submitted in partial fulfilment of the requirements for the award of Doctor of Philosophy at the University of Southampton

January 2001

Supervisor: Professor Lajos Hanzo
Dipl Ing, MSc, PhD, SMIEEE
Chair of Telecommunications
Department of Electronics and Computer Science
University of Southampton
Southampton SO17 1BJ
United Kingdom

UNIVERSITY OF SOUTHAMPTON

ABSTRACT

FACULTY OF ENGINEERING AND APPLIED SCIENCE
DEPARTMENT OF ELECTRONICS AND COMPUTER SCIENCE

Doctor of Philosophy

Adaptive Modulation and Adaptive Antenna Assisted Wireless TDMA/CDMA Networks

by Jonathan S. Blogh

The performance of a Frequency Division Multiple Access (FDMA)/Time Division Multiple Access (TDMA) based cellular mobile network invoking the 7-cell Fixed Channel Allocation (FCA) algorithm and a Dynamic Channel Allocation (DCA) algorithm - the Locally Optimised Least Interference Algorithm (LOLIA) - in conjunction with frequency re-use exclusion zones of both 7 and 19 adjacent cells was investigated. Single element antennas, as well as two- and four-element adaptive antenna arrays located at the base stations were used and the system's performance was evaluated in a Line-Of-Sight (LOS) propagation environment. This work was then extended by investigating the network capacity, when subjected to a three-ray multipath channel, both with and without Power Control (PC). Furthermore, the potential network capacity gains achieved by Adaptive Quadrature Amplitude Modulation (AQAM) techniques integrated with PC were also considered. Additionally, the effects of two different interference environments, namely the "desert-island" and the "wrap-around" scenarios on network capacity were studied.

Similarly, the network capacity of a Code Division Multiple Access (CDMA) based, Universal Mobile Telecommunication System (UMTS) Terrestrial Radio Access (UTRA)-like cellular mobile network was then investigated. The relative performance of four different soft handover algorithms was compared in terms of the network capacity, size of the Active Base station Set (ABS) and the mean transmission powers, for both non-shadowed and log-normal shadow faded propagation environments. The capacity gains achieved with the advent of two- and four-element adaptive antenna arrays were then investigated, under both non-shadowed and shadow-faded conditions. Further results were presented, whilst performing independent up- and down-link beamforming. Finally, the performance benefits of AQAM both with and without beamforming, in conjunction with shadow fading were determined.

List of Publications

1. **J. S. Blogh, P. J. Cherriman and L. Hanzo** "Adaptive Beamforming Assisted Dynamic Channel Allocation", Proceedings of IEEE VTC 1999, Houston, USA, 16-19 May 1999, pp 199-203.

2. **J.S. Blogh, P.J. Cherriman and L. Hanzo** "Dynamic Channel Allocation Using Adaptive Antennas and Power Control", Proceedings of 4th ACTS Mobile Communications Summit, Sorrento, Italy, 8-11 June 1999, pp 943-948.

3. **J.S. Blogh, P.J. Cherriman and L. Hanzo** "Dynamic Channel Allocation Techniques Using Adaptive Modulation and Adaptive Antennas", Proceedings of IEEE VTC 1999 Fall, Amsterdam, The Netherlands, 19-22 September, 1999, pp 2348-2352.

4. **J.S. Blogh, P.J. Cherriman and L. Hanzo** "Comparative Study of Dynamic Channel Allocation Algorithms", *accepted for publication in IEEE Transactions on Vehicular Technology.*

5. **J.S. Blogh, P.J. Cherriman and L. Hanzo** "Adaptive Antenna Array Assisted Dynamic Channel Allocation Techniques", *accepted for publication in IEEE Journal on Selected Areas in Communications.*

6. **J.S. Blogh, P.J. Cherriman and L. Hanzo** "Dynamic Channel Allocation Techniques using Adaptive Modulation and Adaptive Antennas", *accepted for publication in IEEE Journal on Selected Areas in Communications.*

7. **J. S. Blogh and L. Hanzo** "The network performance of multi-rate FDD-mode UMTS", *submitted to VTC 2001 Spring, Tel Aviv, Israel.*

Contents

Chapter 1

Introduction

1.1 Background and Overview

Wireless communications is experiencing an explosive growth rate. This high demand for wireless communications services requires higher and higher system capacities. The simplest solution would be to allocate more bandwidth to these services, but the electromagnetic spectrum is a limited resource, which is becoming increasingly congested [1]. Therefore, the efficient use of the available frequencies is paramount [1, 2].

Digital techniques have already improved upon the capacity attained using analogue technology, whilst achieving better performance. However, more efficient techniques allowing multiple users to share the available frequencies are necessary. Classic techniques of supporting a multiplicity of users are frequency, time, polarisation, code or spatial division multiple access [3]. In Frequency Division Multiple Access [4, 5] the available frequency spectrum is divided into frequency bands, each of which is used by a different user. Time Division Multiple Access (TDMA) [4, 5] allocates each user a given period of time, referred to as a time slot, over which their transmission may take place. The transmitter must be able to store the data to be transmitted and then transmit it at a proportionately increased rate during its time slot constituting a fraction of the TDMA frame duration. Alternatively, Code Division Multiple Access (CDMA) [4, 5] allocates each user a unique code. This code is then used to spread the data over a wide bandwidth shared with all users. For detecting the transmitted data the same unique code, often referred to as the user signature, must be used.

The increasing demand for spectrally efficient mobile communications systems motivates our quest for more powerful techniques. With the aid of spatial processing at a cell site, optimum receive and transmit beams can be used for improving the system's performance

in terms of the achievable capacity and the quality of service measures. This approach is usually referred to as Spatial Division Multiple Access (SDMA) [6, 3] which enables multiple users in the same cell to be accommodated on the same frequency and time slot by exploiting the spatial selectivity properties offered by adaptive antennas [7]. In contrast, if the desired signal and interferers occupy the same frequency band and time slot, then "temporal filtering" cannot be used to separate the signal from the interference. However, the desired and interfering signal usually originate from different spatial locations and this spatial separation may be exploited, in order to separate the desired signal from the interference using a "spatially selective filter" at the receiver [8, 9, 10]. As a result, given a sufficiently large distance between two users communicating in the same frequency band, there will be negligible interference between them. The larger the number of cells in a region, due to using small cells, the more frequently the same frequency is re-used and hence higher teletraffic density per unit area can be carried.

However, the distance between co-channel cells must be sufficiently high, so that the inter-cell interference becomes lower than its maximum acceptable limit [3]. Therefore, the number of cells in a geographic area is limited by the base stations' transmission power level. A method of increasing the system's capacity is to use 120° sectorial beams at different carrier frequencies [11]. Each of the sectorial beams may serve the same number of users as supported in ordinary cells, while the Signal-to-Interference Ratio (SIR) can be increased due to the antenna's directionality. The ultimate solution, however, is to use independently steered high gain beams for supporting individual users [3].

Adaptive Quadrature Amplitude Modulation (AQAM) [12, 13] is another technique by which gains in spectral efficiency may be achieved. The idea behind adaptive modulation is to select a specific modulation mode, from a set of modes, according to the instantaneous radio channel quality [12, 13]. Thus, if the channel quality exhibits a high instantaneous SINR, then a high-order modulation mode may be employed, enabling the exploitation of the temporarily high channel capacity. In contrast, if the channel has a low instantaneous SINR, using a high-order modulation mode would result in an unacceptable Frame Error Ratio (FER), and hence a more robust, but lower throughput modulation mode would be invoked. Hence, adaptive modulation not only combats the effects of a poor quality channel, but also attempts to maximise the throughput, whilst maintaining a given target FER. Thus, there is a trade-off between the mean FER and the data throughput, which is governed by the modem mode switching thresholds. These switching thresholds define the SINRs, at which the instantaneous channel quality requires changing the current modulation mode, i.e. where an alternative AQAM mode must be invoked.

This thesis studies the network capacity gains that may be achieved through the employment of adaptive antenna arrays and adaptive modulation techniques in both FDMA/TDMA and CDMA based mobile cellular networks.

1.2 Organisation of the Thesis

- **Chapter 2:** The principles behind beamforming and the various techniques by which it may be implemented are presented. From this the concept of adaptive beamforming is developed, and temporal as well as spatial reference techniques are examined. Performance results are then presented for three different temporal-reference based adaptive beamforming algorithms, namely the Sample Matrix Inversion (SMI), Unconstrained Least Mean Squares (ULMS) and the Normalised Least Mean Squares (NLMS) algorithms.

- **Chapter 3:** A brief summary of possible methods used for modelling the performance of an adaptive antenna array is provided. This is followed by an overview of fixed and dynamic channel allocation. Multipath propagation models are then considered for use in our network simulations. Next, metrics are developed for characterising the performance of mobile cellular networks and our results are presented for simulations conducted under Line-Of-Sight (LOS) propagation conditions, both with and without adaptive antennas. Further results are then given for identical networks under multipath propagation conditions, which are then extended to power-controlled scenarios using both fixed and adaptive QAM techniques. These network capacity results were obtained for both "island" type simulation areas, and an infinite plane, using wraparound techniques, which will be defined later in Sections 3.7.1.

- **Chapter 4:** This chapter describes the 3rd generation mobile cellular network, known as UTRA - the UMTS Terrestrial Radio Access - network, and then presents network capacity results obtained under various propagation conditions, in conjunction with different soft handover threshold metrics. The performance benefits of adaptive antenna arrays are then analysed, both in a non-shadowed environment, and inflicted by log-normal shadow fading having frequencies of 0.5 Hz and 1.0 Hz . This work was then extended by invoking adaptive modulation techniques, which were studied when the channel conditions were impaired by shadow fading.

- **Chapter 5:** Conclusions and further work.

1.3 Contributions of the Thesis

- Study of network performance gains using adaptive antenna arrays at the base station in an FDMA/TDMA cellular mobile network [14, 15].
- Study of network performance gains using adaptive antenna arrays with power control at the base station in an FDMA/TDMA cellular mobile network [16, 17].
- Design of a combined power control and adaptive modulation assisted channel allocation algorithm, and characterisation of its performance in an FDMA/TDMA cellular mobile network [17, 18].
- Comparing the performance of various UTRA soft-handover techniques.
- Quantifying the UTRA network capacity under various channel conditions.
- Evaluating UTRA network performance with the aid of adaptive antenna arrays.
- Demonstrating the benefits of adaptive modulation in the context of both FDMA/TDMA and CDMA cellular mobile networks.

Chapter 2

Intelligent Antenna Arrays and Beamforming

2.1 Introduction

Adaptive beamforming was initially developed in the 1960s for the military applications of sonar and radar, in order to remove unwanted noise and jamming from the output. The first fully adaptive array was conceived in 1965 by Applebaum [19], which was designed to maximise the Signal-to-Noise Ratio (SNR) at the array's output. An alternative approach to cancelling unwanted interference is the Least Mean Squares (LMS) error algorithm of Widrow [20]. While a simple idea, satisfactory performance can be achieved under specific conditions. Further work on the LMS algorithm, by Frost [21] and Griffiths [22], introduced constraints to ensure that the desired signals were not filtered out along with the unwanted signals. The optimisation process takes place as before, but the antenna gain is maintained constant in the desired direction. For stationary signals, both algorithms converge to the optimum Wiener solution [3, 21, 23]. A different technique was proposed in 1969 by Capon [24] using a Minimum-Variance Distortionless Response (MVDR) or the Maximum Likelihood Method (MLM). In 1974, Reed *et al.* demonstrated the power of the Sample-Matrix Inversion (SMI) technique, which determines the adaptive antenna array weights directly [25]. Unlike the algorithms of Applebaum [19] and Widrow [20], which may suffer from slow convergence if the eigenvalue spread of the received sample correlation matrix is relatively large, the performance of the SMI technique is virtually independent of the eigenvalue spread.

In recent years the tight frequency reuse of cellular systems has stimulated renewed research interests in the field [6, 3, 23, 26]. In this thesis we will attempt to review the

recent literature and highlight the most important research issues for UMTS , HiperLAN and WATM applications, while providing some performance results. We commence in Section 2.2 by reviewing beamforming and its potential benefits, then we provide a generic signal model in Section 2.2.3 and we describe the processes of element and beam space beamforming. In Section 2.3 we highlight a range of adaptive beamforming algorithms and consider the less commonly examined downlink scenario in Section 2.3.5. Lastly in Section 2.3.6 we provide some performance results and outline our future work.

2.2 Beamforming

The signals induced in different elements of an antenna array are combined to form a single output of the array. This process of combining the signals from the different elements is known as beamforming. This section describes the basic characteristics of an antenna, the advantages of using beamforming techniques in a mobile radio environment [6, 3], and a generic signal model for use in beamforming calculations. For further details on the associated issues the reader is referred to [6, 3, 8, 19, 20, 21, 22, 23, 25, 26, 27, 28, 29, 30, 31].

2.2.1 Antenna Array Parameters

Below we provide a few definitions used throughout this report in order to describe antenna systems:

Radiation Pattern The radiation pattern of an antenna is the relative distribution of the radiated power as a function of direction in space. The radiation pattern of an antenna array is the product of the element pattern and the array factor, both of which are defined below. If $f(\theta, \phi)$ is the radiation pattern of each antenna element and $F(\theta, \phi)$ is the array factor, then the array's radiation pattern, $G(\theta, \phi)$, which is also referred to as the beam pattern, is given by

$$G(\theta, \phi) = f(\theta, \phi)F(\theta, \phi). \tag{2.1}$$

Figure 2.1 gives an example of a stylised antenna element response, an array factor of an 8 element linear array with an element spacing of $\lambda/2$ steered at 0° and the radiation pattern, which results from combining the two.

Array Factor The array factor, $F(\theta, \phi)$, is the far-field radiation pattern of an array of isotropically radiating elements, where θ is the azimuth angle and ϕ is the elevation angle.

Main Lobe The main lobe of an antenna radiation pattern is the lobe containing the

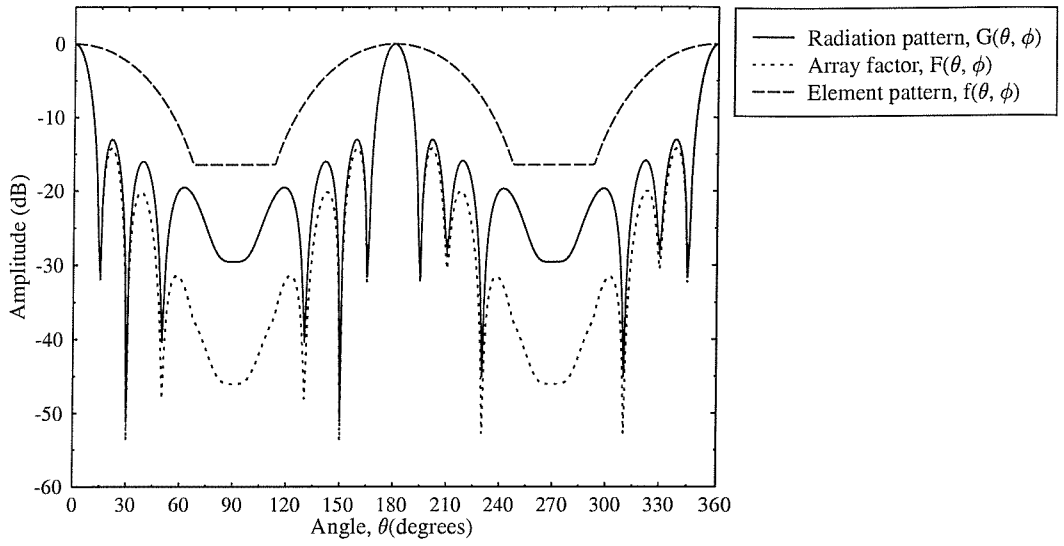

Figure 2.1: The array factor of an eight element linear array with an element spacing of $\lambda/2$ steered at 0°, the response of each antenna element and the radiation pattern resulting from combining the two.

direction of maximum radiated power.

Sidelobes Sidelobes are lobes of the antenna radiation pattern, which do not constitute the mainlobe. They allow signals to be received in directions other than that of the main lobe and hence they are undesirable, but they are also unavoidable.

Beamwidth The beamwidth of an antenna is the angular width of the main lobe. The 3dB beamwidth is the angular width between the points on the main lobe that are 3dB below the peak of the main lobe. A smaller beamwidth results from an array of a greater aperture size, which is the distance between the two farthest elements of the array.

Antenna Efficiency Antenna efficiency is the ratio of the total power radiated by the antenna to the total power input to the antenna.

Grating Lobes When the distance between the antenna array elements, d, exceeds $\lambda/2$, spatial under-sampling of the received radio frequency carrier wave takes place, causing secondary maxima [2, 28], referred to as grating lobes, to appear in the radiation pattern, which can be clearly seen in Figure 2.2. The spatial under-sampling results in ambiguities in the directions of the arriving signals, which manifests itself as copies of the main lobe in

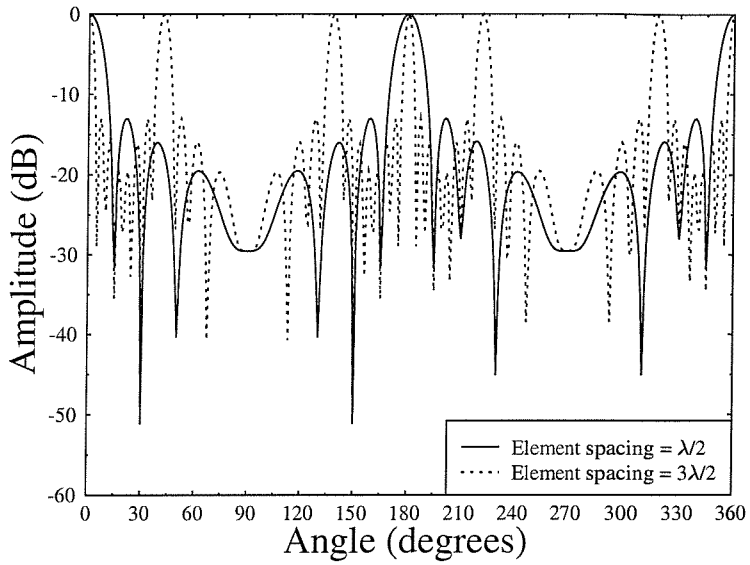

Figure 2.2: The array factor of an eight element uniform linear array with element spacing of $\lambda/2$ and $3\lambda/2$. The grating lobes associated with the spatial under-sampling-induced secondary maxima of the radiated carrier wave are clearly visible for the case when the element spacing is $3\lambda/2$.

unwanted directions. The grating lobe phenomenon in spatial sampling is analogous to the well known aliasing effect in temporal sampling [28]. Therefore, the distance, d, between adjacent sensors in the array must be chosen to be less than or equal to $\lambda/2$, if grating lobes are to be avoided [28, 32]. However, an inter-element spacing of greater than $\lambda/2$ improves the spatial resolution of the array [2], i.e. reduces the 3dB beamwidth as shown in Figure 2.2, and reduces the correlation between the signals arriving at adjacent antenna elements.

2.2.2 The Potential Benefits of Antenna Arrays in Mobile Communications

2.2.2.1 Multiple Beams [6]

The formation of multiple beams, or sectorisation, uses multiple antennae at the base station in order to form beams that cover the whole cell site [32]. For example, three beams, each with a beamwidth of 120° may cover the entire 360° as seen in Figure 2.3. The coverage area of each beam may be regarded as a separate cell, with frequency assignment and handovers

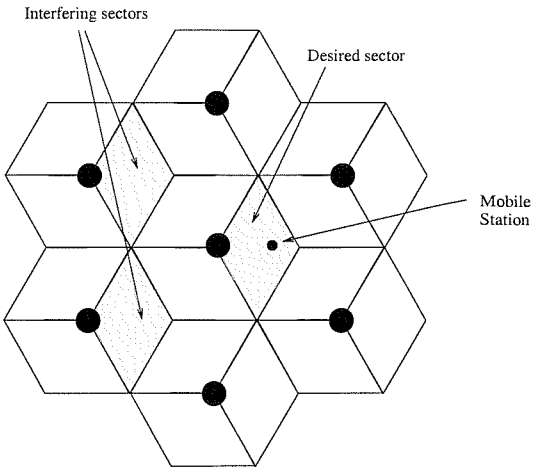

Figure 2.3: An example of sectorisation, using three sectors per base station, showing the reduced levels of interference with respect to an omni-directional base station antenna scenario.

between beams performed in the usual manner [33]. No intelligence is required to locate a subscriber within a beam and to connect that beam to a radio channel unit. The use of multiple beams results in a reduction of the co-channel interference. In the uplink scenario, the signal received from the mobile station constitutes interference at only two base stations, and additionally in only one sector. In the downlink, the situation is similar, only now the sectors which can interfere with the user in the central cell are the images of the interfering sectors on the uplink [34], again, as shown in Figure 2.3.

2.2.2.2 Adaptive Beams [6]

The combined antenna array is used to find the location of each mobile, and then beams are formed, in order to cover different mobiles or groups of mobiles [35, 36]. Each beam having its own coverage area may be considered as a co-channel cell, and thus be able to use the same carrier frequency [7, 32]. In conventional sectorisation the location of the beams is fixed, while the adaptive system allows the beams to cover specific areas of the cell within which users are located [37]. In intelligent near-future systems the beams may follow the mobiles, which benefit from the concentrated transmission power, with inter-beam handovers occurring as necessary.

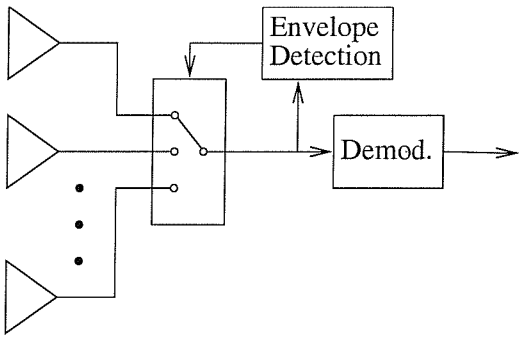

Figure 2.4: Switched-diversity combining.

2.2.2.3 Null Steering [6, 38]

In contrast to steering beams towards mobiles, null steering creates spatial radiation nulls towards co-channel mobiles [39]. The realisation of true nulls or zero response is not possible due to practical considerations, such as the isolation of the radio frequency components. The formation of spatial radiation nulls in the antenna response towards co-channel mobiles reduces the co-channel interference both on the uplink and the downlink [2, 35].

2.2.2.4 Diversity Schemes [6, 40]

The simplest and most commonly used diversity scheme is *switched diversity*. In this scheme the system switches between antennae, such that only one is in use at any one time [1, 41], as shown in Figure 2.4. The switching criterion is often the loss of received signal level at the antenna being used. The switching may be performed at the Radio Frequency (RF) stage, avoiding the need for a down-converter for each antenna.

Selection diversity is a more sophisticated version of switched diversity, where the system can monitor the signal level on all of the antennae simultaneously, and select the specific branch exhibiting the highest SNR at any given time, thus requiring an RF front-end for each antenna in the system [1], as seen in Figure 2.5.

In a Rayleigh fading environment, the fading at each branch can be assumed to be independent provided that the antennae are sufficiently far apart. If each branch has an instantaneous SNR of γ_l, the probability density function of γ_l is given by [3]

$$p(\gamma_l) = \frac{1}{\Gamma} e^{\frac{-\gamma_l}{\Gamma}} \tag{2.2}$$

where Γ denotes the mean SNR at each branch. The probability that a single branch has a

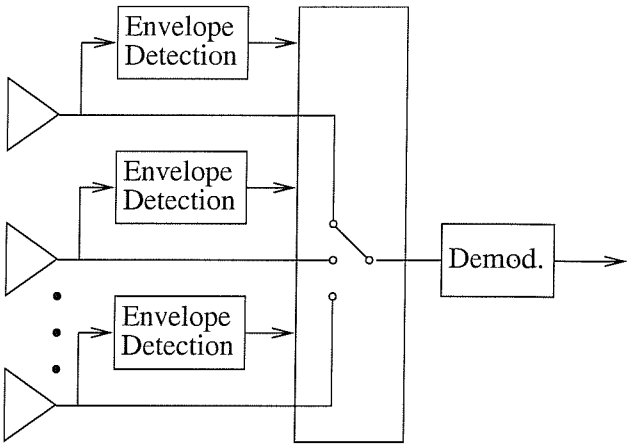

Figure 2.5: Selective-diversity combining.

SNR less than some threshold γ is given by [3]

$$P[\gamma_l \leq \gamma] = \int_0^{\infty} p(\gamma_l) d\gamma_l = 1 - e^{-\frac{\gamma}{\Gamma}}. \tag{2.3}$$

Therefore, the probability that all the branches fail to achieve an SNR higher than γ is [3]:

$$P_L(\gamma) = P[\gamma_1, \gamma_2, \ldots, \gamma_L \leq \gamma] = \left(1 - e^{-\frac{\gamma}{\Gamma}}\right)^L, \tag{2.4}$$

from which the probability density function of the fading magnitude in conjunction with selection diversity can be obtained,

$$p_L(\gamma) = \frac{d}{d\gamma} P_L(\gamma) = \frac{L}{\Gamma}\left(1 - e^{-\frac{\gamma}{\Gamma}}\right)^{L-1} e^{-\frac{\gamma}{\Gamma}}, \tag{2.5}$$

leading to the average SNR, $\bar{\gamma}$, of selection diversity assisted Rayleigh fading channels as [3]:

$$\bar{\gamma} = \int_0^{\infty} \gamma p_L(\gamma) d\gamma = \Gamma \sum_{l=1}^{L} \frac{1}{l}. \tag{2.6}$$

In maximal ratio combining the signal of each antenna is weighted by its instantaneous Signal-to-Noise Ratio (SNR). The weighted signals are then combined to form a single output as shown in Figure 2.6. It has been shown that the maximal ratio combining technique is optimal, if the diversity branch signals are uncorrelated and follow a Rayleigh distribution [42], and the noise is Gaussian distributed with zero mean. If each branch has a gain, g_l, the output of the combiner is [3]

$$s_L = \sum_{l=1}^{L} g_l s_l, \tag{2.7}$$

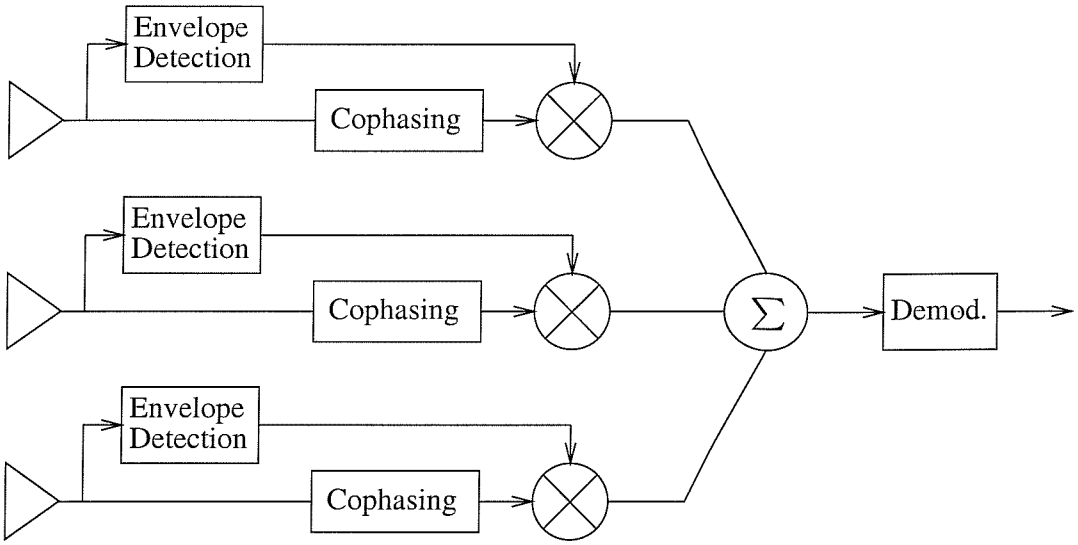

Figure 2.6: Optimal Combining.

and if each branch has the noise power, σ_n^2, the total noise power at the output of the combiner is [3] :

$$\sigma_N^2 = \sigma_n^2 \sum_{l=1}^{L} g_l^2. \tag{2.8}$$

Therefore, the SNR at the output of the combiner is given by

$$\gamma_L = \frac{s_l^2}{2\sigma_N^2}. \tag{2.9}$$

It can be easily shown that γ_L is maximised, when $g_l = s_l^2/\sigma_n^2$, which is the SNR in each branch. The expansion of Equation 2.9 is thus

$$\gamma_L = \frac{1}{2} \frac{\left(\sum_{l=1}^{L} \frac{s_l^2}{\sigma_n^2} s_l\right)^2}{\sigma_n^2 \sum_{l=1}^{L} \left(\frac{s_l^2}{\sigma_n^2}\right)^2} = \frac{1}{2} \sum_{l=1}^{L} \frac{s_l^2}{\sigma_n^2} = \sum_{l=1}^{L} \gamma_l. \tag{2.10}$$

As γ_L has a chi-squared distribution [3], the probability density function of γ_L is [3] :

$$p(\gamma_L) = \frac{\gamma_L^{L-1} e^{-\frac{\gamma_L}{\Gamma}}}{\Gamma^L (L-1)!}. \tag{2.11}$$

The probability that γ_L is less than some threshold, γ, is [3]

$$P[\gamma_L \leq \gamma] = \int_0^{\gamma} p(\gamma_L) d\gamma_L = 1 - e^{-\frac{\gamma}{\Gamma}} \sum_{l=1}^{L} \frac{(\frac{\gamma}{\Gamma})^{l-1}}{(l-1)!}. \tag{2.12}$$

The expectation of Equation 2.12, $\bar{\gamma}_L$, is the average SNR at the output of the combiner :

$$\bar{\gamma}_L = \sum_{l=1}^{L} \bar{\Gamma} = L\Gamma, \tag{2.13}$$

where Γ is the mean SNR at each branch.

Optimal combining processes the signals received from an antenna array such that the contribution from unwanted co-channel sources is reduced, whilst enhancing that of the desired signal. The explicit knowledge of the directions of the interferences is not necessary, but some characteristics of the desired signal are required in order to protect it from cancellation as if it were an unwanted co-channel source [6]. A popular technique is to use a reference signal, such as a channel sounding sequence, which must be correlated with the desired signal. The scheme then phase-coherently combines all the signals that are correlated with the reference signal, whilst simultaneously cancelling the waveforms that are not correlated with this signal, resulting in the removal of co-channel interferences.

A base station using an optimal combining antenna array may adjust the array weights during the receive cycle, in order to enhance the signal arriving from a desired mobile. A system using the same frequency for receiving and transmitting the signals in different time slots, such as in the Time Division Duplex (TDD) Digital European Cordless Telephone (DECT) [43, 44] system may be able to use the complex conjugate of these weights during the transmit cycle in order to pre-process the transmit signal and to enhance the signal received at the desired mobile, whilst suppressing this signal at the other mobiles. This process relies on the fact that the weights were adjusted during the receive cycle to reduce co-channel interference, thus placing nulls in the directions of co-channel mobiles [6]. Therefore, by employing the complex conjugate of these weights during the transmit cycle, the same antenna pattern may be produced, resulting in no energy transmitted towards the co-channel mobiles [6].

2.2.2.5 Reduction in Delay Spread and Multipath Fading

Delay spread is caused by multipath propagation, where a desired signal arriving from different directions is delayed due to the different distances travelled [37]. In transmit mode an intelligent antenna is able to focus the energy in the required direction, assisting in reducing the multipath reflections and thus delay spread. In receive mode the antenna array is able to perform optimal combining after delay compensation of the multipath signals incident upon it [1]. Those signals whose delays cannot be compensated for may be cancelled by the formation of nulls in their directions [45].

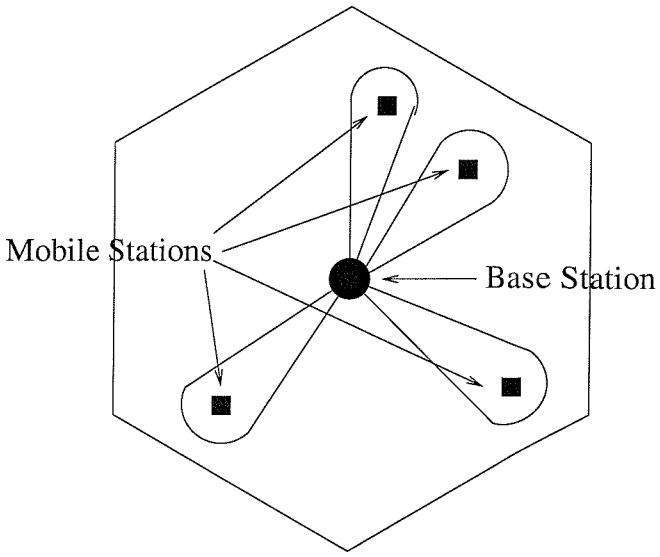

Figure 2.7: A cell layout showing how an antenna array can support many users on the same carrier frequency and timeslot with the advent of spatial filtering or Space Division Multiple Access (SDMA).

The directive nature of an antenna array also results in a smaller spread of Doppler frequencies encountered at the mobile [46]. For an omni-directional antenna at both the base station, and at the mobile the Direction-Of-Arrival (DOA) at the mobile is uniformly distributed. Hence the Doppler spectrum is given by Clarke's model [42] as :

$$S_r(f) = \frac{A_o^2}{\pi f_m \sqrt{1-(f/f_m)^2}}, \qquad |f| < f_m. \tag{2.14}$$

where A_o is the mean power transmitted and $f_m = v/\lambda$ is the maximum Doppler shift, where v is the velocity of the mobile and λ is the carrier wavelength. However, if a directional antenna is used at the base station then the Doppler power spectral density is given by [46] :

$$S_r(f) = \frac{A_o^2}{f_m \sqrt{1-(f/f_m)^2}}[f_\theta(\phi_v + |\cos^{-1}(f/f_m)|) + f_\theta(\phi_v - |\cos^{-1}(f/f_m)|)], \qquad |f| < f_m, \tag{2.15}$$

where ϕ_v, as shown in Figure 2.8, is the direction of motion of the mobile with respect to the direction of the base station from the mobile and $f_\theta()$ is the PDF of the DOA of the multipath components at the mobile, as given by [46] :

$$f_\theta(\theta) = \begin{cases} \frac{R^2}{I}, & -\theta_1 < \theta \leq \theta_1 \\ \frac{(D\tan(\alpha))^2}{I(\sin(\theta)+\cos(\theta)\tan(\alpha))^2}, & \theta_1 < |\theta| \leq \theta_2 \\ \frac{R^2}{I}, & \theta_2 < \theta \leq -\theta_2 \end{cases} \tag{2.16}$$

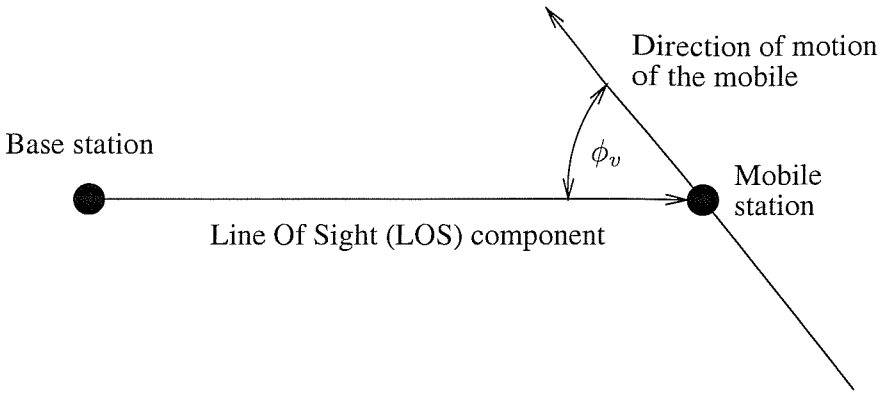

Figure 2.8: Illustration of the Line Of Sight (LOS) component arriving at the mobile from the base station showing the direction of motion of the mobile, ϕ_v.

where

$$I = 2R^2(\pi + \theta_1 - \theta_2) + 4D\sin(\alpha)\sqrt{R^2 - D^2\sin^2(\alpha)}. \tag{2.17}$$

Furthermore, 2α is the beamwidth of the so-called idealised "flat-top" directional antenna, which has zero gain except over the angular spread of 2α, where the gain is 1, R is the radius of the circular area containing all the scatters and D is the separation distance between the base station and the mobile. Finally, θ_1 and θ_2 are constants calculated using $\theta = \cos^{-1}\left[\frac{D}{R}\sin^2(\alpha) \pm \frac{\cos(\alpha)}{R}\sqrt{R^2 - D^2\sin^2(\alpha)}\right]$. Figures 2.9(a), 2.9(b) and 2.9(c) show example Doppler spectra for beamwidths of 2, 10 and 20 degrees for a mobile moving at angles of 0, 45 and 90 degrees with respect to the main LOS component, with a base station to mobile distance of 3km and the scatterers all located within a circle of 1km radius of the mobile.

2.2.2.6 Reduction in Co-channel Interference

An antenna array allows the implementation of spatial filtering, as shown in Figure 2.7, which may be exploited in both transmitting as well as receiving modes in order to reduce co-channel interferences [1, 2, 47, 48]. When transmitting, the antenna is used to focus the radiated energy in order to form a directive beam in the area, where the receiver is likely to be. This in turn means that there is less interference in the other directions, where the beam is not pointing. The co-channel interference generated in transmit mode may be further reduced by forming beams exhibiting nulls in the directions of other receivers [6, 49]. This scheme deliberately reduces the transmitted energy in the direction of co-channel receivers and hence requires prior knowledge of their positions.

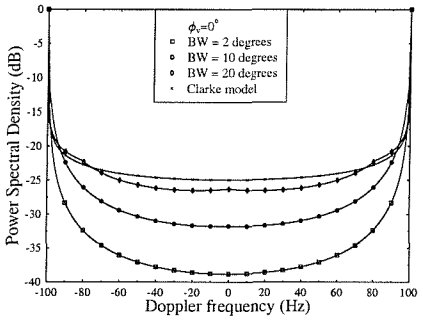

(a) Mobile's direction, $\phi_v = 0°$.

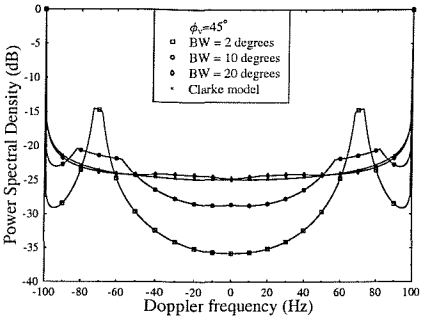

(b) Mobile's direction, $\phi_v = 45°$.

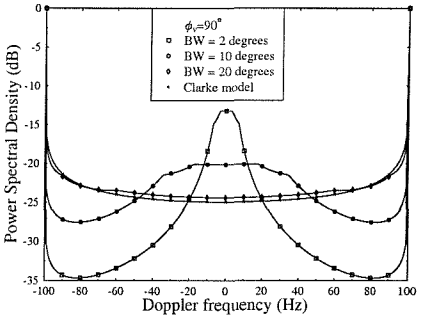

(c) Mobile's direction, $\phi_v = 90°$.

Figure 2.9: Doppler spectra at the mobile, when using a directional antenna at the base station, and an omnidirectional antenna at the mobile, is compared with Clarke's model. $R = 1$km, $D = 3$km, $f_m = 100$Hz.

The employment of antenna arrays for reducing co-channel interference in the receive mode has been reported widely [6, 1, 2, 37, 45, 49]. It does not require knowledge of the co-channel interference, but must have some information concerning the desired signal, such as the direction of its source, a reference signal, such as a channel sounding sequence, or a signal that is correlated with the desired signal.

2.2.2.7 Capacity Improvement and Spectral Efficiency

The spectral efficiency of a network refers to the amount of traffic a given system with a certain spectral allocation could handle. An increase in the number of users of the mobile communications system without a loss of performance increases the spectral efficiency.

Channel capacity refers to the maximum data rate a channel of a given bandwidth can sustain. An improved channel capacity leads to an ability to support more users of a specified data rate, implying a better spectral efficiency. The increased quality of service that results from the reduced co-channel interference and reduced multipath fading [34, 45] upon using smart antennae may be exchanged for an increased number of users [2, 36].

2.2.2.8 Increase in Transmission Efficiency

An antenna array is directive in nature, having a high gain in the direction where the beam is pointing. This property may be exploited in order to extend the range of the base station, resulting in a larger cell size or may be used to reduce the transmitted power of the mobiles. The employment of a directive antenna allows the base station to receive weaker signals than an omni-directional antenna. This implies that the mobile can transmit at a lower power and its battery life becomes longer, or it would be able to use a smaller battery, resulting in a smaller size and weight, which is important for hand-held mobiles. A corresponding reduction in the power transmitted from the base station allows the use of electronic components having lower power ratings and therefore, lower cost.

2.2.2.9 Reduction in Handovers

When the amount of traffic in a cell exceeds the cell's capacity, cell splitting is often used in order to create new cells [2], each with its own base station and frequency assignment. The reduction in cell size leads to an increase in the number of handovers performed. By using antenna arrays to increase the capacity of a cell [1] the number of handovers required may actually be reduced. Since each beam tracks a mobile [2], no handover is necessary, unless different beams using the same frequency cross each other.

2.2.3 Signal Model

Consider an array of L omni-directional antenna elements situated in the far field of a sinusoidal point source, as shown in Figure 2.10. Given that the array element separation is d and the plane wavefront is impinging upon the array at an angle of θ with respect to the array normal, the wavefront arrives at the $l+1^{th}$ element before arriving at the l^{th} element. Again, as seen in Figure 2.10, the extra distance that the wavefront must travel to reach the l^{th} element relative to the $l+1^{th}$ element is $d\sin\theta$. However, for an arbitrary array of L elements the relative delays, assuming that the point of zero delay is the origin, are given by

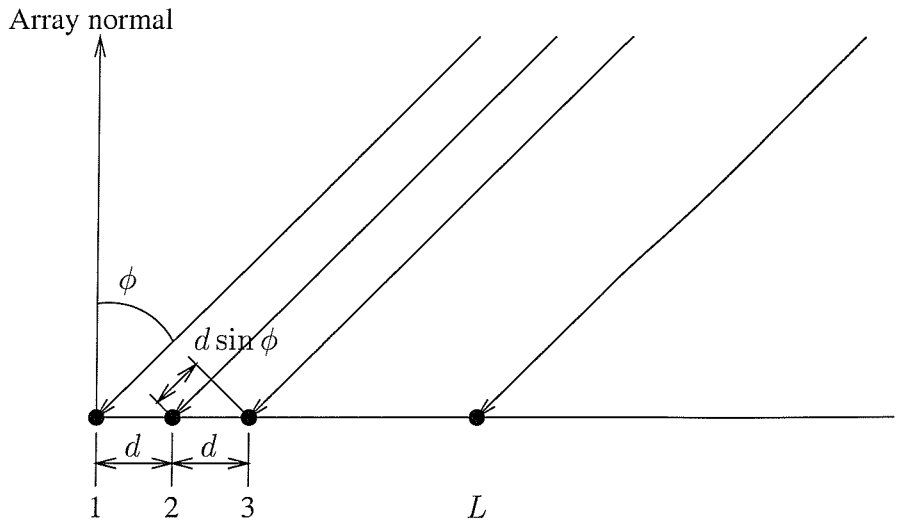

Figure 2.10: Reception by a uniformly spaced linear antenna array.

$$t_l(\theta) = \frac{x_l \sin\theta + y_l \cos\theta}{c}, \qquad l = 1, \ldots, L \tag{2.18}$$

where c is the speed of wave propagation, i.e. the speed of light, while x_l and y_l are, the x and y-coordinates of the l^{th} element with respect to the origin located at (0,0). The extra cosine term is due to the potential y-offset from the x-axis of the array elements which is zero, and thus omitted, from the example shown in Figure 2.10. The signal, $x_{l,i}(t)$, induced in the l^{th} element due to the i^{th} source can be expressed as

$$x_{l,i}(t) = m_i(t)e^{j\omega t_l(\theta)}, \tag{2.19}$$

with $m_i(t)$ denoting the complex modulating function. This expression is based upon the narrow-band assumption for array signal processing, which assumes that the bandwidth of the signal is sufficiently small, so that the weighting co-efficients maintain a constant phase variation across all of the antenna array elements.

Assuming M directional sources and isotropic background noise, the total signal at the l^{th} element is

$$x_l = \sum_{i=1}^{M} m_i(t)e^{j\omega t_l(\theta)} + n_l(t), \tag{2.20}$$

where $n_l(t)$ is a random noise component on the l^{th} antenna array element, which includes background noise and electronic noise. It is assumed to be white noise with a mean of zero and a variance of σ_n^2.

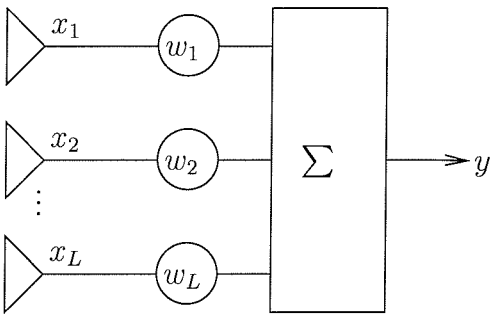

Figure 2.11: A beamformer sums the weighted antenna element signals, yielding the received signal $y(t) = \sum_{l=1}^{L} w_l^* x_l(t)$.

The array factor, $F(\theta)$ which was introduced in Section 2.2.1 may be calculated thus as:

$$F(\theta) = \sum_{l=1}^{L} w_l e^{-j\omega t_l(\theta)}, \tag{2.21}$$

where w_l is the complex weighting applied to the l^{th} element to steer the antenna beam in the direction of θ_0. The maximum value of $F(\theta)$ will occur when $\theta = \theta_0$, as shown previously in Figure 2.1.

Consider the narrow-band receiving beamformer, shown in Figure 2.11, where signals from each element are multiplied by a complex weight, $w_l, l = 1, \ldots, L$ and summed, in order to form the array output. The array output, $y(t)$ in Figure 2.11, at time t is given by

$$y(t) = \sum_{l=1}^{L} w_l^* x_l(t), \tag{2.22}$$

where * denotes the complex conjugate, $x_l(t)$ is the signal arriving from the l^{th} element of the array, and w_l is the weight applied to the l^{th} element. Representing the weights of the beamformer of Figure 2.11 as:

$$\underline{w} = [w_1, w_2, \ldots, w_L]^T, \tag{2.23}$$

and the signals induced in all elements as

$$\underline{x} = [x_1(t), x_2(t), \ldots, x_L(t)]^T, \tag{2.24}$$

the output of the beamformer receiver in Figure 2.11 becomes

$$y(t) = \underline{w}^H \underline{x}(t), \tag{2.25}$$

where the superscripts T and H, respectively, denote the transpose and complex conjugate transpose (Hermitian transpose) of a vector or matrix.

Let R define the L-by-L correlation matrix of the signal received by the L elements :

$$R = E[\underline{x}(t)\underline{x}^H(t)] = E\left\{ \begin{bmatrix} x_1(t) \\ x_2(t) \\ \vdots \\ x_L(t) \end{bmatrix} \begin{bmatrix} x_1^*(t) & x_2^*(t) & \dots & x_L^*(t) \end{bmatrix} \right\}. \tag{2.26}$$

The correlation matrix R may be expressed in the expanded form:

$$R = \begin{bmatrix} r(0) & r(1) & \dots & r(L-1) \\ r(-1) & r(0) & \dots & r(L-2) \\ \vdots & \vdots & \ddots & \vdots \\ r(-L+1) & r(-L+2) & \cdots & r(0) \end{bmatrix}. \tag{2.27}$$

The element $r(0)$ on the main diagonal is always real-valued. For complex-valued data, the remaining elements of R assume complex values. The correlation matrix of a stationary discrete-time stochastic process is Hermitian [28], i.e. $R^H = R$. Alternatively, this may be written as $r(-k) = r^*(k)$, where $r(k)$ is the autocorrelation function of the stochastic process for a lag of k. Therefore, Equation 2.27 may be rewritten as

$$R = \begin{bmatrix} r(0) & r(1) & \dots & r(L-1) \\ r^*(1) & r(0) & \dots & r(L-2) \\ \vdots & \vdots & \ddots & \vdots \\ r^*(L-1) & r^*(L-2) & \cdots & r(0) \end{bmatrix}. \tag{2.28}$$

The elements of the matrix, R, denote the correlation between the output signals of the various antenna elements of Figure 2.11. For example, R_{ij} denotes the correlation between the i^{th} and the j^{th} elements of the array. Given that the steering vector associated with the direction θ_i, or the i_{th} source, can be described by an L-dimensional complex vector $\underline{s}_i$ as [23],

$$\underline{s}_i = [\exp(j\omega t_1(\theta_i)), \dots, \exp(j\omega t_L(\theta_i))]^T, \tag{2.29}$$

where L is the number of elements in the antenna array, and t_i is the time delay taken by a plane wave arriving from the i^{th} source, located in the direction θ_i, and measured from the element at the origin, then the correlation matrix, R, of the array elements' outputs in Figure 2.11 may be expressed as [23] :

$$R = \sum_{i=1}^{M} p_i \underline{s}_i \underline{s}_i^H + \sigma_n^2 I, \tag{2.30}$$

where p_i is the power of the i^{th} source, σ_n^2 is the noise power and I is the identity matrix.

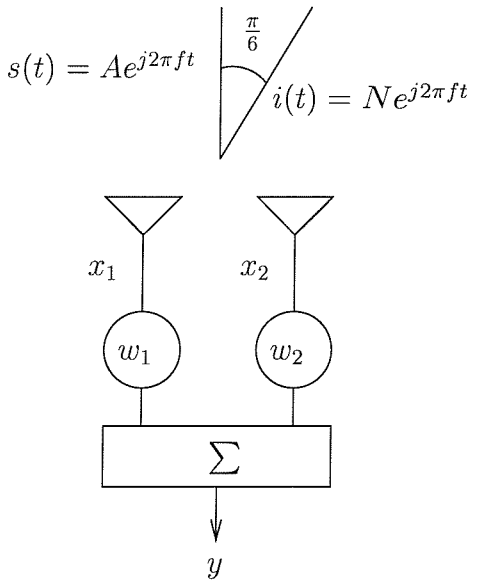

Figure 2.12: Example of a beamforming receiver problem with a wanted signal at 0° and interfering signal at 30° using an array element spacing of $\lambda/2$.

Using matrix notation, the correlation matrix, R, may be expressed in the following form [23, 50]:

$$R = ASA^H + \sigma_n^2 I = U\Lambda U^H, \tag{2.31}$$

where $S = E[\underline{s}_i \underline{s}_i^H]$ is the covariance matrix of the array elements' outputs in Figure 2.11, $A = [\underline{s}_1, \underline{s}_2, \ldots, \underline{s}_M]$, is the $L \times M$ matrix of steering vectors, Λ =diag$[\lambda_1, \lambda_2, \ldots, \lambda_L]$ is a diagonal matrix of real eigenvalues of R and U contains the corresponding unit-norm eigenvectors of R.

2.2.4 A Beamforming Example

Consider the antenna array shown in Figure 2.12, which consists of two omni-directional antenna elements having a spacing of $\frac{\lambda}{2}$. The desired unmodulated carrier signal, $s(t) = Ae^{j2\pi ft}$, arrives from the angle of θ_s=0 radians. The interfering signal, $i(t) = Ne^{j2\pi ft}$, arrives from the direction of θ_i=$\frac{\pi}{6}$ radians or 30°. Both signals have the same frequency, f. The signal arriving from each antenna array element is multiplied by a variable complex weight, and the weighted signals are then summed in order to form the array output. The array output due to the desired signal is

$$y_s(t) = Ae^{j2\pi ft}(w_1 + w_2). \tag{2.32}$$

For the array output, $y(t)$ in Figure 2.12, to be the desired signal $s(t)$, the following equation must be satisfied :

$$Ae^{j2\pi ft}(w_1 + w_2) = Ae^{j2\pi ft}, \tag{2.33}$$

which leads to

$$\begin{aligned} \Re[w_1] + \Re[w_2] &= 1 \\ \Im[w_1] + \Im[w_2] &= 0. \end{aligned} \tag{2.34}$$

The interfering signal arrives at the second array element with a phase lead of $\frac{\pi}{2}$ relative to the first element, since their spacing is $\lambda/2$ and the angle of incidence is 30°. Therefore, the array output due to the interfering signal is

$$y_i(t) = w_1 N e^{j2\pi ft} + w_2 N e^{j(2\pi ft + \pi/2)}. \tag{2.35}$$

For this to become zero we require that :

$$\begin{aligned} \Re[w_1] - \Re[w_2] &= 0 \\ \Im[w_1] + \Im[w_2] &= 0. \end{aligned} \tag{2.36}$$

Solving the simultaneous Equations 2.34 and 2.36 yields

$$w_1 = 0.5 - j0.5, w_2 = 0.5 + j0.5. \tag{2.37}$$

The beam pattern obtained using these weights is shown in Figure 2.13. The desired signal at 0° is attenuated by about 3dB, but the unwanted interference at an angle of 30° is subjected to an attenuation of more than 30dB. This example shows, how beamforming and the cancellation of unwanted interferences may be accomplished. However, a practical beamformer does not require the information regarding the location, number and nature of the signal sources.

2.2.5 Analogue Beamforming

An antenna array consists of a number of antenna elements, the outputs of which are combined via an amplitude and phase control network, in order to form a desired antenna beam [36]. It is possible to perform analogue beamforming at the RF stage [36], using phase shifters and amplifiers, however, the high specification required of these devices renders them costly. An alternative solution is to down-convert the RF signal to an Intermediate Frequency (IF) and to perform the beamforming at the IF stage [3]. The disadvantage of this technique is that each antenna must have its own RF-to-IF receiver. Multiple beamformers

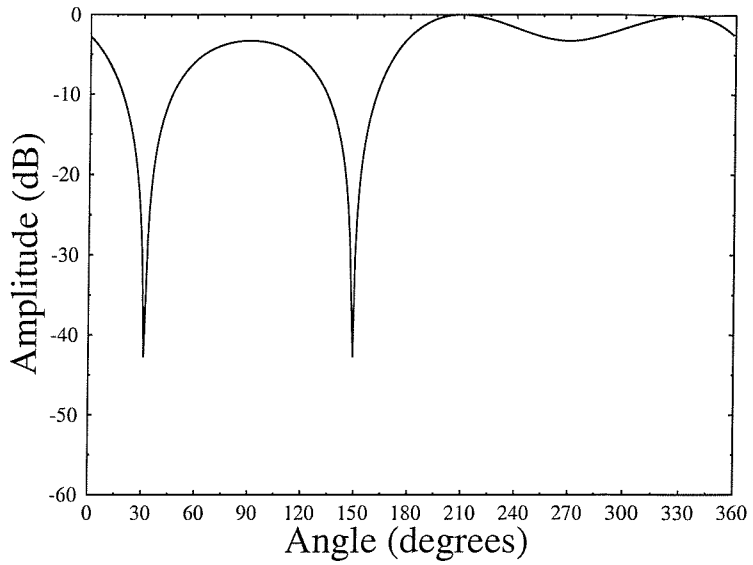

Figure 2.13: The beam pattern produced using Equation 2.21 for a two element array with an element spacing of $\lambda/2$ and element weights of $0.5 \pm j0.5$. The desired signal is at 0°, the interference is at 30°, while SNR=9.0dB and INR=9.0dB.

must be used to form multiple beams, resulting in the distribution of the signal energy across all the formed beams. The output SNR is thus reduced, when the lower signal energy of the beams is combined with the increased noise injected by the increased number of RF and IF stages.

2.2.6 Digital Beamforming

The philosophy of digital beamforming is similar to that of analogue beamforming in that they both adjust the amplitude and phase of the signal arriving from each antenna element, but they use different techniques to reach the same objective. The digitisation of the signal received at each antenna element ensures a higher information processing accuracy [38]. The RF signal received at each element is either digitised at RF or down-converted to IF and then digitised using an Analogue-to-Digital Convertor (ADC). The digital baseband signals then represent the amplitudes and phases of the signals received at each element of the array [38]. The process of beamforming weights these digital signals, thereby adjusting their amplitudes and phases, such that when added together they form the desired beam [36]. The receivers used in a digital beamforming system need not be as closely matched in phase

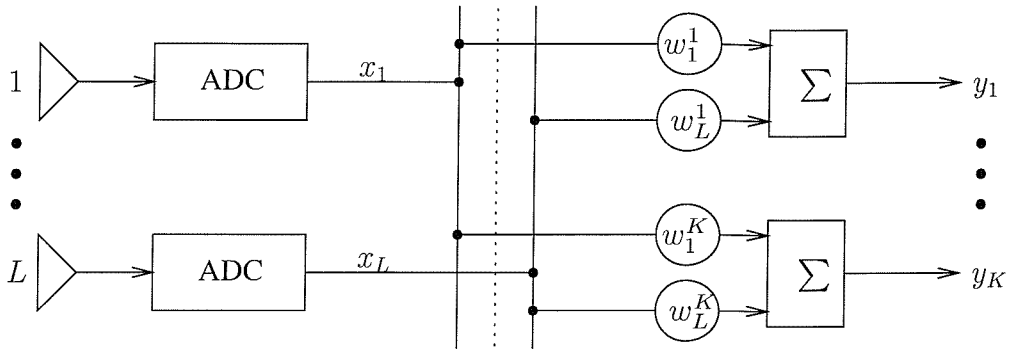

Figure 2.14: An element-space beamformer receiver with L antenna elements capable of forming K beams.

and amplitude, as in an analogue network, since a calibration process can be performed by the controlling software, and any discrepancies can be removed by adjusting the weights appropriately [38].

2.2.7 Element-Space Beamforming

The beamforming process described in Sections 2.2.3-2.2.6 is referred to as element-space beamforming, where the digitised data signals, x_l, $l = 1, \cdots, L$, received from the array elements are directly multiplied by a set of weights, $w_l, l = 1, \ldots, L$, in order to form a beam at the desired angle, θ_k. By multiplying the received data signals, $x_1, \ldots, x_L$, by different sets of weights, w_l^k, where $l = 1, \cdots, L$, and $k = 1, \ldots, K$, *it is possible to form beams steered in any direction,* θ_k, where, again $k = 1, \ldots, K$. More explicitly, by multiplying the signal received at each antenna element by a given complex-valued weight, which may be different for each antenna element, the desired signal may be recovered. Each of the beamformers creates an independent beam, at an angle, θ_k, for receiving an arbitrary mobile's signal, by applying independent weights, w_l^k, $l = 1, \ldots, L$, $k = 1, \ldots, K$, to the array signals, yielding :

$$y(\theta_k) = \sum_{l=1}^{L} w_l^{k*} x_l, \qquad k = 1, \ldots, K \tag{2.38}$$

where $y(\theta_k)$ is the output of the beamformer in the direction of source k, $k = 1, \ldots, K$, which is located at the angle θ_k, $x_l(t)$ is a sample from the l^{th} array element and $w_l^k, l = 1, \cdots, L$ represents the weights for forming a beam at angle θ_k. This equation is very similar to Equation 2.22, except for the addition of the superscript k, $k = 1, \ldots, K$ denoting the k^{th} beam.

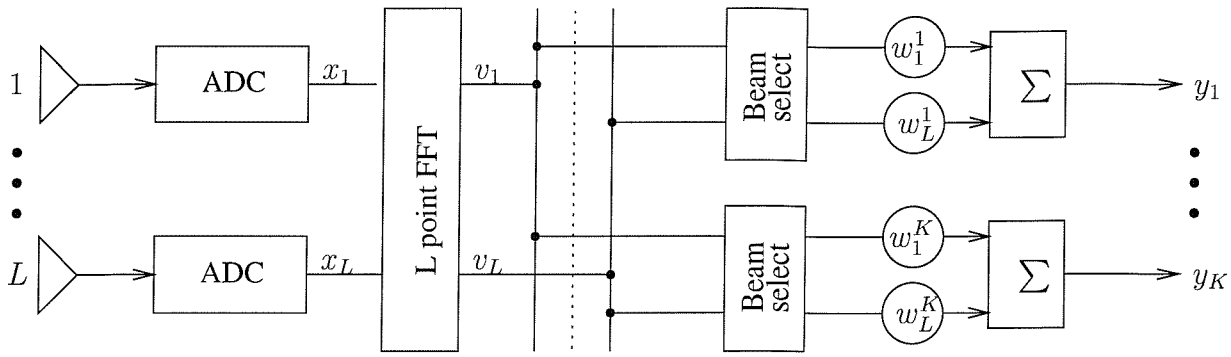

Figure 2.15: A beam-space beamformer receiver with L antenna elements capable of forming K beams [3].

Figure 2.14 shows an element-space beamformer with L antenna elements, capable of forming K independent beams for receiving K mobiles' signals. Each of the K beams may independently reject sources of interference, whilst receiving the desired signal.

2.2.8 Beam-Space Beamforming

In contrast to the method of element-space beamforming, where the signals arriving from each of the L elements are weighted and summed to produce the desired output, the beam-space technique forms multiple fixed beams, using a fixed beamforming network, which may be spatially orthogonal. The output of each beam is then weighted and the resultant signals are combined to produce the desired output [3, 23, 27, 28]. The signals from the beams, which are not used to supply the desired response may be used to cancel unknown interference [28].

Assuming that the outputs from each antenna element are equally weighted and have a uniform phase delay, the response of the array, the array factor $F(\Phi, \alpha)$ in Equation 2.21, produced by an incident plane wave arriving at the antenna array from direction θ, measured with respect to the normal of the antenna array, is given by [28]

$$F(\Phi, \alpha) = \sum_{n=-N}^{N} e^{jn\Phi} e^{-jn\alpha}, \tag{2.39}$$

where $L = (2N + 1)$ is the total number of elements in the array, $\Phi = \frac{2\pi d}{\lambda} \sin\theta$ is the electrical angle, where d is the inter-elemental distance and α is a constant known as the

uniform phase factor. Substituting Φ into Equation 2.39 leads to

$$F(\Phi, \alpha) = \sum_{n=-N}^{N} e^{j\omega t_n(\theta)} e^{-jn\alpha}, \tag{2.40}$$

where $t_n(\theta) = \frac{d \sin\theta}{c}$ and c is the propagation velocity of the received signal. This equation corresponds to Equation 2.21.

For $d = \lambda/2$, we have $\Phi = \pi \sin\theta$ [28]. Summing the geometric series in Equation 2.39, leads to [28]

$$F(\Phi, \alpha) = \frac{\sin[\frac{1}{2}(2N+1)(\Phi - \alpha)]}{\sin[\frac{1}{2}(\Phi - \alpha)]}. \tag{2.41}$$

By assigning different values to α, the main beam of the antenna may be swept across the range, $-\pi \leq \Phi \leq \pi$. In order to generate an orthogonal set of $2N = L - 1$ beams, the uniform phase factor, α, may be assigned the following values [28]:

$$\alpha = \frac{\pi}{2N+1} k, \qquad k = \pm 1, \pm 3, \cdots, \pm 2N - 1. \tag{2.42}$$

Figure 2.16 illustrates the variations in the magnitude of the array factor, $F(\Phi, \alpha)$, with $-\pi \leq \Phi \leq \pi$ for the case of $2N + 1 = 5$ elements and $\alpha = \pm\pi/5, \pm 3\pi/5$. The orthogonal beams generated by the beamforming network represent $2N$ independent directions, one per beam. Depending on the target direction of interest, a particular beam of the set is identified as the main beam and the remainder are viewed as auxiliary beams. From Figure 2.16 it can be seen that each of the auxiliary beams has a null in the direction of the main beam. Because of the fixed nature of these unweighted beams formed by the fixed beamformers of Figure 2.15, individual beam control requires interpolation between beams in order to fine-steer the resultant beam and linear combination of auxiliary beams to create nulls in the direction of interfering sources. Alternatively, beam-space beamforming requires a set of beam-space combiners to generate weighted outputs as shown in Figure 2.15. The Fast Fourier Transform (FFT) block in the diagram generates the orthogonal beams, the process by which this is done is analogous to the performance of an FFT in the time-domain, where it may be viewed as a bank of non-overlapping narrow-band filters whose passbands span the frequency of interest [28]. Hence, the L point FFT generates L spatially orthogonal beams.

2.3 Adaptive Beamforming

An antenna array uses an array of simple antennae, such as omni-directional antennae, and combines the signal induced in these antennae to form the array output. Each antenna

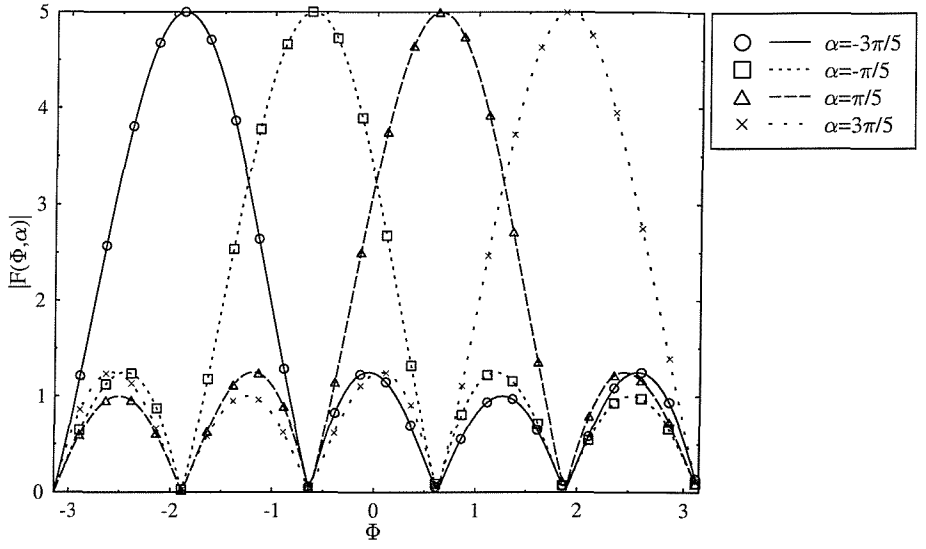

Figure 2.16: The array factor, $F(\Phi, \alpha)$, of a five element antenna array using beam-space beamforming showing the four spatially orthogonal beams that may be generated.

forming part of the array is known as an element of the array. The direction where the maximum gain would appear is controlled by adjusting the phase between the different antenna elements. The phase and gain of the signals induced in each array element is adjusted such that the signals due to a source in the direction in which maximum gain is required are added in-phase. An adaptive antenna adjusts these phases and gains, known as weights, so that when the outputs from the antenna elements are combined, the desired output is achieved [6, 29]. The properties of the antenna array may be varied over time in order to optimise the system's performance with respect to different optimisation criteria. This criteria can include maximum power, maximum Signal to Noise Ratio (SNR), minimum interference and maximum Signal to Interference plus Noise Ratio (SINR) [27]. Depending upon the operational environment that the antenna is currently in, it can change its performance metric and control algorithm, in order to provide the best service for the users of the network [51]. For example, conventional beamforming/diversity may be used to give maximum received signal power, while a null steering algorithm results in minimum interference. Finally, maximising the SINR corresponds to optimum diversity combining. Given these examples and the generic optimisation criteria to maximise reliable information flow to users with minimum required resources such as power and bandwidth, it is plausible

that using a range of different schemes may be necessary. The term intelligent antenna encompasses the technologies of diversity combining [6, 40, 1, 3, 41, 52], adaptive beamforming [6, 3, 8], optimum combining [6, 3], adaptive matching of the antenna's impedance to the receiver [53, 54], and space division multiple access [6, 8, 55, 56].

An adaptive antenna's parameters are automatically adjusted, in order to obtain an optimal or near-optimal array output. The optimisation cost-function and the method used to achieve this state are dependent upon the optimisation algorithm chosen. The need for an adaptive solution is obvious, once one considers that interference is seldom constant in either terms of either time or space and a fixed antenna response would be of little, if any, use.

2.3.1 Fixed Beams

The simplest technique of improving the system's performance is to use fixed multiple beams for both reception and transmission at the base station [32]. The strongest beam in the uplink will also be used for the downlink, since this is deemed to be the beam targeted at the desired user. On the uplink, the base station determines the direction of the path on which the strongest component of the desired signal arrives at the base station. On the downlink, the base station points a beam in the corresponding direction. Although this simple technique is not optimal, the SINR achievable at the mobile can be improved.

Leth-Espensen *et al.* [36] describe a system of array processing, where an algorithm searches through the 22 fixed beams that may be generated by the antenna array, in order to find the strongest receiver beam of the desired signal. More explicitly, an exhaustive search is performed over nine delay taps and the 22 directions until the tap and direction, which result in the maximum received power are obtained. The estimated Direction of Arrival (DoA) was compared to the actual DoA found using a Global Positioning System (GPS) receiver. When averaging the received signals over 21 GSM transmission bursts (21 $\times$ 8 $\times$ 576 μs $\approx$ 100ms) the direction estimates occasionally indicated a direction quite different from that of the mobile. This was attributed to the received signal's lack of power due to undergoing a deep fade at that time. Increasing the number of bursts, over which the received signal was averaged, to 104 ($\approx$480ms) gave significantly improved results. The performance of eight element arrays processing either 22 beams or eight beams as well as that of four element arrays processing eight or four beams were compared. The average performance gain of the eight element array using 22 beams over that of a single element was 9.8dB. For the eight element, eight beam antenna the corresponding improvement was 8.8dB and for the four element, eight beam array the gain was 8.7dB. Finally, the gain

offered by the four beam, four element array was 5.4dB.

In a switched beam system [33] a mobile station is located within a specific antenna beam and the antenna is then switched in the required operational mode in order to communicate with the specific user supported by the selected beam. If one considers a cell split into three sectors, each of 120° coverage, the available channels are divided equally amongst the sectors. No intelligence is required to locate a mobile station within a sector and to initiate a call. In the event of the mobile station changing sector a handover is performed. An intelligent antenna system is able to switch from a given beam to a new beam without necessitating a handover, i.e. any of the beams can be assigned to one or more of the transceivers. Therefore, should all the users be located in one sector, then as many users as there are transceivers can be served. In contrast, using a conventionally sectorised base station the transceivers in the empty sectors would not be used, while calls in the high-traffic sectors would be blocked [33].

2.3.2 Temporal Reference Techniques

Temporal reference techniques refer to the design of array processors which optimise the receive antenna array weights, in order to be able to identify a known sequence at the output of the antenna array. This known desired sequence is termed the reference signal, which must be specifically designed so as to be easily identifiable, for example with the aid of a high auto-correlation peak, while being readily distinguishable from or uncorrelated with unwanted interferences and noise sources [3, 20, 30]. For example, in GSM [11] there are eight different channel sounding sequences used for identifying the eight co-channel base stations, therefore, inevitably, co-channel interferers will use identical sounding sequences to those used by the desired mobile user, hence the system may become unable to distinguish between the wanted signal and a co-channel interferer [1]. The spreading codes used in CDMA are inherently unique and they are therefore suitable for use as the user specific sequence. A significant advantage of the temporal reference technique is that, unlike the spatial reference approach, it does not need careful characterisation of the antenna array. Effects such as mutual coupling between the antenna array elements are readily handled by the adaptation routine, since the array weights are adjusted automatically, in order to cancel them [1].

Figure 2.17 shows the structure of a temporal reference based beamformer, where the array output is subtracted from the reference signal, $r(t)$ which assists in identifying the desired user, in order to generate the error signal $\epsilon(t) = r(t) - \underline{w}^H \underline{x}(t)$, which is then used to control the weights. The weights are adjusted such that the Mean Squared Error (MSE)

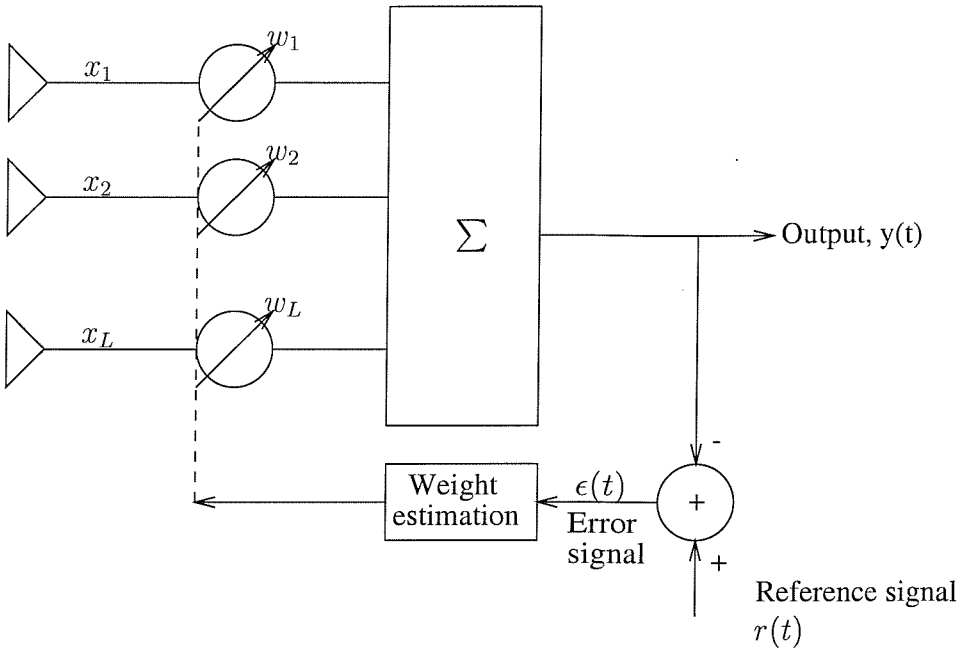

Figure 2.17: The structure of a temporal reference based beamformer with L antenna elements.

between the array output and the reference signal is minimised, where the error is expressed as :

$$\epsilon^2(t) = [r(t) - \underline{w}^H \underline{x}(t)]^2. \tag{2.43}$$

Taking the expected values of both sides of Equation 2.43 we get

$$E[\epsilon^2(t)] = E[r^2(t)] - 2\underline{w}^H \underline{z} + \underline{w}^H R \underline{w}, \tag{2.44}$$

where $\underline{z} = E[\underline{x}(t)r^*(t)]$ is the cross-correlation between the reference signal and the array signal vector $\underline{x}(t)$ and $R = E[\underline{x}(t)\underline{x}^H(t)]$, as defined in Equations 2.26 and 2.27, is the correlation matrix of the array output signals.

The MSE surface is a quadratic function of the complex array weight vector $\underline{w}$ and it is minimised by setting its gradient with respect to $\underline{w}$ equal to zero :

$$\nabla_{\underline{w}}(E[\epsilon^2(t)]) = -2\underline{z} + 2R\underline{w} = 0, \tag{2.45}$$

yielding the well-known Wiener-Hopf equation for the optimal weight vector [3, 20, 23, 27, 28, 30] in the form of :

$$\underline{w}_{opt} = R^{-1}\underline{z}. \tag{2.46}$$

The Minimum Mean Square Error (MMSE) at the output of the array processor, also known as the Wiener filter, using these weights is given by [23] :

$$MMSE = E[|r(t)|^2] - \underline{z}^H R^{-1} \underline{z}. \tag{2.47}$$

In [57] a 16-bit reference signal was used in order to uniquely identify the mobiles. This contribution proposes an adaptive antenna algorithm suitable for GSM and the urban environment, since this is where the highest capacity is generally needed. More specifically, the 16-bit reference signal used in this system is the GSM equaliser's training sequence, which is one of the eight legitimate 16-bit codes exhibiting the highest main-peak to side-peak ratio in its auto-correlation function, which were found by exhaustive computer search of all 2^{16} possible sequences. These 16-bit sequences were then extended to 26 bits by quasi-periodically repeating five bits at both ends of the sequence. Neighbouring base stations, and hence their mobiles, use a different one from the set of eight codes, as detailed in [11]. The algorithm described in this paper [57] calculates the initial weight vector using just the known training sequence. This weight vector is then applied to all the data in the burst and the result is passed to the GSM channel equaliser in order to detect the unknown bits. The detected bits are then input to the GSM modulator, in order to construct a modulated reference waveform for the entire burst and a new weight vector is calculated. This weight vector is applied to the whole data burst and the result is again passed to the GSM equaliser. Therefore, the Signal-to-Interference and Noise Ratio (SINR) is improved for the whole burst, rather than just for the training sequence. In the simulations carried out in [57] the process was repeated for a maximum of 20 iterations or until the same data bits were returned twice. It was found that the typical number of iterations required was three or four. The effect of varying the number of antenna elements was investigated. If the multipath components of the wanted signal are sufficiently delayed, so that they are uncorrelated with the reference signal, they are cancelled. These delayed paths can be exploited, if tapped delay-line filters are used in conjunction with amplitude and phase weighting of the antenna elements. The paper presents results for an eight element linear array with up to three taps.

Barrett and Arnott [1] describe a similar system, in which the modulated training sequence is compared to the signal at the array's output. After the training sequence has been received and the data detection begins, the system switches into decision directed mode, in which the demodulator decisions are remodulated in order to form the reference signal on the basis of the total received burst. Provided that the error rate is adequate (better than 10^{-2}), a reference signal generated by this method would allow the system to track interference changes in the propagation environment. Field trials were conducted

for a system using an eight element adaptive antenna. The data received at each antenna was digitised and stored, in order to allow offline processing, enabling the comparison of different processing functions operating on the basis of the same recorded data. The results show a substantial improvement in terms of the demodulated SNR, when compared to that of a single element antenna. The optimum combining was implemented by updating the array weights every transmission burst (every 10ms), and each update used 100 data snapshots taken from within the burst. The reference signal was obtained using decision directed operation (no training sequence was used) and the weights were updated using the Normalised Least Mean Squares (NLMS) algorithm. The amplitude resolution of the data and weights was eight bits. The results using optimum combining were found to be superior to those obtained using selection diversity.

2.3.2.1 Least Mean Squares

The Least Mean Squares (LMS) algorithm is the most common technique used for continuous adaptation [3, 20, 23, 28, 30]. It is based on the steepest-descent method, a well-known optimisation technique that recursively computes and updates the weight vector. The algorithm updates the weights at each iteration by estimating the gradient of the quadratic error surface and then changing the weights in the direction opposite to the gradient by a small amount in an attempt to minimise the Mean Square Error (MSE), as seen in Figure 2.18. The desired response, generated for example by inputting the reference sequence to the modulator is supplied to the algorithm, allowing the estimation error and thus the error surface, to be calculated. The constant that determines the amount by which the weights are adjusted during each iteration is referred to as the step size. When the step size is sufficiently small, the process leads these estimated weights to the near-optimal weights in Figure 2.18, whilst large step sizes allow faster convergence, but exhibit a larger residual MSE due to the non-optimal weights [28].

The updated value of the weight vector at time $n+1$ is computed using [3, 8, 23, 27, 28, 29, 58] :

$$\underline{w}(n+1) = \underline{w}(n) - \frac{1}{2}\mu\nabla(J(n)), \tag{2.48}$$

where $\underline{w}(n+1)$ denotes the new weights computed at the $(n+1)^{th}$ iteration; μ is the positive step size that controls the rate of convergence and hence determines how close the estimated weights approach the optimal weights and $\nabla(J(n))$ is an estimate of the gradient of the MSE, $J(n)$, where $J(n)$ is given by [23] :

$$J(n) = E[|r(n+1)|^2] + \underline{w}^H(n)R\underline{w}(n) - 2\underline{w}^H(n)\underline{z}, \tag{2.49}$$

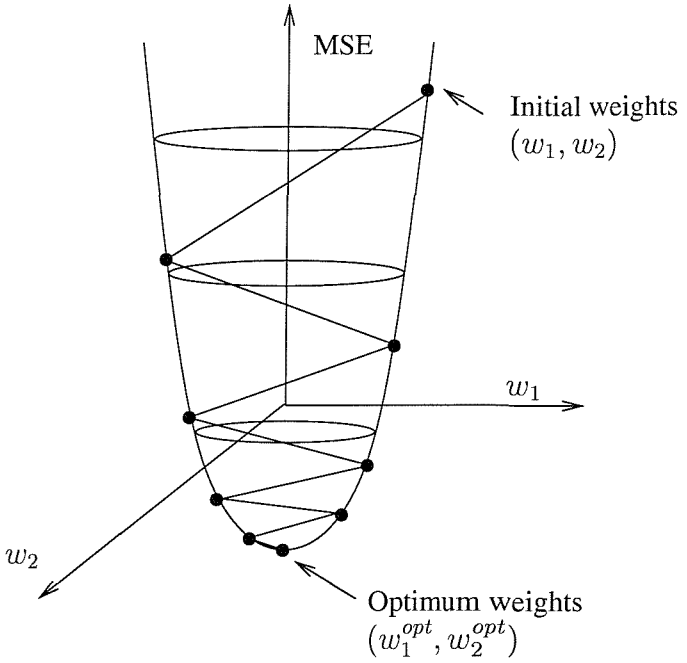

Figure 2.18: An example of the quadratic error surface and the weights of a two element system following the negative direction of the gradient in order to minimise the Mean Square Error (MSE).

where $r(n+1)$ is the reference signal at time $n+1$ and $\underline{z} = E[\underline{x}(t)r^*(t)]$ is the cross-correlation vector between the input vector $\underline{x}(n)$ and the desired response $r(n)$, while the correlation matrix, R, was defined in Equations 2.26 and 2.27.

Differentiating Equation 2.49 with respect to $\underline{w}(n)$ gives :

$$\nabla(J(n)) = 2R\underline{w}(n) - 2\underline{z}. \tag{2.50}$$

Therefore, the instantaneous estimate of the gradient vector becomes :

$$\begin{aligned} \hat{\nabla}(J(n)) &= 2\underline{x}(n)\underline{x}^H(n)\underline{w}(n) - 2\underline{x}(n)r^*(n) \\ &= -2\underline{x}(n)\epsilon^*(n), \end{aligned} \tag{2.51}$$

where $\epsilon^*(\underline{w}(n))$ is the error between the array output and the reference signal, which is formulated as :

$$\epsilon^*(n) = r(n) - \underline{x}^H(n)\underline{w}(n). \tag{2.52}$$

The array output in Figure 2.17 is given by :

$$y(n) = \underline{w}^H(n)\underline{x}(n). \tag{2.53}$$

Upon substituting Equation 2.52 in Equation 2.48 the weight adaptation equation becomes:

$$\underline{w}(n+1) = \underline{w}(n) + \mu \underline{x}(n)\epsilon^*(n). \tag{2.54}$$

Therefore, as Equation 2.52 shows, the estimated gradient, $\hat{\nabla}(J(n))$, is a function of the error, $\epsilon(n)$, between the array output, $y(n)$, and the reference signal, $r(n)$, and the received array signals, $\underline{x}(n)$, after the n^{th} iteration. Convergence is guaranteed only, if [23, 29],

$$0 < \mu < \frac{1}{\lambda_{max}}, \tag{2.55}$$

where λ_{max} is the maximum eigenvalue of R, the correlation matrix of Equations 2.26 and 2.27. Therefore, the eigenvalue spread or ratio of the matrix R controls the rate of convergence [28] according to :

$$\chi(R) = \frac{\lambda_{max}}{\lambda_{min}}, \tag{2.56}$$

where $\chi(R) \geq 1$.

Under these conditions the algorithm is stable and the mean value of the estimated array weights converges to the values of the optimal weights. Within these bounds, the speed of adaptation and also the noise contaminating the weight vector are both determined by the size of μ. Since the trace of R is given by the sum of the diagonal elements of R [28], λ_{max} therefore cannot be greater than the trace of R, that is,

$$\lambda_{max} \leq tr[R] = \sum_{i=1}^{L} \lambda_i \tag{2.57}$$

where L is the number of antenna elements, and λ_i is the i^{th} eigenvalue of R. Hence we have:

$$0 < \mu < \frac{1}{tr[R]}. \tag{2.58}$$

This is a more restrictive bound on μ, than Equation 2.55, but it is much easier to apply, because the elements of R and the signal power can generally be more readily estimated, than the eigenvalues of R. The efficiency of the LMS algorithm has been shown to approach a theoretical limit for adaptive algorithms, when the eigenvalues of R are equal or nearly equal [59]. When the eigenvalues of the correlation matrix R are widely spread, i.e. $\chi(R) = \frac{\lambda_{max}}{\lambda_{min}} \gg 1$, then, according to Haykin [28], the excess mean-squared error produced by the LMS algorithm with respect to the minimum is determined primarily by the largest eigenvalues [28], and the time taken for the average weight vector to converge is limited by

the smallest eigenvalues. However, as the spread of the eigenvalues increases, the highest acceptable value of the stepsize μ required for maintaining stability decreases inevitably, resulting in slower convergence to the optimal weights. Selecting too small a value for μ results in a slow rate of convergence, and in a non-stationary environment may cause the estimated weights to lag behind the evolution of the optimal weights [38], a phenomena known as the weight vector lag. Alternatively, using too high a value for μ allows the vicinity of the solution point to be reached more rapidly, but the weights then wander around a larger region and cause a weight mis-adjustment error, as was demonstrated in Figure 2.18 [60]. This is due to μ being equivalent to the reciprocal of the memory of the system, where a large value of μ uses fewer samples to estimate R, and hence a degraded estimation is performed, resulting in an increase in the average excess mean-squared error after adaptation.

2.3.2.2 Normalised Least Mean Squares Algorithm

In the LMS algorithm, the correction $\mu\underline{x}(n)\epsilon^*(n)$ applied to the weight vector at time $n+1$ in Equation 2.54 is directly proportional to the input vector $\underline{x}(n)$. Therefore, when $\underline{x}(n)$ is large, the LMS algorithm experiences a gradient noise amplification problem [28]. Therefore an algorithm which normalises the weight vector correction with respect to the squared Euclidean norm of the input vector $\underline{x}(n)$ at time n can be invoked. At the n^{th} iteration the step size is then given by [23, 28] :

$$\mu(n) = \frac{\mu_0}{\underline{x}^H(n)\underline{x}(n)} = \frac{\mu_0}{\|\underline{x}(n)\|^2}, \tag{2.59}$$

where μ_0 is a constant. The normalised LMS algorithm is convergent in the mean-square sense, if $0 < \mu_0 < 2$ [28]. However, if the input vector $\underline{x}(n)$ is small, then numerical problems may arise due to the associated division by a small number. Therefore Equation 2.59 may be modified to:

$$\mu(n) = \frac{\mu_0}{a + \|\underline{x}(n)\|^2}, \tag{2.60}$$

where $a > 0$. Hence, the weight update formula of Equation 2.54 is modified to:

$$\underline{w}(n+1) = \underline{w}(n) + \frac{\mu_0}{a + \|\underline{x}(n)\|^2}\underline{x}(n)\epsilon^*(n). \tag{2.61}$$

2.3.2.3 Sample Matrix Inversion

The Sample Matrix Inversion (SMI) algorithm is a method of directly calculating the antenna array weights based on an estimate of the correlation matrix, $R = E[\underline{x}(t)\underline{x}^H(t)]$ of

the adaptive array output samples. The Wiener-Hopf solution for the optimal weights is repeated here from Equation 2.46, for convenience :

$$\underline{w}_{opt} = R^{-1}\underline{z}, \tag{2.62}$$

where $\underline{z} = E[\underline{x}(t)r^*(t)]$ is the cross-correlation between the reference signal, $r(t)$ and the array output signal, $\underline{x}(t)$. If the signal, noise and interference characteristics are stationary, then the correlation matrix can be evaluated and the optimal solution for the adaptive weights can be computed directly using the above equation, with the aid of matrix inversion. In practice however, due to the non-stationary mobile environments encountered, the adaptive processor must continually update the weight vector, in order to meet the new conditions imposed by the time-varying mobile environment. This need to regularly update the weight vector leads to the requirement of obtaining estimates of R and $\underline{z}$ in a finite observation interval, and thus to obtain a weight vector estimate. This approach is termed block-adaptive, where the statistics are estimated from a temporal block of data and are used in a periodic optimum weight calculation process. In the GSM system [11] it may be possible to use the synchronisation/channel sounding sequence in each burst to recompute the antenna array weights for each 4.615ms burst.

If the cross-correlation vector $\underline{z} = E[\underline{x}(t)r^*(t)]$ is assumed to be known, then the optimal weight vector estimate, $\underline{\hat{w}}$ of Equation 2.62, for the situation when $\underline{x}(t)$ contains the reference-signal related desired signal, where $\hat{R}_{xx}$ is the block based estimate of the true correlation of the array's output samples, namely that of R_{xx}, may be determined using

$$\underline{\hat{w}}_1 = \hat{R}_{xx}^{-1}\underline{z}. \tag{2.63}$$

However, in the scenario when the received signal $\underline{x}(t)$ contains either noise of the interfering users' signals rather than the desired signal, the estimate of the correlation matrix R_{xx} is denoted by $\hat{R}_{nn}$, and the optimal antenna weights may be calculated thus according to :

$$\underline{\hat{w}}_2 = \hat{R}_{nn}^{-1}\underline{z}. \tag{2.64}$$

Therefore, the Signal-to-Noise Ratio (SNR) at the output of the combiner seen in Figure 2.17 may be written as [30] :

$$\left(\frac{s}{n}\right)_i = \frac{\underline{\hat{w}}_i^H \underline{s}\underline{s}^H \underline{\hat{w}}_i}{\underline{\hat{w}}_i^H R_{nn} \underline{\hat{w}}_i}, \tag{2.65}$$

where i assumes values of 1 or 2, according to the first or second scenarios above, and $\underline{s}$ denotes the reference-signal related desired signal component of the array output signal vector $\underline{x}$. The SNR $(s/n)_2$ is only defined during those time intervals, when a reference-signal related desired signal is actually present; the weight adjustment is assumed to take place when the desired signal is absent.

The estimate of the sample correlation matrix can be evaluated according to:

$$\hat{R}_{xx} = \frac{1}{N}\sum_{n=1}^{N} \underline{x}(n)\underline{x}^H(n), \tag{2.66}$$

where N is the size of the observation interval expressed in terms of the number of array output samples considered. Again, this approach is termed block-adaptive, where the statistics are estimated from a temporal block of data and used during the optimum weight calculation process. Given that each element of the matrix, $\hat{R}_{xx}$, is a random variable, the output SNR is also a random variable [25, 30]. The maximum achievable SNR at the output of the combiner seen in Figure 2.17 that may be obtained is :

$$SNR_{opt} = \underline{s}^H R_{nn}^{-1} \underline{s}. \tag{2.67}$$

The actual SNRs obtained using $\underline{\hat{w}}_1$ and $\underline{\hat{w}}_2$ may be normalised as follows [25, 30] :

$$\rho_i = \frac{(s/n)_i}{SNR_{opt}}. \tag{2.68}$$

Reed [25] examined the number of samples, N, required in order to achieve a high-quality estimate of the noise- or interference-related co-variance matrix, R_{nn}, and derived the expected value of the normalised SNR at the output of the combiner seen in Figure 2.17, which was found to be :

$$E[\rho_2] = \frac{N+2-L}{N+1}, \tag{2.69}$$

where L is the number of elements in the antenna array.

The expectation of the normalised SNR in Equation 2.69 using the antenna weights calculated on the basis of the noise- or interference-only related co-variance matrix, is plotted in Figure 2.19 for two, four and eight element antenna arrays. Explicitly, Figure 2.19 suggests that as long as, N, the number of samples used to estimate the noise- or interference-related correlation matrix, R_{nn}, is greater than twice the number of antenna elements, the loss in $E[\rho_2]$ due to non-optimal weights is less than 3dB. The expected values of $E[\rho_2]$ evaluated from Equation 2.69 are compared to values determined using simulations. The simulation based and theoretical SNRs were in good agreement. It is interesting to note that although both the normalised simulated and theoretical SNRs approach unity, implying approaching the optimum SNR in Equation 2.67, however the rate of convergence for both the theoretical and simulated values slows down, as the number of antenna elements used to form the antenna array increases. This is expected, since as the number of antenna array elements increases, so does the optimum SNR that may be obtained according to Equation 2.67, as also seen in Figure 2.20.

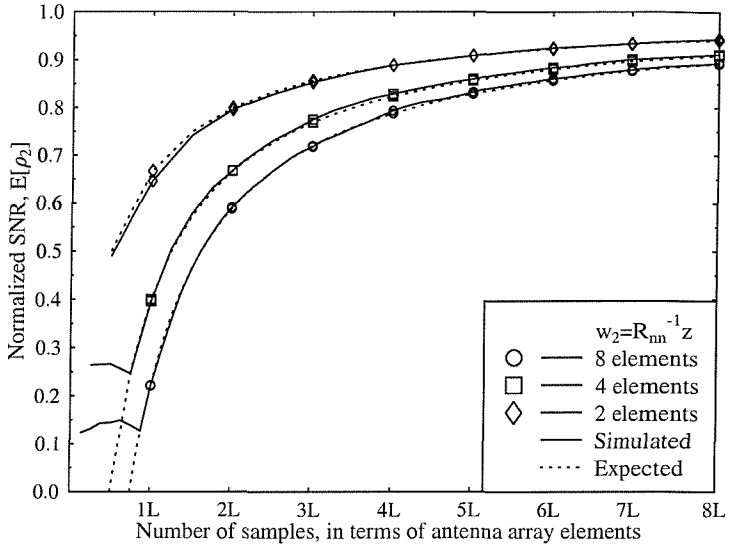

Figure 2.19: The expected normalised Signal-to-Noise Ratio (SNR), $E[\rho_2]$ evaluated from Equation 2.69, for various numbers of array output samples, in terms of the number of antenna array elements, used to construct the noise- or interference-only correlation matrix. Simulated results for identical scenarios are also presented for comparison. The SNR at each antenna array element was 12.0dB.

Thus far we have assumed the knowledge of the cross-correlation vector $\underline{z}$, which is unrealistic in a practical system. Therefore, the optimal weight vector may be determined with the aid of the estimated cross-correlation vector $\hat{\underline{z}}$ according to :

$$\underline{\hat{w}}_2 = \hat{R}_{xx}^{-1}\hat{\underline{z}}, \tag{2.70}$$

where $\hat{\underline{z}}$ is the sample cross-correlation vector given by

$$\hat{\underline{z}} = \frac{1}{N}\sum_{n=1}^{N}\underline{x}(n)r^*(n), \tag{2.71}$$

and $r(n)$ is the reference signal.

The normalised SNR for a two element antenna array was determined by simulation using Equation 2.70, for estimating the optimum antenna array weights, is presented in Figure 2.21. This figure shows that the SNR of the received signal, using the antenna weights determined when the desired signal was present, is significantly lower, than when using the weights obtained when the desired user's signal was absent. The simulated SNR, for the

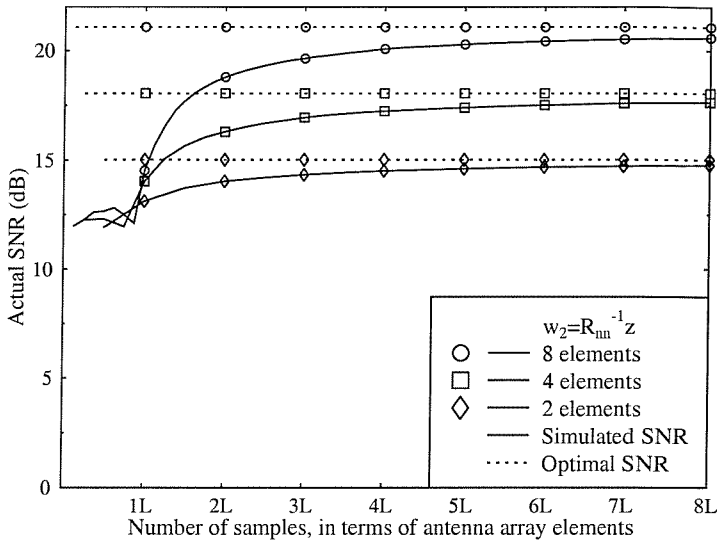

Figure 2.20: The SNR at the output of the array combiner determined by simulation and the optimal SNR according to Equation 2.67 for a varying number of array output samples, in terms of the number of antenna array elements, used to construct the noise- or interference-only correlation matrix. The SNR at each antenna array element was 12.0dB.

case of two antenna elements, when the desired signal was received is significantly higher than that predicted theoretically by Equation 2.68, although this phenomenon does not appear for the four and eight element antenna arrays characterised in Figure 2.22.

The SNR obtained using Equation 2.70 is shown to be comparable to the SNR obtained with the noise- or interference-only correlation matrix, R_{nn}, which is because the estimates $\hat{\underline{z}}$ and $\hat{R}_{xx}$ are highly correlated under strong desired signal conditions, and the errors in each estimate tend to compensate each other, thus yielding an improved weight estimate and faster convergence. Improvement of the transient response through careful selection of the initial weight vector is possible by invoking the following relationship [30] :

$$\hat{\underline{w}}_1 = \left[\frac{1}{N} \left(\sum_{n=1}^{N} \underline{x}(n) \underline{x}^H(n) + \alpha I \right) \right]^{-1} \underline{z} \tag{2.72}$$

where α is a scalar constant and I is the $N \times N$ identity matrix.

The estimate of R may be updated, when new samples arrive from the antenna, according

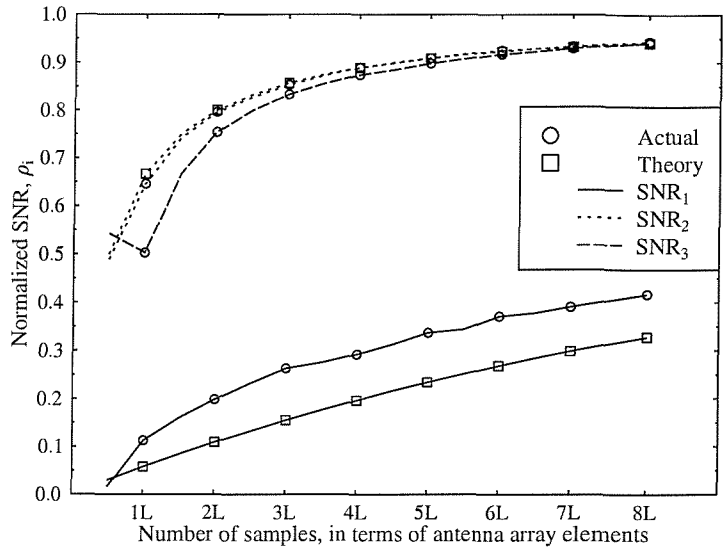

Figure 2.21: The normalised Signal-to-Noise Ratio (SNR), ρ_i, for various numbers of array output samples, in terms of the number of antenna array elements. Results are shown for $\underline{w}_1 = \hat{R}_{xx}^{-1}\underline{z}$, $\underline{w}_2 = \hat{R}_{nn}^{-1}\underline{z}$, and $\underline{w}_3 = \hat{R}_{xx}^{-1}\hat{\underline{z}}$ for both theory, according to Equations 2.63, 2.64 and 2.70, and simulation. The antenna array consisted of two antenna elements, separated by $\lambda/2$, and the SNR at each of which was 12.0dB.

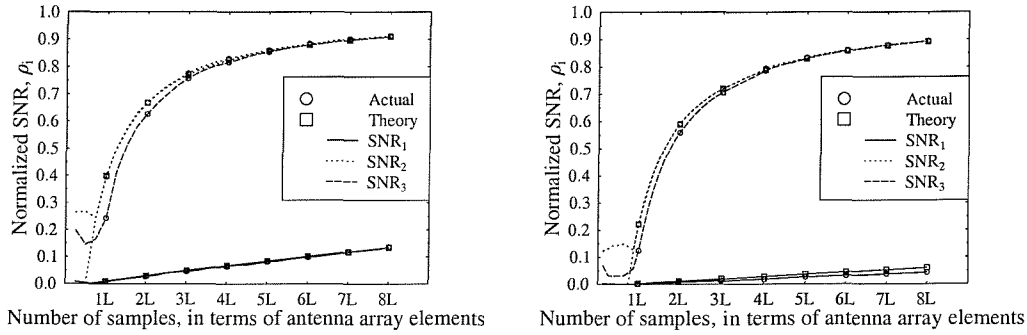

(a) Four elements

(b) Eight elements

Figure 2.22: The normalised Signal-to-Noise Ratio (SNR), ρ_i, for various numbers of samples, in terms of the number of antenna array elements. Results are shown for $\underline{w}_1 = \hat{R}_{xx}^{-1}\underline{z}$, $\underline{w}_2 = \hat{R}_{nn}^{-1}\underline{z}$, and and $\underline{w}_3 = \hat{R}_{xx}^{-1}\hat{\underline{z}}$ for both theory, according to Equations 2.63, 2.64 and 2.70, and simulation. The antenna elements were separated by $\lambda/2$. The SNR at each antenna element was 12.0dB.

to [23]:

$$\hat{R}(n+1) = \frac{n\hat{R}(n) + \underline{x}(n+1)\underline{x}^H(n+1)}{n+1}, \tag{2.73}$$

and a new estimate of the weights $\underline{\hat{w}}(n+1)$ at time instant $n+1$ may be made. The expression of the optimal weights in Equation 2.46 requires the inverse of R, and this process of estimating R and then its inverse may be combined to update the inverse of R from the array signal samples, $\underline{x}(n)$, using the Matrix Inversion Lemma [23, 27] which is given in its general form as:

$$(A + XX^H)^{-1} = A^{-1} - \frac{A^{-1}XX^HA^{-1}}{1 + X^HA^{-1}X}, \tag{2.74}$$

thus leading to:

$$\hat{R}^{-1}(n) = (n+1)\hat{R}^{-1}(n-1) - \frac{(1+\frac{1}{n})\hat{R}^{-1}(n-1)\underline{x}(n)\underline{x}^H(n)\hat{R}^{-1}(n-1)}{n + \underline{x}^H(n)\hat{R}^{-1}(n-1)\underline{x}(n)}, \tag{2.75}$$

with

$$\hat{R}^{-1}(0) = \frac{1}{\epsilon_0}I, \qquad \epsilon_0 > 0, \tag{2.76}$$

where I is the $N \times N$ identity matrix. This method of estimating the array weights using the inverse update technique is known as the Recursive Least Squares (RLS) algorithm.

Unlike for the LMS algorithms, the performance of the SMI algorithm is almost independent of the eigenvalue spread of R and it is similar to that of the steepest descent algorithm using a correlation matrix, R, of equal eigenvalues [27]. The matrix estimation in Equation 2.66 is only suitable for use in a stationary environment [27]. In a time varying environment a de-weighted matrix estimate may be more applicable [58], yielding:

$$\hat{R}(n) = \alpha\hat{R}(n-1) + (1-\alpha)\underline{x}(n)\underline{x}^H(n) \qquad 0 < \alpha < 1 \tag{2.77}$$

where α is the so-called 'forgetting factor'.

Hence, Equation 2.75 becomes

$$\hat{R}^{-1}(n) = \alpha^{-1}\hat{R}^{-1}(n-1) - \frac{(1-\alpha)\alpha^{-2}\hat{R}^{-1}(n-1)\underline{x}(n)\underline{x}^H(n)\hat{R}^{-1}(n-1)}{1 + (1-\alpha)\alpha^{-1}\underline{x}(n)\hat{R}^{-1}(n-1)\underline{x}^H(n)}. \tag{2.78}$$

The vector, $\underline{\hat{z}} = E[\underline{x}(n)r^*(n)]$, containing the correlation between the reference signal, $r(n)$, and the array output signals, $\underline{x}(n)$, must also be updated for each block of N received samples according to:

$$\underline{\hat{z}} = \frac{1}{N}\sum_{n=1}^{N}\underline{x}(n)r^*(n). \tag{2.79}$$

If an error term, $e = \hat{\underline{z}} - \underline{z}$, between the estimate of the correlation vector $\underline{z}$ and its actual value, is used to represent the errors due to the estimation process, we may write

$$e = \hat{R}\underline{w}_{opt} - \underline{z}. \tag{2.80}$$

Therefore, the weight vector derived using the SMI method is a least squares solution. It can be shown theoretically that the array weights derived by the SMI approach converge more rapidly towards their final values than those generated by the LMS algorithm. However, there are practical difficulties associated with the employment of the SMI algorithm. Specifically, the inversion of the potentially large correlation matrix, R, requires a high complexity. Specifically, the complexity of the matrix inversion is proportional to L^3, where L is the matrix dimensionality, and it is thus very computationally expensive. However, the matrix inversion may be avoided by using the recursive techniques of Equation 2.75.

In [48] Strandell *et al.* investigated the performance of an adaptive antenna system using the SMI adaptation algorithm. The system was integrated into an existing DCS-1800 base station and used the 26-bit equaliser training sequence in each traffic burst as the reference signal. The performance of the adaptive antenna was evaluated in the laboratory initially, so as to avoid multipath propagation. It was shown that the algorithm was capable of suppressing an interferer, when the power of the interferer was within the dynamic range of the Analogue-to-Digital Converter (ADC) used to digitise the signals arriving at the antenna array elements. The ADC had an eight-bit resolution giving approximately a 48dB dynamic range spanning from -32dBm to -80dBm. Consequently, below -80dBm the interferer is buried in the noise and no suppression is possible. Therefore, stronger interferers are suppressed more effectively than weak ones. The adaptive antenna was found to improve the SIR by more than 30dB in conjunction with an interferer power at -40dBm and a desired input signal power between -70dBm and -40dBm. When either of the signal levels exceeded the dynamic range of the ADC, the SIR improvement was very low, even less than 0dB in some circumstances.

The performance of the antenna was then evaluated in an open terrain environment, with no obstacles within 500m of the antenna. It was found that even though there was some array pattern distortion, or angular pointing error in the direction of the main beam, the interfering signal located at an angle of 90° with respect to the desired signal was suppressed by about 25dB relative to the main beam. The pointing error of the main beam was due to the relatively short, 26-bit training sequence used, leading to a poorly estimated array output correlation matrix, when the desired signal was present in the matrix [61]. A solution to this problem is the positive diagonal loading technique [61], where adding a small value to the diagonal elements of the matrix results in faster weight convergence. In conjunction with

a perfectly estimated array output correlation matrix all the noise eigenvalues are identical and equal to the noise variance [48]. In contrast, a poor estimate of the array output correlation matrix gives non-identical eigenvalues, resulting in a distorted array pattern. If the loading value is larger than the noise eigenvalues, but smaller than the eigenvalues of the desired and interfering signal, then the overall noise level is increased, resulting in almost identical noise eigenvalues [62]. The loading value l was chosen so that $l/\sigma^2 \approx 10^2$ [61]. The diagonal loading decreases the SIR, but increases the SNR due to the lower sidelobe levels, leaving the SINR unchanged [61]. The SIR improvement achieved by the adaptive antenna was measured for Direction-Of-Arrival (DOA) separations ranging from 2.5° to 180° at a constant input SIR of 20dB. The interference suppression capability varied from 31dB for a 180° angular separation to 26dB for a 2.5° separation. However, as a consequence of the limited array beamwidth, the SNR gain decreased upon decreasing the DOA separation, reaching a minimum of -10dB at 5° separation.

2.3.2.4 Recursive Least Squares

The RLS algorithm exploits the matrix inversion lemma defined in Equation 2.74 for updating the antenna array element weights. As the RLS algorithm utilises information contained in the array's combiner output data as shown by Equations 2.74 and 2.75, extending back to the time when the algorithm was initiated, the rate of convergence is typically an order of magnitude higher than that of the LMS algorithm. This performance improvement, however, is achieved at the expense of a substantial increase in computational complexity.

The correlation matrix, R of the array output, at time n, may be updated thus according to [3, 23, 28] :

$$R(n) = \delta_0 R(n-1) + \underline{x}(n)\underline{x}^H(n), \tag{2.81}$$

where, similarly to Equation 2.77, the 'forgetting factor', δ_0, is used to de-emphasise old array output samples. The value $1/(1-\delta_0)$ is known as the memory of the algorithm, and for example when $\delta_0 = .99$, the memory of the algorithm is approximately 100 samples, while $R(n-1)$ is the previous value of the correlation matrix, R, at time $n-1$.

Similarly, the cross-correlation vector between the array output signal and the desired signal may be calculated as :

$$\underline{z}(n) = \delta_0 \underline{z}(n-1) + \underline{x}(n)r(n). \tag{2.82}$$

Equation 2.46 states how the optimal receive antenna weights may be obtained, which is

repeated here for convenience :

$$\underline{w}_{opt} = R^{-1}\underline{z}, \tag{2.83}$$

leading to,

$$\begin{aligned} \underline{\hat{w}}(n) &= R^{-1}(n)\underline{z} \\ &= \delta_0 R^{-1}(n)\underline{z}(n-1) + R^{-1}(n)\underline{x}(n)r^*(n), \end{aligned} \tag{2.84}$$

where

$$R^{-1}(n) = \frac{1}{\delta_0}\left[R^{-1}(n-1) - \frac{R^{-1}(n-1)\underline{x}(n)\underline{x}^H(n)R^{-1}(n-1)}{\delta_0 + \underline{x}^H(n)R^{-1}(n-1)\underline{x}(n)}\right] \tag{2.85}$$

with

$$R^{-1}(0) = \frac{1}{\epsilon_0}I, \qquad \epsilon_0 > 0, \tag{2.86}$$

as in Equation 2.76, when using the SMI algorithm. Therefore, with the aid of:

$$R^{-1}(n) = \frac{1}{\delta_0}\left[R^{-1}(n-1) - q(n)\underline{x}^H(n)R^{-1}(n-1)\right], \tag{2.87}$$

where

$$q(n) = \frac{R^{-1}(n-1)\underline{x}(n)}{\delta_0 + \underline{x}^H(n)R^{-1}(n-1)\underline{x}(n)} \tag{2.88}$$

we arrive at [28, 3],

$$\underline{w}(n) = \underline{w}(n-1) + q(n)[r^*(n) - \underline{w}^H(n-1)\underline{x}(n)], \tag{2.89}$$

where the square-bracketed term represents the error, $e(n) = r^*(n) - y(n)$ between the desired signal and the array output signal after processing. As can be seen from Equation 2.85, the inversion of the correlation matrix, $R(n)$ required by Equation 2.83, has been replaced by the simple update formula of Equation 2.87, requiring scalar division, thus significantly reducing the complexity imposed.

2.3.3 Spatial Reference Techniques

Spatial reference adaptation [1, 3, 8, 19, 20, 21, 22, 23, 50] relies on information regarding the direction of arrival of the desired signal and its multipath components. There are numerous different methods for obtaining estimates of the DOA information with the aid of the received antenna array signals [3, 23, 50]. Wave-number estimation techniques [3, 23, 24, 50] are based on the decomposition of the array output correlation matrix, $R = E[\underline{x}(t)\underline{x}^H(t)]$,

whose terms consist of estimates of the correlation between the signals at the elements of the antenna array in Figure 2.10. The so-called MUltiple SIgnal Classification (MUSIC) algorithm [3, 23, 50] and the Estimation of Signal Parameters by Rotational Invariance Techniques (ESPRIT) both use this approach [23, 50]. However, these algorithms are not effective for detecting coherent signals [23, 50]. The parametric estimation techniques [23, 50] are mainly maximum likelihood estimation (MLE) based algorithms, where the ML estimates of desired parameters, such as the angles of arrival, are the ones for which the likelihood function is maximised. These techniques impose a high computational complexity and also require the antenna array to be accurately calibrated. Again, further information concerning these algorithms may be found in [7, 9, 23, 63].

2.3.3.1 Antenna Calibration

Antenna calibrating procedures [7, 35, 64] can be readily incorporated in a digital beamforming array, facilitating the realisation of highly selective antenna patterns exhibiting ultra-low sidelobes. The feature of self-calibration is an advantage, but may indeed also be an essential requirement for a system employing an array of elemental receivers constituted by multiple, cascaded active components [38, 7]. Several techniques are available, such as the injection of precise radio frequency test signals at the receiver front-ends [35, 48], focusing on a source at a known position in the near or far-field, or employment of a known, well defined scatterer of the transmitted signal.

In order to improve the SIR of the signal received by an adaptive antenna array, nulls can be created in the antenna array's radiation pattern in the direction of strong co-channel interferers. However, the depth and angular position of these nulls are very sensitive to phase and amplitude errors within the antenna array [7]. The performance of RF components generally varies over temperature, time and frequency. A study conducted by Tsoulos and Beach [7] found that a temperature variation of 14°C to 27°C resulted in a maximum amplitude variation of ± 1.5dB and a $\pm 180^\circ$ maximum phase error across the antenna array. Performing a calibration of phase and amplitude mis-matches between the antenna array elements at the time of manufacture would not take into account temperature variations and ageing effects [35]. Reference [7] noted that even under the same room temperature the amplitude and phase mismatches varied from day to day. Therefore, an online calibration procedure is required that can take place, whilst the base station continues to function normally. Only the active components have to be calibrated, the passive components are assumed to be less susceptible to temperature and time. After calibration the amplitude mismatch was limited to ± 0.04dB and the phase mismatch to $\pm 0.4^\circ$.

The calibration process of an 8×8 element receiver antenna array developed for the pan-European TSUNAMI (II) SDMA Field Trial was described by Passman and Wixforth in [64]. The aim of the calibration procedure was to reduce the phase error to less than 3° and the amplitude error to less than 0.5dB. The receive antenna array, as shown in Figure 2.23, consists of ten linearly spaced active subarrays, each of which consists of eight vertically separated single antenna elements. The 1st and 10th subarrays act as dummy elements in an attempt to maintain a consistent mutual coupling between subarrays across the entire array. The provision of circuitry to allow the reception of both vertically and horizontally polarised signals at each of the eight subarrays implies that the reception of 16 different polarisations is possible. The calibration of the antenna can be separated into two stages, namely the offline calibration after manufacture and the online calibration performed during operation. The offline calibration measures the characteristics of the passive components in the signal path and assumes that the 16:1 Wilkinson divider and the 20dB directional couplers are stable over both time and temperature. More specifically, the online calibration procedure uses the Wilkinson divider and the directional couplers to inject a calibration signal into each of the eight signal paths dedicated to horizontal polarisation and the eight paths for vertical polarisation. The magnitude and phase response of these 16 signal paths is then measured in the baseband in order to characterise the entire antenna system. However, fully characterising this antenna array receiver at all of the frequencies of interest would generate vast amounts of data, and require an impractical length of time.

Fortunately, it is possible to use a reduced set of measurements [64]. Measurements of the antenna array's forward transfer function, S_{21}, between the central calibration port and the 16 receiver ports for both the vertically and horizontally polarised signals were found to be essential, for characterising the calibration network itself. Phase differences of up to 20° and amplitude variations of 2dB were measured between two seemingly identical calibration signal paths, despite the symmetrical layout of the Wilkinson divider [64]. Further measurements of S_{21} between each subarray port and all other subarray ports, in order to account for mutual coupling of the subarrays showed coupling levels of below -30dB between all ports. Thus far, the characterisation of the calibration network has required 16 phase and magnitude values, while the mutual coupling between the subarrays necessitated a further $(2 \times 8)^2 = 256$ readings. Additionally, any imbalances between subarrays in the magnitude radiation patterns over all specified azimuth and elevation angles must also be measured, leading to a still significant amount of information that must be processed.

Simmonds and Beach [35] described how an 8 element adaptive antenna array can be calibrated, with no interruption to the network, for both transmission and reception. The

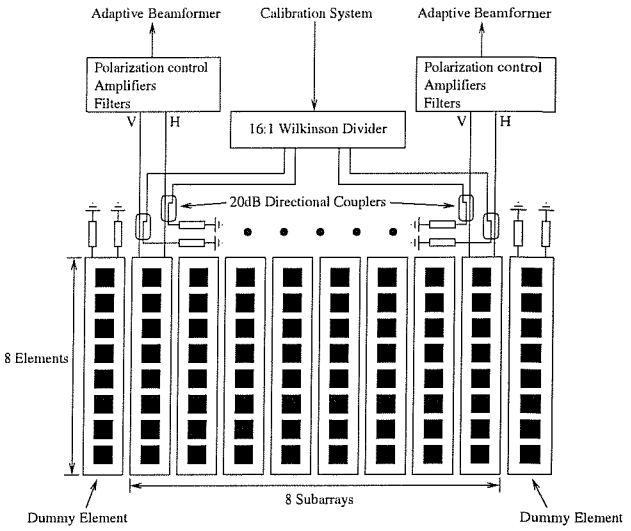

Figure 2.23: Block diagram of the 8×8 element antenna array receiver and in-built calibration system of Passman and Wixforth showing the horizontal and vertical polarisation ports [64].

aim of the scheme was to achieve a post-calibration accuracy of 3° phase and 0.5dB magnitude error across the array. The design of the process allows the receive calibration to be performed during the unallocated timeslots within the DCS1800 frame structure. A Continuous Wave (CW) signal is injected simultaneously into each of the receiver antenna array elements via directional couplers and a power divider/combiner. Digital attenuators allow the injected signal strength to be varied over a range of 60dB in 2 to 3dB steps. The errors associated with the received signal phase and amplitude are measured in the baseband and the beamformer weights are adjusted appropriately, in order to produce the desired beam pattern. Moreover, the same technique cannot be used for transmitter calibration, since this would result in spurious RF transmission. In the proposed scheme the transmitter would be calibrated in the even timeslots, except for timeslot zero, which is used for the Broadcast Control CHannel (BCCH) in DCS1800 and GSM [35]. Each branch of the antenna array is sampled using the directional couplers and the resulting signals are down-converted to baseband. These 8-bit quantised I and Q samples are compared to the baseband digital beamformer outputs, in order to obtain the correction factor required for each array path.

2.3.4 Blind Adaptation

Blind adaptation [3, 23, 50] of the array weights has several advantages over both the spatial [6, 7, 9, 23, 50, 63] and temporal reference [6, 1, 3, 20, 30, 57] based systems of Sections

2.3.3 and 2.3.2. Temporal reference assisted systems must achieve synchronisation and perform demodulation, before weight adaptation can commence, whereas spatial reference aided systems require very strictly calibrated hardware and rely on DoA information. However, the typically large angular spread of the incoming signals in small picocells makes this difficult to attain. In contrast, a blind adaptation scheme [3, 23, 50, 56] does not require training sequences or any information concerning the antenna array's geometry. Dispensing with the reference or training sequence results in potentially increased data rates. For example, a capacity increase of 17% can be achieved in the uplink for GSM [56] upon invoking blind joint space-time equalisation. However, using for example the so-called constant modulus adaptive algorithm [65] can lead to the capture of interfering signals instead of the wanted signal, an issue argued more explicitly in [66, 67].

2.3.4.1 Constant Modulus Algorithm

The Constant Modulus (CM) algorithm [65] operates on the principle that the amplitude of the receive antenna array output should remain constant, unless the interference causes fluctuations. If the transmitted signal, $s(n)$, has a constant envelope, then the combiner output, $y(n)$ in Figure 2.17, should also have a constant envelope. However, if multipath fading occurs, then the combiner output, $y(n)$, will have a fluctuating envelope. The objective of CM beamforming [3, 23, 50] is to restore the array output to a constant envelope signal, on average. This can be accomplished by adjusting the array weight vector, $\underline{w}$, in such a way, so as to minimise a certain cost function.

In the classic paper by Godard [65], who used the CM property in order to carry out blind channel equalisation, the criterion was to minimise the functions $D^{(p)}$, referred to as the dispersion of order p ($p > 0$ integer), defined by

$$D^{(p)}(n) = E\Big[(|y(n)|^p - R_p(n))^2\Big], \tag{2.90}$$

with R_p being real positive constants given by :

$$R_p(n) = \frac{E[|a(n)|^{2p}]}{E[|a(n)|^p]}, \tag{2.91}$$

where $a(n)$ is the transmitted data symbol. The standard cost function of [3, 23, 65]

$$G^{(p)}(n) = E\Big[(|y(n)|^p - |a(n)|^p)^2\Big], \tag{2.92}$$

which is not used in blind array weight adaptation, is independent of the carrier phase but depends on the magnitude of the antenna array's output signal, $|y(n)|$, and that of the transmitted signal, $|a(n)|$. In contrast, the function $D^{(p)}$, used in the CM algorithm is independent of both the carrier phase and the data symbol's magnitude [65].

The most often used practical case is that of $p = 2$, where

$$D^{(2)}(n) = E[(|y(n)|^2 - R_2(n))^2], \tag{2.93}$$

with

$$R_2 = \frac{E[|a(n)|^4]}{E[|a(n)|^2]}, \tag{2.94}$$

and the cost function, $D^2(n)$, is effectively the mean squared error between the magnitude of the antenna array's output signal squared and the constant $R_2(n)$. Hence, again, the main difference between the conventional cost function of Equation 2.92 and that of the constant modulus algorithm in Equation 2.90 is that the constant modulus algorithm does not assume the knowledge of the data sequence's magnitude, $|a(n)|$, it rather attempts to minimise the difference with respect to the constant quantity $R_2(n)$, which is related to the moments of $|a(n)|$ by Equation 2.94. In other words, the CM beamforming algorithm directs the combiner's output to a constant envelope.

In [23] a cost function is given in the form of :

$$J(n) = \frac{1}{2}E[(|y(n)|^2 - y_0^2)^2], \tag{2.95}$$

where y_0 is the desired amplitude in the absence of interference.

The objective is to find a set of values for the array weight vector, $\underline{w}$, that will minimise the given cost function. This may be accomplished using the following equation [23] :

$$\underline{w}(n+1) = \underline{w}(n) - 2\mu(|y(n)|^2 - y_0^2)y(n)\underline{x}(n+1), \tag{2.96}$$

or employing the update formula of [3] :

$$\underline{w}(n+1) = \underline{w}(n) + \mu[R_p(n) - |y(n)|^2]y(n)\underline{x}(n), \tag{2.97}$$

which are used in a steepest descent fashion to update the array weights and are essentially identical, apart from Equation 2.96 using the current sample, $\underline{x}(n+1)$, of the array's output, while Equation 2.97 using the previous sample, $\underline{x}(n)$. These equations are identical to the update regime of Equation 2.54 used in the LMS algorithm, with the only difference being the error term.

There are two conditions, which may lead to a zero-gradient situation, where the algorithm stops adapting. The first is the condition of $|y(n)| = 1$, which represents the desired convergence optimum. The second is $y(n) = 0$, which also forces the gradient to become zero. However, fortunately this is not a practical problem, since the point $y(n) = 0$ is not a stable equilibrium and the system noise moves the weight vector from this zero-gradient

point. A further problem in a hostile fading environment is that the beamformer may incorrectly select the interference as the signal to process, so as to maintain a constant modulus, rather than the desired signal.

In [56] a blind array weight adaptation technique was described by Laurila, which performs joint space-time equalisation, separation and detection of multiple unsynchronised co-channel digital signals. The scheme exploits the facts that the signals are of fixed symbol rate, have a CM and a Finite Alphabet (FA) of symbols. Simulations were conducted for an eight-element Uniform Linear Array (ULA) with an element spacing of $\lambda/2$ [56]. The equaliser order was five. Although the simulation parameters were not optimised, the system gave results demonstrating that comparable BER can be achieved, when compared to reference-assisted adaptation methods.

2.3.5 Adaptive Arrays in the Downlink

Adaptive arrays have been more often studied for receiving uplink data at the base station. However, they are equally suitable for transmitting data by the base station in the downlink. It is possible to steer a transmitting array in the same way as one used for reception, so as to minimise the downlink interference inflicted upon co-channel mobiles. The wide frequency separation between the uplink and downlink frequency bands used in the Frequency Division Duplexing (FDD) GSM system, for example, results in uncorrelated fading between the up- and the down-link. Therefore, the weights calculated for reception are typically unsuitable for employment in transmit mode. In contrast, in a Time Division Duplexing (TDD) system, such as UTRA [11] it may be possible to re-use the receive mode weights, provided that the location of the mobile has not changed significantly between timeslots, i.e. if the duration of the timeslots is sufficiently short.

In the uplink scenario, the receive array can adapt to changes in the propagation medium by observing its own outputs and modifying its own processing, since there is an in-built feedback mechanism, as was shown in Figure 2.17. When used in the transmit mode, an adaptive antenna array at the base station needs an additional feedback signal from the mobile receivers, in order to give the base station a means of measuring its own beam patterns. The array, by directing a mainlobe towards a mobile, could nonetheless produce a spurious fade in the desired signal or inflict interference upon other mobiles.

The scheme proposed by Gerlach and Paulraj [68] uses feedback of the signals received at the mobiles, in order to calculate the transmitter antenna weights to employ. The paper describes a system, where data transmission is temporarily halted in for the transmission of probing signals. Each probing signal is sent on an orthogonal channel in the time, frequency

or code domain so that the receivers may measure the response of each probing signal. The responses to each of the probing signals at each of the receivers are fed back to the transmitter, allowing the channel responses to be estimated. Simulations were performed, by Gerlach and Paulraj [68], which showed that at a low mobile speed of 2.5 miles per hour (mph) adequate signal separation required a data feedback rate in the order of a few kbit/s, making the approach only viable for static or slow-moving receivers. It is worth noting here that the 3G UTRA system has a total control channel rate of about 10 kbit/s.

Further to this scheme, Gerlach and Paulraj [69] presented a method, which reduces the feedback rate by exploiting that as the array's weight vector fluctuates due to the mobile receiver's motion, the weight vector's fluctuations will be confined to a certain subspace of its total vector space. In contrast to the channel weight vector itself, the channel vector's subspace is much more stable during the mobile's motion, and this fact can reduce the required feedback rates. The method is best suited to environments having either a low number of propagation paths, or for several paths approaching the base station from similar angles. This implies that there must be only a few scattering bodies near to the base station. As the mobile receiver moves, its array weight vector varies at the fast fading rate, but the fluctuations are confined to the subspace Ψ_k, where the subscript k denotes the k^{th} mobile, which varies slowly. A beamformer based on this more stable subspace structure, rather than the array weight vector, will need a lower feedback rate. Hence, the subspace structure tends to be more useful, when the subspace dimension, $\dim[\Psi_k]$, is small. The subspace dimension, $\dim[\Psi_k]$, will only be small however, if the number of propagation paths is low or if all of the paths have approximately the same angle of departure from the array. The paper derives a subspace beamformer and presents results obtained using simulations. The required feedback rate for a mobile moving at 35mph was estimated to be 250 bits/s. While this is a best-case estimate, it is significantly reduced in comparison to the rate in [68] and it is also less than the feedback rate used for power control in Qualcomm's IS-95 cellular system [69]. Hence, such a regime could realistically be used in a UTRA-type system.

Martin and Gaspard [32] presented a system based on the Discrete Fourier Transform (DFT) Beamspace technique. Each user's signal was transmitted on the particular DFT beam, which offered the largest mean power level during the uplink reception. With a four-element linear array the system provided a 175% radio capacity gain over a conventional base station. An eight-element array resulted in a gain of 200% in radio capacity. However, the downlink capacity using this method was not matched to the uplink capacity. Similarly enhanced downlink capacity was achieved using exact DOA information, where the downlink's transmission beam was steered in the direction of the strongest multipath component received at the uplink. This provided an estimated 350% increase in radio capacity.

Monot *et al.* [49] also used a DOA based system. Their prototype implemented the Capon [24] and the MUSIC [3, 23, 50] algorithms using a five element antenna array, and it was reported to have successfully estimated the DOA of the different paths, in an environment consisting of one main path and a set of spatially dispersed other paths.

2.3.6 Adaptive Beamforming Performance Results

The performance of the SMI algorithm of Section 2.3.2.3 using the direct matrix inversion formula of Equation 2.70 and the iterative matrix inversion lemma in Equation 2.75 as well as that of the ULMS and NLMS algorithms of Sections 2.3.2.1 and 2.3.2.2 was compared for identical scenarios. The effects of varying the reference signal lengths and the SNR as well as INR on the level of interference rejection were measured. For the situations exposed to different SNRs and INRs, the eigenvalue spread $\chi(R)$ of Equation 2.56 is summarised in Table 2.1.

SNR (dB)	INR (dB)	$\chi(R)$
3.0	3.0	4.4
3.0	9.0	8.3
3.0	27.0	402.2
9.0	3.0	8.3
9.0	9.0	5.4
9.0	27.0	120.6
27.0	3.0	403.3
27.0	9.0	120.6
27.0	27.0	5.8

Table 2.1: Eigenvalue spread, $\chi(R) = \frac{\lambda_{max}}{\lambda_{min}}$, of Equation 2.56 evaluated for the array output cross-correlation matrix, R, for different values of SNR and INR.

The effects of varying the reference signal length, the signal-to-noise, and the interference-to-noise ratios on the interference rejection achieved were evaluated and a complexity analysis was performed. The ability of the various beamforming algorithms to combine multipath signals, whilst rejecting interference was also investigated. The modulation scheme used in the simulations was BPSK. Our associated results are summarised in the forthcoming sections.

2.3.6.1 Two Element Adaptive Antenna Using Sample Matrix Inversion

Recall that the SMI algorithm of Section 2.3.2.3 directly inverts the sample correlation matrix, $\hat{R}_{xx} = E[\underline{x}(t)\underline{x}^H(t)]$, in order to find the optimal antenna element weights according

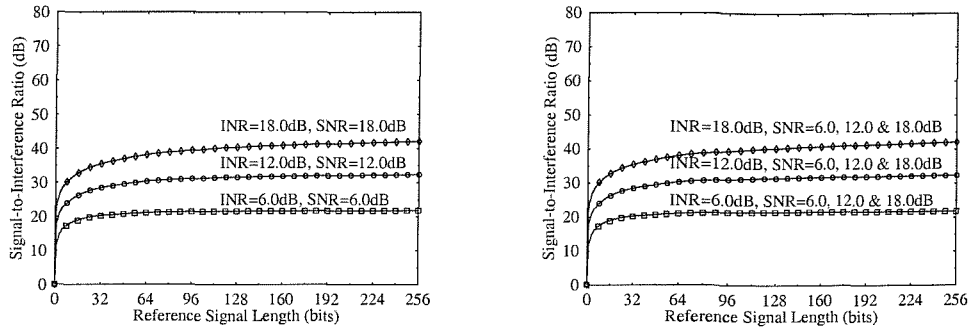

(a) Equal SNR and INR

(b) Unequal SNR and INR

Figure 2.24: The interference rejection achieved using **SMI** beamforming upon varying the reference signal lengths for a two element antenna array using an element spacing of $\lambda/2$. The source was at 0° and the interferer at 30°, whilst $\epsilon_0 = \mathbf{0.01}$ evaluating 10000 averaged runs over a Gaussian channel.

to Equation 2.70. Specifically, we have $\underline{\hat{w}}_3 = \hat{R}_{xx}^{-1}\underline{\hat{z}}$, where $\underline{\hat{z}}$ is the sample cross-correlation vector between the array output vector, $\underline{x}$, and the reference signal, r. The iterative version of this technique, as described in Section 2.3.2.3, forms the inverse of the sample correlation matrix, $\hat{R}_{xx}^{-1}$, based on the received signal samples using Equation 2.75, and iteratively updates it according to :

$$\hat{R}^{-1}(n) = \hat{R}^{-1}(n-1) - \frac{\hat{R}^{-1}(n-1)\underline{x}(n)\underline{x}^H(n)\hat{R}^{-1}(n-1)}{1+\underline{x}^H(n)\hat{R}^{-1}(n-1)\underline{x}(n)}, \tag{2.98}$$

with $\hat{R}^{-1}(0) = \frac{1}{\epsilon_0}I$ where ϵ_0 is a scalar value greater than zero.

The interference rejection achieved using the SMI algorithm as a function of the reference signal length is shown in Figure 2.24(a) for equal values of SNR and INR, i.e. for equal signal and interferer powers. The graph also shows how the interference rejection increases, as the SNR and INR are increased. The performance of the direct inversion method of Equation 2.70 and the iterative method of Equation 2.75 was found to be identical using a value of $\epsilon_0 = 0.01$ in Equation 2.76 to initialise the estimate of R^{-1}. For a setting of $\epsilon_0 = 0.3$ the difference between the rejection levels was of the order of 0.01dB, while a 0.1dB interference rejection reduction resulted from $\epsilon_0 = 0.9$. As stated earlier in Section 2.3.2.3, an adequate performance can be achieved after processing only $2M$ data samples, where M is the number of sources present, which was two in this case. Figure 2.24(b) shows that the interference rejection is only affected by the INR and appears to be independent of the SNR.

The rate at which the interference rejection increases, as the SNR and INR improve is

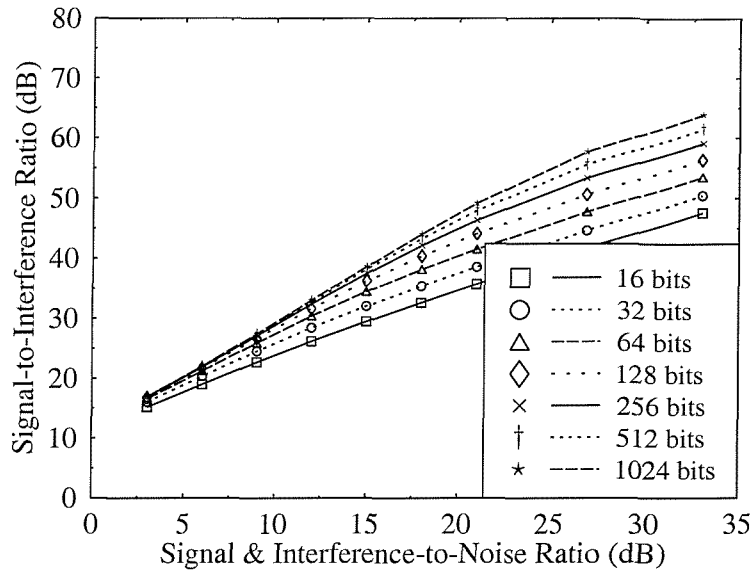

Figure 2.25: The interference rejection achieved versus SNR and INR using **SMI** beamforming upon varying the reference signal lengths for a two element antenna array using an element spacing of $\lambda/2$, at **equal SNR and INR**. The source was at 0° and the interferer at 30°, whilst $\epsilon_0 = \mathbf{0.01}$ evaluating 10000 averaged runs over a Gaussian channel.

shown in Figure 2.25. The increased SNR and INR values allow for more accurate estimates of the array output cross-correlation matrix, R, thus resulting in improved interference rejection. The rate of increase of the interference rejection slows down as the SNR and INR increase, since the limit of the estimation accuracy is approached. As expected, the longer reference lengths allow for a better estimate of R and hence exhibit higher interference rejection levels for sufficiently high SNR and INR values. In contrast, for low SNR and INR the estimation quality of R is poor, resulting in marginal performance improvements due to extending the reference sequence length.

2.3.6.2 Two Element Adaptive Antenna Using Unconstrained Least Mean Squares

The Unconstrained Least Mean Squares (ULMS) technique [3, 20, 21, 22, 23] of beamforming was described in more detail in Section 2.3.2.1 but is based around the weight update formula of Equation 2.54, i.e. $\underline{w}(n+1) = \underline{w}(n) - \mu \underline{x}(n)\epsilon^*(n)$, where μ is a constant controlling the rate of convergence and $\epsilon(n)$ is the error between the combiner output, $y(n)$, and the reference

signal, $r(n)$. For each array output sample, $x(n)$, the new antenna element weights are calculated, in order to minimise the mean square error between the measured array output and the desired array output.

The performance of the ULMS algorithm of Section 2.3.2.1 was studied using $\mu = 0.0000005$, $\mu = 0.00005$, $\mu = 0.0005$ in Equation 2.54 and varying the prevalent SNR and INR. It was found that convergence was extremely slow using $\mu = 0.0000005$, and a reasonable level of interference rejection required an SNR and INR of 33.0dB in conjunction with a reference length of 1024 bits. This shows the dependence of the ULMS algorithm upon the received signal strength, which is evidenced by Figures 2.26, 2.27(a) and 2.27(b). Additionally, Figure 2.29(a) shows that step size is insufficient to allow convergence to an acceptable level of interference rejection regardless of the reference length or the number of iterations. In contrast, using a value of $\mu = 0.00005$ in Figure 2.26 results in significantly faster convergence for all SNRs and INRs, where best performance was achieved by the stronger signals. However, the step size is excessive for SNRs and INRs in excess of about 20dB and the phenomenon of weight jitter can be seen becoming apparent. Figure 2.28 illustrates this further since it can be seen that the interference rejection achieved actually decreases for high SNRs and INRs upon increasing the number of iterations. Again, this phenomenon is due to weight jitter around the optimal solution for high values of SNR as well as INR and it becomes more prevalent for a large step size of 0.0005, which may be seen in Figure 2.29(b). Increasing the step size to 0.0005 results in a levelling off or even a reduction in the interference rejection achieved, as shown in Figure 2.27(b). Therefore, if the step size, μ, is chosen to be small, weak signals associated with low SNRs and INRs limit the convergence speed and may not be of much practical use, while strong signals allow for rapid convergence, as displayed in Figure 2.26. However, if μ is large then the convergence is rapid even for weak signals, but the algorithm exhibits weight jitter, resulting in poor performance and potential instability.

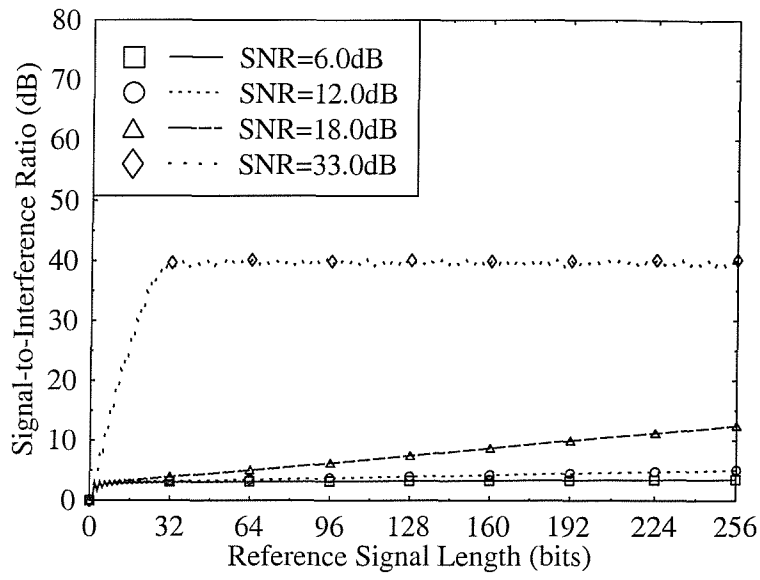

Figure 2.26: The interference rejection achieved using **ULMS** beamforming upon varying the reference signal lengths, a two element antenna array, using an element spacing of $\lambda/2$, at **equal SNR and INR**. The source was at 0° and the interferer at 30°, whilst μ = **0.00005** evaluating 10000 averaged runs over a Gaussian channel.

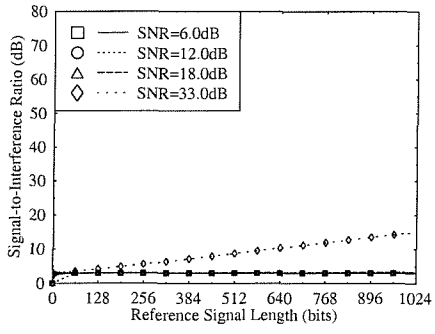

(a) μ = **0.0000005**

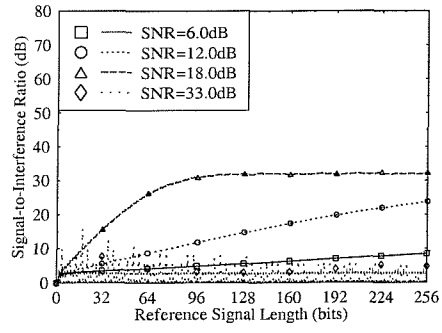

(b) μ = **0.0005**

Figure 2.27: The interference rejection achieved using **ULMS** beamforming upon varying the reference signal lengths for a two element antenna array using an element spacing of $\lambda/2$, at **equal SNR and INR**. The source was at 0° and the interferer at 30° evaluating 10000 averaged runs over a Gaussian channel.

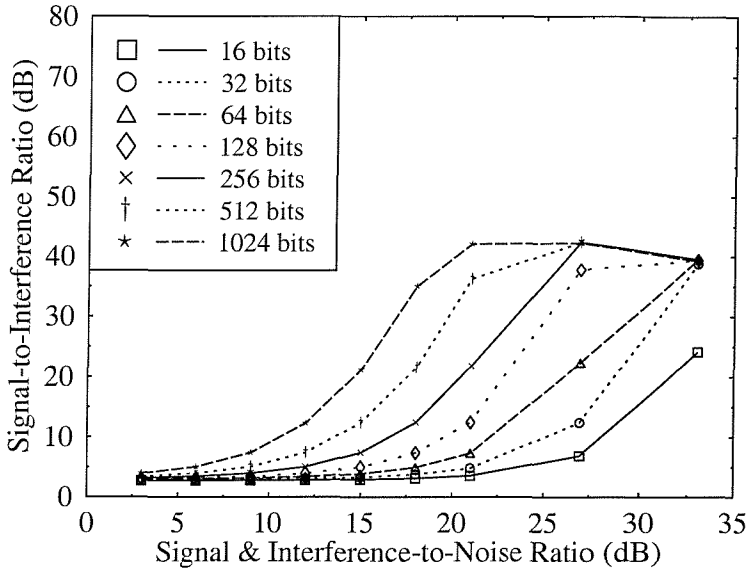

Figure 2.28: The interference rejection achieved using **ULMS** beamforming upon varying the reference signal lengths, SNR and INR. A two element antenna array was used with an element spacing of $\lambda/2$, at **equal SNR and INR**. The source was at 0° and the interferer at 30° while $\mu = \mathbf{0.00005}$ evaluating 10000 averaged runs over a Gaussian channel.

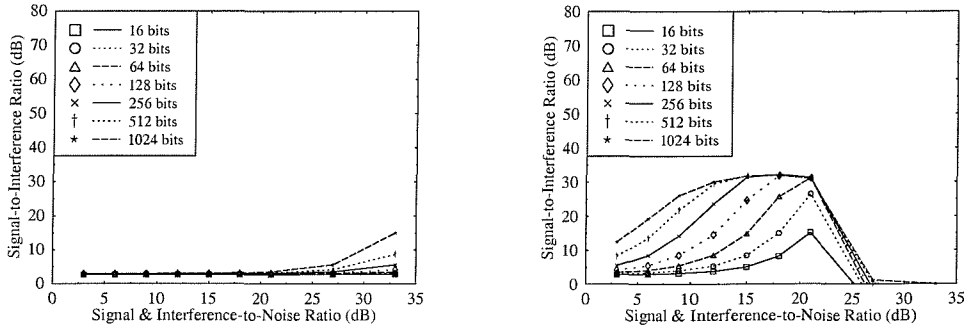

(a) $\mu = \mathbf{0.0000005}$ (b) $\mu = \mathbf{0.0005}$

Figure 2.29: The interference rejection achieved using **ULMS** beamforming upon varying the reference signal lengths, SNR and INR. A two element antenna array was used with an element spacing of $\lambda/2$, at **equal SNR and INR**. The source was at 0° and the interferer at 30° evaluating 10000 averaged runs over a Gaussian channel.

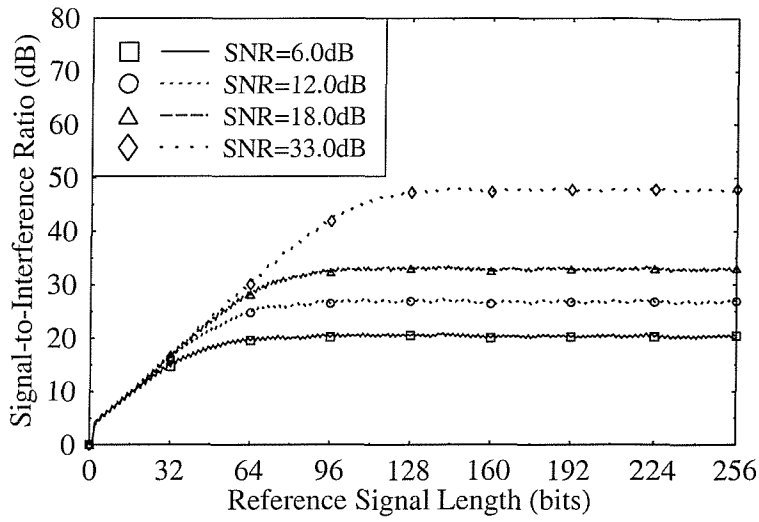

Figure 2.30: The interference rejection achieved using **NLMS** beamforming upon varying the reference signal lengths for a two element antenna array with an element spacing of $\lambda/2$, at **equal SNR and INR**. The source was at 0° and the interferer at 30° whilst $\mu_0 = \mathbf{0.2}$ evaluating 10000 averaged runs over a Gaussian channel.

2.3.6.3 Two Element Adaptive Antenna Using Normalised Least Mean Squares

The Normalised Least Mean Squares (NLMS) algorithm [23, 28] of Section 2.3.2.2 uses a data dependent step size calculated using Equation (2.59), namely $\mu(n) = \frac{\mu_0}{||\underline{x}(n)||^2}$, in order to eliminate the deficiencies of the ULMS method of Section 2.3.2.1. Figure 2.30 characterises the algorithm's convergence, when $\mu_0 = 0.2$ in Equation 2.59.

When compared to the performance of the algorithm using the larger step sizes of $\mu_0 = 0.5$ and $\mu_0 = 1.0$ in Figures 2.31 and 2.32, it can be seen that for a small reference signal length the level of interference rejection is increased in conjunction with the larger step sizes, due to their faster rates of convergence. However, after the final interference rejection level has been reached, the algorithm performs better for smaller step sizes, attaining a higher level of interference rejection at the end of the convergence phase, and significantly lower weight jitter. For example, using $\mu_0 = 1.0$ when the SNR and INR was 6.0dB, the interference rejection became approximately 15dB exhibiting a jitter of $\pm$2.5dB. In the case of $\mu_0 = 0.2$, the interference rejection was 20dB exhibiting virtually no jitter effects. The performance difference became even more marked for higher SNR and INR levels.

Figures 2.33(a), 2.33(b) and 2.33(c) demonstrate how the interference rejection increases,

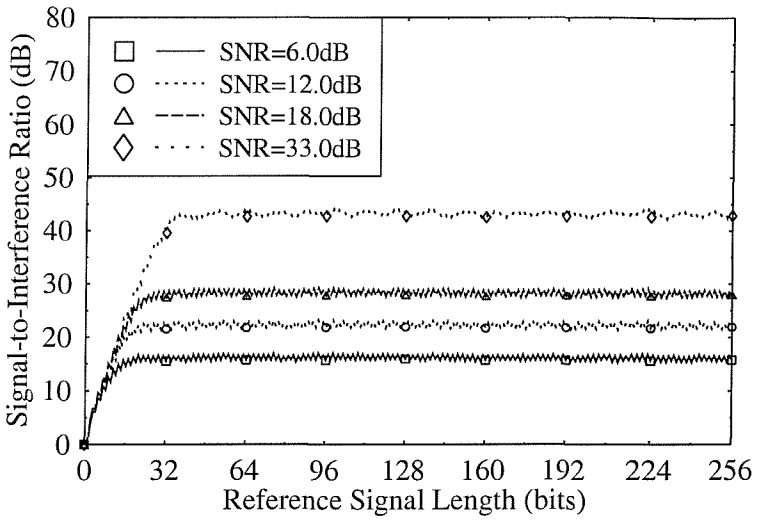

Figure 2.31: The interference rejection achieved using **NLMS** beamforming upon varying the reference signal lengths for a two element antenna array with an element spacing of $\lambda/2$, at **equal SNR and INR**. The source was at 0° and the interferer at 30° whilst $\mu_0 = \mathbf{0.5}$ evaluating 10000 averaged runs over a Gaussian channel.

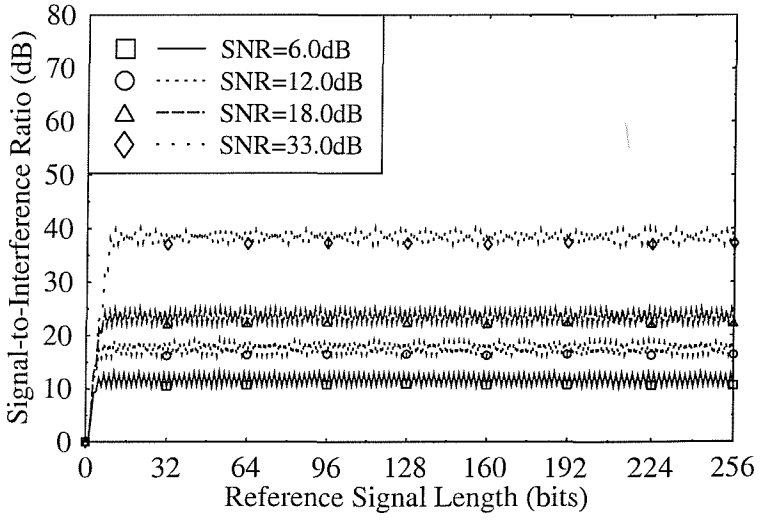

Figure 2.32: The interference rejection achieved using **NLMS** beamforming upon varying the reference signal lengths for a two element antenna array with an element spacing of $\lambda/2$, at **equal SNR and INR**. The source was at 0° and the interferer at 30° whilst $\mu_0 = \mathbf{1.0}$ evaluating 10000 averaged runs over a Gaussian channel.

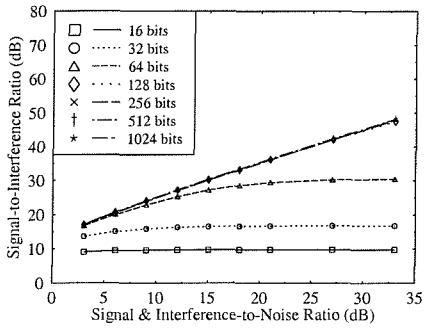

(a) $\mu_0 = 0.2$

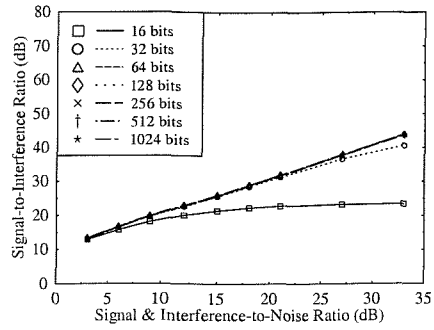

(b) $\mu_0 = 0.5$

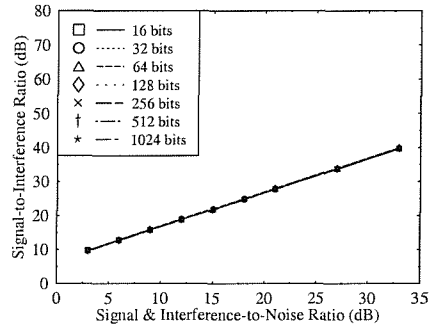

(c) $\mu_0 = 1.0$

Figure 2.33: The interference rejection achieved using **NLMS** beamforming upon varying the reference signal lengths, and SNR and INR, for a two element antenna array with an element spacing $\lambda/2$, at **equal SNR and INR**. The source was at 0° and the interferer at 30° evaluating 10000 averaged runs over a Gaussian channel.

as the SNR and INR improve. When $\mu_0 = 0.2$, the rate of convergence is too slow for the optimal solution to be reached for reference signal lengths of 16 and 32 bits. For a reference signal length of 64 bits, a near optimal solution is obtained at low values of SNR and INR but as the SNR and INR increase, the performance of the algorithm does not improve beyond a certain point. This performance limitation experience for short reference signal lengths is due to the limited estimation quality of the mean of the received signal. Using a larger step size, hence allowing for faster convergence, resulted in shorter reference signal lengths converging to the optimal weights, although the final value of interference rejection reached did not match that of the smaller step sizes.

The performance of the NLMS beamforming algorithm for unequal values of the SNR

and the INR is portrayed in Figures 2.34(a), 2.34(b) and 2.34(c). From these figures it can be seen that as the INR improves, i.e. as the interference power increases, so does the interference rejection, regardless of the SNR. However, for a given level of interference, better interference rejection is achieved for a higher SNR, although the rate of convergence may be slower, as seen for the case when we have SNR=18.0dB and the INR=6.0dB. Faster convergence was observed for higher values of the INR, for a given SNR. However, for a high INR associated with a low SNR, i.e. for example for SNR=6.0dB and INR=18.0dB, significant weight jitter occurred, whilst fast convergence was maintained. Therefore, when the power spread of the received signals is substantial, the NLMS adaptive beamforming algorithm does not perform as well as the SMI algorithm. In contrast, when the range of input powers is smaller, the algorithm performs well and for more than six antenna elements, this is achieved at a lower complexity, than that of the SMI algorithm, as will be shown in Section 2.3.6.5.

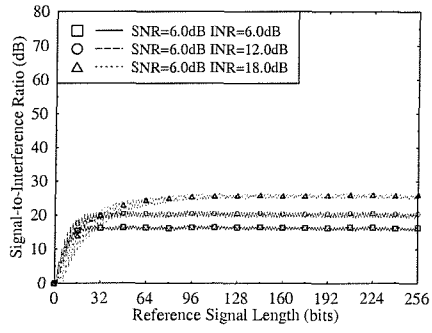

(a) Signal-to-Noise Ratio = **6.0dB**

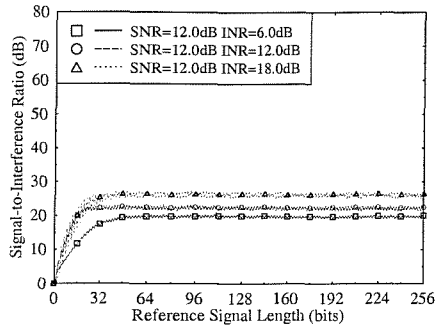

(b) Signal-to-Noise Ratio = **12.0dB**

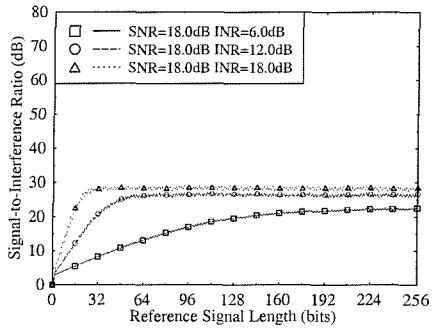

(c) Signal-to-Noise Ratio = **18.0dB**

Figure 2.34: The interference rejection achieved using **NLMS** beamforming upon varying the reference signal lengths, and SNR and INR, for a two element antenna array with an element spacing $\lambda/2$, at **unequal SNR and INR**. The source was at $0°$ and the interferer at $30°$ whilst $\mu_0 = \mathbf{0.5}$ evaluating 10000 averaged runs over a Gaussian channel.

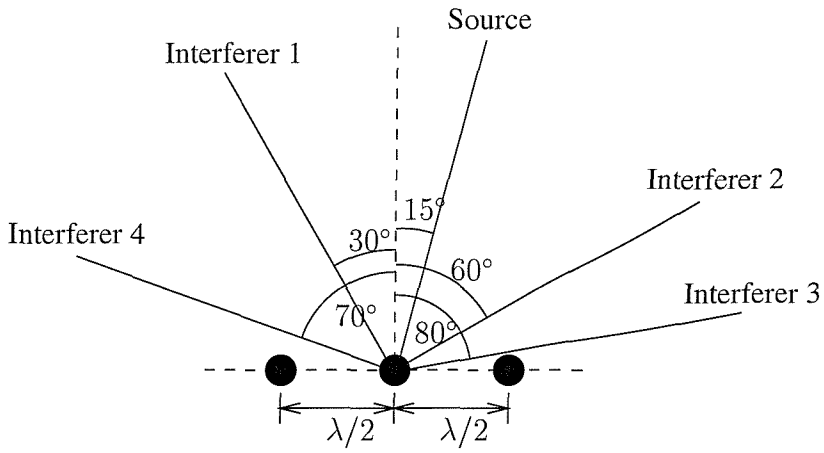

Figure 2.35: Locations of the desired source and the interferers with respect to the three element linear array with $\lambda/2$ element spacing.

2.3.6.4 Performance of a Three Element Adaptive Antenna Array

The interference rejection capabilities of a three element uniformly spaced linear adaptive array were investigated upon increasing the number of interference sources. The purpose of these experiments was to determine how the array behaved, when the total number of sources and interferers exceeded the degrees of freedom of the array, which was defined as the number of sources and/or interferences that may simultaneously be steered towards or nulled. The source was located at 15°, interferer 1 was at -30°, interferer 2 at 60°, interferer 3 was located at 80° and lastly, interference source 4 at -70°. It was assumed that the sources were point sources located in the far-field of the antenna array, benefiting from pure line of sight propagation without multipaths. Figure 2.35 shows the locations of the desired source and the interfering sources graphically. The simulations were carried out in conjunction with a 256-bit reference signal using the SMI and NLMS algorithms.

From the antenna array beam patterns portrayed in Figure 2.36 it can be observed that successful nulling of the interference source was accomplished for all the scenarios considered. A minimum interference rejection of 40dB was attained for an INR of 9dB, and when the INR was increased to 21dB, an even higher rejection was achieved.

Figure 2.37 shows the array response for the situation where two interferers are incident upon the antenna array, having equal signal strengths to that of the desired signal. For the cases illustrated in Figure 2.37(a), where one of the sources of interference is at a -30° angle with respect to the array, good rejection of both sources of interference is achieved, whilst maintaining a perfect response in the direction of the desired source. Even for the

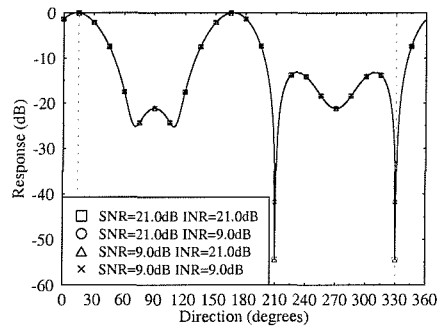

(a) Source located at 15°, interference at −30°.

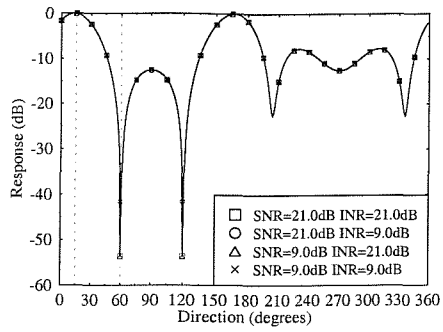

(b) Source located at 15°, interference at 60°.

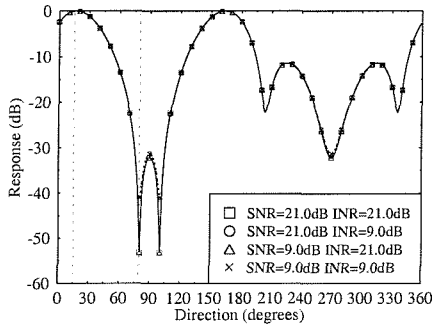

(c) Source located at 15°, interference at 80°.

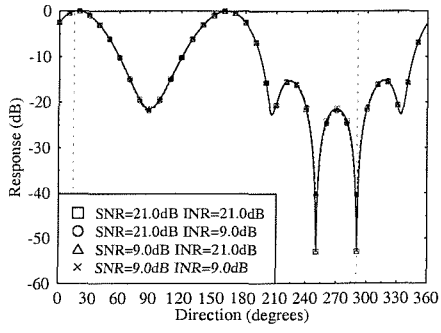

(d) Source located at 15°, interference at −70°.

Figure 2.36: Beam patterns of a three element uniformly spaced linear array with an inter-element spacing of $\lambda/2$ with one desired source and **one source of interference**. The **SMI** beamforming algorithm was used with a reference length of 256 bits.

situation, where the interference sources are located fairly close to each other, i.e. at -30° and -70°, strong nulling is maintained. Placing the interferers closer together, at angles of 60° and 80°, resulted in an interference rejection of over 45dB, albeit exhibiting some beam and null mis-alignment. Spreading the interferers further apart, with each one tending to "end-fire" at opposite ends of the array leads to some beam mis-steering, but nevertheless, maintaining good rejection of the sources of interference. Separating the interferers further so that they were located at -70° and 80° yielded significantly poorer results with an average interference rejection of about 25dB. However, this is still perfectly acceptable and levels significantly higher than this would be unrealisable due to hardware limitations.

From Figure 2.38 it can be seen that, if two sources of interference are present, and one

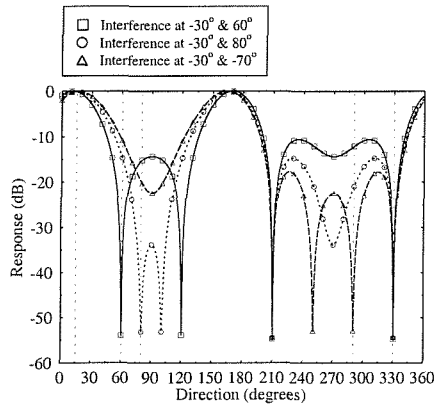

(a) Source located at 15°, interferers located at **-30°** and, **80°** or **-30°** and **-70°**.

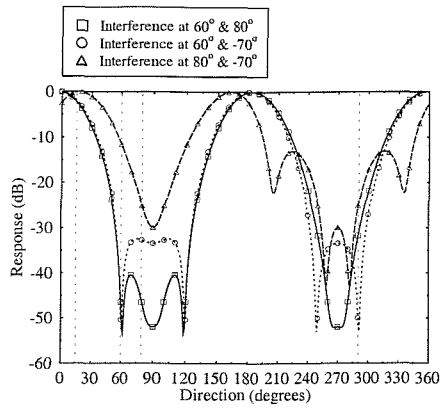

(b) Source located at 15°, interferers located at **60°** and **80°**, or **60°** and **-70°**, or **80°** and **-70°**.

Figure 2.37: Beam patterns of a three element uniformly spaced linear array having an inter-element spacing of $\lambda/2$ in conjunction with one desired source and **two sources of interference**. The **SMI** beamforming algorithm was used with a reference length of 256 bits.

of them is weaker than the other, then the stronger one will be nulled more effectively than the weaker one. The SNR of the desired signal does not appear to affect the interference rejection.

When three sources of interference and one desired signal source are incident upon a three element antenna array, the performance of the array is reduced compared to the situation, when fewer sources impinge upon the array concurrently. In Figure 2.39(a) it can be seen that an interference rejection ratio of at least 15dB is achieved for all of the interference sources simultaneously, where greater than 20dB rejection ratios are also frequently obtained. The results presented in Figure 2.39(b) are better than those in Figure 2.39(a), exhibiting a minimum interference rejection of 25dB. Therefore, the interference rejection obtainable when the number of sources equals the number of antenna elements appears to be dependent upon the location of the sources, but on average a good interference rejection performance is observed. Reducing the SNR from 21dB to 9.0dB, whilst keeping the INR at 21dB produced the results depicted in Figure 2.40. The beam patterns in this figure are similar in form to those of Figure 2.39, where the Interference-to-Noise Ratios was 21dB, but the depths of the nulls are shallower. Although the nulls are less deep, the INRs are not as high, so the resultant SIR should not be any higher. Furthermore, the nulls are generally still more than 15 to 20dB deep, which should be sufficient for effective interference rejection.

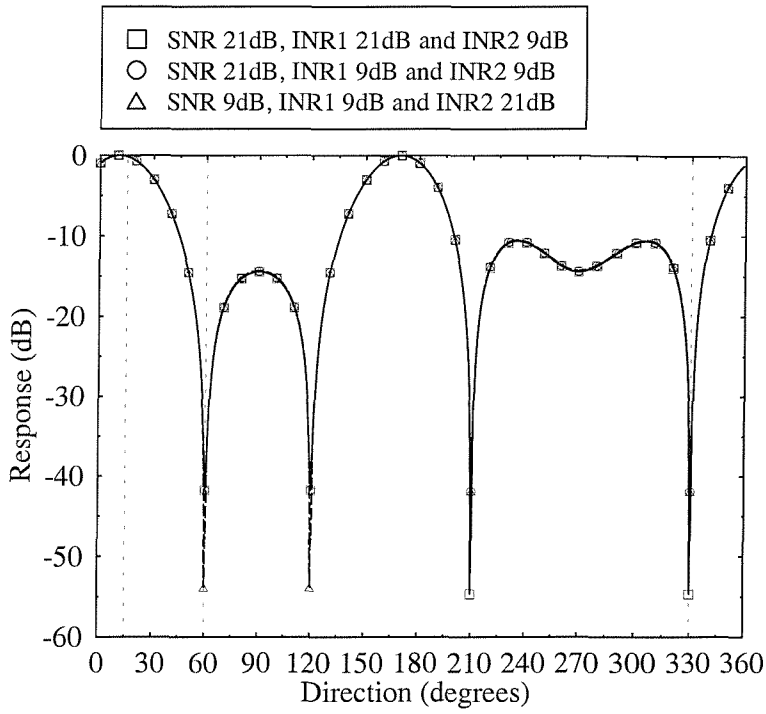

Figure 2.38: Beam patterns of a three element uniformly spaced linear array having an inter-element spacing of $\lambda/2$ in conjunction with one desired source and **two sources of interference** with **unequal powers**. The **SMI** beamforming algorithm was used with a reference length of 256 bits. The desired source was at 15°, interference source 1 was located at -30° and interferer 2 at 60°.

The performance of the three element antenna array when the desired source and the four interfering sources, all exhibiting equal signal power, are incident upon it, is shown in Figure 2.41(a). The antenna array response is virtually identical for the scenario when all the sources have SNRs of 21dB, to that when the SNRs are equal to 9dB. The array succeeds in suppressing all of the interference sources by at least 15dB, where one of the interferers is nulled by more than 40dB. In the situation when one of the interference sources has an INR of 9dB, as in Figure 2.41(b), it is nulled less strongly, than in the case of an INR of 21dB. Although the associated null-depth was reduced from 43dB to 29dB, due to the associated 21-9=12dB decrease in the power of the interferer, the SIR only fell by 2dB to 20dB. However, the rejection of the other interference sources increased slightly.

The beam patterns obtained for exactly the same scenarios, except using the NLMS beamforming algorithm along with $\mu_0 = 0.5$, are presented in Figures 2.42 to 2.46. From the graphs in Figure 2.42 it can be observed that the nulls formed by the NLMS adaptive

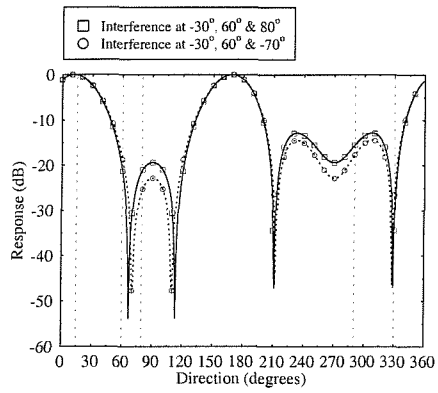

(a) Source located at 15°, interferers located at **-30°**, **60°** and **80°** or **-30°**, **60°** and **-70°**.

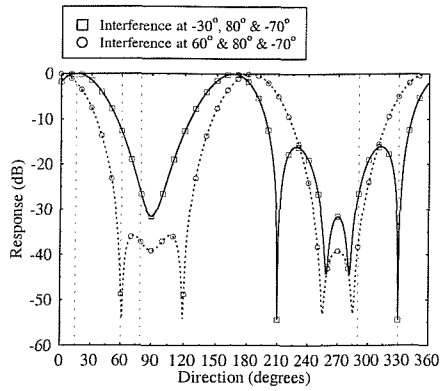

(b) Source located at 15°, interferers located at **-30°**, **80°** and **-70°**, or **60°**, **80°** and **-70°**.

Figure 2.39: Beam patterns of a three element uniformly spaced linear array having an inter-element spacing of $\lambda/2$ in conjunction with one desired source and **three sources of interference**. The **SMI** beamforming algorithm was used with a reference length of 256 bits. The SNR and INRs were **21.0dB**

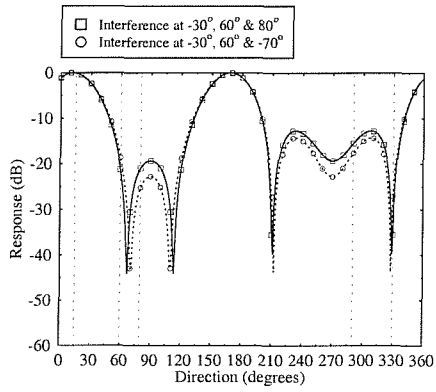

(a) Source located at 15°, interferers located at **-30°**, **60°** and **80°** or **-30°**, **60°** and **-70°**.

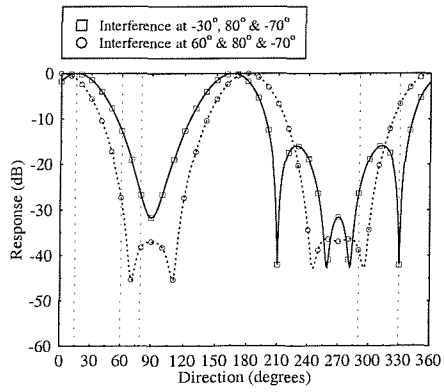

(b) Source located at 15°, interferers located at **-30°**, **80°** and **-70°**, or **60°**, **80°** and **-70°**.

Figure 2.40: Beam patterns of a three element uniformly spaced linear array having an inter-element spacing of $\lambda/2$ in conjunction with one desired source and **three sources of interference**. The **SMI** beamforming algorithm was used with a reference length of 256 bits. The SNR was **21.0dB** whilst the INRs were **9.0dB**

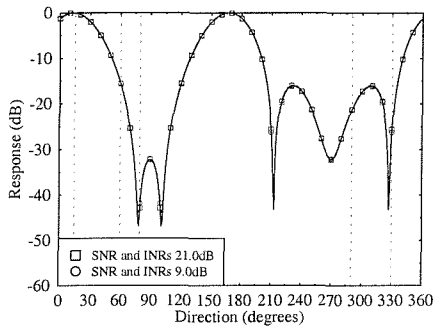

(a) Equal SNR and INR of 21.0dB.

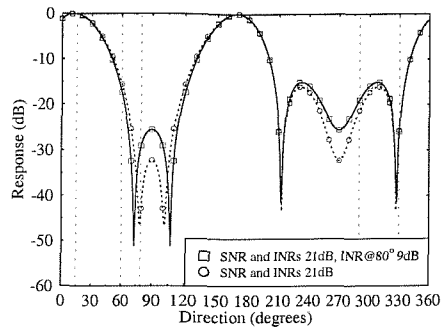

(b) Comparison between all SNRs and INRs of 21.0dB, and all at 21.0dB except the interferer at 80° which has an INR of 9.0dB.

Figure 2.41: Beam patterns of a three element uniformly spaced linear array having an inter-element spacing of $\lambda/2$ in conjunction with one desired source located at 15°, and **four sources of interference** located at **-30°**, **60°**, **80°** and **-70°**. The **SMI** beamforming algorithm was used with a reference length of 256 bits.

beamforming algorithm are not as deep as those of the SMI algorithm. As for the SMI algorithm, the null depths are also shallower, when the INRs are lower.

In the case of two sources of interference, as shown in Figure 2.43, the algorithm has again successfully nulled the sources, albeit with a lower attenuation than that achieved by the SMI algorithm as may be seen in Figure 2.37. This is, however of purely academic interest, since null depths of 50dB would be unrealisable. For three interferers, all having the same power as the desired source, this phenomenon persists, as it does when the interference sources are of lower power. However, in Figure 2.45(b) the interference rejection for the source at an angle of 60° is significantly lower at 20dB, than that obtained using the SMI algorithm, which was 27dB. For deep nulls this difference would have little impact, but at these levels of interference rejection, it may be problematic.

Figure 2.46 shows the beam patterns encountered, when four sources of interference and one desired source are present simultaneously. In conjunction, with the NLMS beamforming algorithm the levels of interference rejection for each interference source are lower, than those obtained using the SMI algorithm. Specifically, the associated reductions vary from only 2dB to 17dB, having a mean difference of about 8dB.

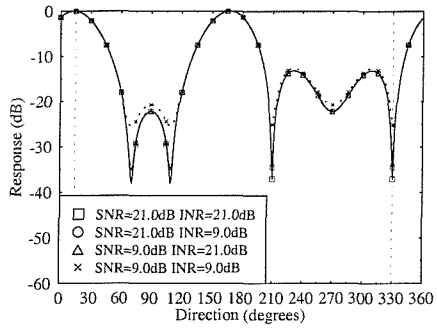

(a) Source located at 15°, interference at −30°.

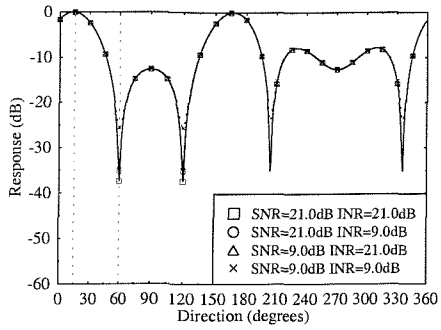

(b) Source located at 15°, interference at 60°.

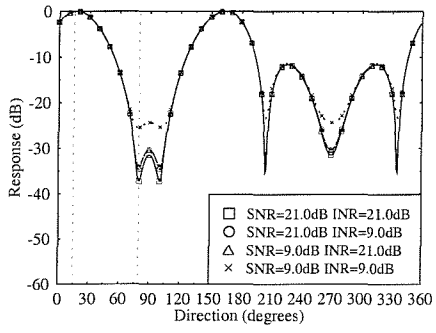

(c) Source located at 15°, interference at 80°.

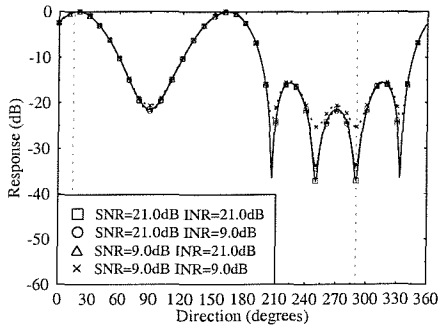

(d) Source located at 15°, interference at −70°.

Figure 2.42: Beam patterns of a three element uniformly spaced linear array with an inter-element spacing of $\lambda/2$ with one desired source and **one source of interference.** The **NLMS** beamforming algorithm was used with a reference length of 256 bits.

2.3.6.5 Complexity analysis

The direct matrix inversion algorithm requires the average of the cross-correlation matrix, R, which is a square-shaped matrix of size L, where L is the number of antenna elements. In order to calculate each element of the matrix, R, N complex multiplications and $N-1$ complex additions must be performed, where N is the sample size, in bits, used to generate the cross-correlation matrix, R. Due to the Hermitian nature of the matrix, R, it is only necessary to execute these instructions $L(L+1)/2$ times, rather than L^2 times, as would be expected.

Therefore, $NL(L+1)/2$ complex multiplications and $L(L+1)(N-1)/2$ complex additions

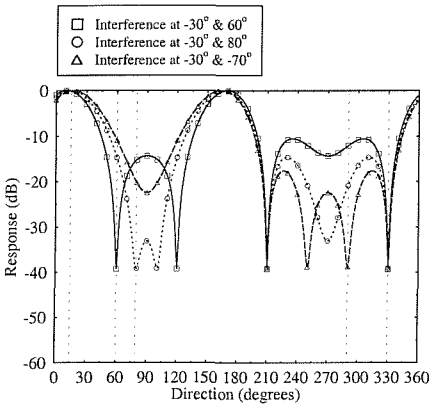

(a) Source located at 15°, interferers located at **-30°** and, **80°** or **-30°** and **-70°**.

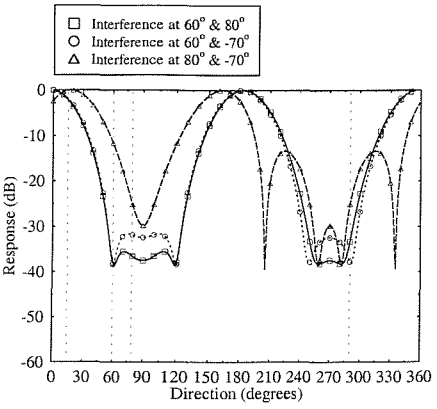

(b) Source located at 15°, interferers located at **60°** and **80°**, or **60°** and **-70°**, or **80°** and **-70°**.

Figure 2.43: Beam patterns of a three element uniformly spaced linear array with an inter-element spacing of $\lambda/2$ with one desired source and **two sources of interference**. The **NLMS** beamforming algorithm was used with a reference length of 256 bits.

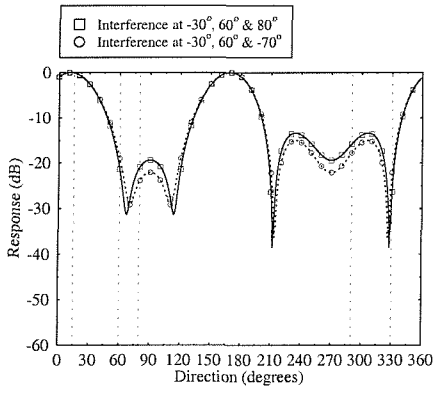

(a) Source located at 15°, interferers located at **-30°**, **60°** and **80°** or **-30°**, **60°** and **-70°**.

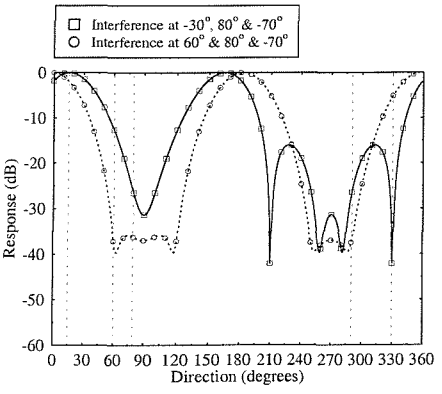

(b) Source located at 15°, interferers located at **-30°**, **80°** and **-70°**, or **60°**, **80°** and **-70°**.

Figure 2.44: Beam patterns of a three element uniformly spaced linear array with an inter-element spacing of $\lambda/2$ with one desired source and **three sources of interference**. The **NLMS** beamforming algorithm was used with a reference length of 256 bits. The SNR and INRs were **21.0dB**

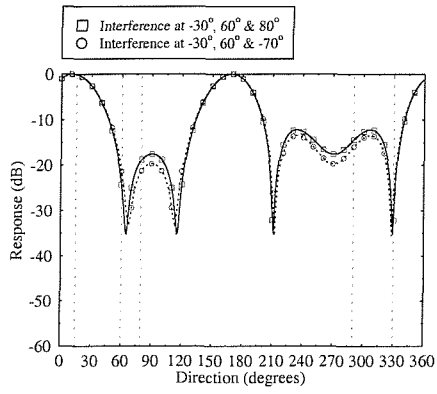

(a) Source located at 15°, interferers located at **-30°**, **60°** and **80°** or **-30°**, **60°** and **-70°**.

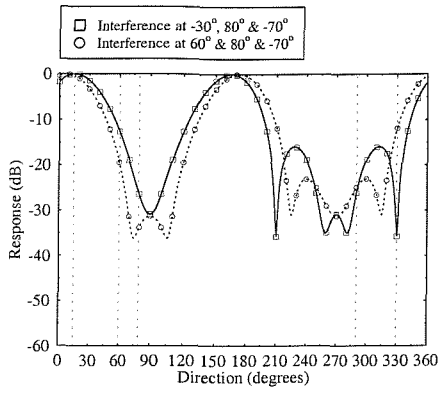

(b) Source located at 15°, interferers located at **-30°**, **80°** and **-70°**, or **60°**, **80°** and **-70°**.

Figure 2.45: Beam patterns of a three element uniformly spaced linear array with an inter-element spacing of $\lambda/2$ with one desired source and **three sources of interference**. The **NLMS** beamforming algorithm was used with a reference length of 256 bits. The SNR was **21.0dB** whilst the INRs were **9.0dB**

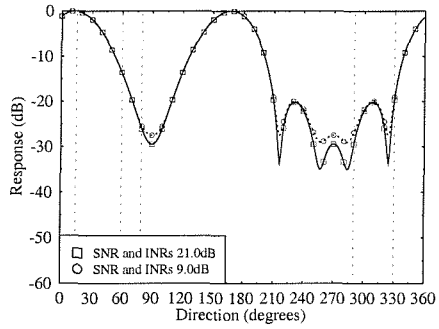

(a) Equal SNR and INR of 21.0dB.

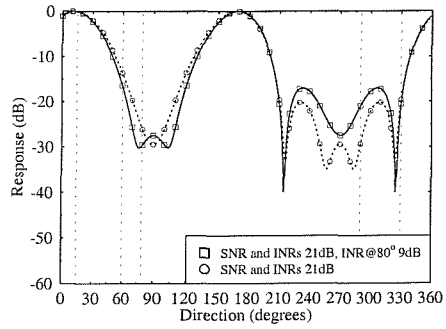

(b) Comparison between all SNRs and INRs of 21.0dB, and all at 21.0dB except the interferer at 80° which has an INR of 9.0dB.

Figure 2.46: Beam patterns of a three element uniformly spaced linear array with an inter-element spacing of $\lambda/2$ with one desired source located at 15°, and **four sources of interference** located at **-30°**, **60°**, **80°** and **-70°**. The **NLMS** beamforming algorithm was used with a reference length of 256 bits.

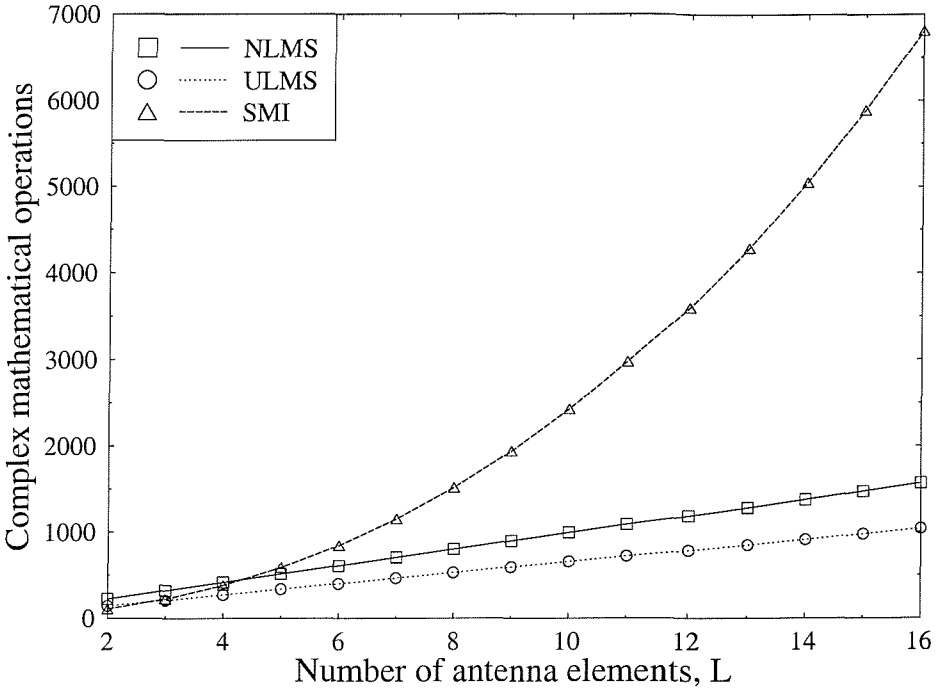

Figure 2.47: The relative complexities of the SMI, ULMS and NLMS beamforming algorithms for a reference signal length, N, of 16 symbols.

are required to form the matrix, leading to a total of $L(L+1)(2N-1)/2$ complex operations. However, assuming that a Multiply-and-ACcumulate (MAC) instruction exists in the implementation, this complexity figure reduces to $NL(L+1)$. The Hermitian cross-correlation matrix, R, must then be inverted requiring $L^3/2+L^2$ complex operations [25], rather than the usual L^3 operations required for a non-Hermitian matrix. In order to calculate the correlation between the reference signal and the array output vector requires a further L complex multiplications and $L-1$ complex additions, reducing to L complex operations assuming a MAC instruction. Then, from the inverted matrix, R^{-1}, and the correlation vector, $\underline{z}$, the weight vector, $\underline{w}$, may be obtained after L^2 complex operations. Therefore, the total complexity of the SMI beamforming algorithm is, $L(L+1)(2N-1)/2+L^3/2+2L^2+2L-1$ complex operations.

The ULMS adaptive beamformer requires only $2L+1$ complex multiplications and $2L$ complex additions per iteration, rendering it the least complex algorithm. However, the NLMS technique is more practical, since its performance is less dependent upon the input power. The additional complexity associated with this algorithm is the $L+1$ complex multiplications and L complex additions required to calculate the current value of μ. Therefore,

the final complexity of the NLMS algorithm is equivalent to $3L+2$ complex multiplications and $3L$ complex additions, per bit received. Hence, the total number of complex operations required by the NLMS beamforming algorithm is $N(3L+2+3L) = N(6L+2)$. The relative complexities of the three algorithms are shown in Figure 2.47 for a fixed reference signal length of 16 symbols. The figure shows how the ULMS and NLMS algorithm complexities increase linearly as the number of antenna array elements increases, whilst the number of complex operations required by the SMI algorithm increases exponentially.

2.4 Conclusions

In this chapter we commenced in Section 2.2.2 by considering the possible applications of antenna arrays and their related benefits. A signal model was then described in Section 2.2.3 and a rudimentary example of how beamforming operates was presented. Section 2.3 highlighted the process of adaptive beamforming in conjunction with several different temporal reference techniques detailed, along with the approaches of spatial reference techniques and the associated process of antenna array calibration. The challenges that must be overcome before beamforming for the downlink becomes feasible were also discussed in Section 2.3.5.

In Section 2.3.6 results were presented showing how the SMI, ULMS and NLMS beamforming algorithms of Sections 2.3.2.3, 2.3.2.1 and 2.3.2.2 behaved for a two element adaptive antenna having varying eigenvalue spread and reference signal length. The SMI algorithm was shown to converge very rapidly, irrespective of the eigenvalue spread, and the level of interference rejection was found to be purely dependent upon the interference power, regardless of the desired signal power. However, in Section 2.3.6.2 the convergence characteristics of the ULMS adaptive beamforming algorithm were shown to be heavily dependent upon both the desired signal power and the interfering signal powers. The NLMS algorithm, in contrast, was found to be far superior in this respect, and considering its significantly lower complexity than that of the SMI technique, offered good performance.

The performance of the SMI and NLMS algorithms was then compared in Section 2.3.6.4 for a three element antenna array with one desired source and between one and four sources of interference. The results obtained in Section 2.3.6.4 further evidenced the better performance of the SMI algorithm, but as was shown in Section 2.3.6.5, this was achieved at a much higher complexity, which became more significant when the number of array elements was greater than four. For a small number of elements, the SMI algorithm was found to have a lower complexity than both the ULMS and the NLMS techniques, but as the number of antenna elements used in the array increased, the complexity of the SMI method grew

exponentially, whereas, for the LMS routines it increased only linearly. Therefore, for about ten array elements, the complexity of the SMI algorithm was between three and four times that of the NLMS technique.

In the next chapter we consider the performance benefits that may be obtained with the advent of adaptive antenna arrays in a cellular radio network.

Chapter 3

Adaptive Arrays in an FDMA/TDMA Network

3.1 Introduction

Cellular networks are typically interference limited, with co-channel interference arising from cellular frequency reuse, ultimately limiting the quality and capacity of wireless networks [70, 71]. However, Adaptive Antenna Arrays (AAAs) are capable of exploiting the spatial dimension in order to mitigate this co-channel interference and thus to increase the achievable network capacity [6, 3, 23, 31, 39, 72]. Since an AAA may receive signals with a high gain from one direction, whilst nulling signals arriving from other directions, it is inherently suited to a CCI-limited cellular network. Thus a beam may be formed to communicate with the desired mobile, whilst nulling interfering mobiles [6]. Assuming that each mobile station is uniquely identifiable, it is a relatively simple task to calculate the antenna array's receiver weights, so as to maximise the received SINR. The use of adaptive antenna arrays in a cellular network is an area of intensive research and adaptive antenna array's have been studied widely in the context of both interference rejection and in single-cell situations [1, 45, 48, 51, 57, 58]. More recently, work has been expanded to cover the analysis and performance benefits of using base stations equipped with adaptive antenna arrays across the whole of a cellular network [2, 55, 73].

A further approach to improving the network performance is the employment of Dynamic Channel Allocation (DCA) techniques [74, 75, 76, 77, 78, 79, 80, 81, 82], which offer substantially improved call-blocking, packet dropping, and grade-of-service performance in comparison to Fixed Channel Allocation (FCA). A range of so-called distributed DCA algorithms were investigated by Chuang *et al.* [80] where a given physical channel could be

invoked anywhere in the network, provided that the associated channel quality was sufficiently high. As compromise schemes, locally optimised distributed DCA algorithms were proposed, for example, by Delli Priscoli *et al.* [83, 84], where the system imposed an exclusion zone for reusing a given physical channel around the locality, where it was already assigned.

In Sections 3.2.1-3.2.3 we briefly consider how an adaptive antenna array may be modelled for employment in a network level simulator, followed by a short overview of a variety of channel allocation schemes in Section 3.3. This section also provides a brief performance summary of the various channel allocation schemes based on our previous work [15, 85], which suggested for the scenarios considered [15, 85] that the Locally Optimised Least Interference Algorithm (LOLIA) provided the best overall compromise in network performance terms. Section 3.4 presents a theoretical analysis of the performance of an adaptive antenna in a cellular network. A summary of several multipath propagation models is given in Section 3.5, with particular emphasis on the Geometrically Based Single-Bounce Statistical Channel Model [86, 87]. The potential methods of cellular network performance evaluation are described in Section 3.6, as are the parameters of the network simulated in later sections. Simulation results for Fixed Channel Allocation (FCA) and two Dynamic Channel Allocation (DCA) schemes using single element antennas, as well as two- and four-element adaptive antenna arrays for Line-Of-Sight (LOS) scenarios are presented and analysed in Section 3.7.2.1. Furthermore, simulation-specific details of the multipath model are given in Section 3.7.1, with the associated results obtained for the FCA and the LOLIA in the context of two, four and eight element adaptive antenna arrays presented in Section 3.7.2.2. Performance results for a network using power control over a multipath channel in conjunction with two and four element adaptive antenna arrays are provided in Section 3.7.2.3, followed by the description of a network using Adaptive Quadrature Amplitude Modulation (AQAM) in Section 3.7.2.4.

Performance results were also obtained for AQAM and the FCA algorithm as well as the LOLIA, with both two- and four-element adaptive antenna arrays. Results using the "wraparound" technique, described in Section 3.7.1, which removes the cellular edge effects observed at the simulation area perimeter of a "desert-island" scenario, are then presented in Sections 3.7.3.1-3.7.3.4. Finally, a performance summary of the investigated networks is given in Section 3.8.

3.2 Modelling Adaptive Antenna Arrays

The interference rejection achieved by an antenna array is determined by both the direction of arrival of the interference and the angle of arrival of the desired signal (where direction of arrival and angle of arrival may be used interchangeably), and therefore, ultimately by the angular separation between the two. The number of interferers and their signal strengths also affects the achievable attenuation of each of the interferers. This section attempts to derive a simple relationship between these factors for low-complexity modelling of an adaptive antenna array.

3.2.1 Algebraic Manipulation with Optimal Beamforming

Given that the steering vector associated with the direction θ_i of the i_{th} source can be described by an L-dimensional complex vector $\underline{s}_i$ as [23],

$$\underline{s}_i = [\exp(j\omega t_1(\theta_i)), \ldots, \exp(j\omega t_L(\theta_i))]^T, \tag{3.1}$$

where L is the number of elements in the antenna array, and t_i is the time delay experienced by a plane wave arriving from the i^{th} source direction, θ_i, and measured from the antenna element at the origin. Then the correlation matrix, R, of the steering vector $\underline{s}_i$, may be expressed as [23]:

$$R = \sum_{i=1}^{M} p_i \underline{s}_i \underline{s}_i^H + \sigma_n^2 I, \tag{3.2}$$

where p_i is the power of the i^{th} source, σ_n^2 is the noise power and I is the identity matrix.

Assuming optimal beamforming under the constraint of a unit response in the wanted user's direction, then the weight vector of the AAA is [23]:

$$\underline{w} = \frac{R^{-1}\underline{s}_0}{\underline{s}_0^H R^{-1} \underline{s}_0}. \tag{3.3}$$

The array factor, $F(\theta)$, in the direction θ may be formulated as [39]:

$$F(\theta) = \sum_{l=1}^{L} w_l e^{-j\omega t_l(\theta)}. \tag{3.4}$$

Therefore, given that the desired signal arrives from the direction θ_0, and an interfering signal arrives from the angle θ_1, the corresponding array responses are $F(\theta_0)$ and $F(\theta_1)$, respectively. Hence, the level of interference rejection, $F(\theta_0) - F(\theta_1)$, when one desired signal

and one interfering signal are received at a two-element antenna array, may be calculated using Equation 3.4 to be:

$$F(\theta_0) - F(\theta_1) = \frac{(2p_1 + \sigma_n^2)e^{\frac{j\omega\lambda\sin\theta_0}{2c}} - (p_1 + \sigma_n^2)e^{\frac{j\omega\lambda(2\sin\theta_0 - \sin\theta_1)}{2c}} - p_1 e^{\frac{j\omega\lambda\sin\theta_1}{2c}}}{(2p_1 + 2\sigma_n^2)e^{\frac{j\omega\lambda\sin\theta_0}{2c}} - p_1 e^{\frac{j\omega\lambda\sin\theta_1}{2c}} - p_1 e^{\frac{j\omega\lambda(2\sin\theta_0 - \sin\theta_1)}{2c}}}, \quad (3.5)$$

where the term interference rejection is defined as the difference between the array response in the direction of the desired signal source and the array response in the direction of the interfering source.

As can be seen from this equation, there is a non-linear relationship between the two angles of arrival and the achievable interference rejection. Furthermore, the achievable interference rejection is independent of the desired signal's received power, p_0, and it is solely dependent upon the power of the interfering signal, p_1. Expanding this technique to either an antenna array having more elements or to catering for more interfering sources, or to multiple incident beams, led to overly complicated expressions which would be too complex to evaluate in real-time. In order to avoid the associated complexity, the quantities required for interference rejection in a given scenario could be stored in lookup tables. However, the size of the table required to store all of the information would be impractical. For example, for the desired source, one dimension would be required for the angle of arrival and then another one for every interference source. Two further table dimensions would be required to store the angle of arrival and interference power. Therefore, the simple situation involving just one interferer, with a received power dynamic range of 40dB, would require an array of $180 \times 180 \times 40 = 1,296,000$ elements, at an angular resolution of 1°, and an interferer power resolution of 1 dB. For two interference sources this figure increases to $180 \times 180 \times 40 \times 180 \times 40 = 0.3312 \times 10^9$ elements, which is clearly excessive.

3.2.2 Using Probability Density Functions

Due to the inherent complexities of performing large-scale network simulations, whilst invoking the required beamforming operations, we conducted an investigation into the probability distribution of the interference rejection ratio achieved by an adaptive antenna array. For our initial studies a two element antenna array with the elements located $\lambda/2$ apart was considered, with one desired source and one interfering source. Therefore, the average interference rejection achieved in decibels, for a given source-direction and power as well as interferer-direction and power could be determined. Unfortunately, as it can be seen from Figure 3.1(a), the achievable interference rejection was not based upon a linear relationship between the two angles of arrival. Furthermore, Figure 3.1(b) illustrates that the interference rejection achieved was also related to the power, or the Signal-to-Noise Ratio (SNR),

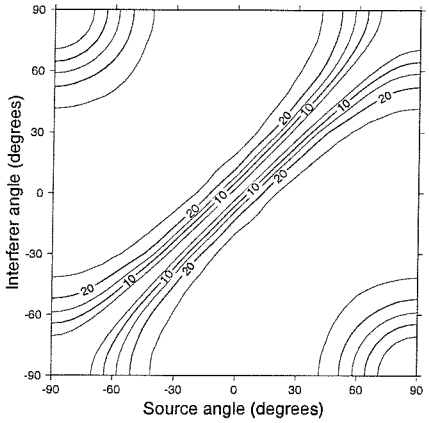

(a) Desired signal SNR = 3.0 dB, Interference SNR = 3.0 dB

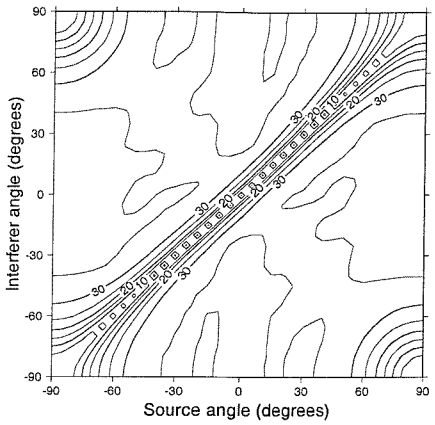

(b) Desired signal SNR = 3.0 dB, Interference SNR = 12.0 dB

Figure 3.1: Contour plots of interference rejection achieved using a four element antenna array with an inter-element spacing of $\lambda/2$ using SMI beamforming with a reference signal length of 16 bits. The angles of arrival of the signals from the desired source and the interfering source were swept over the range, -90 degrees to +90 degrees.

of the undesired interference source, which was 3 dB or 12 dB. As it was found in Section 3.2.1, attempting to construct a model or probability density function to cater for these parameters was not easily achievable. Rather than attempting to find the Probability Density Function (PDF) relating the two angles of arrival and interference power to the interference rejection achieved, a brief study was initiated for determining the PDF of the interference rejection achieved with respect to the angular separation between the desired signal and interfering signal. Figure 3.2 shows the probability density function of interference rejection achieved for one interference source and one desired source versus their angular separation. As this figure shows, the distribution of the interference rejection varies significantly, as the separation between the sources changes. As a consequence of the PDF's dependence on the angular separation encountered, modelling the achievable interference rejection expressed in decibels is an arduous task. Due to the complex nature of the PDF illustrated in Figure 3.2, an analysis of a smaller range of angles of arrival was conducted, in order to construct a piecewise valid model. The results are displayed in Figures 3.3(a) and 3.3(b) for angle of arrival spreads of $\pm 30°$ and $\pm 10°$, respectively. While these PDFs appear to be considerably simpler than that in Figure 3.2, it was not possible to match the PDFs to any commonly known distributions. Additionally, no information was available with regard to the correlation between successive interference rejection values. For these reasons, and due to the difficulties associated with adding multipath, it was decided to cease work on constructing

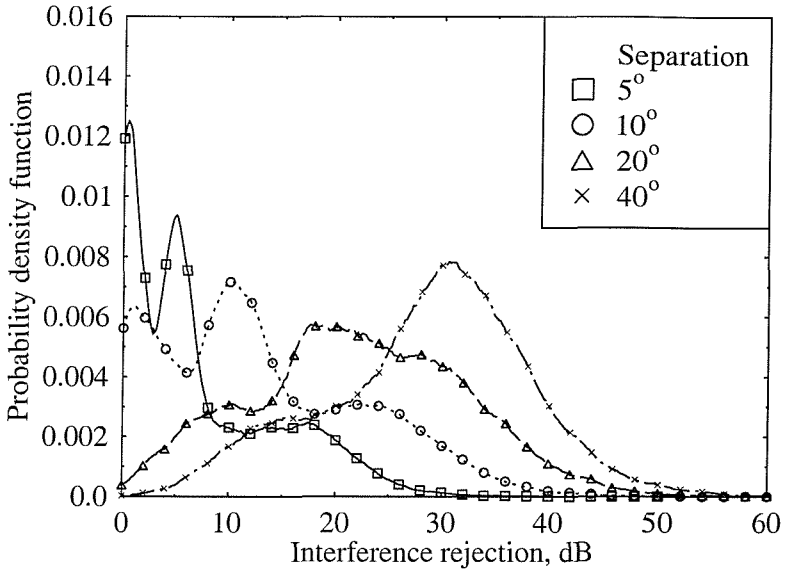

Figure 3.2: The PDF of the interference rejection (dB) achieved for various angular separations of the desired signal and the interfering signal. The angles of arrival of both signals were varied over the range of - 90 to +90 degrees and were of equal power. The antenna array consisted of two elements separated by $\lambda/2$.

a suitable interference rejection model and instead to implement an actual SMI beamformer within the simulation program as described in the following section.

3.2.3 Sample Matrix Inversion Beamforming

The process of defining a suitable model of an adaptive antenna array was becoming increasingly complex, resulting in the decision to implement an SMI beamformer in the simulation software. The SMI beamforming algorithm of Section 2.3.2.3, was chosen due to its independence from the received signal strengths, as well as due to its fast convergence with the aid of few data samples and for the sake of its good overall performance in terms of its interference rejection capability. The reference signal was chosen to be eight bits in length as a compromise between the quality of the sample correlation matrix, R, and the computational complexity required. Since a cellular network is an interference limited system, the addition of noise to the received signal vector was neglected. A result of this was that occasionally the correlation matrix, R, was non-invertible, which was remedied by diagonally augmenting the matrix with a positive constant as it was suggested in [48, 61, 62]. The addition of

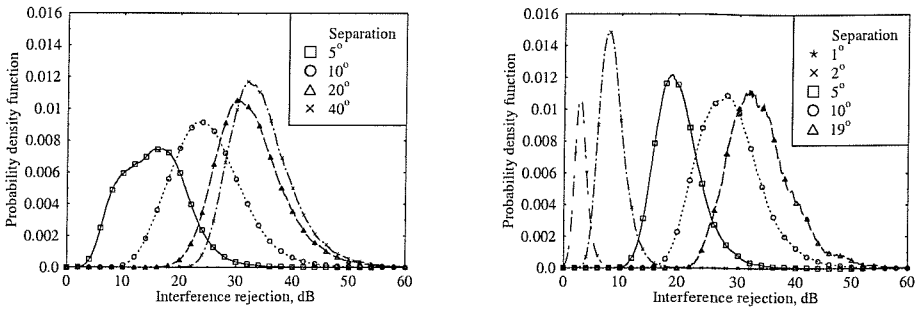

(a) Angular spread=±30°.

(b) Angular spread=±10°.

Figure 3.3: The PDF of the interference rejection achieved for the desired signal and the interfering signal angular separations of 5, 10 and 20 degrees. The desired signal and the interfering signal were of equal power. The antenna array consisted of two elements separated by $\lambda/2$.

multipaths simply required the direction of arrival, and the strength of the multipath rays at the antenna array to be determined before adding these received signal vectors to the total received signal vector of the antenna array. In both the line-of-sight and the multipath scenarios, the transmit/receive channel was assumed to be frequency invariant, thus allowing the same antenna pattern to be used in both the up- and the down-links.

3.3 Channel Allocation Techniques

Channel assignment is the process of allocating a finite number of channels to the various base stations and mobile phones in the cellular network. In a system using fixed channel assignment, the channels are assigned to different cells during the network planning stage, and the assignment is rarely altered to reflect changes in traffic levels. A channel is assigned to a mobile at the commencement of the call and the mobile communicates with its base station on this channel until either the call terminates or the mobile leaves the current cell. Dynamic channel allocation, however, assigns a channel that best meets the channel selection criteria, which may be the channel experiencing the minimum interference level, depending upon the cost function used.

3.3.1 Fixed Channel Allocation

In Fixed Channel Allocation (FCA), the available radio spectrum is divided into sets of frequencies. One or more of these sets is then assigned to each base station on a semi-permanent basis. The minimum distance between two base stations, which have been assigned the same set of frequencies, is referred to as the "reuse distance". This distance is chosen such that the co-channel interference is within acceptable limits, when the interferers are at least the reuse distance away from each other. The assignment of frequency sets to base stations is based on a pre-defined reuse pattern. The group of cells that contains one of each of the frequency sets is referred to as the frequency reuse cluster. The less cells in a reuse cluster, the more bandwidth-efficient the frequency reuse pattern, and the higher the user capacity in terms of the number of users supported per unit area per Hertz. However, small reuse clusters typically exhibit an increased co-channel interference, which has to be tolerated by the transceiver.

As mentioned above, in FCA the assignment of frequencies to cells is considered to be semi-permanent. However, the assignment can be modified, in order to accommodate the teletraffic demand changes experienced in the network. FCA schemes are simple, however, modifying them to adapt to changing traffic conditions or user distributions can be problematic. Hence FCA schemes have to be designed carefully, in order to remain adaptable and scalable, as the number of mobile subscribers increases.

A commonly used FCA cluster size is the seven-cell reuse cluster, providing coverage over regular hexagonal shaped cells, which is shown in Figure 3.4. Each cell in the seven-cell reuse cluster has six co-channel interfering cells at a distance D, the reuse distance. This reuse pattern provides the same number of channels at each cell site, and hence the same system capacity. Therefore, the teletraffic capacity is distributed uniformly across all of the cells. Since traffic distributions are not uniform in practice, such a system can lead to inefficiencies. For example, under a non-uniform traffic loading, some cells may have no spare capacity, and hence new calls in these cells are blocked, however, nearby cells may have spare capacity [88].

3.3.2 Dynamic Channel Allocation

While fixed channel allocation schemes are common in most existing cellular radio systems, the cost of increasing their teletraffic capacity can become prohibitive. In theory, the use of Dynamic Channel Allocation (DCA) allows the employment of all carrier frequencies in every cell, thereby ensuring significantly higher capacity, provided the transceiver-specific

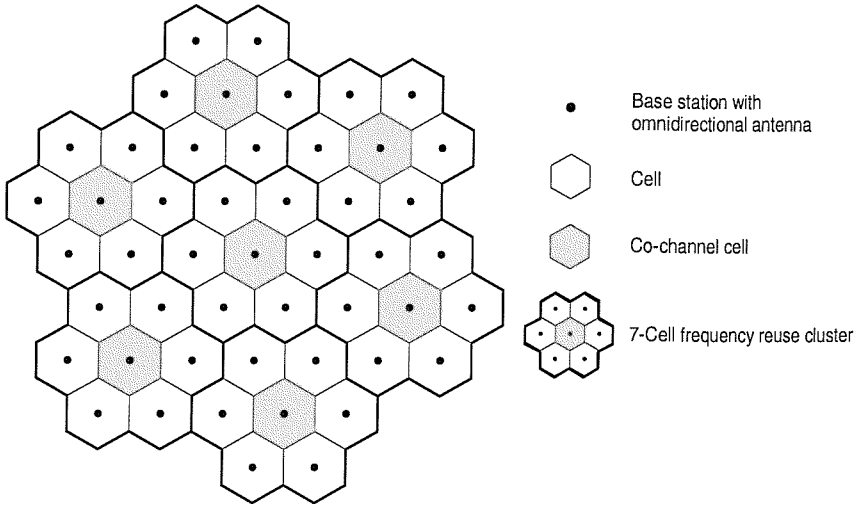

Figure 3.4: A commonly employed frequency reuse pattern for Fixed Channel Assignment (FCA) algorithms. The frequency spectrum is divided into seven frequency sets, one set assigned to each cell, yielding a so-called 7-cell reuse cluster. The shaded cells represent cells assigned the same frequency set.

interference constraints can be met. Therefore, it is feasible to design a mobile radio system, which configures itself to meet the required capacity demands as, and when, they arise.

In contrast to fixed assignment, in dynamic assignment strategies the traffic cells have no channels assigned to themselves. Instead, all call attempts are referred to the Mobile Switching Centre (MSC), which manages all channel assignments in its region. Each time a call attempt arrives, the base station asks the MSC for the channel having the minimum cost to be assigned. The cost function depends on the future call blocking probability, usage frequency of the candidate channel, the reuse distance of the channel, and so on. The MSC decides, on a call-by-call basis, which channel to assign to which call attempt by searching for the available channel for which the cost function is minimum. It needs to have information regarding the channel occupancy distributions under the current traffic conditions and other network directed criteria, as well as radio channel quality estimates of the individual mobiles [89]. This information is then used to decide which channel to allocate or whether to allocate a channel at all. It is sometimes better not to allocate a channel, if it is likely to inflict severe interference upon another user, potentially forcibly terminating existing calls or preventing the setup of new calls. Ideally, the channel quality measurements should be made at both the mobile and the base station. Channel allocation decisions that are based upon only one of the measurements can in some circumstances cause severe interference, leading to possible termination of the new call as well as potentially curtailing

an existing call supported by the same channel in the vicinity. If measurements are made at both the mobile and the base station, then the measurements have to be compared, requiring additional signalling, which increases the call setup time. The call setup time is longer in DCA algorithms than in FCA due to the time required to make measurements and to compare them. This can be a problem, especially when a handover is urgently required.

Probably the simplest DCA algorithm is to allocate the least interfered channel available to users requesting a channel. By measuring the received power within unused channels, effectively the noise plus interference power on that channel can be jointly measured. By allocating the least interfered channel, the new channel is unlikely to be interfered and hence it is unlikely to inflict too much interference upon channels already allocated. This works well for lightly loaded systems, but the algorithm's performance is seriously impaired in high-load scenarios, when FCA would work better. Some algorithms give better performance than others, but only in certain conditions. Most DCA algorithms' objectives can be classified into two types; those that attempt to reduce interference, and those that attempt to maximise the channel utilisation in order to achieve spectral compactness.

In previous work [15, 85, 88], a comparative study of a range of DCA algorithms was conducted and it was found that the algorithm, which gave the best overall compromise in terms of the desired performance measures was the Locally Optimised Least Interference Algorithm (LOLIA). The results in Table 3.1 indicate the achievable network capacities, without AAAs and without shadow fading, for various DCA algorithms and for the FCA algorithm. Below we briefly define the various DCA algorithms. The Least Interference Algorithm (LIA) [80] always assigns the channel suffering from the least interference, which minimises the system's interference load. A more advanced version of this scheme is the Least interference below Threshold Algorithm (LTA) [80], which attempts to maintain the amount of interference below a given threshold. The threshold is determined by the transceiver's interference rejection tolerance expressed in terms of the SINR required for attaining its target Frame Error Ratio (FER). In contrast, the Highest interference below Threshold Algorithm (HTA) [80] allocates the most interfered channel, whose interference is below the maximum acceptable level. A technique similar to the LTA is the Lowest Frequency below threshold Algorithm (LFA) [80], which attempts to reduce the number of carrier frequencies in use simultaneously, whilst allocating the least interfered channel exhibiting an interference level below the given threshold. And finally, the Locally Optimised Most Interference Algorithm (LOMIA) selects the most interfered channel, rather than the least interfered one, as in the Locally Optimised Least Interference Algorithm (LOLIA). Hence, our investigations presented here continue the work on LOLIA by combining it with adaptive beamforming and other network capacity enhancement techniques.

Algorithm	Number of users supported by network	
	Conservative	**Lenient**
	P_{FT}=1%, P_{low}=1%	P_{FT}=1%, P_{low}=2%
	GOS=4%, P_B=3%	GOS=6%, P_B=5%
FCA	820	1120
HTA	1435	1520
LFA	1555	1705
LOMIA (n=19)	1505	2040
LTA	1815	1830
LIA	1820	1820
LOLIA (n=7)	1860	2115
LOLIA (n=19)	1935	2005

Table 3.1: Maximum number of mobile users that can be supported by the various DCA algorithms [85].

3.3.2.1 Locally Optimised Least Interference Algorithm

The LOLIA makes its channel allocation decisions by always allocating the least interfered available channel to the next allocation request. The LOLIA however will not allocate an otherwise adequate quality channel, if it is used in any of the nearest n neighbouring cells. Thereby the nearby BSs exchange their information concerning channels that are currently being used. This requires a fast backbone network, but it is not reliant on central control. The overall level of interference in the system can be reduced by increasing the number of "excluded" cells, which are classed as neighbouring cells. However, the larger n, the more calls are blocked, since there will be less available channels, which are not used by the nearest n BSs. Figure 3.5 shows the arrangement of neighbouring cells for $n = 7$ and $n = 19$. The n parameter effectively imposes a minimum reuse distance constraint upon the algorithm.

3.3.3 The Effect of Handovers

A handover or handoff event occurs, when the quality of the communications channel used degrades, and hence the call is switched to a newly allocated channel. If the new channel belongs to the same base station, this action is referred to as an intra-cell handover. Generally an intra-cell handover is performed, either when the channel quality degrades due to co-channel interference or in order to increase the system's performance and capacity. Inter-cell handovers occur typically, when the mobile approaches the fringes of the cell area, and hence the signal strength degrades, requiring a handover to a nearer base station.

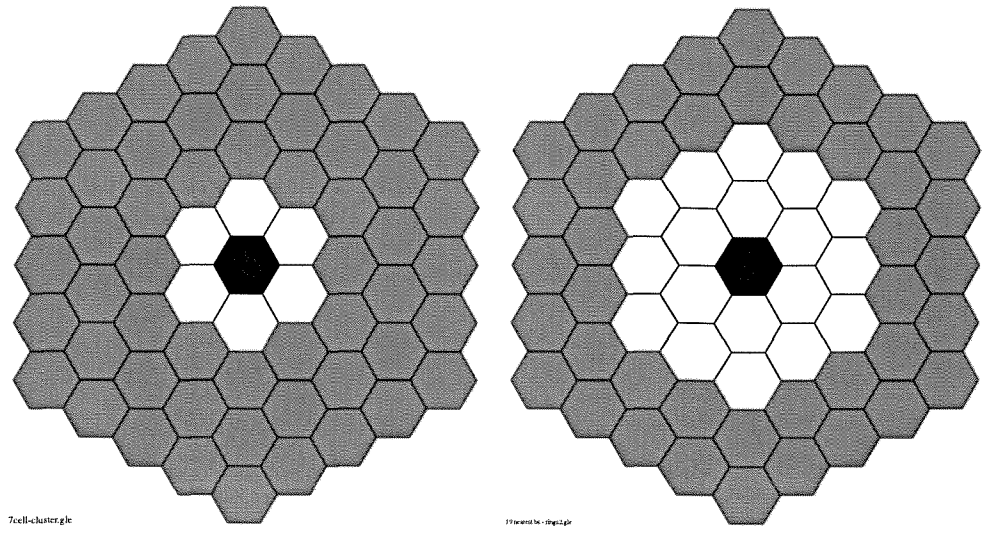

(a) 7 nearest base stations monitored. (b) 19 nearest base stations monitored.

Figure 3.5: The nearest neighbour constraint for $n = 7$ and $n = 19$ for the Locally Optimised Least Interference Algorithm (LOLIA) as described in Section 3.3.2.1.

Handovers have a substantial effect on the performance of channel allocation algorithms. At high traffic loads the majority of forced call terminations are due to the lack of availability of channels to handover to, rather than due to interference. This can be a particular problem in microcellular systems, where the rate of handovers is significantly higher than in normal cellular systems.

3.4 Analysis of an Adaptive Antenna Array in a Cellular Network

Here, a study into the usage of an adaptive antenna array in a cellular network is conducted. A theoretical analysis of such a system is performed and the results are presented for later comparison with simulated results. To simplify this process the following assumptions were made :

- There is a uniform distribution of users in each cell.
- There is a blocking probability of P_B in all cells.
- The omni-directional base station antenna has an ideal beam pattern, giving a uniform circular coverage.

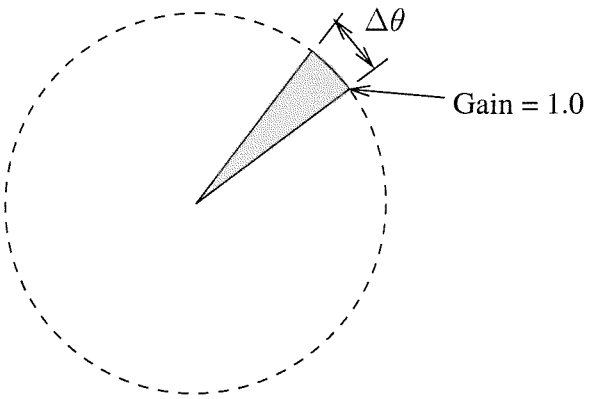

Figure 3.6: Beam pattern of an ideal beamformer with beamwidth $\Delta\theta$.

- The adaptive base station antenna array can generate m ideal beams, each with a gain of 1.0 over a beamwidth of $\Delta\theta = 2\pi/m$ radians, and a gain of 0.0 over the remaining angular sector, as shown in Figure 3.6

The blocking probability, P_B, is the fraction of attempted calls that cannot be allocated a channel. If the traffic intensity offered is a Erlangs, then the actual traffic carried is $a(1 - P_B)$ Erlangs. The Erlang is a measure of offered tele-traffic, which indicates the quantity of traffic on a channel or group of channels per unit time. This gives a channel usage efficiency of [2] :

$$\eta = \frac{a(1 - P_B)}{N}, \tag{3.6}$$

where N is the total number of channels allocated per cell.

It was also assumed that the main beam formed by the adaptive antenna was centred about the angle of arrival of the desired mobile's signal and that the mobile was tracked with no error. Additionally, all interfering sources outside the main beam were assumed to be nulled successfully. The ideal beamformer model used has a single mainlobe with a unity-gain beamwidth of $\Delta\theta$ and sidelobes of zero gain, as shown in Figure 3.6. When the desired signal's power, S, does not exceed the co-channel interference power I by the required protection ratio, γ, an "outage" will occur, i.e. we fail to obtain satisfactory reception at the mobile in the presence of interference with the probability of [2, 90, 91, 92]:

$$P(\text{outage}) = P(S \leq \gamma I) = P(S/I \leq \gamma) = P(SIR \leq \gamma), \tag{3.7}$$

where SIR is the signal-to-interference ratio. In other words, $P(\text{outage})$ is the probability of the power of the signal being insufficient to provide reliable communications due to the

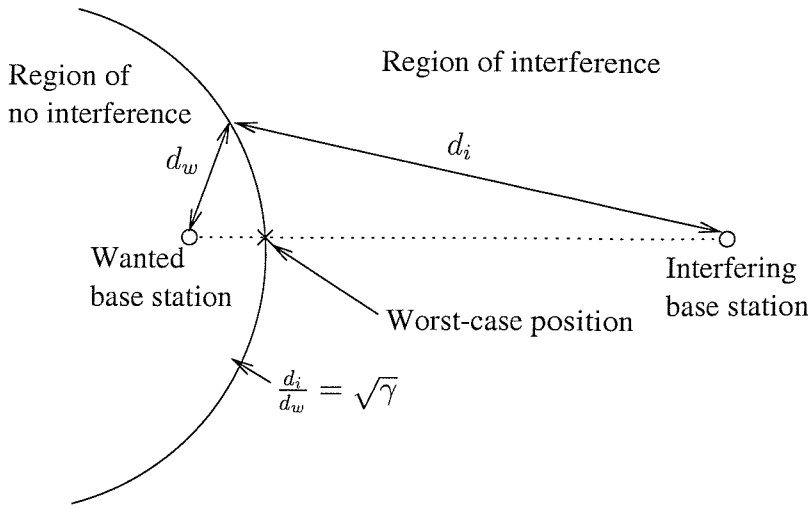

Figure 3.7: Contour defining interference regions in a downlink scenario using omnidirectional antennas.

interference in the channel. Considering only the propagation path loss, but no fast- and shadow-fading, we have $SIR = S/I = d_i^2/d_w^2 \leq \gamma$, hence for a given interference protection ratio, a locus defined by $d_i/d_w = \sqrt{\gamma}$ can be drawn, as in Figure 3.7. This defines a region, where the signal-to-interference ratio necessary for reliable downlink (DL) communications is maintained, and a region where interference occurs.

In a cellular network employing base station (BS) adaptive antenna arrays, the occurrence of co-channel interference is a statistical phenomenon dependent upon the number of co-channel interferers and on the positions of these interferers in the co-channel cells. In general the uplink (UL) and downlink (DL) interference calculations are different and hence they have to be considered separately. The total probability of co-channel interference-induced outage can be evaluated by [2, 73, 92]:

$$P(\text{outage}) = P(SIR \leq \gamma) = \sum_{n=1}^{N} P(SIR \leq \gamma | n) P(n), \tag{3.8}$$

where N is the total number of co-channel interferers, usually restricted to the first tier of interferers, shown in white in Figure 3.5(a), i.e., to six, $P(SIR \leq \gamma|n)$ is the conditional probability of co-channel interference, $P(SIR \leq \gamma)$ given n interferers. Furthermore, $P(n)$ is the probability that there are n active interfering co-channel cells. Therefore, if the activation of channels is assumed to be independent and identically distributed, $P(n)$ has the form of a binomial PDF [2, 55, 92]:

$$P(n) = \binom{6}{n} p^n (1-p)^{6-n}, \tag{3.9}$$

where p is the probability of finding one interfering co-channel active. The probability p that a single co-channel BS has an active DL co-channel interferer, given that the wanted mobile has been assigned that DL channel already, is [2]:

$$p = \frac{\text{number of active channels}}{\text{total number of channels}} = \frac{a(1-P_B)}{N} = \eta. \tag{3.10}$$

Therefore, the probability that n co-channel interfering BSs are using the same DL channel as the wanted mobile for its reception becomes:

$$P(n) = \binom{6}{n}\eta^n(1-\eta)^{6-n}. \tag{3.11}$$

Hence, from Equations (3.8) and (3.11) we have:

$$P(\text{outage}) = P(SIR \leq \gamma) = \sum_{n=1}^{N} P(SIR \leq \gamma|n)\binom{6}{n}\eta^n(1-\eta)^{6-n}. \tag{3.12}$$

In conjunction with an omnidirectional BS antenna, the probability of an active DL co-channel interferer was given by η, the channel usage efficiency. For an adaptive BS antenna, forming m beams per cell, there will always be six DL beams targeted at the wanted mobiles from the six co-channel base stations. Therefore, for an adaptive base station antenna [2, 55] we have:

$$\begin{aligned} p &= \begin{pmatrix}\text{probability that the beam pointing at the desired} \\ \text{mobile also contains an interfering mobile}\end{pmatrix} \\ &= \frac{\text{number of active channels in beam}}{\text{total number of channels}} \\ &= \frac{a(1-P_B)/m}{N} = \frac{\eta}{m}. \end{aligned} \tag{3.13}$$

Hence, for an adaptive BS antenna array with m beams per BS we have:

$$P(n) = \binom{6}{n}\left(\frac{\eta}{m}\right)^n\left(1-\frac{\eta}{m}\right)^{6-n}, \tag{3.14}$$

leading to the overall outage probability for a BS adaptive antenna array in the form of:

$$P(\text{outage}) = P(SIR \leq \gamma) = \sum_{n=1}^{N} P(SIR \leq \gamma|n)\binom{6}{n}\left(\frac{\eta}{m}\right)^n\left(1-\frac{\eta}{m}\right)^{6-n}. \tag{3.15}$$

where $P(SIR \leq \gamma|n)$ is the conditional outage probability, which is dependent on the mean received signal power and the mean received interference power.

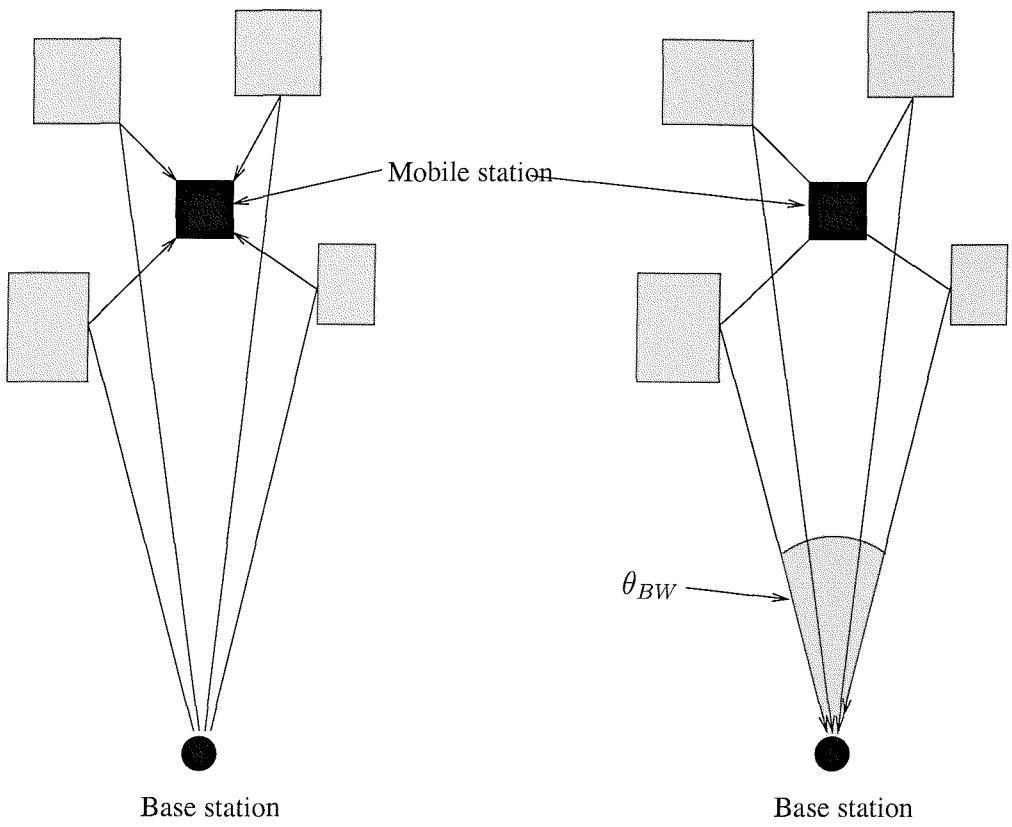

Figure 3.8: Macrocellular up- and down-link multipath scattering scenarios.

3.5 Multipath Propagation Environments

In Section 3.2 various situations were investigated where only a direct Line-Of-Sight (LOS) link existed between the base station and the mobile handset. However, in a real environment, a phenomenon known as multipath scattering takes place, which results in the presence of numerous signal components, or multipath components, at the receiver. This is due to reflections, diffractions and signal scattering, caused by objects in the path between the transmitter and the receiver. A simple figure showing an example of the multipath propagation channel is shown in Figure 3.8. Each signal component experiences a different path attenuation and phase rotation, which determines the received signal's amplitude, carrier phase shift, time delay, angle of arrival and Doppler shift [42]. In general, each of these components will be time-varying. We note here that the various uplink and downlink scenarios will be considered in more depth in Figure 3.19 during our further discourse.

Figure 3.8 shows the multipath environment that may be found on the up- and down-links in a macrocellular environment. It is usually assumed that the scatterers surrounding the

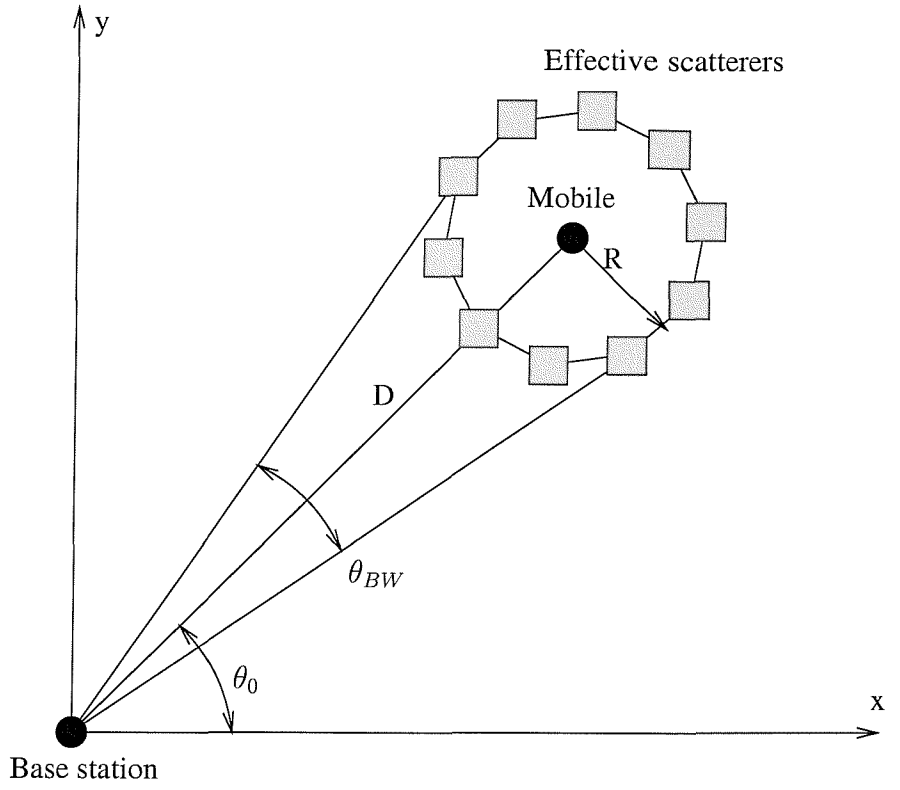

Figure 3.9: Lee's model for multipath scattering using N scatterers in a circle of radius R around the mobile station.

mobile station are at about the same height as or are higher than the mobile. This implies that the received signal at the mobile antenna arrives from all directions after bouncing from the surrounding scatterers, as illustrated in Figure 3.8. Under these conditions it is assumed that the downlink Direction-Of-Arrival (DOA) at the mobile is uniformly distributed over $[0, 2\pi]$ [42, 86]. However, the uplink DOA of the received signal at the base station is quite different. In a macrocellular environment, the base station is typically positioned higher than the surrounding scatterers. Hence, the received signals at the base station result predominantly from the scattering process in the vicinity of the mobile station, as it may be seen in Figure 3.8. The uplink multipath components are restricted to a smaller angular region, θ_{BW}, and hence the distribution of the uplink DOA is no longer uniform over $[0, 2\pi]$. Many different models have been developed for use in different applications. Below a brief description of some of the models follows, but for a more detailed exposition the reader is referred for example, to Ertel *et al.* [86]. The macrocellular models are all based around the same principle of placing a number of scatterers near the mobile station in a given pattern, obeying a geographic probability distribution. In Lee's model, the scatterers are evenly spaced on a circular ring about the mobile, as shown in Figure 3.9. Assuming that the N

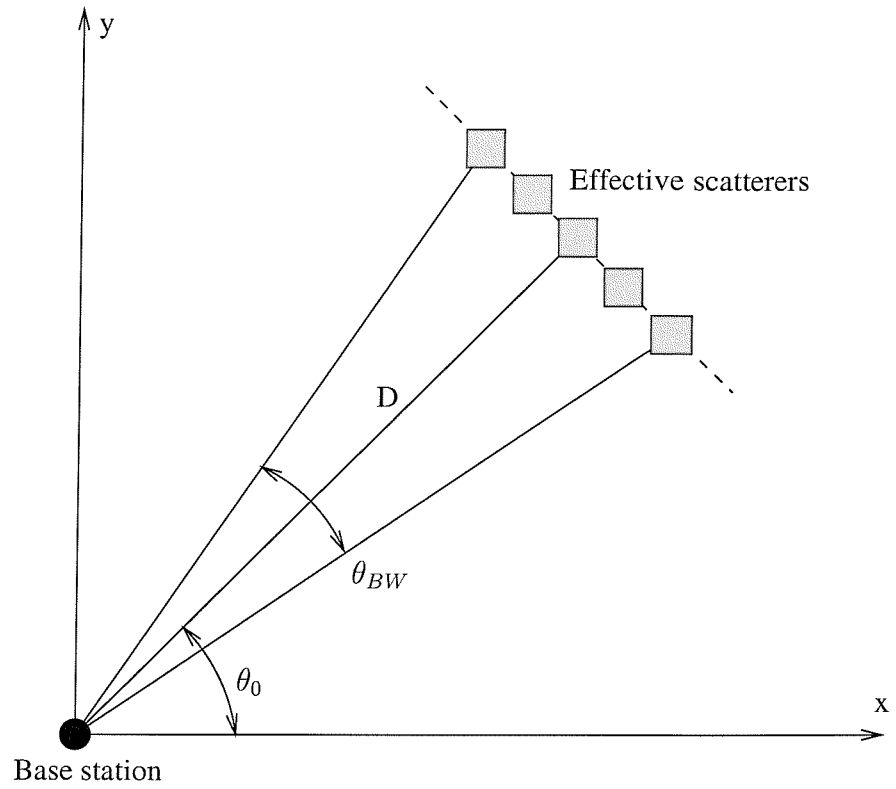

Figure 3.10: The Discrete Uniform Distribution model for multipath scattering using a line of N scatterers centred about the line of sight to the mobile.

scatterers are uniformly spaced on the circle having a radius R and orientated such that a scatterer is located along the LOS path, the discrete DOAs are [86]:

$$\theta_i \approx \frac{R}{D} \sin\left(\frac{2\pi}{N} i\right), \qquad i = 0, 1, \ldots, N-1. \tag{3.16}$$

However, the model was originally designed simply for providing information regarding the signal correlations of the multipath components and when used to provide DOA and Time-Of-Arrival (TOA) information, the simulated results are not consistent with measurements [86].

A model similar to Lee's, known as the discrete uniform distribution, evenly spaces N scatterers within a narrow beamwidth centred about the LOS to the mobile, as shown in Figure 3.10. According to [86], the discrete possible DOAs, assuming that N is odd, are given by:

$$\theta_i = \frac{1}{N-1} \theta_{BW} i, \qquad i = -\frac{N-1}{2}, \ldots, \frac{N-1}{2}. \tag{3.17}$$

The Geometrically Based Single-Bounce (GBSB) Statistical Channel Models are defined by a spatial scatterer density function. This model involves randomly placing scatterers in the scatterer region according to the spatial scatterer density function. From the location of each of the scatterers, the DOA, TOA, and signal amplitude can be determined. The Geometrically Based Single-Bounce Circular Model (GBSBCM) is shown in Figure 3.11, which was found to be suitable for macrocellular modelling, since it assumes that all the scatterers lie within the radius R about the mobile and $R < D$ [86]. An alternative spatial distribution of the scatterers, known as the Geometrically Based Single-Bounce Elliptical Model (GBSBEM) [86, 87], assumes that the scatterers are uniformly distributed within an ellipse, as shown in Figure 3.12, where the base station and the mobile station are the foci of the ellipse, and the parameters a_m and b_m are the semi-major and semi-minor axis values, which may be calculated as [86, 87]:

$$a_m = \frac{c\tau_m}{2} \qquad b_m = \frac{1}{2}\sqrt{c^2\tau_m^2 - D^2}, \tag{3.18}$$

where τ_m is the maximum time of arrival to be considered, D is the distance between the transmitter and the receiver and c is the velocity of light in free space. This model was proposed for microcellular environments [87], where the antenna heights are relatively low, and therefore, multipath scattering near the base station is equally likely, as scattering near the mobile station [87].

The GBSBEM may be used to generate the path time delay, τ_i, the angle of arrival, ϕ_i, the direction of departure, Φ_i, the power of the multipath component, P_i, and the phase angle, α_i. However, here we are only concerned with the angle of arrival information at the base station. The Cumulative Density Function (CDF) of the angle of arrival, ϕ_i, conditioned on the normalised multipath delay, $r_i = c\tau_i/D = \tau_i/\tau_0$, is given as [87]:

$$F_{\phi|r}(\phi_i|r_i) = \begin{cases} \frac{1}{2\pi}\cos^{-1}\left(\frac{1-r_i\cos\phi_i}{r_i-\cos\phi_i}\right) - \frac{\sqrt{r_i^2-1}\sin(-\phi_i)(1-r_i\cos\phi_i)}{2\pi(2r_i^2-1)(r_i-\cos\phi_i)^2} & -\pi \le \phi_i \le 0 \\ 1 - \frac{1}{2\pi}\cos^{-1}\left(\frac{1-r_i\cos\phi_i}{r_i-\cos\phi_i}\right) + \frac{\sqrt{r_i^2-1}\sin(\phi_i)(1-r_i\cos\phi_i)}{2\pi(2r_i^2-1)(r_i-\cos\phi_i)^2} & 0 \le \phi_i \le \pi. \end{cases} \tag{3.19}$$

The conditional probability density function of ϕ_i, may be found by differentiating Equation (3.19) with respect to Φ leading to :

$$f_{\phi|r}(\phi|r_i) = \frac{(r_i^2-1)^{3/2}(r_i^2 - 2r_i\cos\phi + 1)}{\pi(2r_i^2-1)(r_i-\cos\phi)^3} \qquad -\pi \le \phi \le \pi, \tag{3.20}$$

which is plotted in Figure 3.13 for various values of the normalised multipath delay, r_i. From this figure it can be seen that as the normalised multipath delay increases, the distribution of the angles-of-arrival tends to the uniform distribution, since the longer the delays, the greater the distance travelled, which results in a wider range of angles-of-arrival. In contrast,

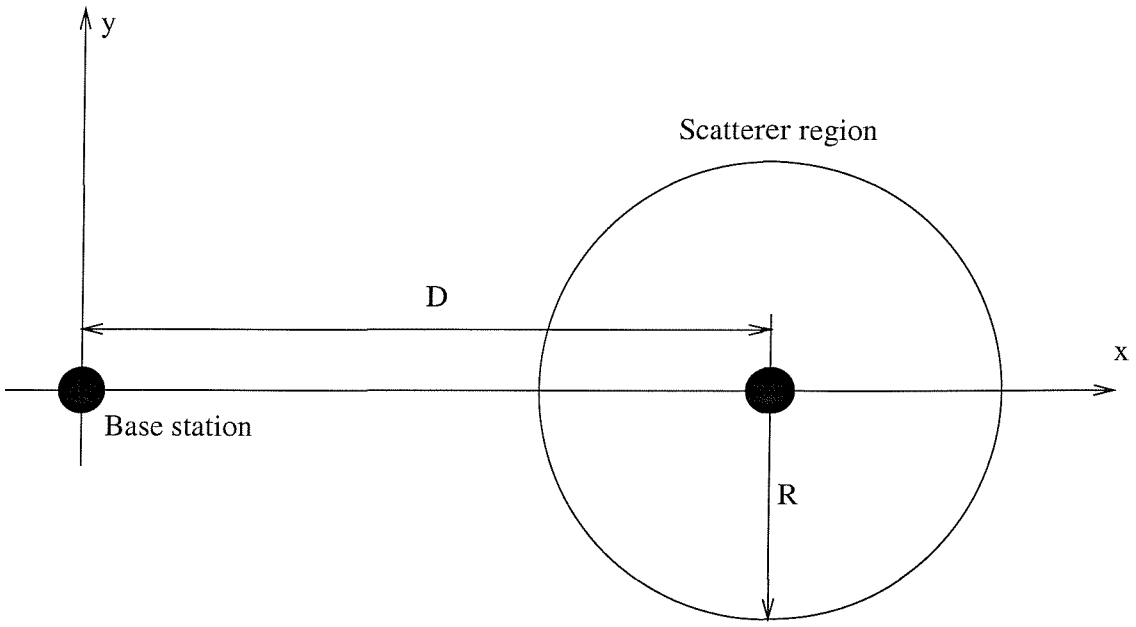

Figure 3.11: The Geometrically Based Single-Bounce Circular Model (GBSBCM), which is suitable for use as a macrocellular model, showing the region in which the scatterers are located.

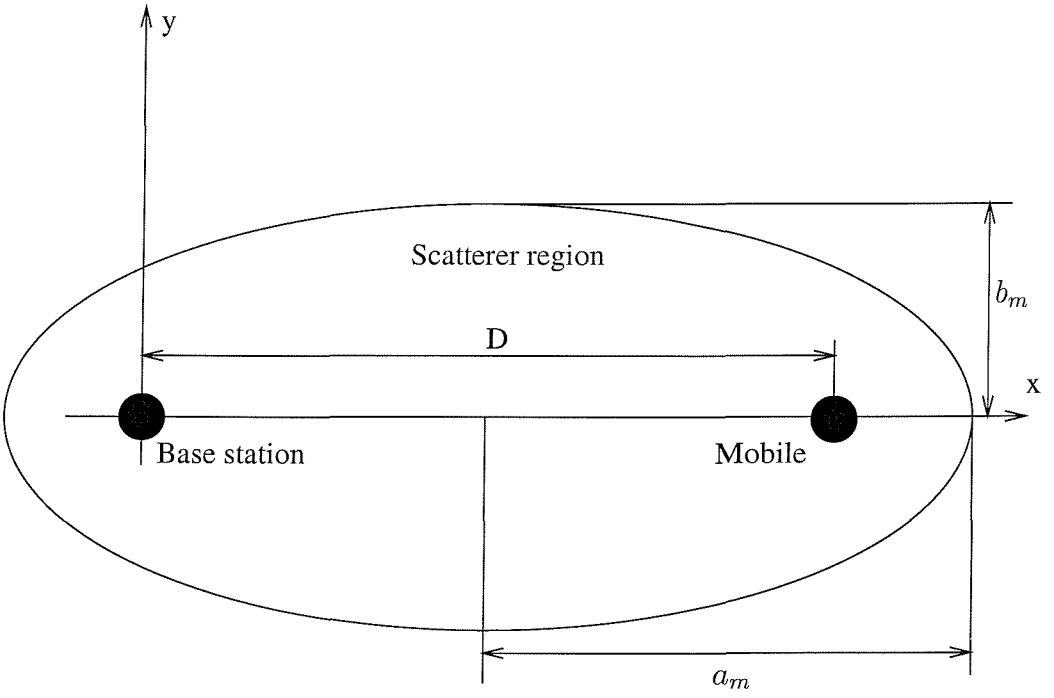

Figure 3.12: The Geometrically Based Single-Bounce Elliptical Model (GBSBEM), which is suitable for use as a microcellular model, showing the region in which the scatterers are located.

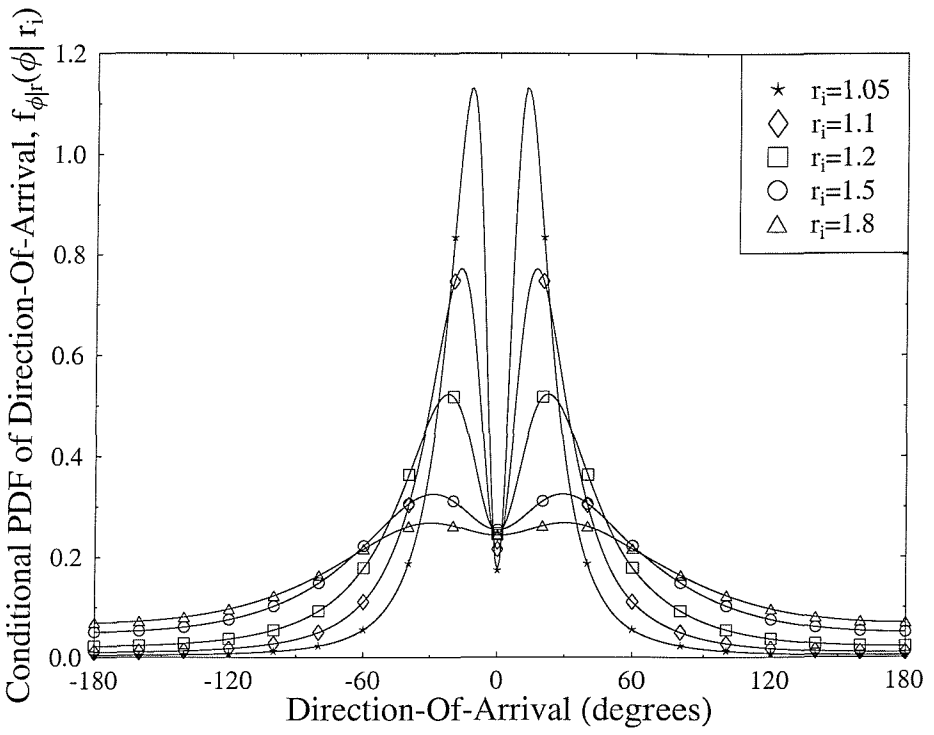

Figure 3.13: Probability density function of angle-of-arrival conditioned on the normalised multipath delay, r_i, for various values of r_i, evaluated from Equation 3.20.

a small value of r_i concentrates the multipath components around the angle-of-arrival of the direct path component.

In simulating multipath component parameters, it is necessary to generate samples of random variables from specified distributions. The normalised path delay, r_i, of the i^{th} multipath component, may be calculated thus as [87]:

$$r_i = \sqrt{\frac{1}{2} + \frac{1}{2}\sqrt{1 + 4\beta^2 x_i^2}}, \tag{3.21}$$

where x_i is a uniformly distributed random variable, denoted by $U(0,1)$, ranging from 0 to 1 and $\beta = r_m\sqrt{r_m^2 - 1}$ depends on the maximum value of the normalised path delay, r_m. The maximum normalised path delay, r_m, may be determined by the four different selection criteria summarised in Table 3.2 [87].

Again, using large values of r_m results in a near-uniform distribution of the angles of arrival, whereas small values of r_m gives low-delay multipath components clustered in angle of arrival about the direct LOS path component.

From normalised path delay r_i and y_i, a uniformly distributed random variable, again

Criteria	Expression
Maximum path delay, τ_m	$r_m = \tau_m/\tau_0$
Fixed threshold, T (in dB), with path loss exponent n	$r_m = 10^{(T-L_r)/10n}$
Fixed delay spread, σ_τ	$r_m = 3.24(\sigma_\tau/\tau_0) + 1$
Maximum excess delay, σ_e	$r_m = (\tau_0 + \tau_e)/\tau_0$

Table 3.2: Selection criteria for choosing r_m, the maximum normalised path delay [86, 87].

formulated as $U(0,1)$, over 0 to 1, it is now possible to determine the angle-of-arrival of the i^{th} multipath component by solving $y_i = F_{\phi|r}(\phi_i|r_i)$ for ϕ_i, where $F_{\phi|r}(\phi_i|r_i)$ is defined in Equation (3.19).

The corresponding Cumulative Density Function (CDF) is a smooth and monotonic function of the angle-of-arrival, as illustrated in Figure 3.14. The figure shows that, if the normalised path delay, $r_i = 1$, then the angle-of-arrival is 0°, and that as r_i increases, so does the spread of values of the angle-of-arrival.

Therefore, to summarise, the process of generating the angles-of-arrival obeying the required distribution the following sequence of operations must be performed:

- Determine r_m for the scenario under consideration.
- Calculate $\beta = r_m\sqrt{r_m^2 - 1}$.
- Generate $x_i = U(0,1)$.
- Calculate $r_i = \sqrt{\frac{1}{2} + \frac{1}{2}\sqrt{1 + 4\beta^2 x_i^2}}$.
- Generate $y_i = U(0,1)$.
- Solve Equation (3.19) for ϕ_i, given y_i using numerical methods.

3.6 Network Performance Metrics

There are several performance metrics that can be used to quantify the quality of service provided by a cellular network. The following performance metrics have been widely used in the literature and were also advocated by Chuang *et al.* [80]:

- New Call Blocking probability, P_B.
- Call Dropping or Forced Termination probability, P_{FT}.

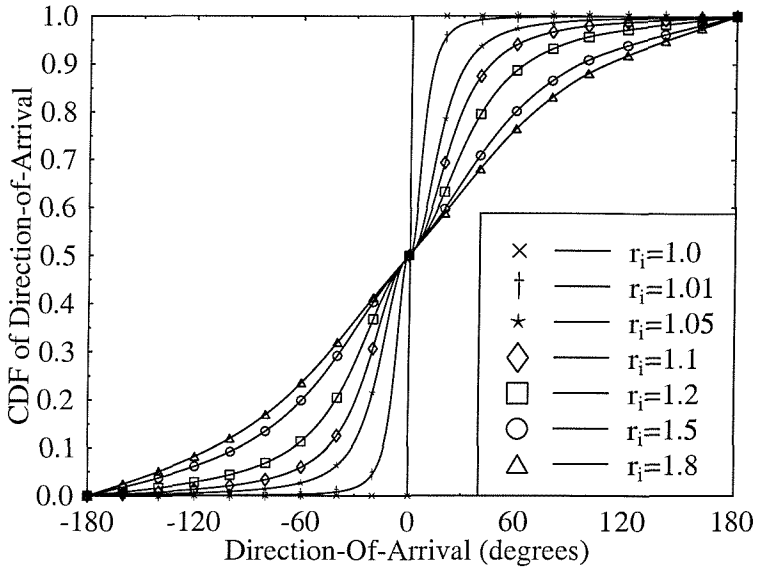

Figure 3.14: Cumulative density function of the angle-of-arrival conditioned on the normalised multipath delay, r_i, for various values of r_i.

- Probability of low quality connection, P_{low}.
- Probability of Outage, P_{out}.
- Grade Of Service, GOS.

The new call blocking probability, P_B, is defined as the probability that a new call is denied access to the network. This may occur because there are no available channels at the desired base station or the available channels are subject to excessive interference. A low new call blocking probability is desirable, however, it must frequently be traded off against a low call dropping probability which is more important for user satisfaction.

The call dropping probability, or the forced termination probability, P_{FT}, is the probability that a call is forced to terminate prematurely. This may be due to insufficient SINR during the call, which is not remedied by an intra-cell handover, either due to a lack of available channels, or still insufficiently high SINR, which leads to successive outages and eventually a dropped call. Calls may also suffer from forced termination, when a mobile enters a heavily loaded cell, which either suffers from poor SINR or has no available channels for the mobile to handover to.

The probability of a low quality connection is defined as:

$$\begin{aligned} P_{low} &= P\{SINR_{uplink} < SINR_{req} \text{ or } SINR_{downlink} < SINR_{req}\} \\ &= P\{min(SINR_{uplink}, SINR_{downlink}) < SINR_{req}\}. \end{aligned} \tag{3.22}$$

This performance measure allows for the comparison of algorithms, that may have similar call blocking and dropping characteristics, with respect to their quality of service provision for calls in progress. The probability of a low quality access is the probability that either the up- or the down-link signal quality is below the level required by the transceiver for maintaining our target performance of 5% Frame Error Ratio (FER) [93]. $SINR_{req}$ is the required reallocation SINR threshold, i.e. the SINR necessary to maintain an FER of 5%. If this SINR requirement was not satisfied, then a low quality outage would occur, and a handover request would be signalled to the base station. The Probability of Outage, P_{out}, is defined as the probability that the lower of the up- and down-link SINR values is below the threshold at which the call is deemed to be in outage, i.e. the SINR resulting in 10% FER or higher. A prolonged outage results in the call being dropped.

The Grade Of Service (GOS) was defined by [80]:

$$\begin{aligned} GOS &= P\{\text{unsuccessful or low-quality call access}\} \\ &= P\{\text{call is blocked}\} + P\{\text{call is admitted}\} \times \\ &\quad P\{\text{low signal quality and call is admitted}\} \\ &= P_B + (1 - P_B)P_{low}, \end{aligned} \tag{3.23}$$

which is interpreted in verbal terms as the probability of unsuccessful network access (blocking), or low quality access, provided that a call is admitted to the system.

In order to compare our network performance results attained by fixed and various dynamic channel allocation algorithms, with and without adaptive antenna arrays at the base station, it was necessary to consider more than one performance metric. For example, an algorithm may perform very well in one respect, yet have poor performance, when measured using an alternative metric. Therefore, it was decided to invoke two different scenarios :

- A *conservative scenario*, where the maximum acceptable value, for the call blocking probability, P_B, is 3%, for the call dropping probability, P_{FT}, is 1%, for P_{low} is 1%, and for the GOS is 4%.
- A *lenient scenario*, where the maximum acceptable value, for the call blocking probability, P_B, 5%, for the call dropping probability, P_{FT}, is 1%, for P_{low} is 2%, and for the GOS is 6%.

It must be noted that the maximum allowable GOS does not have to obey Equation 3.23 for the given values of P_B and P_{low}, since they may be traded off against each other, and thus the GOS represents a form of "user satisfaction". In the lenient case the GOS is 6% rather than the expected 7%, since it may be unacceptable for the user to suffer both a P_B of 5% and a P_{low} of 2%. Therefore, the "user satisfaction" may be maintained with any allowable combination of P_B and P_{low}, as long as they remain below their limits and the overall measure, GOS, remains below its limit.

3.7 Network Performance Results

Section 3.7.1 describes the processes involved in the simulator used to obtain the network performance results, such as the adaptive beamforming techniques, new call generation and handover queues as well as the multipath propagation model. Section 3.7.2.1 presents our simulation results obtained for the FCA and LOLIA DCA algorithms with a single element antenna, as well as two and four element adaptive antenna arrays, assuming a LOS propagation environment. Further results are presented in Section 3.7.2.2 which were obtained using the multipath channel of Section 3.7.1, using two, four and eight element adaptive antenna arrays. Section 3.7.2.3 characterises the network performance of using two and four element antenna arrays, in the multipath propagation environment, in conjunction with power control. This is further expanded upon in Section 3.7.2.4, where power control assisted Adaptive Quadrature Amplitude Modulation (AQAM) with is employed.

Sections 3.7.3.1-3.7.3.4 present our results for similar scenarios generated using the "wrap-around" rather than the "desert-island" technique, which eliminates the edge effects associated with the reduced interference levels encountered at the boundary of the simulation area. This process is described in Section 3.7.1. Finally, Section 3.7.2.7 provides a summary of the results obtained in this section.

3.7.1 System Simulation Parameters

The performance of the various channel allocation algorithms was investigated in a GSM-like [94] microcellular system, the parameters of which are defined in Table 3.3. The propagation environment was modelled using the power pathloss model having a pathloss exponent of -3.5. The mobile and base station transmit powers were fixed at 10dBm (10mW) for the simulations using no power control. The mobile and base station transmit powers were restricted to the range of -20dBm to +10dBm for the power control assisted and adaptive modulation based simulations. The number of carrier frequencies in the whole

system was limited to seven, each supporting eight timeslots, in order to maintain an acceptable computational load. This implied that the DCA system employing seven carrier frequencies in conjunction with eight time slots, as in GSM, could theoretically handle a maximum of $7 \times 8 = 56$ instantaneous calls at one base station, provided that their quality was adequate. If a channel allocation request for a new call could not be satisfied immediately, it was queued for a duration of up to 5s, after which time, if not satisfied, it was classed as blocked. It was assumed that the network was synchronous from cell to cell, thus channels on different time slots of the same frequency were orthogonal in the time-domain and hence did not interfere with each other. The GSM-like system used a channel bandwidth of 200kHz, but instead of the Gaussian Minimum Shift Keying (GMSK) [11] based modulation scheme, 4-QAM was employed for the sake of increasing the achievable bandwidth efficiency from 1.35 bps/Hz to 1.64 bps/Hz. Hence, the achievable bit rate was 200kHz $\times$ 1.64bps/Hz = 328 kbps. When dividing this bit rate amongst the eight users supported by the eight timeslots, the channel rate of the users, neglecting overheads such as equaliser training sequences, tail sequences, guard periods and channel coding, became $328/8 = 41$ kbps. The call arrivals were Poisson distributed, and hence the call duration and inter-call periods were exponentially distributed [79, 95] with the mean values shown in Table 3.3.

Parameter	**Value**	**Parameter**	**Value**
Noisefloor	-104dBm	Multiple Access	F/TDMA
Frame duration	0.4615ms	Cell radius	218m
BS transmit power	10dBm	MS transmit power	10dBm
BS power control	No	MS power control	No
Number of base stations	49	Handover hysteresis	2dB
Outage SINR threshold	17dB	Re-allocation SINR threshold	21dB
Modulation scheme	4-QAM	Pathloss exponent	-3.5
Number of timeslots	8	Number of carriers	7
Average inter-call-time	300s	Max new-call queue-time	5s
Average call duration	60s	Reference signal modulation	BPSK
Beamforming algorithm	SMI	Reference signal length	8 bits
MS speed	30mph	Number of antenna elements	2, 4 & 8
Pathloss at 1m reference point	0dB	Shadow fading	No
Geometry of antenna array	Linear	Array element spacing	$\lambda/2$
Channel/carrier bandwidth	200kHz		

Table 3.3: Network simulation parameters.

The physical layer was modelled using two parameters, namely the 'Outage SINR' and 'Reallocation SINR', defined as the average Signal-to-Interference+Noise Ratio (SINR) required by a transceiver in order to satisfy the FER requirements over a narrowband Rayleigh

fading channel. More specifically, Pilot Symbol Assisted (PSA) 4-QAM transmitting 2 bits/symbol was assumed, which had an outage SINR of 17 dB and a reallocation SINR of 21 dB [12, 13]. When the signal quality, expressed in terms of the SINR, drops below the 'Reallocation SINR', a low quality access is encountered, and the mobile requests a new physical channel to handover to, thus initiating an intra- or inter-cell handover. If, while waiting for a reallocation handover, the signal quality drops further, below the so-called 'Outage SINR', defined as the SINR required to maintain a 10% FER, then an outage is encountered. A prolonged outage leads to the call being dropped or forcibly terminated. Since a user typically views a dropped call as less desirable than a blocked call, a Handover Queueing System (HQS) was employed. By forming a queue of the handover requests, which have a higher priority during contention for network resources than new calls, it is possible to reduce the number of dropped calls at the expense of a higher blocked call probability. A further advantage of the HQS is that a time window is formed, during which the handover may take place, enabling the user to wait, if necessary, for a slot to become free, thus increasing its chances of a successful handover. This twin-threshold physical layer model is similar to those described by Tekinay *et al.* [96] and Katzela *et al.* [97]. However, the model described here is based on SINR thresholds, rather than on the received power thresholds of Tekinay *et al.* [96] and Katzela *et al.* [97]. A further metric, namely the low signal quality probability, is calculated as the proportion of time that the SINR is below the 'Reallocation SINR' threshold.

Again, the 'Outage SINR' and 'Reallocation SINR' threshold were determined, with the aid of independent bit-level simulations, for BPSK, QPSK/4-QAM and 16-QAM [12, 13], conducted in a Rayleigh fading environment using approximately half-rate Bose-Chaudhuri-Hocquenghem (BCH) codes, which employed bit interleaving over the different number of bits per transmission frame conveyed by the different modem modes [98]. Thus, the 'Reallocation SINR' threshold was determined to be the average SINR required by the specific transceiver employed for maintaining a 5% transmission FER. This SINR value is transceiver dependent and in general can be reduced at the cost of increased transceiver complexity and power consumption. The loss of a maximum of 5% of the speech or video frames can be considered a worst-case scenario for modern 'wireless-oriented', i.e. error-resilient source codecs. Therefore, by setting the reallocation threshold at this level, the system requested handovers to new channels, before the speech or video quality degradation due to excessive FERs became objectionable.

The 'Outage SINR' threshold defines the SINR, below which the system declares that the radio channel has degraded to such a level, as to cause a service outage. If the radio channel continues to be in outage, then the call is forcibly terminated. The 'Outage SINR'

Modulation Scheme	Reallocation SINR threshold (dB) for 5% FER	Outage SINR threshold (dB) for 10% FER
BPSK	17	13
4-QAM	21	17
16-QAM	27	24

Table 3.4: The 'Reallocation SINRs' and 'Outage SINRs' used in the handover process, found by bit-level simulations for BPSK, QPSK/4-QAM, and 16-QAM modems. The 'Reallocation SINR' is the SINR, below which a channel reallocation will be requested, while the 'Outage SINR' is the SINR, below which a service outage is declared. Successive service outages render the call to be forcibly terminated.

threshold was determined by bit-level or physical layer simulations to be the average SINR required for maintaining a 10% FER. Therefore, if the radio channel degrades such that at least 10% of the speech or video frames were lost for some period of time, then the call would be forcibly terminated. The corresponding SINR thresholds based on bit-level simulations of BPSK, QPSK/4-QAM and 16-QAM modems are shown in Table 3.4.

The mobiles were capable of moving freely, at a speed of 30mph, in a fixed random direction, selected at the start of the simulation from a uniform distribution, within the simulation area of 49 traffic cells, each having a radius of 218m. Two different types of simulation area were invoked, the classical "desert island" type and the "wraparound" type. The "desert island" or "urban/sub-urban/rural" environment neglects the interference emanating from the cells surrounding the outside of the simulation area. In other words, the traffic cells at the centre of the simulation area are surrounded by interfering cells and thus are subjected to the highest levels of interference. However, the cells at the edges of the simulation area are not surrounded by interfering cells and hence are subjected to a lower level of interference. This can be likened to an "urban/sub-urban/rural" environment, where the centre cells represent the urban environment and the outer cells are considered to be low traffic-density rural cells in nature. However, this can lead to optimistic results, and hence often a "wraparound" simulation area is used [99, 100]. In order to facilitate the employment of an infinite plane of simulation area, a tessellating rhombic simulation area was used. Hence, the simulation area was replicated around itself, or tiled to form a larger, or effectively infinite, simulation area. More explicitly, mobile stations and their signals were "wrapped around" from one side of the network to the other [99, 100]. Hence, for example, a mobile station in call, which leaves the network at its edge, re-enters the network at the opposite side, whilst inflicting Co-Channel Interference (CCI) to **all** users, which may be positioned at any location in the network. Figure 3.15 depicts this scenario graphically.

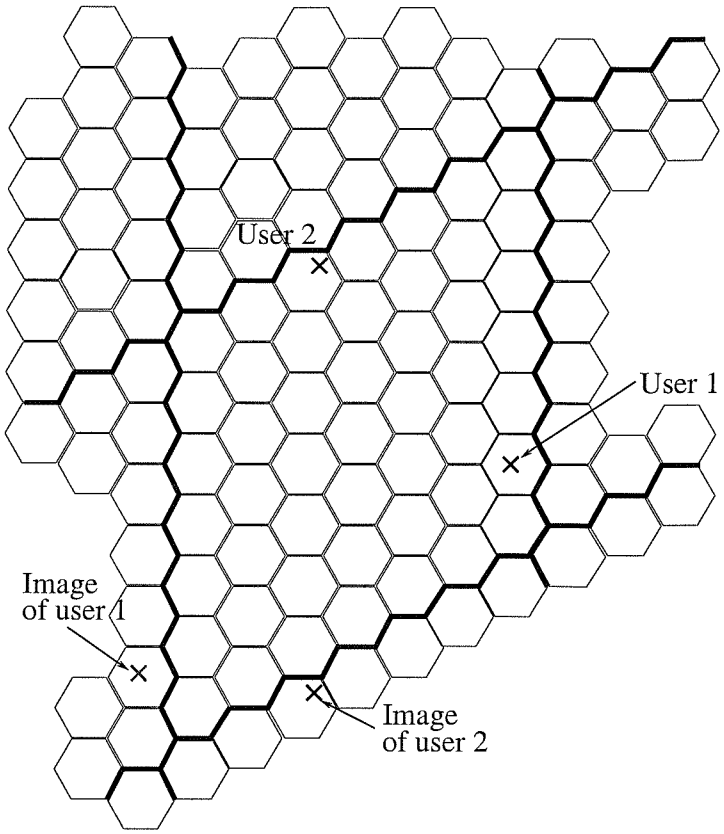

Figure 3.15: The 7x7 rhombic simulation area showing a user and its "wrapped" image.

The receiver antenna array weights were calculated using the Sample Matrix Inversion (SMI) algorithm [23, 25, 30], which determines the value of the AAA weights, such that they are optimised with respect to the received SINR [30]. In order to calculate the receiver antenna weights using the SMI algorithm, an eight-symbol long BPSK reference signal was assigned to the desired mobile. The remaining seven orthogonal eight-symbol duration BPSK reference symbols were then assigned to the interfering mobiles. However, any of these seven codes were allocated to more than one mobile, if the number of interferers was higher than seven. Thus, the desired mobile was uniquely identifiable, with the aid of its reference signal and the receiver antenna weights were optimised for obtaining the maximum received SINR, as detailed in Section 2.3.2.3. The calculation of the receiver antenna array weights was performed on a transmission frame-by-frame basis, leading to updated up- and down-link SINRs every transmission frame.

The base station's receiver antenna weights calculated for up-link reception may not be suitable for the down-link transmission due to the generally uncorrelated up- and down-link channels of Frequency Division Duplexed (FDD) systems. However, forming a feedback

loop by transmitting the mobiles' received reference signals back to the base station, and thus conveying the quality of the received reference signals, enables the employment of an iterative adaptive beamforming algorithm and would allow the base station to use the down-link weights as proposed in [68, 69]. In a Time Division Duplexed (TDD) system having a sufficiently short dwell time, the AAA weights calculated for up-link reception can also be used for down-link transmission, since the propagation channel does not vary significantly between the up- and down-link timeslots [6]. However, the system considered here is an FDD based network, and hence the assumption of channel predictability should therefore give an upper limit to the performance gains that may be achieved using an adaptive array. From now on we assume that the base station's receive and transmit, or up- and down-link, beam patterns are identical.

An example of the adaptive antenna array beam patterns generated by two element adaptive antenna arrays is shown in Figure 3.16. In this figure the mobiles are denoted by the use of small squares, while the base stations are represented by black filled circles. The solid black lines from the base stations to the users show the direction that the antenna array is steered in, and the gain in that direction. The half-tone grey lines pointing towards the mobiles represent the interfering signals, where the length of these lines is proportional to the gain of the antenna array in that direction. As it can be seen from the figure, the main beamwidth is large and, although there is some beneficial interference nulling, its extent is limited. For the four element adaptive antenna array, as in Figure 3.17, the beams in the direction of the desired users are significantly narrower, and hence the interference sources are nulled much more strongly, as indicated by the shortened half-tone lines. In both Figures 3.16 and 3.17 it can be seen that the antenna array beam patterns formed are symmetrical in the y-axis, as a direct consequence of the linear array geometry with the antenna array elements located on the y-axis. Using an alternative array geometry, such as a square or circle, would prevent this beam pattern symmetry from occurring and thus could potentially improve the achievable performance.

Both a purely Line-Of-Sight (LOS) propagation environment and a multipath propagation environment were considered. This multipath environment consisted of the Line-Of-Sight (LOS) ray and two additional rays, each having a third of the power of the LOS ray. The angles-of-arrival at the base station were determined using the Geometrically Based Single-Bounce Elliptical Model (GBSBEM) of Section 3.5 [86, 87], with its parameters chosen such that the multipath rays had one-third of the received power of the direct ray. The multipath received power criteria of Table 3.2 was used to determine the value of r_m to be used in the GBSBEM. Specifically, we opted for $r_m = 10^{(T-L_r)/10n}$, where T is the received power value in dBW, L_r is the reflection loss and n is the pathloss exponent. Furthermore, T was set

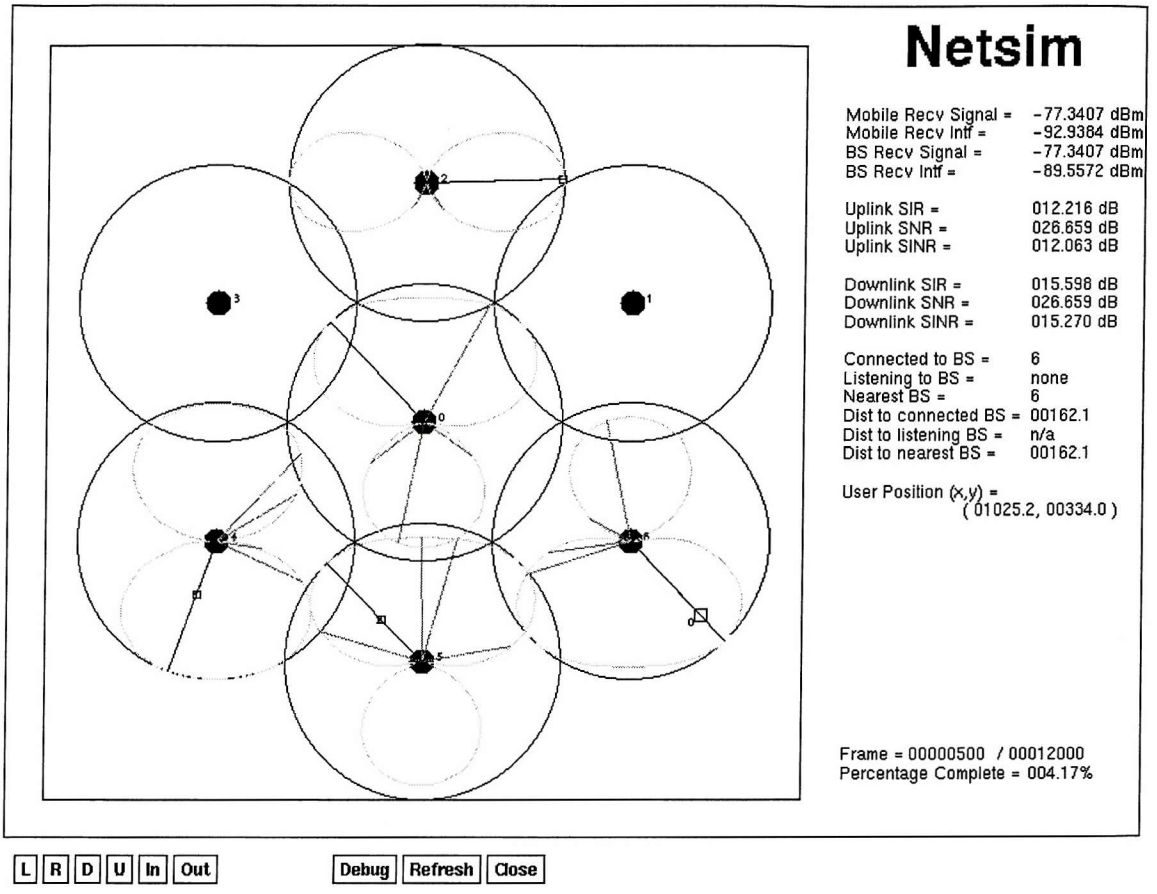

Figure 3.16: Screenshot of the simulation software, "Netsim", for a 7-cell, 5-user simulation, showing the identical up- and down-link, or receive and transmit, beam patterns generated by the adaptive antenna arrays using **2 elements** spaced by $\lambda/2$ on the y-axis. The squares represent the mobiles, with the large black circles denoting the base stations. The black lines from the base stations, passing through the squares representing the mobiles, show the array gain in the desired direction. The half-tone grey lines point in the direction of interfering sources, where the length of the line indicates the antenna gain in that direction.

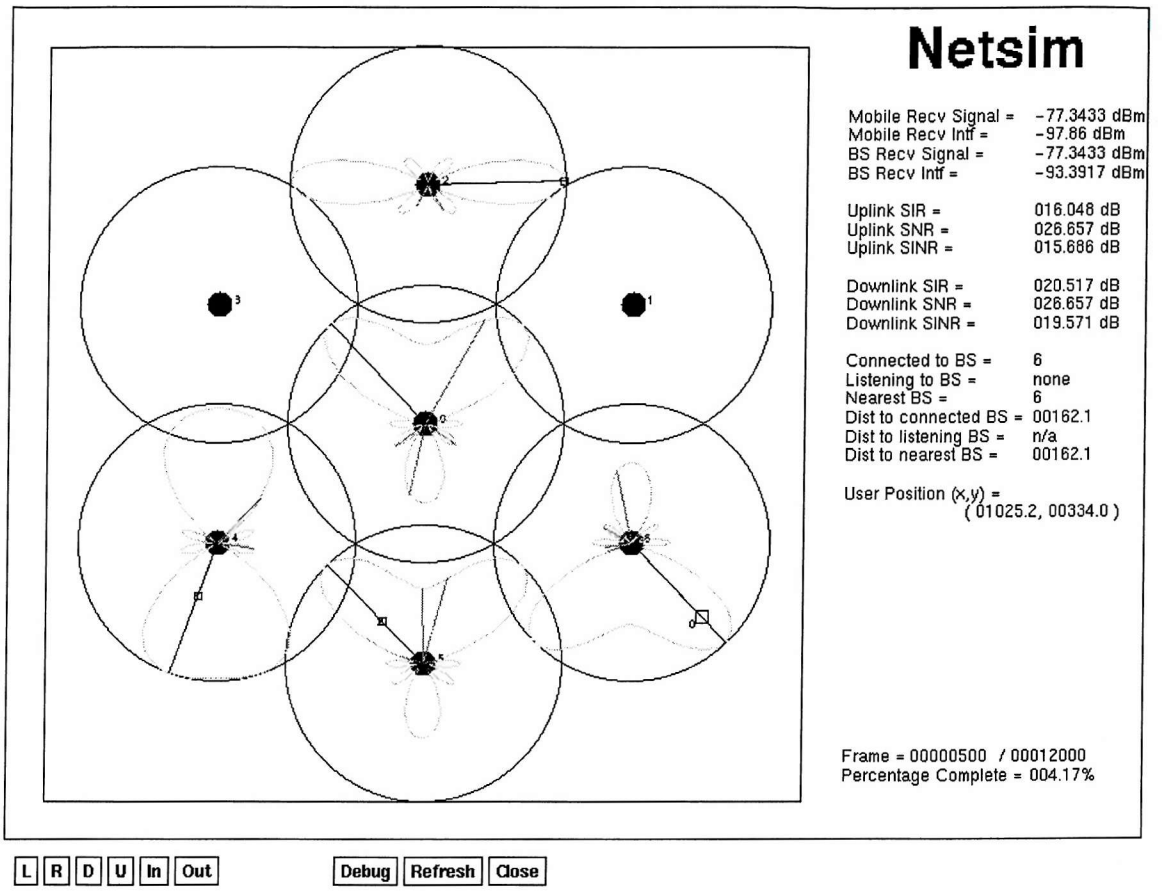

Figure 3.17: Screenshot of the simulation software, "Netsim", for a 7-cell, 5-user simulation, showing the identical up- and down-link, or receive and transmit, beam patterns generated by the adaptive antenna arrays using **4 elements** spaced by $\lambda/2$ on the y-axis. The squares represent the mobiles, with the large black circles denoting the base stations. The black lines from the base stations, passing through the squares representing the mobiles, show the array gain in the desired direction. The half-tone grey lines point in the direction of interfering sources, where the length of the line indicates the antenna gain in that direction.

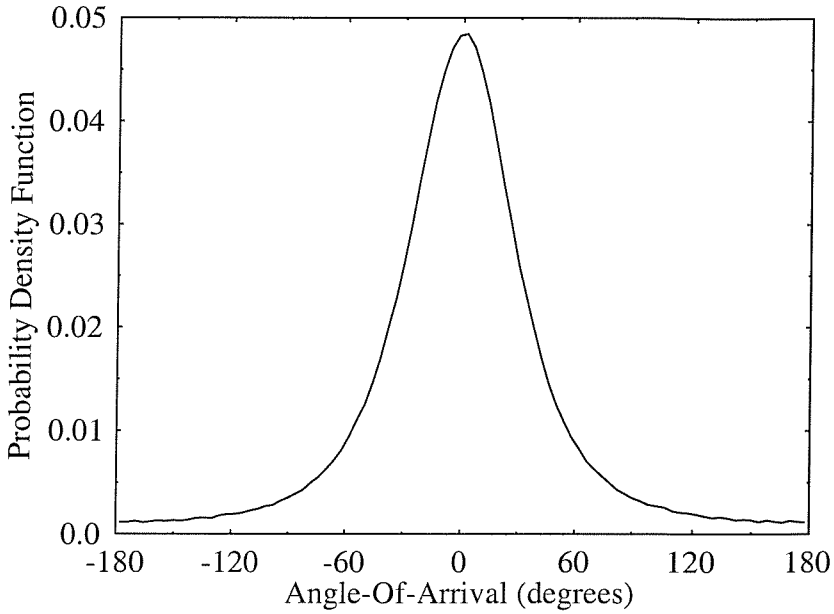

Figure 3.18: Probability density function of the angle-of-arrival of the up-link multipath rays, centred about the angle-of-arrival of the line-of-sight path. Furthermore, $r_m = 1.36874$ and 1 000 000 trials were used.

to 4.8dB with L_r equal to zero in conjunction with a pathloss exponent of 3.5, in order to achieve the desired received signal power of one-third that of the LOS ray. Hence, using the formulae of Section 3.5, $r_m = 10^{(4.8-0.0)/35} = 1.36874$, leading to, $\beta = r_m\sqrt{r_m^2 - 1} = 1.2792$. Since $r_i = \sqrt{\frac{1}{2} + \frac{1}{2}\sqrt{1 + 4\beta^2 x_i^2}}$ where x_i is a uniformly distributed random variable over $[0, 1]$, r_i varies from 1.0 to 1.36874. The PDF of the angle-of-arrival for r_m=1.36874 is shown in Figure 3.18, which was generated using the GBSBEM algorithm of Section 3.5 for 100 000 trials. It was assumed that all of these multipath rays arrived with zero time delay relative to the LOS path, or that a space-time equaliser [39, 45] was employed, thus making full use of the additional received signal energy. However, the numerous extra desired and interfering signals incident upon the antenna array rapidly consume the finite degrees of freedom of the antenna array, limiting its ability to fully cancel each source of interference.

The addition of multipath rays, for both the desired signal and the interference sources, results in many more received up-link signals impinging upon the antenna array at the base station. A result of the increased number of received up-link signals is that the limited degrees of freedom of the base station's adaptive antenna array are exhausted, resulting in

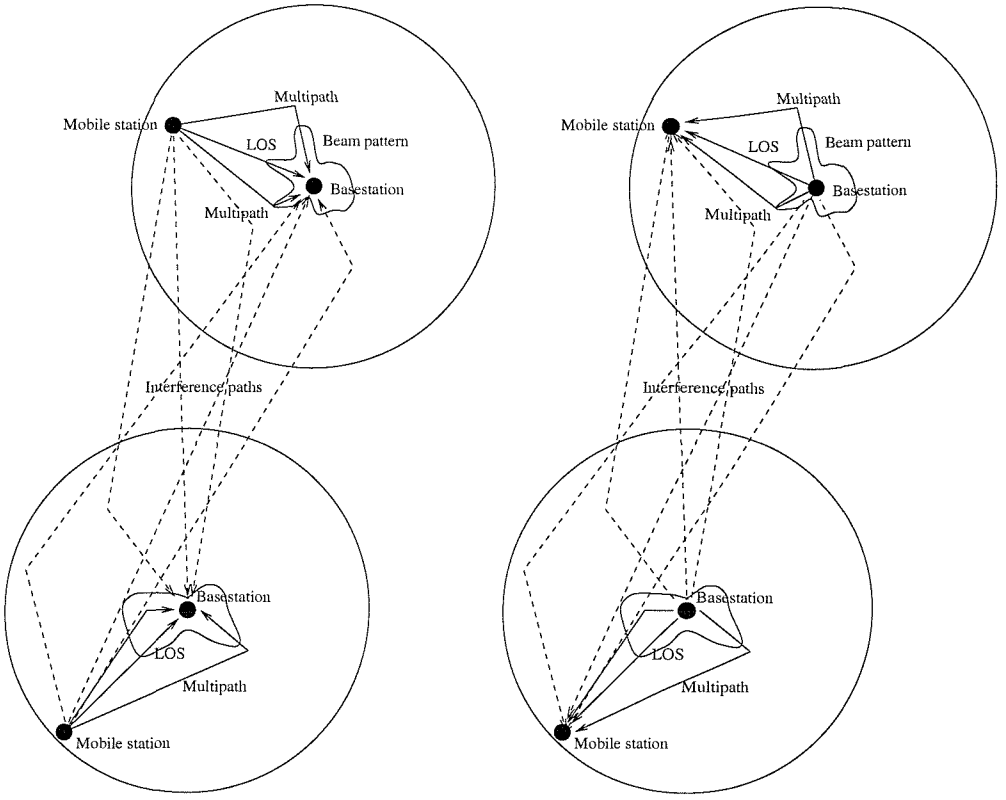

(a) Uplink. (b) Downlink.

Figure 3.19: The multipath environments of both the uplink and downlink, showing the multipath components of the desired signals, the line-of-sight interference and the associated base station antenna array beam patterns.

reduced nulling of the interference sources. A solution to this limitation is to increase the number of antenna elements in the base station's adaptive array, although this has the side effect of raising the cost and complexity of the array. In a macro-cellular system it may be possible to neglect multipath rays arriving at the base station from interfering sources since the majority of the scatterers are located close to the mobile station [42]. In contrast, in a micro-cellular system the scatterers are located in both the region of the reduced-elevation base station and that of the mobile, and hence multipath propagation must be considered. Figure 3.19 shows the simulated environment for both the up- and the downlink, with the multipath components of the desired signal and interference signals clearly illustrated, where the up- and downlinks are assumed to be reciprocal. When the DCA algorithm is "listening", in order to determine the best channel to be selected, only the LOS signals are considered with the multipath signals being neglected by the network simulator. However, at all other times the multipath signals are used in the calculation of the received signal and interference levels.

Figures 3.20, 3.21 and 3.22 show examples of the beam patterns obtained for two, four and eight element adaptive antenna arrays in the presence of multipath propagation. For the two element antenna array, as illustrated in Figure 3.20, the beamwidth of the antenna array is large, thus limiting its efficiency at nulling the sources of interference. Nonetheless, it can be seen from the beam patterns that the arrays are attempting to steer towards the desired signals, and away from the sources of interference. The desired signals are represented by the three black lines, where the black line passing through a square is the direct ray, and the remaining two black lines indicate the multipath rays from the desired user. Observe in the figures that these lines generally end on the unity-gain circles, and therefore are received with a gain of one by the base station. The dark grey lines are the LOS paths from the interference sources, with the two multipath rays of each interferer denoted by the light grey lines. The beam pattern of base station "1" is a good example of how the array is steering towards the desired signal paths, and away from the interference. For base station "5", at the bottom of Figure 3.20, the small angular separation between the arriving signals, and the end-fire location of these sources, makes rejection of the interference harder to accomplish. The use of a four element antenna array, depicted in Figure 3.21, results in more successful nulling of the interference sources, but again, for base station "5" at the bottom, the similar angular location of the desired and interfering sources results in poor interference cancellation performance. Figure 3.22 shows that an eight element adaptive antenna array performs well in most cases, nulling the sources of interference strongly, whilst efficiently steering towards the desired signals. Using an alternative layout of the antenna elements, rather than the uniform linear array, should minimise the possibility of a situation, similar to that of base station "5", where all the sources are located at end-fire, which is the area of poorest performance of the array.

Having described the simulation parameters, in the next section we present our simulation results, quantifying the amount of traffic that can be carried by each of the simulated networks, whilst maintaining the required network quality.

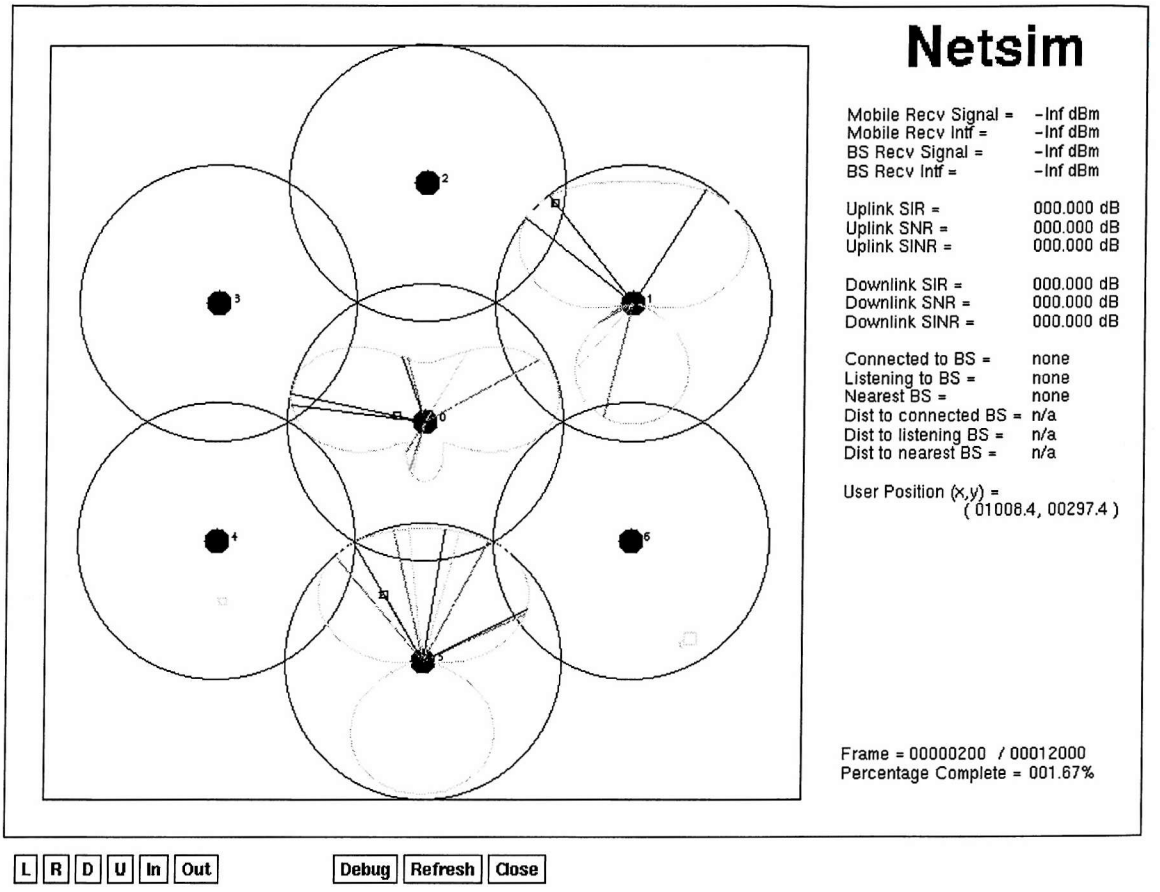

Figure 3.20: Screenshot of the simulation software, "Netsim", for a 7-cell, 5-user scenario, showing the beam patterns generated by the adaptive antenna arrays using **2 elements** spaced by $\lambda/2$ on the y-axis. The squares represent the users, with the large black circles denoting the base stations. The black lines from the base stations, passing through the squares representing the mobiles, show the array gain in the desired direction, the black lines not passing through the squares are the desired user's multipath rays. The dark grey lines are the LOS interference paths, while the interferer's multipath components are illustrated by the light grey lines, where the length of the line is proportional to the corresponding antenna gains in their directions.

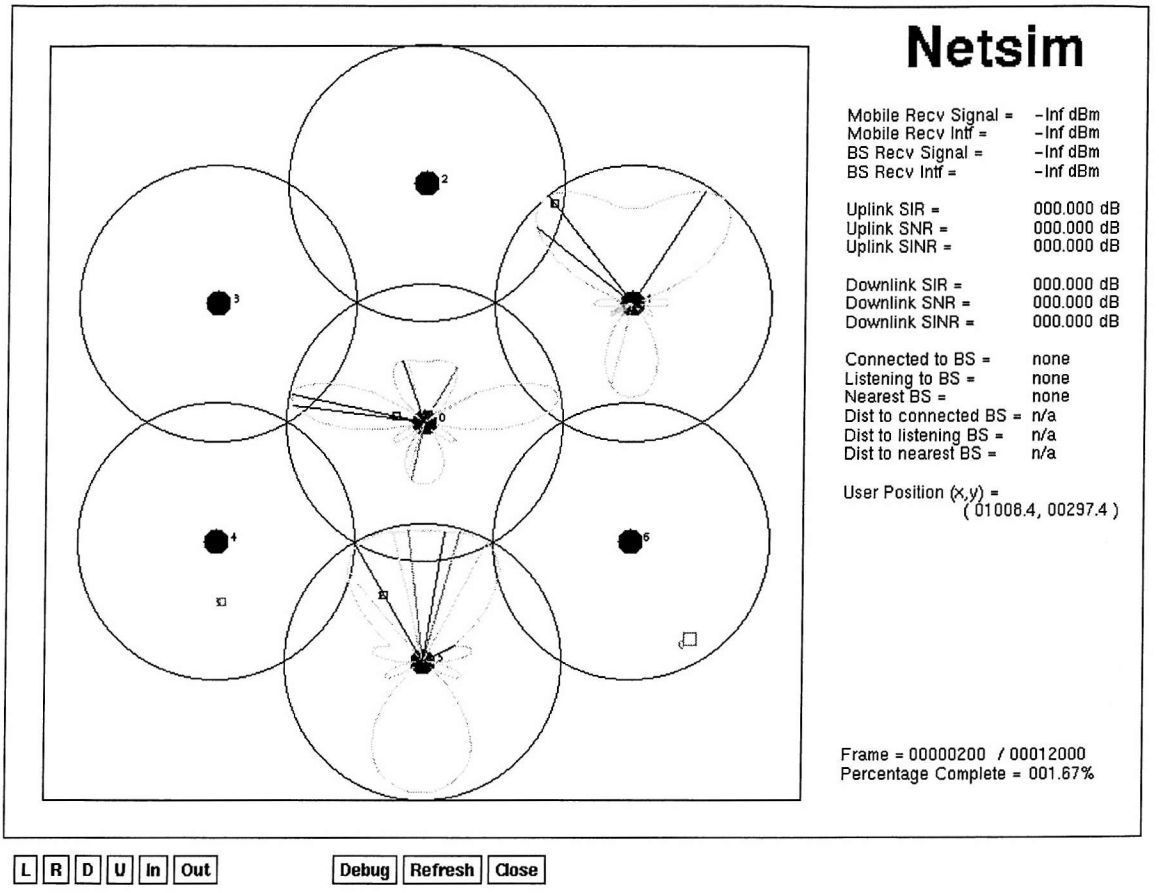

Figure 3.21: Screenshot of the simulation software, "Netsim", for a 7-cell, 5-user scenario, showing the beam patterns generated by the adaptive antenna arrays using **4 elements** spaced by $\lambda/2$ on the y-axis. The squares represent the users, with the large black circles denoting the base stations. The black lines from the base stations, passing through the squares representing the mobiles, show the array gain in the desired direction, the black lines not passing through the squares are the desired user's multipath rays. The dark grey lines are the LOS interference paths, while the interferer's multipath components are illustrated by the light grey lines, where the length of the line is proportional to the corresponding antenna gains in their directions.

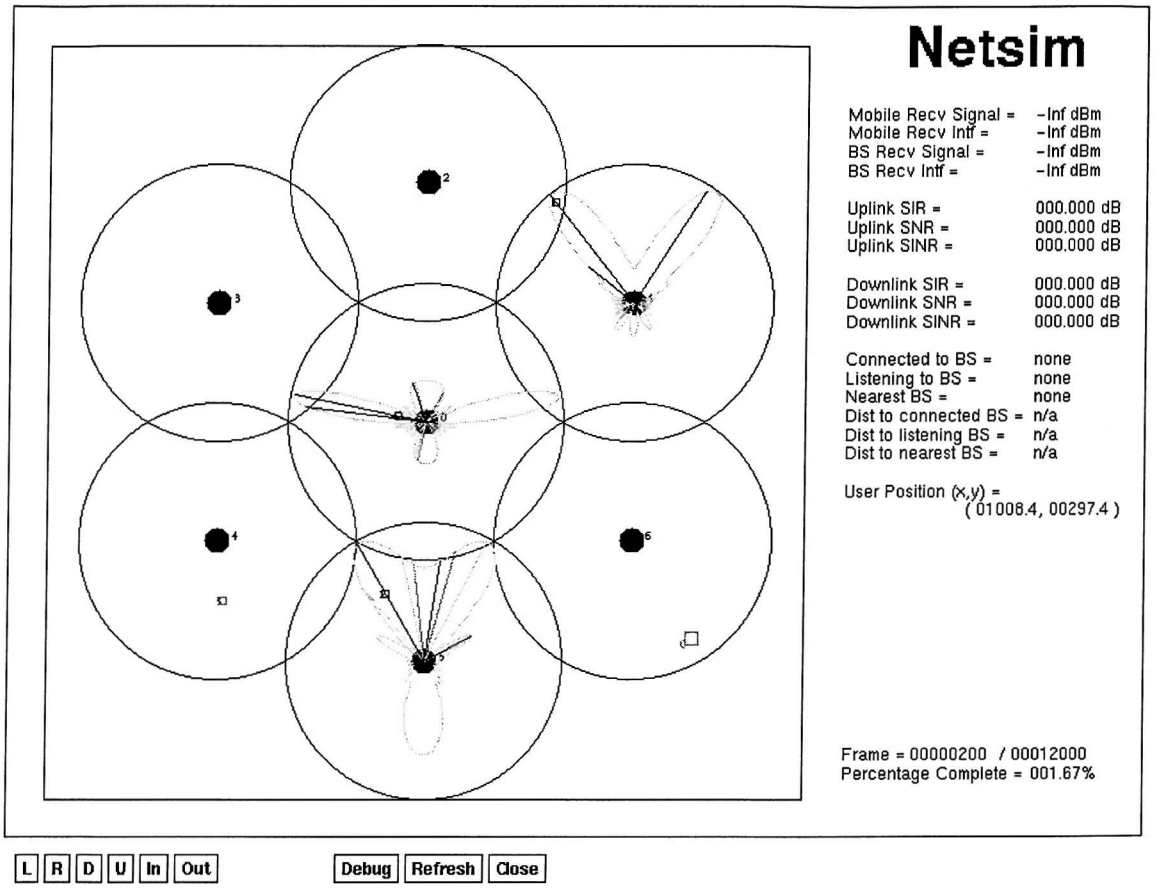

Figure 3.22: Screenshot of the simulation software, "Netsim", for a 7-cell, 5-user scenario, showing the beam patterns generated by the adaptive antenna arrays using **8 elements** spaced by $\lambda/2$ on the y-axis. The squares represent the users, with the large black circles denoting the base stations. The black lines from the base stations, passing through the squares representing the mobiles, show the array gain in the desired direction, the black lines not passing through the squares are the desired user's multipath rays. The dark grey lines are the LOS interference paths, while the interferer's multipath components are illustrated by the light grey lines, where the length of the line is proportional to the corresponding antenna gains in their directions.

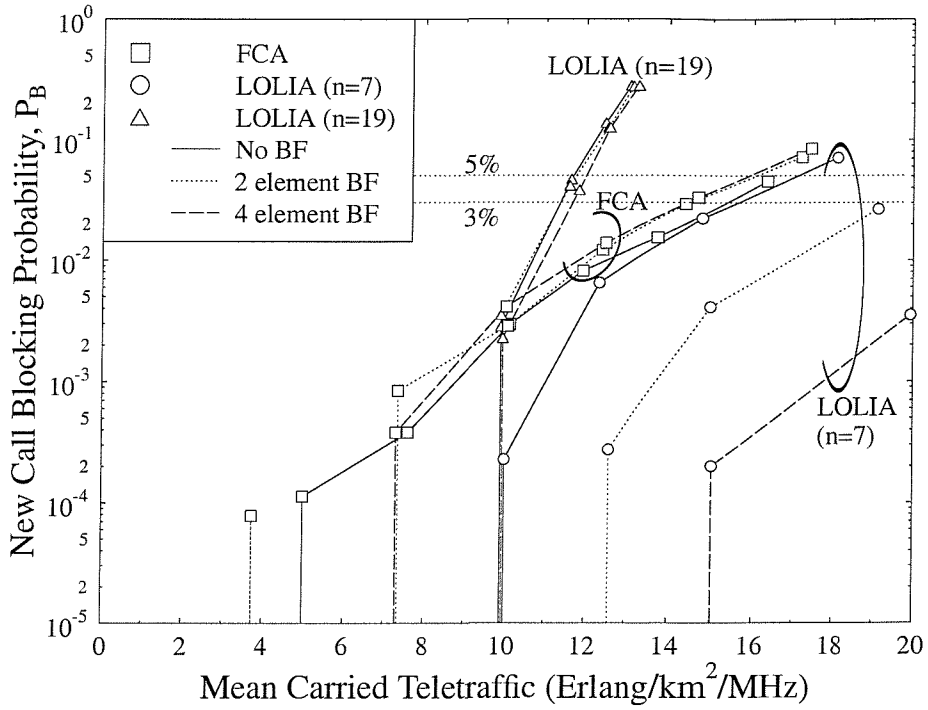

Figure 3.23: New call blocking probability performance versus mean carried traffic, for comparison of the LOLIA, with 7 and 19 "local" base stations, and of FCA using a 7-cell reuse cluster, under a uniform geographic traffic distribution, for a single antenna element as well as for two and four element antenna arrays with beamforming in an **LOS environment**. See Figure 3.29 for the corresponding multipath results.

3.7.2 Non-Wraparound Network Performance Results

The results presented in this section were obtained for the "desert-island" or "urban/sub-urban/rural" scenario, i.e. with the highest levels of interference present at the centre of the simulation area. Results were obtained for single, two and four element antenna arrays over a LOS channel for both the FCA algorithm and the LOLIA with exclusion zones of 7 and 19 cells. This work was then extended to provide network capacity estimates for non-LOS or multipath channels using adaptive antenna arrays comprising two, four and eight elements. Power control and adaptive modulation techniques were also employed for increasing the network capacity further.

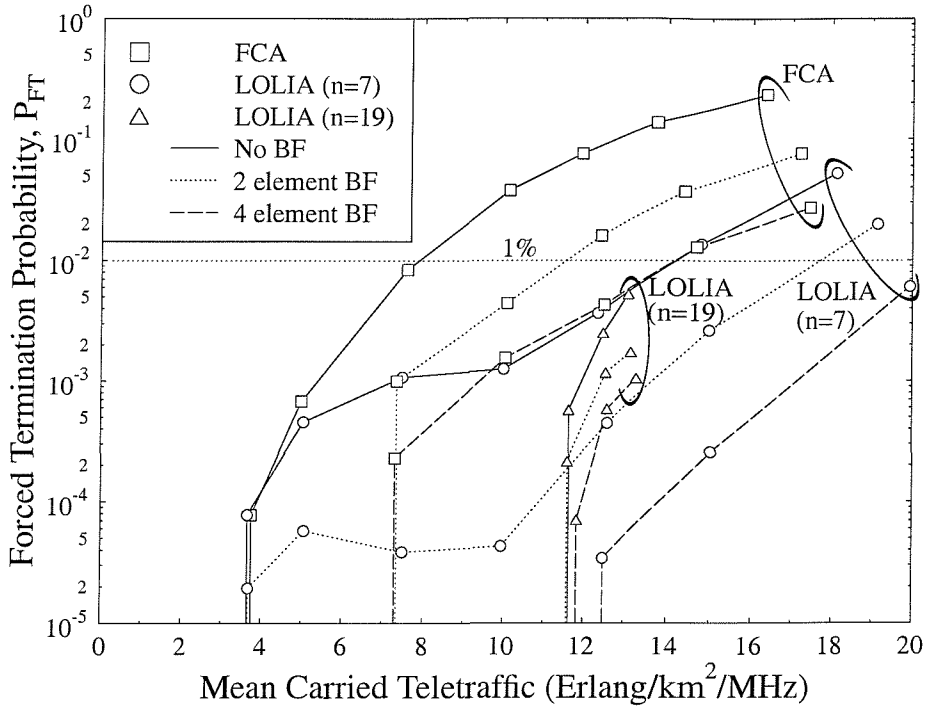

Figure 3.24: Call dropping probability performance versus mean carried traffic, for comparison of the LOLIA, with 7 and 19 "local" base stations, and of FCA using a 7-cell reuse cluster, under a uniform geographic traffic distribution, for a single antenna element as well as for two and four element antenna arrays with beamforming in an **LOS environment**. See Figure 3.30 for the corresponding multipath results.

3.7.2.1 Performance Results over a LOS Channel

Figure 3.23 shows the new call blocking probability for a variety of uniform traffic loads, measured in terms of the mean normalised carried traffic, with units of Erlangs/km^2/MHz. The figure shows that for a given traffic load, both FCA and the LOLIA, using an exclusion zone of $n = 19$ maintained a fairly similar probability of new call blocking, regardless of the number of elements in the antenna array. In the case of the FCA algorithm, this was due to the limited number of frequency/timeslot combinations available as a direct result of the fixed nature of the network. However, for the LOLIA having an exclusion zone of 19 cells, the lack of frequency/timeslot combinations was due to the large exclusion zone. Thus, using the smaller exclusion zone of 7 cells led to a significantly reduced new call blocking probability. The figure also shows that, since the new call blocking probability of the LOLIA using $n = 7$ was reduced, thanks to the adaptive antenna arrays, the new call blocking performance was interference limited. This contrasts with the FCA algorithm

and the LOLIA using $n = 19$, whose new call blocking performance was limited by the availability of frequency/timeslot combinations. It is interesting to note that, in terms of its new call blocking probability, the FCA algorithm performed better using only one antenna element as a result of its significantly increased call dropping probability, which freed up network resources, thus enabling more new calls to start.

The call dropping probability of the FCA algorithm, and that of the LOLIAs is depicted in Figure 3.24 for one, two and four element antenna arrays, when subjected to varying uniform traffic loads. The FCA algorithm suffered from the highest call dropping probability of the three channel allocation schemes. With a four element adaptive antenna array it similarly to the LOLIA using $n = 7$ and a single antenna element for teletraffic loads higher than 10 Erlang/km^2/MHz. For teletraffic levels below this point, the FCA algorithm offered superior performance due to the call dropping probability "floor" experienced by the LOLIA using $n = 7$. The large exclusion zone of the LOLIA using $n = 19$ resulted in a very low probability of forced termination until the system approached its maximum capacity of around 12 Erlang/km^2/MHz, where the dropping probability increased rapidly. However, the performance of the LOLIA with $n = 19$ still exceeded that of both the FCA algorithm and the LOLIA with $n = 7$ due to the low levels of co-channel interference resulting from the high frequency re-use distance associated with the large exclusion zone.

Figure 3.25 shows the probability of low quality access versus various uniform traffic loads. The figure shows our results for the FCA algorithm and the LOLIA for nearest base station constraints of 7 and 19 cells. Again, the LOLIA with $n = 19$ offered the best performance at the lower traffic levels, but the low-quality access probability increased the most rapidly as the traffic load increased. For a given traffic load the LOLIA using $n = 19$ provided the lowest probability of a low quality access. This resulted from the low level of co-channel interference of the network and the interference rejection capabilities of the adaptive antenna arrays. The figure shows that all of the channel allocation schemes benefited from the use of the adaptive antenna arrays.

Figure 3.26 shows the Grade-Of-Service (GOS) for a range of uniform teletraffic loads. The figure shows results for the FCA algorithm and the LOLIAs with nearest base station constraints of 7 and 19 cells, for cases of a single antenna element as well as for two and four element adaptive antenna arrays. The grade of service is better, i.e. lower, for larger exclusion zone size when the traffic load is low, which is reversed for high traffic loads. This is mainly attributable to the higher call blocking probability of the larger exclusion zone of 19 cells, particularly in the region of the highest traffic loads. The GOS for the FCA scheme follows the probability of a blocked call and the dropping probability trends by increasing smoothly and monotonically with the traffic load.

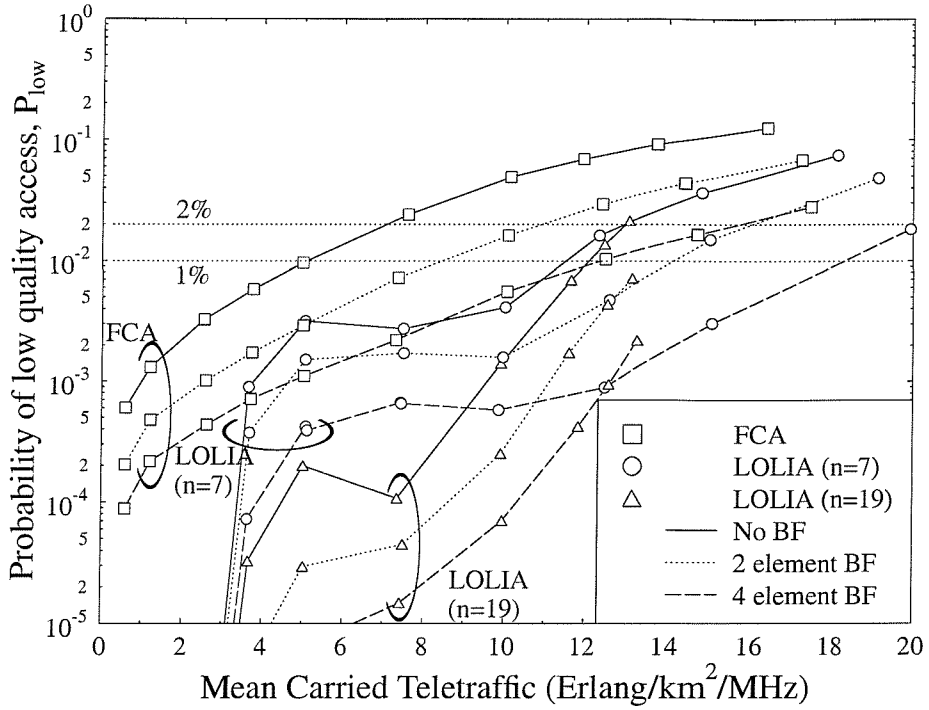

Figure 3.25: Probability of low quality access versus mean carried traffic, for comparison of the LOLIA, with 7 and 19 "local" base stations, and of FCA using a 7-cell reuse cluster, under a uniform geographic traffic distribution, for a single antenna element as well as for two and four element antenna arrays with beamforming in an **LOS environment**. See Figure 3.31 for the corresponding multipath results.

The effect of beamforming on the number of handovers performed can be seen in Figure 3.27. The performance of the LOLIAs was barely altered by the use of beamforming, with both performing the lowest number of handovers per call. At the highest teletraffic loads it can be seen that the LOLIA using an exclusion zone of 7 base stations benefited slightly from the use of the adaptive antenna arrays. In contrast, the number of handovers performed by the FCA algorithm was reduced significantly as a benefit of using adaptive antennas with a maximum reduction in the mean number of handovers performed per call of 69% for two elements, and of 86% for four elements. This translates into a significantly reduced load for the network, since it has to manage far less handovers, therefore reducing the complexity of the network infrastructure. As the network load exceeded about 12 Erlangs/km^2/MHz, the mean number of handovers performed per call dropped due to the excessive call dropping probability, since calls were being dropped before they could handover, thus reducing the number of handovers.

Figure 3.28 portrays the mean carried teletraffic versus the number of mobiles in the

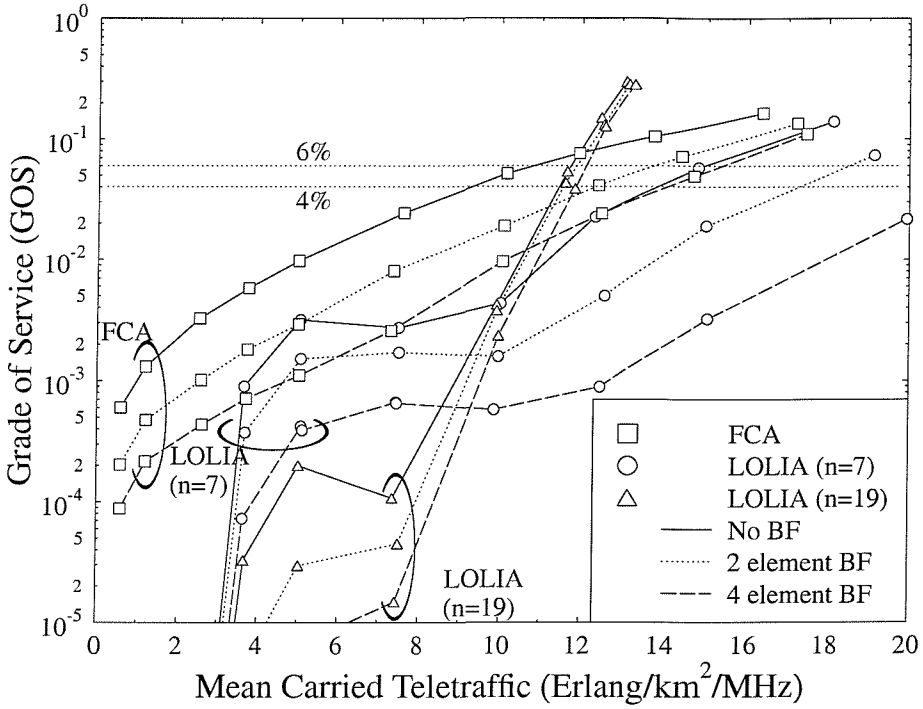

Figure 3.26: Grade-Of-Service (GOS) performance versus mean carried traffic, for comparison of the LOLIA, with 7 and 19 "local" base stations, and of FCA using a 7-cell reuse cluster, under a uniform geographic traffic distribution, for a single antenna element as well as for two and four element antenna arrays with beamforming in an **LOS environment**. See Figure 3.32 for the corresponding multipath results.

simulated system. The figure shows that at low traffic loads both FCA and the LOLIA carry virtually identical amounts of traffic. However, as the mobile density, and hence the traffic load, is increased, the LOLIA with the nearest base station limit of 19 reaches its maximum traffic load and cannot carry further traffic. The large frequency reuse distance of the LOLIA with $n = 19$ resulted in the performance of the network being resource limited, with the associated low levels of co-channel interference restricting the ability of the adaptive antenna arrays to reduce the interference level. Hence, in Figure 3.28 increasing the number of antenna elements constituting the adaptive antenna array does not increase the number of users supported by the network, which is limited by the availability of frequency/timeslot combinations, as indicated by the "flattening" of the performance curve. For FCA and the LOLIA with $n = 7$, the advantage of using adaptive antennas can be seen from the figure, since they enable a higher level of traffic to be carried, at a higher quality, than a system without adaptive antenna arrays. The performance gain attained by the LOLIA, over the FCA algorithm, is also shown in Figure 3.28, which illustrates the increase in carried traffic

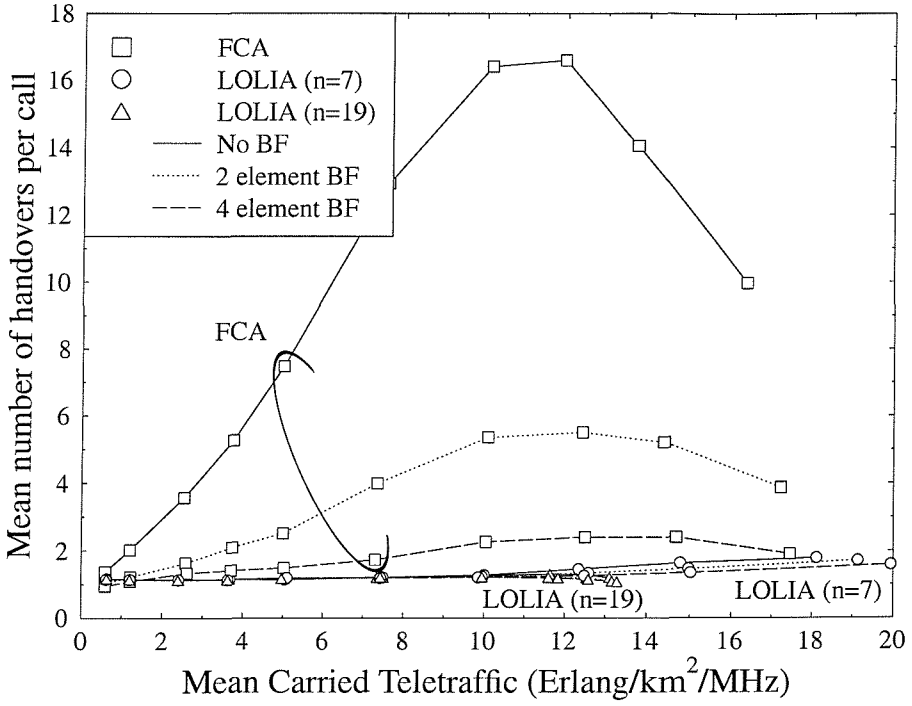

Figure 3.27: The mean number of successful handovers per call versus mean carried traffic, for comparison of the LOLIA, with 7 and 19 "local" base stations, and of FCA using a 7-cell reuse cluster, under a uniform geographic traffic distribution, for a single antenna element as well as for two and four element antenna arrays with beamforming in an **LOS environment**. See Figure 3.33 for the corresponding multipath results.

as a result of the dynamic configurability of DCA schemes.

It can be seen from Table 3.5 that for all of the channel allocation schemes, the use of adaptive antenna arrays at the receiver resulted in increased carried teletraffic, hence supporting a higher number of simultaneous users. The FCA algorithm benefited most from the use of adaptive antennas with a 67% increase in the number of users supported when using two antenna elements and a 144% rise in the carried traffic, when using an adaptive array with four elements. The LOLIA associated with $n = 7$, supported a higher number of users than FCA although the capacity increases obtained through the use of adaptive antenna arrays were more limited. Specifically, a two element array carried an extra 22% of users and with the aid of four elements it supported 58% more users. Using a channel exclusion zone of 19 base stations gave a slight performance advantage over the 7-cell variant for the conservative scenario of Section 3.6, but only without adaptive antennas. Employing adaptive antennas had little effect on the number of users supported by the network using the LOLIA with $n = 19$, increasing the traffic carried by only a small

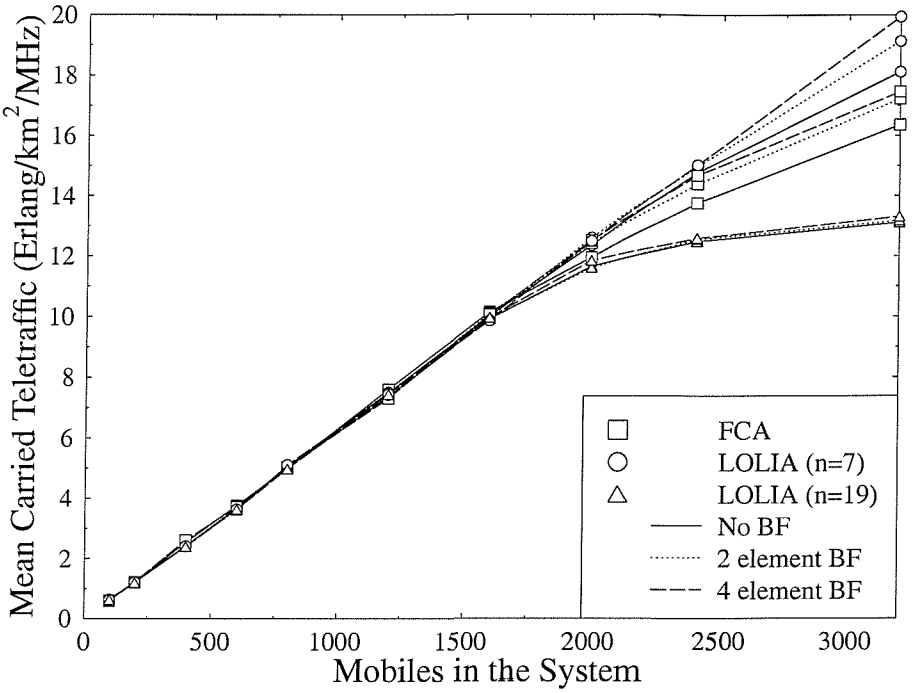

Figure 3.28: Mean traffic carried versus the number of mobiles in the system, for comparison of the LOLIA, with 7 and 19 "local" base stations, and of FCA using a 7-cell reuse cluster, under a uniform geographic traffic distribution, for a single antenna element as well as for two and four element antenna arrays with beamforming in an **LOS environment**. See Figure 3.34 for the corresponding multipath results.

margin. The corresponding multipath results are summarised in Table 3.6 with network configurations common between the two highlighted in bold.

Algorithm	Conservative $P_{FT} = 1\%$, $P_{low} = 1\%$ $GOS = 4\%$, $P_B = 3\%$			Lenient $P_{FT} = 1\%$, $P_{low} = 2\%$ $GOS = 6\%$, $P_B = 5\%$		
	Users	**Traffic**	**Limiting Factor**	**Users**	**Traffic**	**Limiting Factor**
FCA, 1 element	815	5.10	P_{low}	1115	7.05	P_{low}
FCA, 2 elements	**1360**	8.45	P_{low}	**1755**	11.00	P_{low}
FCA, 4 elements	**1985**	12.40	P_{low}	**2710**	15.75	P_{low}
LOLIA (n=7), 1 element	1855	11.50	P_{low}	2110	13.00	P_{low}
LOLIA (n=7), 2 elements	**2260**	14.15	P_{low}	**2600**	16.00	P_{low}
LOLIA (n=7), 4 elements	**2935**	18.30	P_{low}	**>3200**	>20.00	P_{low}
LOLIA (n=19), 1 element	1935	11.35	P_B	2010	11.65	P_B
LOLIA (n=19), 2 elements	**1940**	11.35	P_B	**2045**	11.70	P_B
LOLIA (n=19), 4 elements	**1960**	11.65	P_B	**2090**	12.00	P_B

Table 3.5: Maximum mean carried traffic, and the maximum number of mobile users that can be supported by each configuration whilst meeting the preset quality constraints of Section 3.6. The carried traffic is expressed in terms of normalised Erlangs (Erlang/km^2/MHz), for the network described in Table 3.3 in an **LOS environment**.

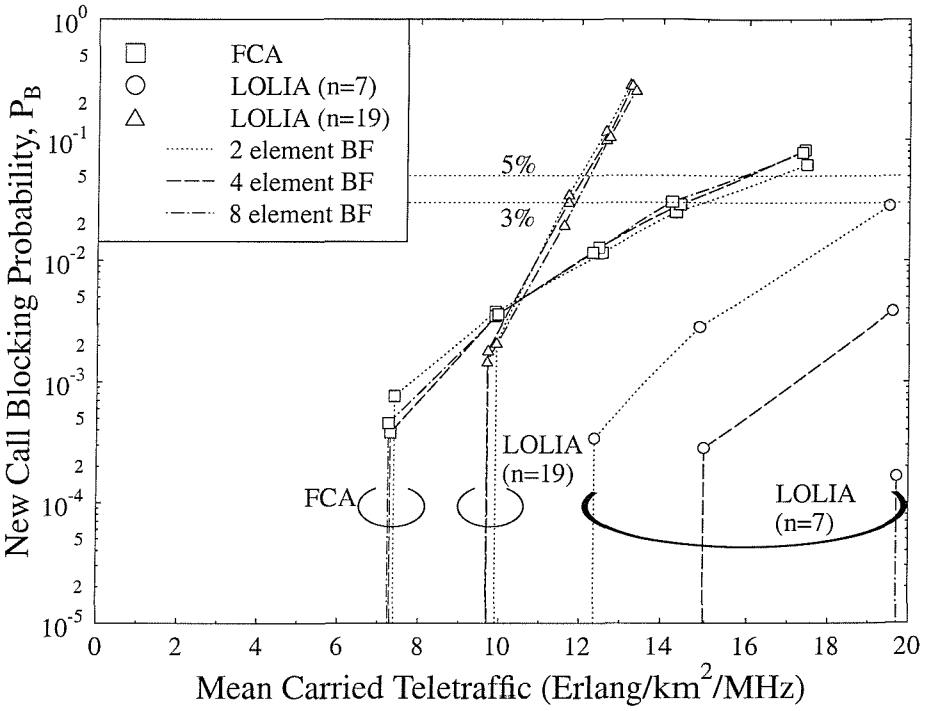

Figure 3.29: New call blocking probability performance versus mean carried traffic, for comparison of the LOLIA, with 7 and 19 "local" base stations, and of FCA using a 7-cell reuse cluster, under a uniform geographic traffic distribution, for two, four and eight element antenna arrays with beamforming in a **multipath environment**. See Figure 3.23 for the corresponding LOS results.

3.7.2.2 Performance Results over a Multipath Channel

Following our previous simulations, where a purely LOS environment existed between the mobiles and their base stations, this section presents our performance results for the multipath environment described in Section 3.7.1, using two, four and eight element adaptive antenna arrays.

Comparing the blocking probabilities of the multipath environment, in Figure 3.29, with those of the LOS environment, which were portrayed in Figure 3.23, reveals that the FCA algorithm and both the LOLIAs behaved similarly in both propagation environments. Again, only the LOLIA with an exclusion zone of 7 base stations benefited from the use of the adaptive antenna arrays in terms of the new call blocking probability.

In Figure 3.30 the probability of a dropped call in a multipath environment is presented which, for the FCA algorithm, was similar under the multipath propagation conditions to that of the LOS scenario in Figure 3.24. The LOLIA using an exclusion zone of 7

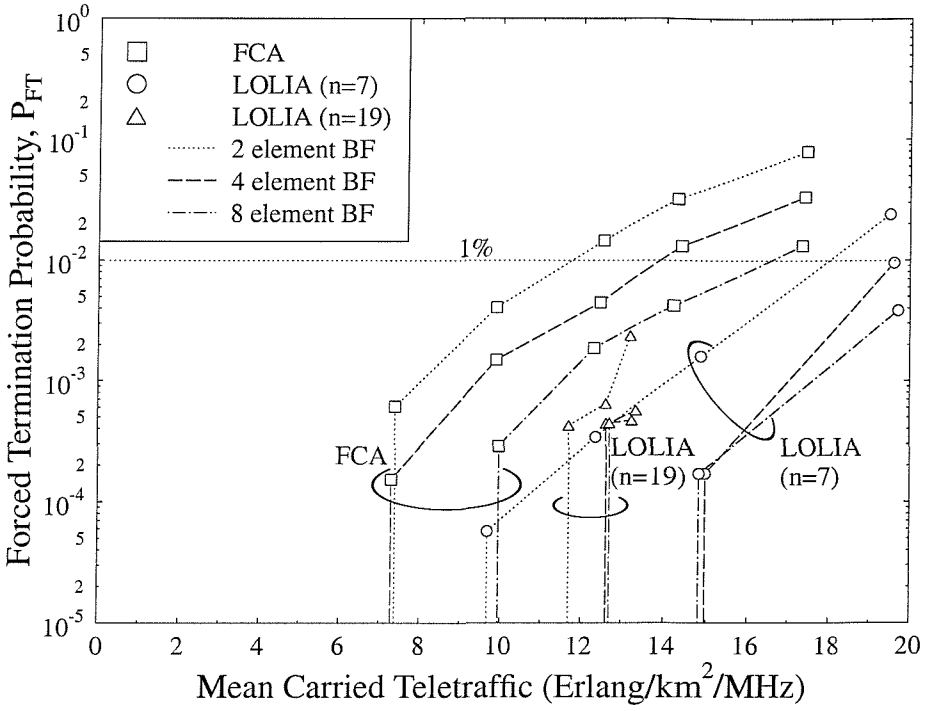

Figure 3.30: Call dropping probability performance versus mean carried traffic, for comparison of the LOLIA, with 7 and 19 'local' base stations, and of FCA using a 7-cell reuse cluster, under a uniform geographic traffic distribution, for two, four and eight element antenna arrays with beamforming in a **multipath environment**. See Figure 3.24 for the corresponding LOS results.

base stations also exhibited call dropping probabilities close to those observed in the LOS scenario, when using a two element adaptive antenna array. In conjunction with a four element antenna array the performance was slightly degraded in the multipath scenario, but using the eight element antenna array resulted in superior performance to that of the four element array in the LOS environment. There was a slight call dropping performance improvement for the LOLIA using $n = 19$.

The probability of low quality access is depicted in Figure 3.31. The FCA algorithm did not perform as well, with respect to the probability of a low quality access, in the multipath propagation environment, when compared to the LOS case of Figure 3.25. The same was true of the LOLIA using $n = 7$ at higher traffic levels, although, at lower levels of traffic the performance in the multipath case was superior. At low levels of traffic the average level of interference was relatively low, and hence the extra signal power received in the multipath environment resulted in a reduced chance of a low quality access occurring. However, at higher levels of teletraffic, the background interference level was higher than in

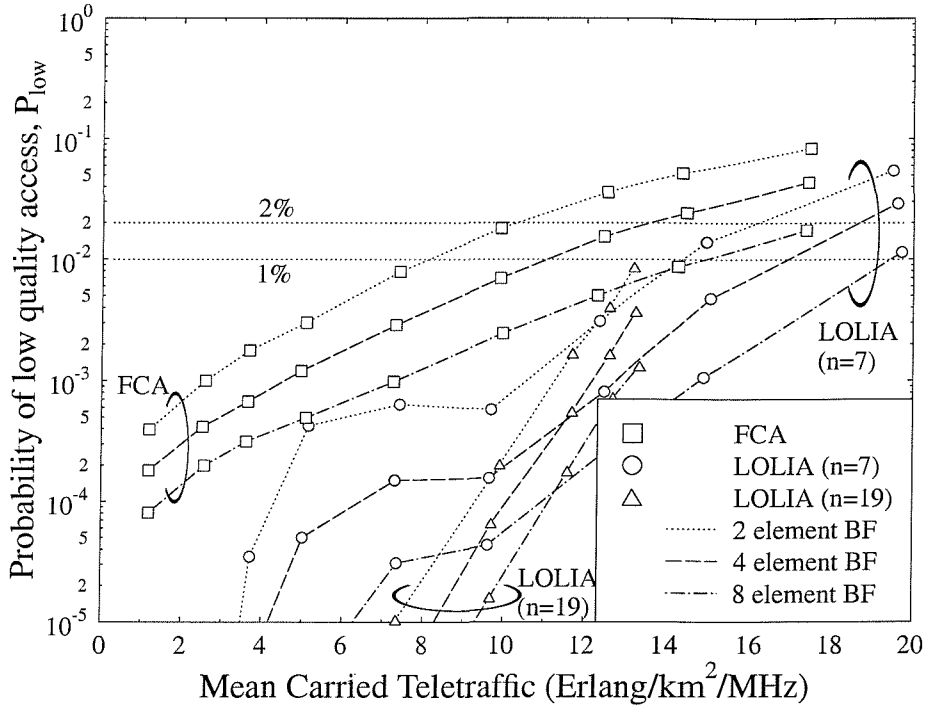

Figure 3.31: Probability of low quality access versus mean carried traffic, for comparison of the LOLIA, with 7 and 19 'local' base stations, and of FCA using a 7-cell reuse cluster, under a uniform geographic traffic distribution, for two, four and eight element antenna arrays with beamforming in a **multipath environment**. See Figure 3.25 for the corresponding LOS results.

the LOS scenario of Figure 3.25, and hence the extra received power had a less beneficial impact, in fact the multipath components created additional interference. The LOLIA using an exclusion zone of 19 base stations and an adaptive antenna array of two elements performed better in the multipath case. However, in conjunction with four elements it offered a superior performance in the LOS scenario of Figure 3.25. Overall, the improvement in the probability of low quality access through increasing the number of adaptive antenna array elements, was reduced in the multipath propagation environment, since the added interference power outweighed the increased received signal power. This ultimately reduced the prevalent SINR even when using adaptive antenna arrays.

As expected on the basis of Equation 3.23, the FCA algorithm and the LOLIA with $n = 19$, offered a similar GOS performance for both the LOS scenario of Figure 3.26 and for the multipath environment. Figure 3.32 also shows that the GOS of the FCA algorithm using a given number of antenna elements is inferior to the GOS of the LOS propagation environment characterised in Figure 3.26, as for the probability of low quality access seen

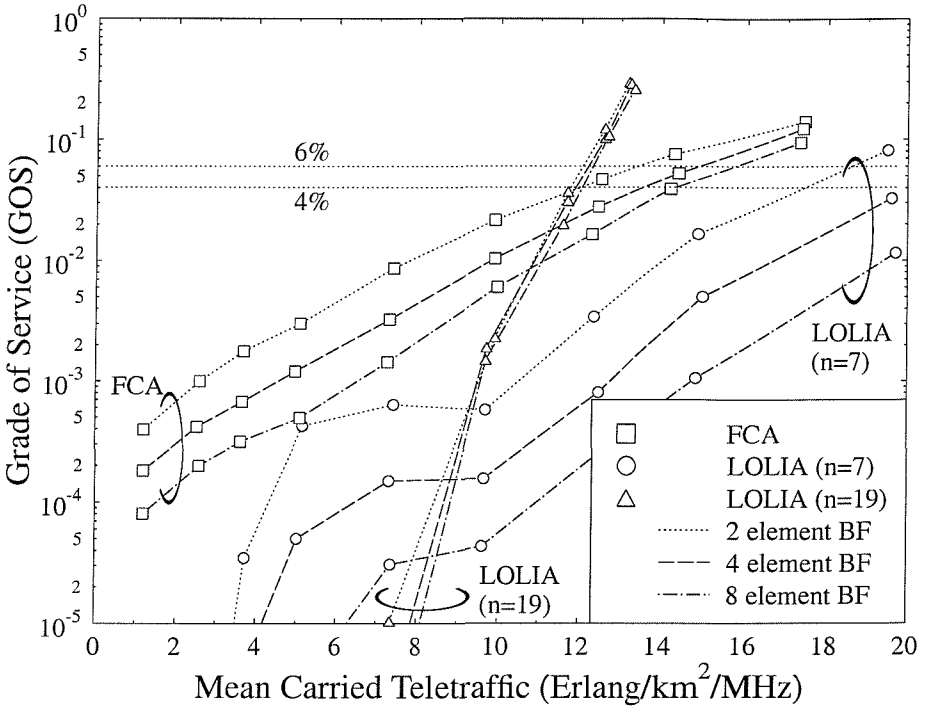

Figure 3.32: Grade-Of-Service (GOS) performance versus mean carried traffic, for comparison of the LOLIA, with 7 and 19 'local' base stations, and of FCA using a 7-cell reuse cluster, under a uniform geographic traffic distribution, for two, four and eight element antenna arrays with beamforming in a **multipath environment**. See Figure 3.26 for the corresponding LOS results.

in Figures 3.25 and 3.31. At network loads of less than about 13 Erlang/km^2/MHz, the GOS of the LOLIA with $n = 7$ was superior to that of the LOS environment in Figure 3.26, however, above this carried traffic value the performance was worse.

Figure 3.33 demonstrates the significant impact that adaptive antennas have on the mean number of handovers per call for the FCA algorithm in a multipath environment. As in the LOS propagation environment characterised in Figure 3.27, more handovers per call were initiated, when using FCA system employing two or four element antenna arrays, than for either of the LOLIAs using a single antenna element. Furthermore, a higher number of handovers was required in the multipath environment, than in the LOS scenario of Figure 3.27, for a given antenna array configuration. The LOLIA schemes performed much fewer handovers than FCA, irrespective of the propagation environment, and generally did not appear to benefit from the employment of adaptive antennas in terms of the required handovers per call.

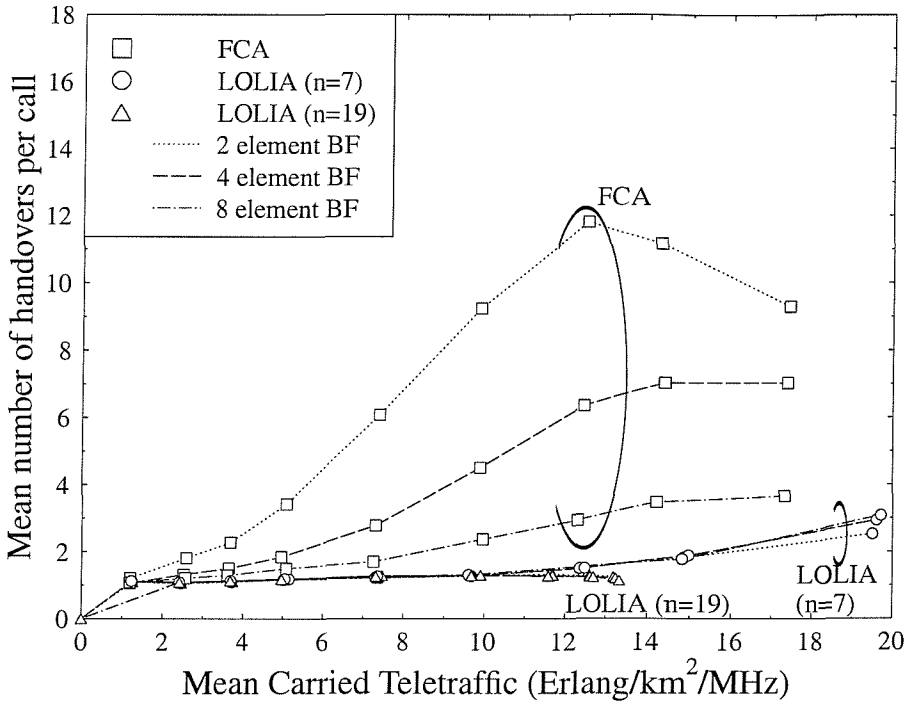

Figure 3.33: Mean number of successful handovers per call versus mean carried traffic, for comparison of the LOLIA, with 7 and 19 'local' base stations, and of FCA using a 7-cell reuse cluster, under a uniform geographic traffic distribution, for two, four and eight element antenna arrays with beamforming in a **multipath environment**. See Figure 3.27 for the corresponding LOS results.

As it can be seen in Figure 3.34 for the adaptive array, the mean levels of carried teletraffic against the number of mobiles in the system followed a near-linear trend, with the capacity of the LOLIA 19 system rolling off above 2000 users, as for the LOS scenario in Figure 3.28. Above this number of users, very little extra teletraffic was carried, with corresponding several orders of magnitude increases of the blocking, dropping and low quality access probabilities as well as that of the GOS measure. For the channel allocation algorithms operating in a multipath rather than LOS environment, increasing the number of antenna elements did not significantly increase the levels of traffic carried, although the network performance improved in other respects, such as for example the call dropping probability.

Table 3.6 presents similar results to Table 3.5, but for a multipath environment. From this table it can be seen that LOLIA 19 actually performed slightly better in the multipath scenario, than in a LOS situation. This was due to the large reuse distance of the system, resulting in the sum of the three desired multipath signals versus the sum of the interfering signals being higher than the ratio of the LOS desired signal power to the LOS interference

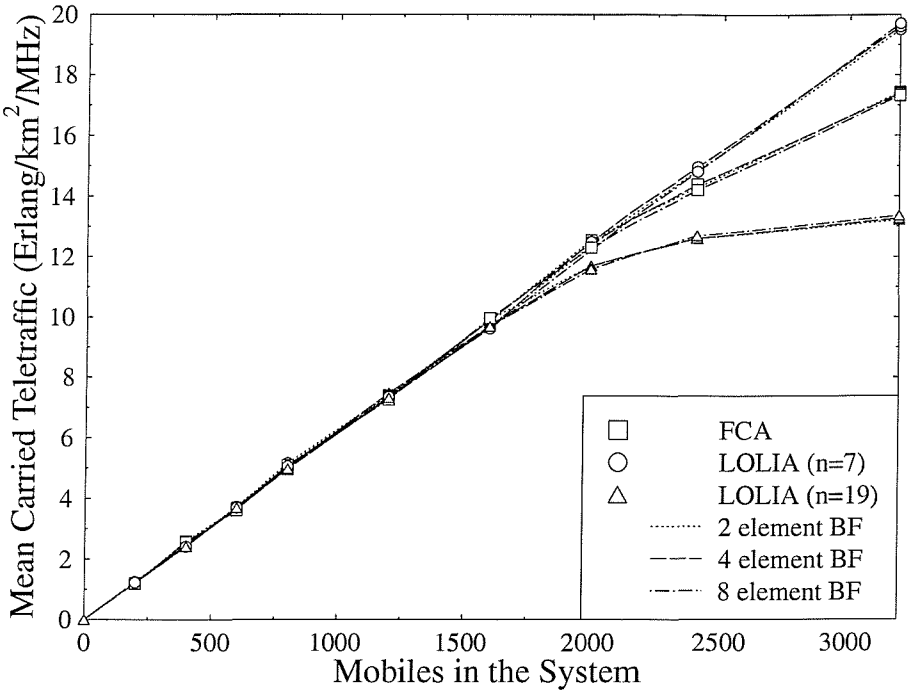

Figure 3.34: Mean traffic carried versus the number of mobiles in the system, for comparison of the LOLIA, with 7 and 19 "local" base stations, and of FCA using a 7-cell reuse cluster, under a uniform geographic traffic distribution, for two, four and eight element adaptive antenna arrays in a **multipath environment**. See Figure 3.28 for the corresponding LOS results.

power. The LOLIA 7 algorithm, however, did not generally benefit from the multipath environment, since the smaller reuse distance resulted in numerous sources of relatively strong interference, all requiring cancellation. Therefore, as the number of antenna elements increased, so should the number of users supported by the network, as a result of the increased number of degrees of freedom, and therefore, the increased number of sources that may be nulled. The results support this expectation with a 17% gain in the number of users, when upgrading the system from two element to four element arrays, and a further 15% improvement in the number of supported users with the aid of eight element antenna arrays instead of the four element arrays. As for the LOS results, the FCA algorithm, again, benefited the most in terms of the number of users supported by the network from the employment of adaptive antenna arrays. The number of users increased by 35%, when doubling the number of antenna elements from two to four, and on doubling from four to eight delivered a further 29% user capacity improvement.

Algorithm	Conservative $P_{FT}=1\%$, $P_{low}=1\%$ $GOS=4\%$, $P_B=3\%$			Lenient $P_{FT}=1\%$, $P_{low}=2\%$ $GOS=6\%$, $P_B=5\%$		
	Users	**Traffic**	**Limiting Factor**	**Users**	**Traffic**	**Limiting Factor**
FCA, 2 elements	**1315**	**8.10**	P_{low}	**1660**	**10.30**	P_{low}
FCA, 4 elements	**1790**	**11.10**	P_{low}	**2240**	**13.60**	P_{low}
FCA, 8 elements	2400	14.20	P_B	2780	15.70	GOS
LOLIA (n=7), 2 elements	**2310**	**14.30**	P_{low}	**2610**	**16.10**	P_{low}
LOLIA (n=7), 4 elements	**2735**	**16.90**	P_{low}	**3035**	**18.65**	P_{low}
LOLIA (n=7), 8 elements	3155	19.45	P_{low}	>3200	>20.00	P_{low}
LOLIA (n=19), 2 elements	**1970**	**11.55**	P_B	**2110**	**11.95**	P_B
LOLIA (n=19), 4 elements	**1990**	**11.65**	P_B	**2155**	**12.05**	P_B
LOLIA (n=19), 8 elements	2095	11.85	P_B	2220	12.20	P_B

Table 3.6: Maximum mean carried traffic, and maximum number of mobile users that can be supported by each configuration, whilst meeting the preset quality constraints of Section 3.6. The carried traffic is expressed in terms of normalised Erlangs (Erlang/km^2/MHz), for the network described in Table 3.3 in a **multipath environment**. The corresponding LOS results are summarised in Table 3.5 with network configurations common between the two highlighted in bold.

3.7.2.3 Performance over a Multipath Channel using Power Control

This section builds on the results obtained in the previous section for a multipath propagation environment. Simulations were conducted for a standard 7-cell FCA scheme and a LOLIA-assisted system using $n = 7$, both invoking power control. The power control algorithm implemented attempted to independently adjust the mobile and base station transmit powers, such that the up- and down-link SINRs were within a given target SINR window. The use of a target window avoided constantly increasing and decreasing the transmission powers, which could lead to potential power control instabilities within the network. Furthermore, using a range of possible transmission powers is analogous to accounting for an inherent power control error plus slow fading phenomenon. The 'Target SINR' given in Table 3.7 is the SINR to be maintained by the power control algorithm. The immediate effect of power control on the SINR versus the mobile's distance from the base station can be seen in Figure 3.35. This figure shows that power control attempts to maintain a constant SINR, sufficiently high for reliable communications across the network, rather than allowing for unnecessarily high SINRs near the base station and providing insufficient levels of SINR far from the base stations, evident for a cordless telephone type network using no power control. It was found that in conjunction with 4-QAM using a target SINR of

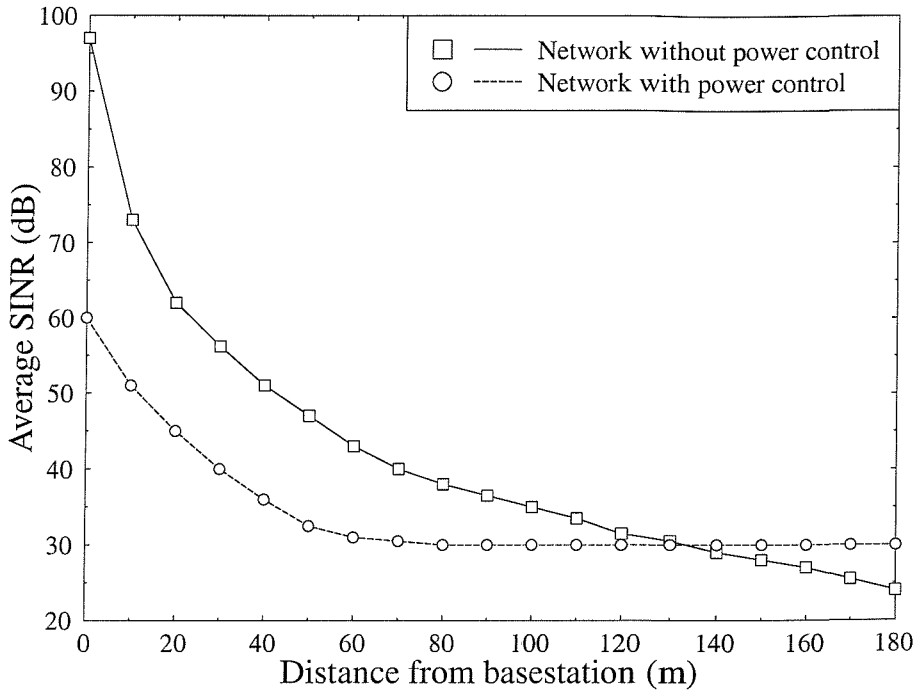

Figure 3.35: Signal-to-Interference plus Noise Ratio (SINR) versus mobile station distance measured from the base station, for networks with and without power control. The unnecessarily high SINR near the base station was a consequence of the base station's inability to power down below the minimum transmit power of -20 dBm, when the mobile station was within a distance of about 60m from the base station.

27dB was most suitable, when using the FCA algorithm. However, the LOLIA required a higher target SINR of 31dB in order to obtain satisfactory call dropping performance, as a result of its dynamic nature causing the interference levels to vary more rapidly than for the FCA algorithm. In other words, the LOLIA required a higher SINR "headroom" above the re-allocation SINR threshold.

Figure 3.36 shows the new call blocking probability versus the mean normalised carried traffic, expressed in terms of Erlangs/km^2/MHz. The figure shows that the blocking performance of the FCA algorithm is limited by the availability of frequency/timeslot combinations, and hence the addition of power control does not improve the new call blocking performance. However, the blocking performance of the LOLIA is not dominated by the availability of frequency/timeslot combinations and hence it can be seen to benefit significantly from using power control.

From Figure 3.37 it can be seen that the Power Control (PC) algorithm substantially

Parameter	Value	Parameter	Value
Noisefloor	-104dBm	Multiple Access	F/TDMA
Frame duration	0.4615ms	Cell radius	218m
Maximum BS transmit power	10dBm	Maximum MS transmit power	10dBm
Minimum BS transmit power	-20dBm	Minimum MS transmit power	-20dBm
Power control stepsize	1dB	Power control hysteresis	3dB
Number of base stations	49	Handover hysteresis	2dB
Outage SINR threshold [93]	17dB	Power control FCA target SINR	27dB
Re-allocation SINR threshold [93]	21dB	Power control LOLIA7 target SINR	31dB
Number of timeslots	8	Number of carriers	7
Average inter-call-time	300s	Max new-call queue-time	5s
Average call length	60s	Reference signal modulation	BPSK
Beamforming algorithm	SMI	Reference signal length	8 bits
MS speed	13.4m/s	Number of antenna elements	2 &4
Pathloss exponent	-3.5	Pathloss at 1m reference point	0dB
Geometry of antenna array	Linear	Array element spacing	$\lambda/2$
Modulation scheme	4-QAM	Channel/carrier bandwidth	200kHz

Table 3.7: Simulation parameters for the FCA, and DCA-assisted networks using power control.

improved the call dropping probability of the FCA algorithm in comparison to the scenario without PC in Figure 3.29. Specifically, at the highest traffic loads, the PC-assisted performance matched that without power control but using antenna arrays with twice the number of antenna elements. At lower levels of traffic, the performance improvement obtained with the aid of power control was even higher, with the two element array results approaching those of the eight element array without power control. However, below approximately 10 Erlang/km^2/MHz a forced termination probability performance plateau was reached as a result of the power control algorithm limiting the maximum SINR. In contrast, when no power control is used and there are few users, the average SINR is very high and consequently fewer calls are dropped.

The performance gain of the LOLIA using power control is lower than that of the FCA algorithm, but still significant, since its performance is about halfway between that of the LOLIA without power control and using the same number of antenna elements, and that with twice the number of antenna elements.

The probability of low quality access of the PC-assisted scenario is shown in Figure 3.38. The corresponding curves for using no PC were plotted in Figure 3.30. The power controlled variant of the FCA algorithm offered a significantly reduced probability of low quality access for a given number of antenna elements. In fact, the probability of low quality access, when

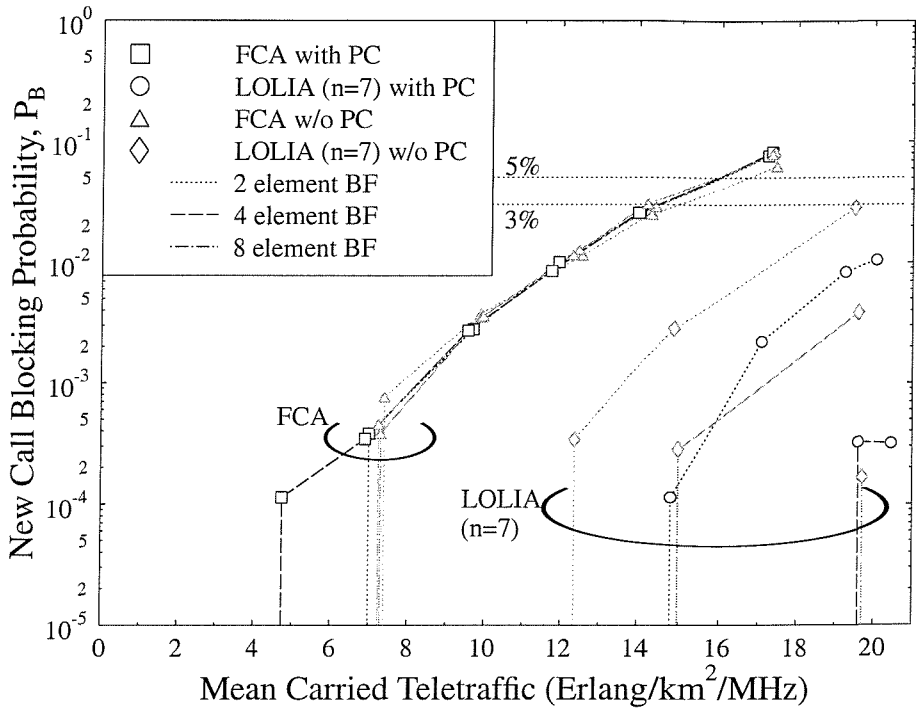

Figure 3.36: New call blocking performance versus mean carried traffic, for comparison of the LOLIA, with 7 'local' base stations, and of FCA using a 7-cell reuse cluster, under a uniform geographic traffic distribution, **with and without power control**, for two and four element antenna arrays with beamforming in a multipath environment.

using power control and a two element adaptive antenna array, was lower than that when using a four element array without power control. The LOLIA also benefited to the same extent, with the probability of low quality access when using the power control algorithm equalling that obtained with the aid of twice the number of antenna elements and no power control.

The GOS illustrated in Figure 3.39 is related to the probability of low quality access by Equation 3.23, hence the close resemblance to Figure 3.38. However, it can be seen that the performance difference of the FCA algorithm using two and four element antenna arrays diminished as a result of their similar new call blocking performances, which dominate the GOS metric of Equation 3.23.

Figure 3.40 shows the mean number of handovers performed per call versus the mean carried teletraffic. From this figure it can be seen that the performance of the FCA algorithm was improved significantly as a result of using the power control algorithm. However, the FCA algorithm still required significantly more handovers per call for maintaining the

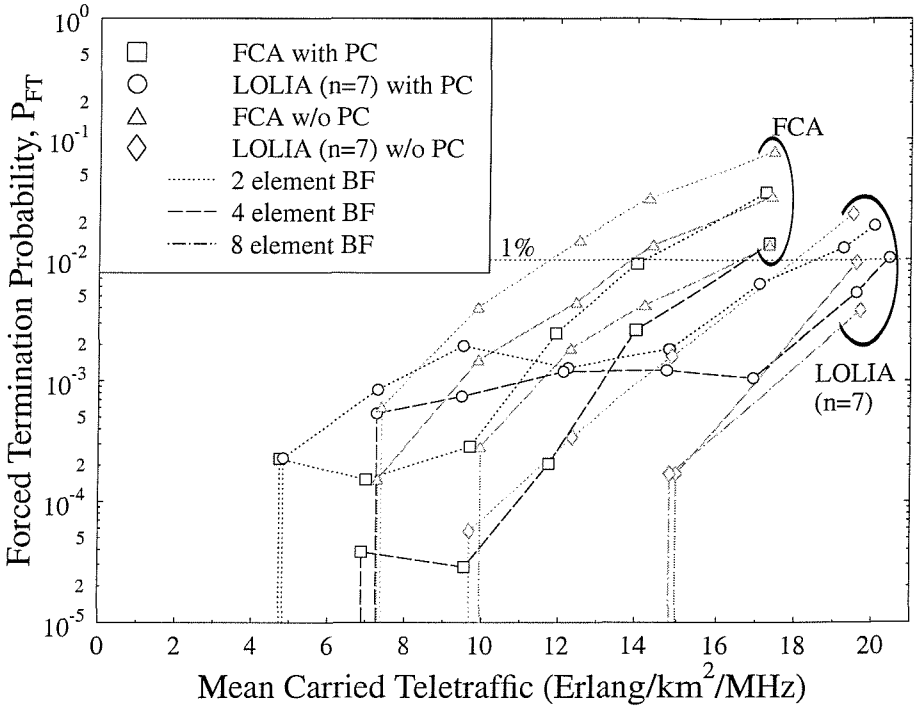

Figure 3.37: Call dropping performance versus mean carried traffic, for comparison of the LOLIA, with 7 'local' base stations, and of FCA using a 7-cell reuse cluster, under a uniform geographic traffic distribution, **with and without power control**, for two and four element antenna arrays with beamforming in a multipath environment.

desired call quality than the equivalent LOLIA based network without power control.

From the mean transmission power results of Figure 3.41 it can be seen that, as expected, the mean transmission power increased as the amount of teletraffic carried increased due to the higher levels of interference to be overcome. At high traffic loads the difference between the mean transmission powers of the mobile stations and the base stations, became more significant for the FCA algorithm. This resulted from the downlink interfering base stations being, on average, farther away from the served mobile, than the interfering mobiles were from the serving base station on the uplink. This was further exacerbated by the omni-directional nature of the mobiles' antennas and the directional nature of the antennas at the base stations. The LOLIA using a 7-cell exclusion zone required a higher mean transmission power, than the FCA algorithm, which was attributed to the higher target SINR required by the LOLIA for maintaining an acceptable call dropping performance. When compared to the fixed transmission power of 10dBm for an identical network operating without power control, the reductions in transmitted power are significant, with a minimum average transmit power

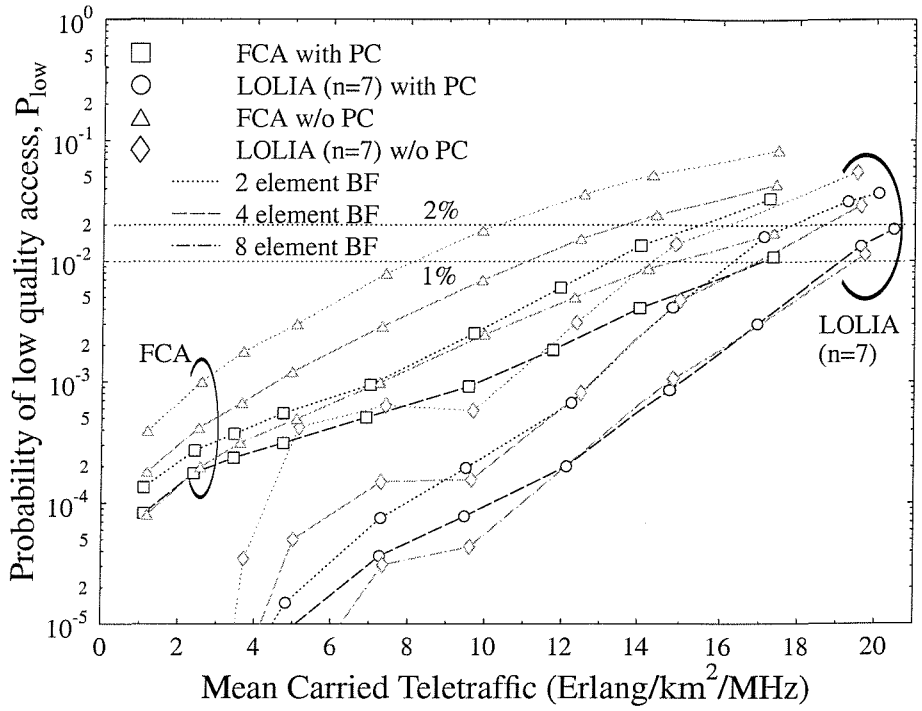

Figure 3.38: Probability of low quality access per call versus mean carried traffic, for comparison of the LOLIA, with 7 'local' base stations, and of FCA using a 7-cell reuse cluster, under a uniform geographic traffic distribution, **with and without power control**, for 2 and 4 element antenna arrays with beamforming in a multipath environment.

reduction of 6dB, which substantially extends the mobile stations' battery lives.

Table 3.8 presents the summary of our results obtained for a network using power control in a multipath environment. The table shows that the use of power control has increased the number of users that may be serviced according to the required network performance criteria. The number of users supported by the network using the FCA algorithm increased by 28% to 70%, with a mean of 54% over the conservative and lenient scenarios. The capacity gains obtained with the aid of power control in a network using the LOLIA 7, however, were lower, namely between 9% and 15%, with a mean of almost 13% for both the conservative and lenient scenarios. Whilst the LOLIA 7 capacity gains are fairly modest, the overall call quality, of the channel allocation techniques has improved for a given level of traffic, when compared to an identical network without power control.

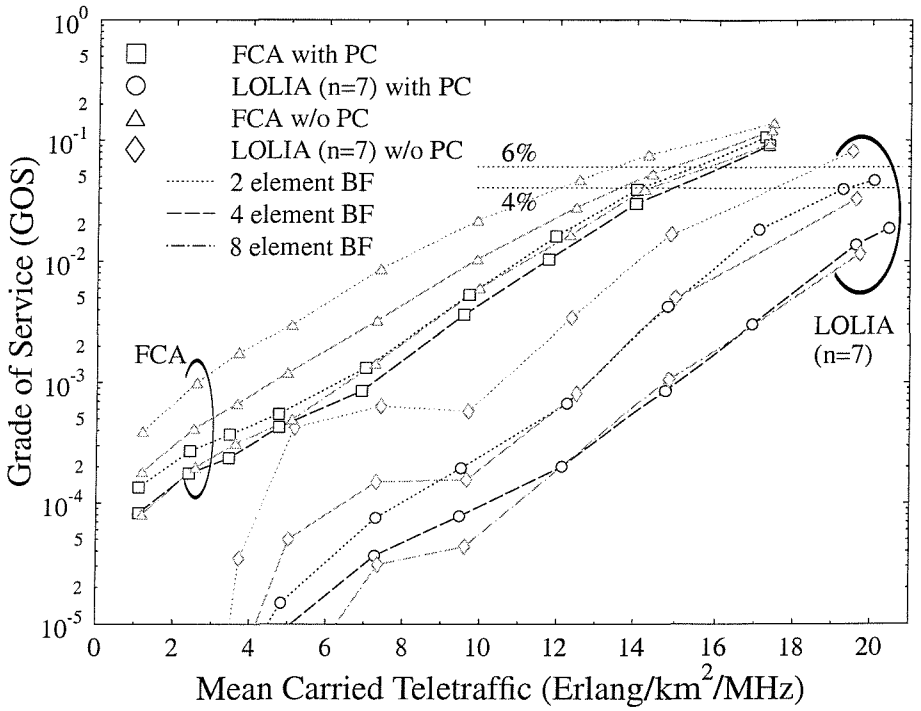

Figure 3.39: Grade-Of-Service (GOS) performance versus mean carried traffic, for comparison of the LOLIA, with 7 'local' base stations, and of FCA using a 7-cell reuse cluster, under a uniform geographic traffic distribution, **with and without power control**, for two and four element antenna arrays with beamforming in a multipath environment.

3.7.2.4 Transmission over a Multipath Channel using Power Control and Adaptive Modulation

The idea behind adaptive modulation is to select a modulation mode according to the instantaneous radio channel quality [12, 13]. Thus, if the channel quality exhibits a high instantaneous SINR, then a high order modulation mode may be employed, enabling the exploitation of the temporarily high channel capacity. In contrast, if the channel has a low instantaneous SINR, using a high-order modulation mode would result in an unacceptable Frame Error Ratio (FER), and hence a more robust, but lower throughput modulation mode would be invoked. Hence, adaptive modulation not only combats the effects of a poor quality channel, but also attempts to maximise the throughput, whilst maintaining a given target FER. Thus, there is a trade-off between the mean FER and the data throughput, which is governed by the modem mode switching thresholds. These switching thresholds define the SINRs, at which the channel is considered unsuitable for a given modulation mode, where an alternative AQAM mode must be invoked.

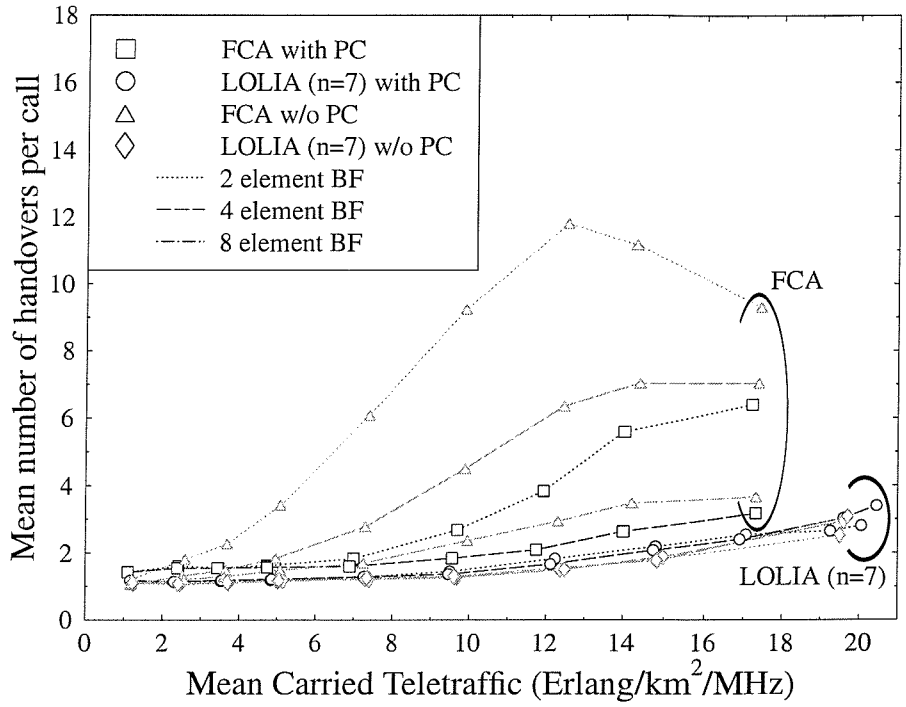

Figure 3.40: Mean number of successful handovers per call versus mean carried traffic, for comparison of the LOLIA, with 7 'local' base stations, and of FCA using a 7-cell reuse cluster, under a uniform geographic traffic distribution, **with and without power control**, for two and four element antenna arrays with beamforming in a multipath environment.

The power control algorithm invoked attempted to independently adjust the mobile and base station powers, such that the up- and down-link SINRs were within a given target SINR window. The employment of a target window avoided constantly increasing and decreasing the transmission powers, which could lead to potential power control instabilities within the network. Furthermore, the affect of a range of different possible transmission powers is analogous to an inherent power control error plus slow fading envelope.

The combination of power control with adaptive modulation leads to several performance trade-offs, which must be considered when designing the power control and modulation mode switching algorithm. For example, the transmitted power could be minimised, which would result in either a high FER and a high throughput, or a low BER and a low throughput. Alternatively, the FER could be lowered even while maintaining a high throughput, when tolerating high transmission powers.

The power control and modulation mode switching algorithm invoked in our simulations attempted to minimise the transmitted power, whilst maintaining a high throughput with

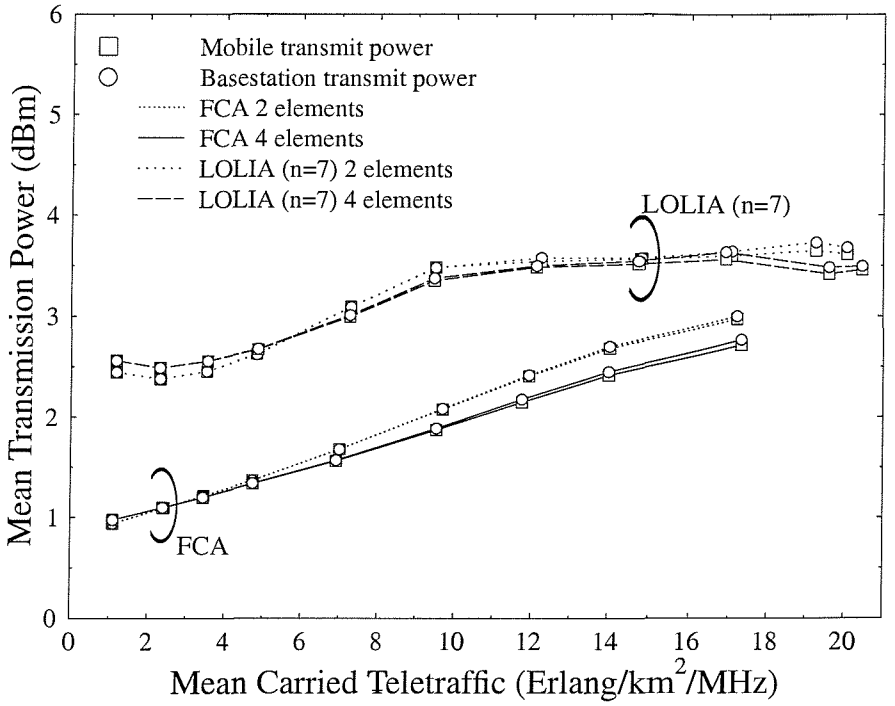

Figure 3.41: Mean transmission power versus mean carried traffic, of the LOLIA, with 7 "local" base stations, under a uniform geographic traffic distribution, **with power control**, for two and four element antenna arrays with beamforming in a multipath environment.

a less than 5% target FER. The pseudo-code of the proposed algorithm is described in the next section.

3.7.2.5 Power Control and Adaptive Modulation Algorithm

```
determine lowest SINR out of up- and down-link SINRs
if in 16-QAM mode
  if lowest SINR < 16-QAM drop SINR
    drop to 4-QAM mode
  else if lowest SINR < 16-QAM reallocation SINR
    if at maximum transmit power
      revert to 4-QAM
    else
      increase transmit power
  else if lowest SINR < 16-QAM target SINR
    if not at maximum power
```

Algorithm	Conservative $P_{FT}=1\%$, $P_{low}=1\%$ $GOS=4\%$, $P_B=3\%$			Lenient $P_{FT}=1\%$, $P_{low}=2\%$ $GOS=6\%$, $P_B=5\%$		
	Users	**Traffic**	**Limiting Factor**	**Users**	**Traffic**	**Limiting Factor**
Without power control						
FCA, 2 elements	**1315**	**8.10**	P_{low}	**1660**	**10.30**	P_{low}
FCA, 4 elements	**1790**	**11.10**	P_{low}	**2240**	**13.60**	P_{low}
FCA, 8 elements	2400	14.20	P_B	2780	15.70	GOS
LOLIA (n=7), 2 elements	**2310**	**14.30**	P_{low}	**2610**	**16.10**	P_{low}
LOLIA (n=7), 4 elements	**2735**	**16.90**	P_{low}	**3035**	**18.65**	P_{low}
LOLIA (n=7), 8 elements	3155	19.45	P_{low}	>3200	>20.00	P_{low}
With power control						
FCA, 2 elements	**2260**	**13.30**	P_{low}	**2455**	**14.25**	P_{FT}
FCA, 4 elements	**2510**	**14.45**	P_B	**2870**	**15.95**	P_B
LOLIA (n=7), 2 elements	**2665**	**16.30**	P_{low}	**2935**	**17.80**	P_{low}
LOLIA (n=7), 4 elements	**3125**	**19.08**	P_{low}	**3295**	**20.42**	P_{FT}

Table 3.8: Maximum mean carried traffic, and maximum number of mobile users that can be supported by each configuration whilst meeting the preset quality constraints of Section 3.6. The carried traffic is expressed in terms of normalised Erlangs (Erlang/km^2/MHz) for the network described in Table 3.7 both **with and without power control** in a **multipath environment**. The figures in bold indicate common network configurations to both the results without power and those with.

```
      increase transmit power
  else if lowest SINR > 16-QAM target SINR+hysteresis
    decrease transmit power
else if in 4-QAM mode
  if lowest SINR < 4-QAM drop SINR
    drop to BPSK mode
  else if lowest SINR < 4-QAM reallocation SINR
    if at maximum transmit power
      revert to BPSK
    else
      increase transmit power
  else if lowest SINR < 4-QAM target SINR
    if not at maximum power
      increase transmit power
  else if lowest SINR > 16-QAM target SINR+hysteresis
    change to 16-QAM mode
```

```
  else if lowest SINR > 4-QAM target SINR+hysteresis
    if at maximum transmit power
      reduce transmit power
    else
      if lowest SINR > 16-QAM drop SINR
        change to 16-QAM
      else
        decrease transmit power
else if in BPSK
  if lowest SINR < BPSK drop SINR
    outage occurs
  else if lowest SINR < BPSK reallocation SINR
    if not at maximum transmit power
      increase transmit power
  else if lowest SINR > 4-QAM target SINR+hysteresis
    change to 4-QAM
  else if lowest SINR > BPSK target_hysteresis
    if at maximum transmit power
      reduce transmit power
    else
      change to 4-QAM
```

Figure 3.42 shows the flowchart of the AQAM and power control decision tree, when in the 4-QAM mode. The first step in the process is to determine the lower of the up- and the down-link SINRs. The next step is to determine, whether the BPSK modulation mode should be selected. The conditions for this to occur are that, either the lower SINR is below the 4-QAM call dropping threshold or that it is below the 4-QAM call reallocation threshold and currently the maximum possible transmission power is used. When in BPSK mode, outages may occur due to an insufficient SINR level, and after a given number of consecutive BPSK mode outages, the call is dropped. If the lower SINR is below the 4-QAM call reallocation threshold, or the SINR is below the 4-QAM target SINR, and the maximum transmission power has not been reached, then the transmit power is increased. However, if the SINR is below the 4-QAM target SINR and the maximum possible transmit power is currently used, then the modem remains in the 4-QAM mode. The 16-QAM mode is chosen, if the SINR is higher than the 16-QAM target SINR, plus the associated hysteresis. Alternatively, the 16-QAM mode is invoked, if the SINR is higher than the 4-QAM target SINR plus the hysteresis, furthermore the transmission power required to obtain this SINR

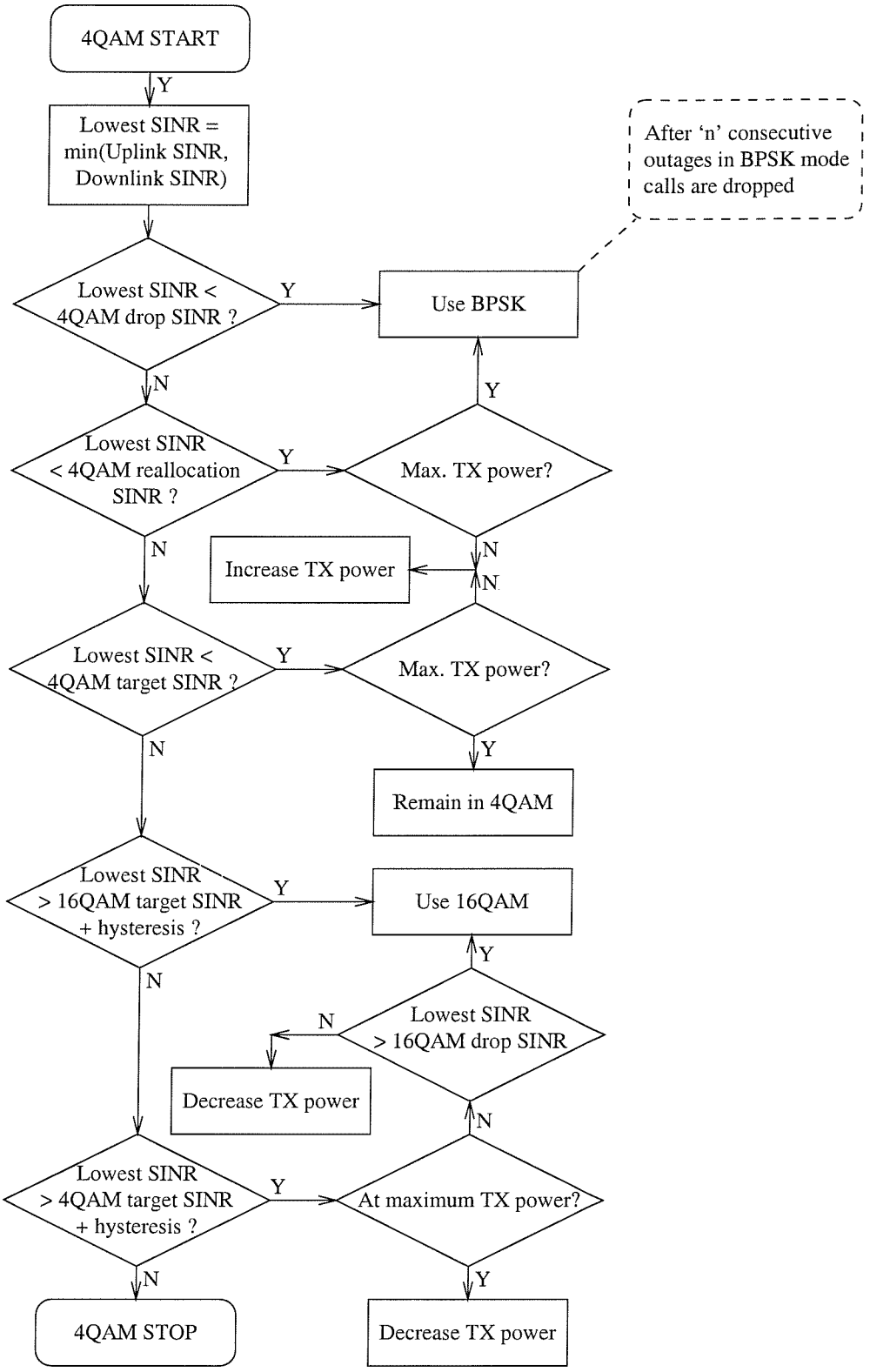

Figure 3.42: The AQAM and power control decision tree for the 4-QAM mode.

is lower than the maximum transmit power, and the SINR is higher than the 16-QAM call dropping SINR. However, if the SINR is below the 16-QAM call dropping SINR or the maximum transmission power is in use, then the transmit power is reduced in an effort to keep the SINR in the 4-QAM mode's target SINR window. The improved SINR achieved using adaptive antenna arrays at the base station facilitates a higher mean network data throughput.

The FER was evaluated for approximately half-rate Bose-Chaudhuri-Hocquenghem (BCH) codes, which employed interleaving over the different number of bits conveyed by the different modem modes within a transmission frame [93]. The 'Reallocation SINR' and the 'Outage SINR' are defined as the average SINRs necessary for satisfying the 5% and 10% maximum FER constraints, respectively, using a given modulation mode such as BPSK, 4-QAM, or 16-QAM. The 'Target SINR' was chosen so as to maximise the network capacity and represents an FER of approximately 2%.

The calculation of the receive antenna arrays weights was performed on a transmission frame-by-frame basis, leading to updated up- and down-link SINRs every transmission frame. These SINR values were then used for selecting the modulation mode and transmission power to be employed, and for determining whether any channel re-allocation was necessary. Hence, frame-by-frame adaptive modulation, power control and dynamic channel allocation was jointly performed.

The system parameters for the network are defined in Table 3.9 and our performance results are provided in the next section.

3.7.2.6 Performance of PC-assisted, AQAM-aided Dynamic Channel Allocation

This section presents the simulation results obtained for a network using burst-by-burst adaptive modulation in order to improve the network's performance. Simulations were conducted for both a standard 7-cell FCA scheme and for the LOLIA using $n = 7$. The benchmark results obtained for a 4-QAM based network using power control were included for comparison purposes. Due to the enhanced network performance resulting from the employment of AQAM, a further constraint of a minimum throughput of 2 bits/symbol was invoked. This ensured a fair comparison with the fixed 4-QAM based network.

Figure 3.43 shows the new call blocking probability versus the mean normalised carried traffic. From this figure it can be seen that in conjunction with the LOLIA there are no blocked calls, except for the highest levels of traffic. In contrast, the performance of the FCA algorithm was degraded by using AQAM. This was the result of the limited

Parameter	Value	Parameter	Value
Noisefloor	-104dBm	Multiple Access	TDMA
Frame length	0.4615ms	Cell radius	218m
Minimum BS transmit power	-20dBm	Minimum MS transmit power	-20dBm
Maximum BS transmit power	10dBm	Maximum MS transmit power	10dBm
Power control stepsize	1dB	Power control hysteresis	3dB
BPSK outage SINR	13dB	BPSK reallocation SINR	17dB
BPSK target SINR	21dB	4-QAM outage SINR	17dB
4-QAM reallocation SINR	21dB	4-QAM target SINR	27dB
16-QAM outage SINR	24dB	16-QAM reallocation SINR	27dB
16-QAM target SINR	32dB	Pathloss exponent	-3.5
Number of base stations	49	Handover hysteresis	2dB
Number of timeslots/carrier	8	Number of carriers	7
Average inter-call-time	300s	Max new-call queue-time	5s
Average call length	60s	Reference signal modulation	BPSK
Beamforming algorithm	SMI	Reference signal length	8 bits
MS speed	30mph	Number of antenna elements	2 & 4
Pathloss at 1m reference point	0dB	Shadow fading	No
Geometry of antenna array	Linear	Array element spacing	$\lambda/2$
Channel/carrier bandwidth	200kHz		

Table 3.9: Simulation parameters for the AQAM based network using power control.

availability of frequency/timeslot combinations restricting the achievable performance gain, since the reduced call dropping probability encouraged the prolonged utilisation of the limited resources. This however, prevented new call setups.

The corresponding call dropping probability is depicted in Figure 3.44, which shows that when invoking adaptive modulation, the FCA algorithm performs better than the LOLIA below a traffic load of about 14 Erlangs/km^2/MHz. Both channel allocation algorithms consistently offered a lower call dropping probability, when employing AQAM compared to when using the fixed-mode 4-QAM modulation scheme. This reduction in the call dropping rate using adaptive modulation was brought about by the inherent ability of the AQAM scheme to be reconfigured to a lower-order, and hence more interference resistant modulation mode, in order to prevent calls from being dropped.

Figure 3.45 shows that the probability of a low quality access was substantially reduced by AQAM for both the FCA scheme and the LOLIA. At lower traffic loads the probability of low quality outage was higher than when using the fixed 4-QAM modulation mode for both of the channel allocation schemes. This was due to the frequent use of the highest order modulation mode, 16-QAM, which was more susceptible to low quality outages. The more frequent usage of the 16-QAM mode by the four element adaptive antenna arrays also

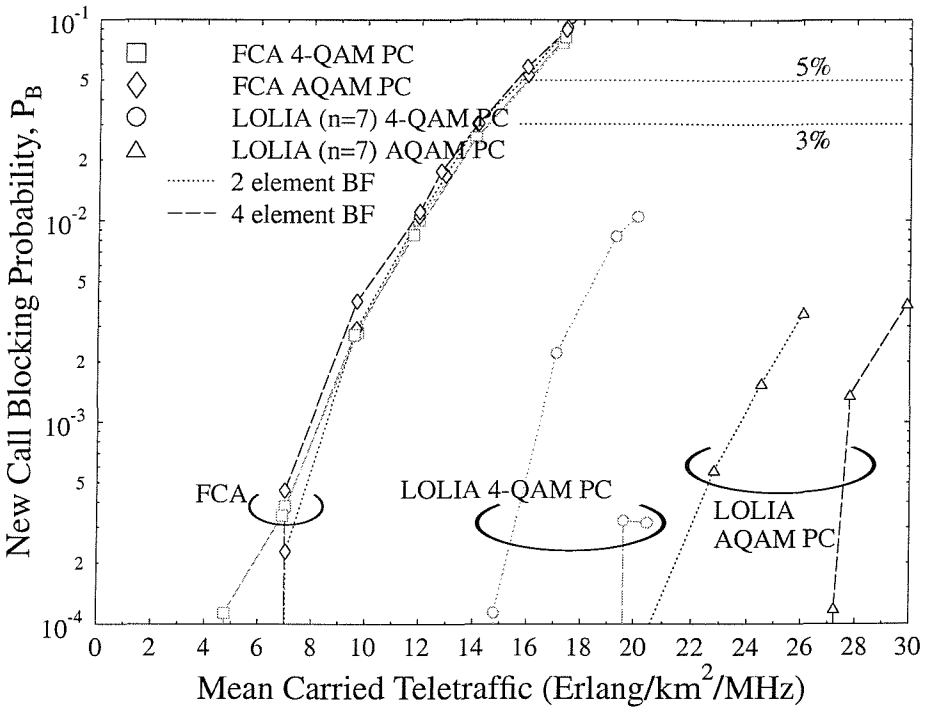

Figure 3.43: New call blocking probability versus mean carried traffic of the LOLIA, with 7 'local' base stations, and of FCA employing a 7-cell reuse cluster, for 2 and 4 element antenna arrays, **with and without AQAM**.

explains their greater probability of low quality outage at the lower traffic levels. However, as the traffic levels increased, the lower order modulation modes were invoked more frequently, and hence when combined with the four element arrays, the system guaranteed a lower probability of low quality outage, than the two element arrays.

From Figure 3.46 it can be seen that the GOS of the FCA algorithm did not benefit from employing AQAM to the same extent as the LOLIA, except at the lower traffic levels when the new call blocking probability does not dominate the overall GOS performance. The LOLIA, however, benefited substantially, as we have also seen for the probability of low quality outages, since its performance was not constrained by its new call blocking probability observed in Figure 3.43 for both 4-QAM and AQAM.

The employment of AQAM, in Figure 3.47, reduced the mean number of handovers per call of the LOLIA at all traffic loads, and of the FCA for the highest traffic loads, although an increased number of handovers were performed by the FCA at lower traffic loads. At these lower traffic loads, more intra-cell handovers were performed by the FCA algorithm, due to the employment of the 16-QAM modulation mode, which required more frequent

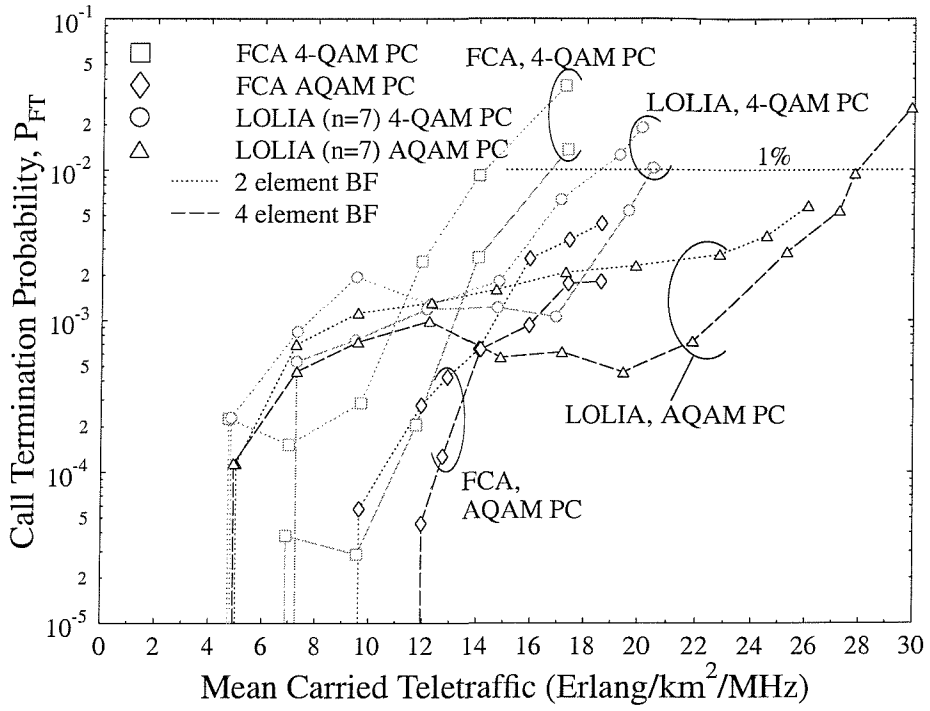

Figure 3.44: Call dropping or forced termination performance versus mean carried traffic of the LOLIA, with 7 'local' base stations, and of FCA employing a 7-cell reuse cluster, for two and four element antenna arrays, **with and without AQAM.**

intra-cell handovers in order to maintain a sufficiently high SINR. However, as the traffic load increased, the lower-order modulation modes were used more frequently, and hence less intra-cell handovers were required, leading to a reduction in the number of handovers performed.

The mean transmission power results of Figure 3.48 demonstrate how the employment of AQAM can reduce the power transmitted both for the up- and the down-link. At low traffic load levels the FCA algorithm performed slightly worse in transmitted power terms, than the LOLIA. However, as the traffic loads increased, the gap became negligible when using two element antenna arrays. However, when using four element antenna arrays, the LOLIA required a higher transmission power at these higher loads. When compared to the fixed transmission power of 10dBm for the network without power control, the employment of AQAM resulted in a significant reduction in the mean transmission power, with a minimum reduction of more than 4dB and a maximum reduction of more than 7dB, in addition to maintaining a superior call quality and mean modem throughput.

The average modem throughput expressed in bits per symbol versus the mean carried

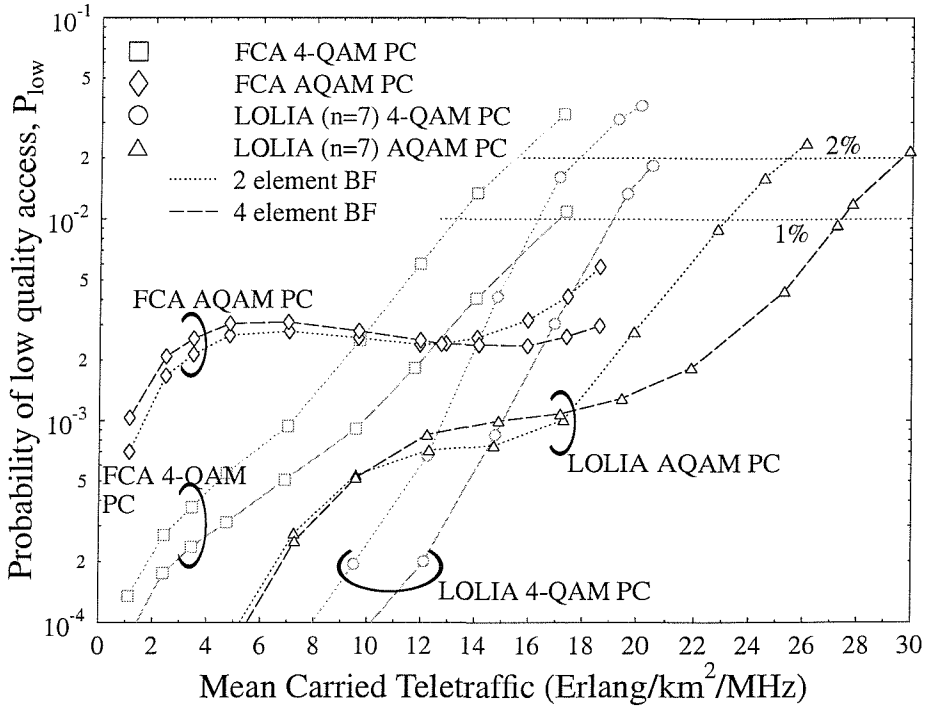

Figure 3.45: Probability of low quality access versus mean carried traffic of the LOLIA, with 7 'local' base stations, and of FCA employing a 7-cell reuse cluster, for two and four element antenna arrays, **with and without AQAM.**

teletraffic is shown in Figure 3.49. The figure shows how the mean number of bits per symbol decreased as the network traffic increased. The FCA algorithm offered the lowest throughput with its performance degrading near-linearly upon increasing the network's traffic load. The LOLIA, especially for the lower levels of traffic, offered a greater modem throughput for a given level of teletraffic carried, with the achievable performance gracefully decreasing, as the carried teletraffic continued to increase. Table 3.10 shows the mean modem throughput in bits per symbol, for the maximum mean carried traffic levels, whilst meeting the predefined quality constraints of Section 3.6.

From Table 3.11 it can be seen that it is the blocking performance of the network using the FCA algorithm which limits its associated network capacity, thus leading to a relatively high mean modem throughput at its user capacity limits. The increase in the modem throughput for the FCA algorithm varied from 35% to 55%, with corresponding user capacity improvements of 6% and -4%, when comparing the AQAM network to 4-QAM. The table also shows that the number of users supported by the FCA network using two element

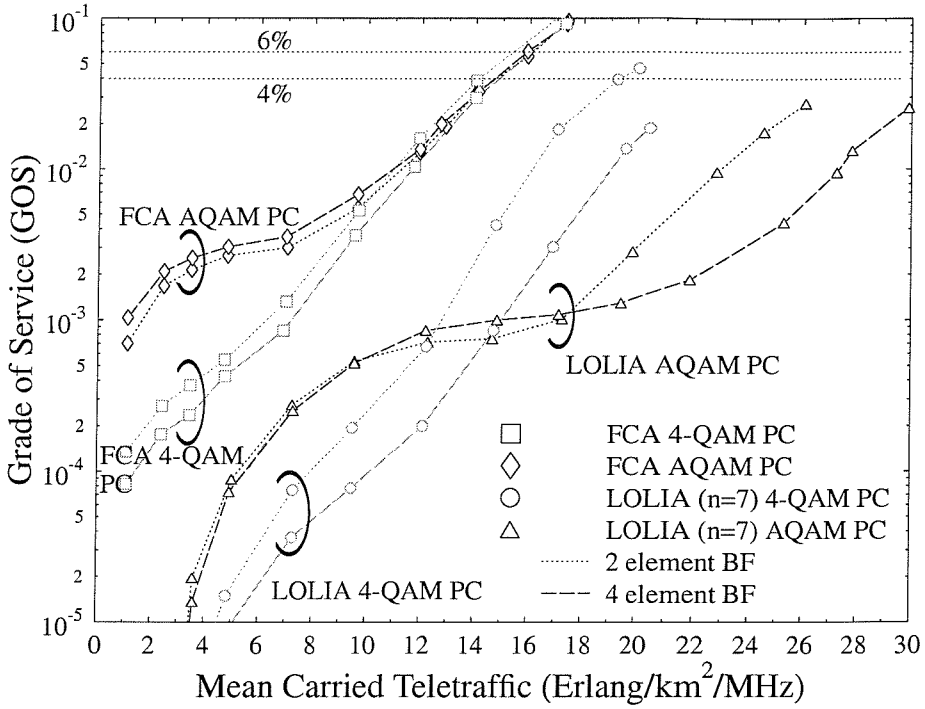

Figure 3.46: GOS performance versus mean carried traffic of the LOLIA, with 7 'local' base stations, and of FCA employing a 7-cell reuse cluster, for two and four element antenna arrays, **with and without AQAM**.

	Conservative $P_{FT} = 1\%$, $P_{low} = 1\%$ $GOS = 4\%$, $P_B = 3\%$ Bits per Symbol	**Lenient** $P_{FT} = 1\%$, $P_{low} = 2\%$ $GOS = 6\%$, $P_B = 5\%$ Bits per Symbol
FCA, 2 elements	2.8	2.7
FCA, 4 elements	3.1	2.9
LOLIA (n=7), 2 elements	2.1	≈2.0
LOLIA (n=7), 4 elements	2.15	2.05

Table 3.10: Mean modem throughput, when supporting the maximum mean carried traffic, whilst meeting the preset quality constraints of Section 3.6. The carried traffic is expressed in terms of normalised Erlangs (Erlang/km^2/MHz) for the network described in Table 3.9 in a **multipath environment with AQAM**.

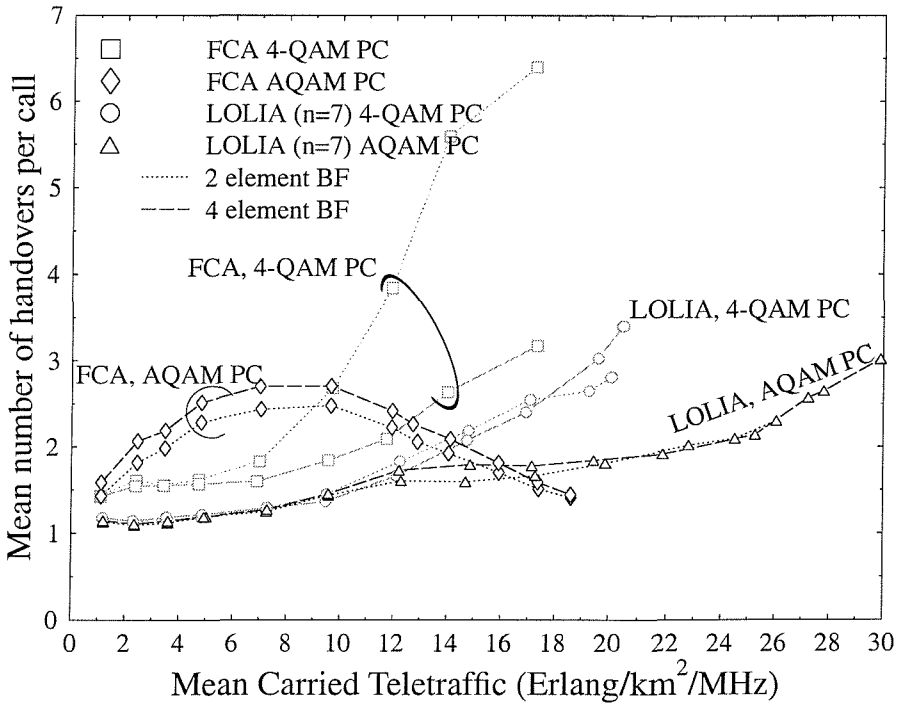

Figure 3.47: Mean number of successful handovers per call versus mean carried traffic of the LOLIA, with 7 'local' base stations, and of FCA employing a 7-cell reuse cluster, for two and four element antenna arrays, **with and without AQAM**.

adaptive antenna arrays increased when using AQAM, which was restricted by the probability of low quality access when using 4-QAM. In contrast, when using four element antenna arrays, the network capacity was limited by the network's new call blocking performance. Hence, using AQAM techniques did not increase the number of users supported. In fact, due to the superior call dropping performance of AQAM, the new call blocking probability increased as a result of the lack of available frequency/timeslot combinations, and hence the number of users supported by the network decreased.

However, the dynamic nature of the LOLIA limited its fixed 4-QAM based network capacity due to its excessive low quality access probability, and thus in all cases, AQAM increased the number of users supported, by 38% to 50%, whilst meeting the required call quality criteria of Section 3.6. The AQAM-induced improvement in mean modem throughput varied from 0% to 7.5% as a result of the particular AQAM implementation used in the simulations. This can be further verified with the aid of Figure 3.48, which shows that the mean transmission powers were not at their maxima and hence both the modem throughput and the probability of low quality access were sub-optimal. In other words,

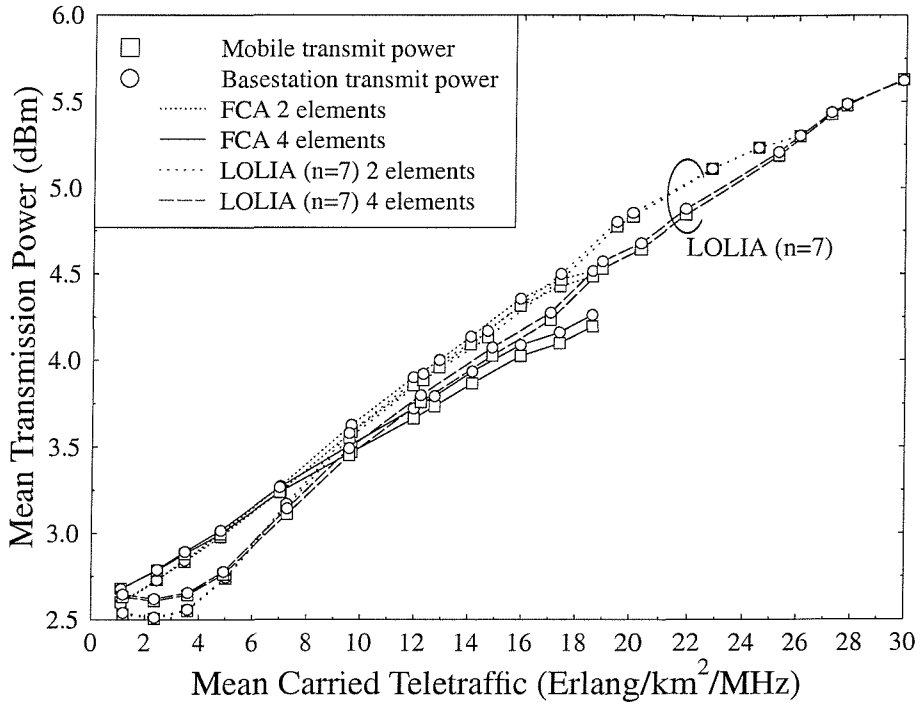

Figure 3.48: Mean transmit power versus mean carried traffic of the LOLIA, with 7 'local' base stations, and of FCA employing a 7-cell reuse cluster, for two and four element antenna arrays, **with and without AQAM.**

had the AQAM algorithm been more aggressive in terms of its transmitted power usage, a reduced probability of low quality access and an increased mean modem throughput would have occurred. However, a trade-off existed, where both the number of users supported and the mean modem throughput were increased, whilst achieving a significant reduction in the mean transmission powers.

3.7.2.7 Summary of Non-Wraparound Network Performance

The performance results summarised in this section can be gleaned from Tables 3.5-3.11. Specifically, in this section simulation results were obtained for a LOS scenario, for both the FCA algorithm and for the LOLIA, which showed that the FCA algorithm benefited the most from the employment of adaptive antenna arrays, with an increase of 144% in the number of users supported by a four element antenna arrays. The corresponding figure was 67% with the aid of two element arrays. The performance of the LOLIA with a 19 base station constraint improved least using adaptive antenna arrays due to the inherently low interference levels present. However, for the LOLIA with a base station constraint of 7,

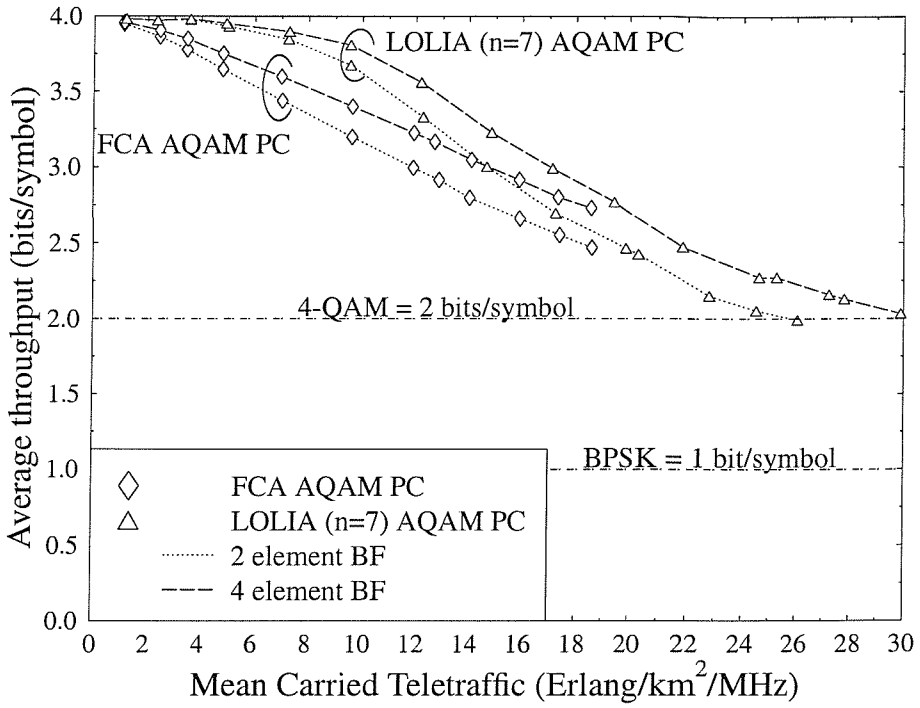

Figure 3.49: Mean throughput in terms of bits per symbol versus mean carried traffic of the LOLIA, with 7 'local' base stations, and of FCA employing a 7-cell reuse cluster, for two and four element antenna arrays, in conjunction **with AQAM**.

using two element adaptive antenna arrays, an extra 22% additional users were supported with the desired performance metric limits of Section 3.6 observed. Using four element adaptive antenna arrays at the base stations led to an increase of 58% in the number of users supported.

Identical simulations with the addition of two multipath rays were then performed. These simulations demonstrated that the LOLIA 19 actually performed better in a multipath scenario, than in a LOS situation. This was due to the large reuse distance of the system, resulting in the sum of the powers of the three desired multipath signals versus the sum of the interfering signal powers being higher, than the ratio of the LOS desired signal power to the interference power. The FCA algorithm, which offered the lowest network capacity in the LOS simulations, also suffered from the greatest capacity reduction in the multipath scenarios. The corresponding network capacities, expressed in terms of the number of users supported, decreased by between 3% and 17%. The number of users supported by the network using the LOLIA 7, was not significantly affected by the multipath propagation environment, with the highest reduction of almost 7% occurring using a four element

Algorithm	Conservative $P_{FT}=1\%$, $P_{low}=1\%$ $GOS=4\%$, $P_B=3\%$			Lenient $P_{FT}=1\%$, $P_{low}=2\%$ $GOS=6\%$, $P_B=5\%$		
	Users	**Traffic**	**Limiting Factor**	**Users**	**Traffic**	**Limiting Factor**
4-QAM with PC						
FCA, 2 elements	2260	13.30	P_{low}	2455	14.25	P_{FT}
FCA, 4 elements	2510	14.45	P_B	2870	15.95	P_B
LOLIA (n=7), 2 elements	2665	16.30	P_{low}	2935	17.80	P_{low}
LOLIA (n=7), 4 elements	3125	19.08	P_{low}	3295	20.42	P_{FT}
AQAM with PC						
FCA, 2 elements	2400	14.00	P_B	2760	15.75	P_B
FCA, 4 elements	2400	14.10	P_B	2710	15.50	P_B
LOLIA (n=7), 2 elements	3675	23.10	P_{low}	4115	25.4	P_{low}
LOLIA (n=7), 4 elements	4460	27.40	P_{low}	4940	29.6	P_{low}

Table 3.11: Maximum mean carried traffic, and maximum number of mobile users that can be supported by each configuration, whilst meeting the preset quality constraints of Section 3.6. The carried traffic is expressed in terms of normalised Erlangs (Erlang/km^2/MHz) for the network described in Table 3.9 in a **multipath environment.**

antenna array employed in the conservative network scenario of Section 3.6. The FCA algorithm benefited the most from increasing the number of elements comprising the adaptive antenna arrays, with a minimum increase of 25% in the number of users supported upon doubling the number of antenna elements. The LOLIA employing a reuse cluster size of seven also performed well, with a user capacity increase of at least 15% for each doubling of the number of antenna elements.

Simulations were then performed in the multipath environment, where the network used the power control algorithm to maintain a fairly constant received SINR across the cell area. It was found that the power control algorithm increased the number of users carried in all the scenarios considered. The FCA algorithm exhibited the greatest gains in terms of the number of users supported by the network. When compared to an identical network without power control, the user capacity increased by 28%-72%, with an average increase of 47%. The LOLIA 7 using power control carried more traffic, than the equivalent power control assisted FCA networks, and the LOLIA 7 system using no power control. When compared to the LOLIA 7 network using no power control, 9% to 15% more users were carried with a satisfactory performance. With respect to an FCA based network using power control, the increase in the number of supported users varied from 9% to almost 25%.

Further experiments were conducted in order to investigate the potential of AQAM techniques to increase network capacity. The gains achievable by the FCA algorithm were restricted by the number of available frequency/timeslot combinations, for both new calls and handovers, and hence the capacity increases were constrained by the new call blocking probability to 6%. However, this limitation to the number of supported users resulted in an increased mean modem throughput of between 2.7 and 3.1 bits per symbol, a reduced mean transmission power, and an overall improvement in call quality. The LOLIA, however, was not constrained by its new call blocking probability and was able to fully exploit the advantages of adaptive modulation. Thus, the LOLIA achieved a minimum network capacity increase of 38% over an identical scenario not using adaptive modulation.

The next section presents similar results but obtained using the "wraparound" technique in an effort to provide an effectively infinite simulation plane with, on average, constant interference levels present over the entire simulation area.

3.7.3 Wrap-around Network Performance Results

This section presents a range of performance results similar to those obtained in the previous section. However, in this section the "wrap-around" technique of Figure 3.7.1 was used to generate results not subjected to the edge effects present at the perimeter of the simulation area. This process was described in Section 3.7.1. Results were obtained for the LOS propagation environment in Section 3.7.3.1 and for the multipath propagation environment of Section 3.7.3.2. Section 3.7.3.3 portrays the results obtained for the multipath propagation environment using power control, and Section 3.7.3.4 presents the network performance using adaptive modulation techniques.

3.7.3.1 Performance Results over a LOS Channel

Firstly we compared the FCA and the LOLIA under uniform geographic traffic distribution conditions using both a single antenna element and adaptive antenna arrays consisting of two and four elements in a LOS propagation environment. The FCA scheme employed a seven-cell reuse cluster, corresponding to one carrier frequency per base station. The LOLIA was used in conjunction with the constraints of seven and nineteen nearest base stations, i.e., $n = 7$ or 19.

As seen in Figure 3.50 the LOLIA using $n = 19$ offered the worst call blocking performance of the three channel allocation schemes, with the AAAs having little beneficial effect. This demonstrated that the limiting factor was not inadequate signal quality for a call to be setup, but the lack of available frequency/timeslot combinations due to the large exclusion zone. The FCA algorithm benefited only to a limited extent from the employment of the AAAs, suggesting that the majority of the blocked calls were as a result of the limited availability of frequency/timeslot combinations. Inadequate signal quality caused the remainder of the blocked calls. The call blocking performance of the LOLIA using $n = 7$ appeared mainly to be interference limited, hence the AAAs guaranteed a significant reduction of the number of blocked calls, particularly for mean carried traffic levels in excess of 9 Erlang/km^2/MHz.

Figure 3.51 shows that - as expected - the FCA algorithm performed the least satisfactorily of the three channel allocation schemes investigated with respect to its call dropping performance. Even in conjunction with a four-element adaptive antenna array, it exhibited a higher call dropping rate than that of either of the LOLIAs ($n = 19$ and $n = 7$). The large exclusion zone of the LOLIA using $n = 19$ led to a low dropping probability of less than 1×10^{-3} for teletraffic loads below approximately 12 Erlang/km^2/MHz. However, the rapid rise in the call dropping probability upon increasing the teletraffic became unacceptable for

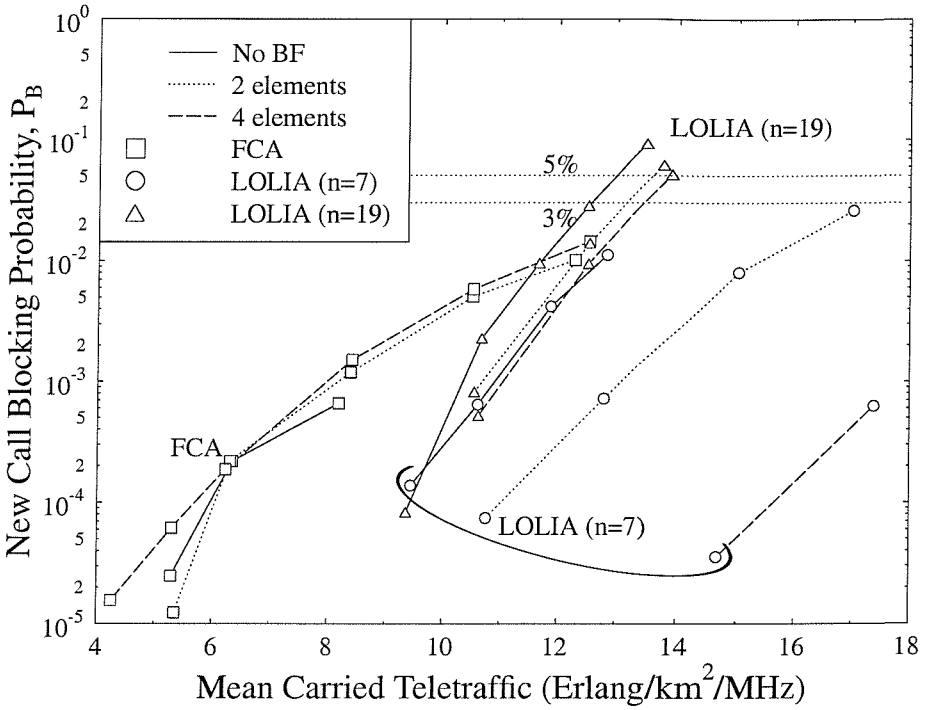

Figure 3.50: New call blocking probability performance versus mean carried traffic, for the LOLIA using 7 and 19 'local' base stations, and for FCA employing a 7-cell reuse cluster, under uniform geographic traffic distribution, for a single antenna element, as well as for two and four element antenna arrays with beamforming in a **LOS environment** using wrap-around. See Figure 3.23 for the corresponding "desert-island" scenario.

teletraffic loads in excess of about 13 Erlang/km^2/MHz. The large exclusion zone of the algorithm prevented from handovers occurring, since there were no free channels available in the vicinity, hence resulting in a high number of dropped calls. Thus, for $n = 19$ the employment of adaptive antenna arrays at the base stations did not improve the performance significantly, unlike for the FCA and LOLIA using $n = 7$, which were predominantly interference limited. The call dropping performance of the LOLIA using $n = 7$ benefited the most from the assistance of adaptive antenna arrays, with the most dramatic gains in call dropping performance at the higher teletraffic levels.

Figures 3.52 and 3.53 show the probability of low quality access and the GOS, which are similar in terms of their trends and are closely related to each other by Equation 3.23. The GOS of the FCA algorithm was dominated by the probability of low quality access, since it had a higher value than the blocking probability. However, the rapid rise of the new call blocking probability of the LOLIA with $n = 19$ caused a steep increase in its GOS, especially when coupled with its rapidly degrading probability of low quality access. All of

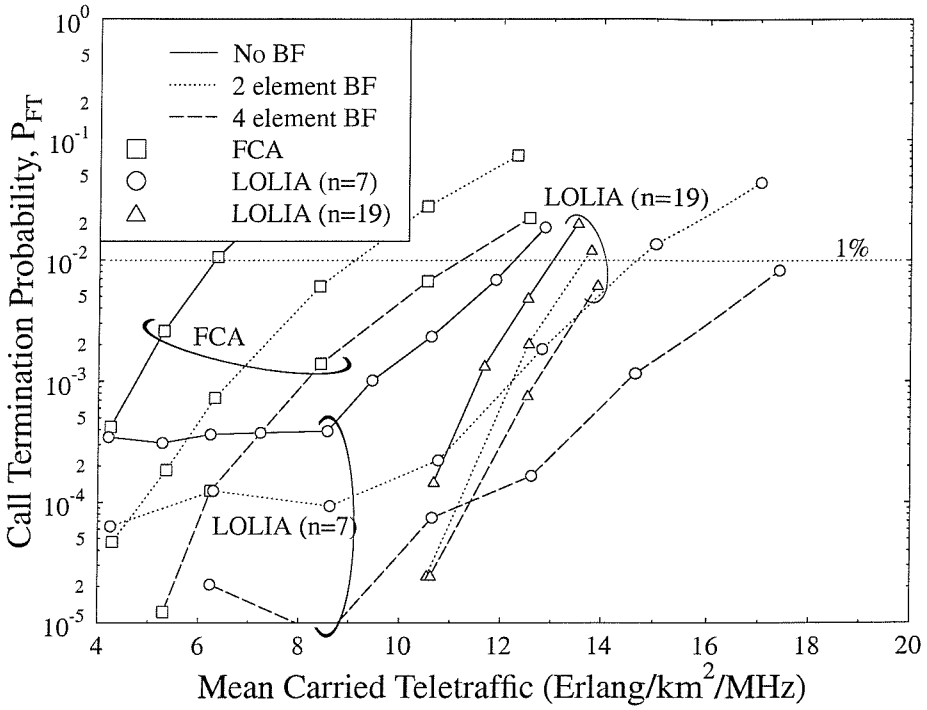

Figure 3.51: Dropping probability performance versus mean carried traffic, for the LOLIA using 7 and 19 'local' base stations, and for FCA employing a 7-cell reuse cluster, under a uniform geographic traffic distribution, for a single antenna element, as well as for two and four element antenna arrays with beamforming in a **LOS environment** using wrap-around. See Figure 3.24 for the corresponding "desert-island" scenario.

the algorithms benefited substantially from the employment of adaptive antenna arrays.

The effect of beamforming on the number of handovers performed can be seen in Figure 3.54. The LOLIAs required the least frequent handovers, with beamforming barely altering the results. In contrast, the number of handovers performed when using the FCA algorithm was reduced significantly due to employing AAAs with a maximum reduction of 72% for two elements, and of 89% for four elements. This translates into a significantly reduced signalling load for the network, since it has to manage far less handovers, therefore reducing the complexity of the network infrastructure.

It can be seen from Table 3.12 that in a LOS environment all of the channel allocation schemes benefit from the use of base station AAAs in terms of an increased level of teletraffic carried, hence supporting an increased number of users. The FCA algorithm benefited most from the employment of AAAs, with a 160% increase in terms of the number of users supported, when using a four-element antenna array. The performance improvements of the

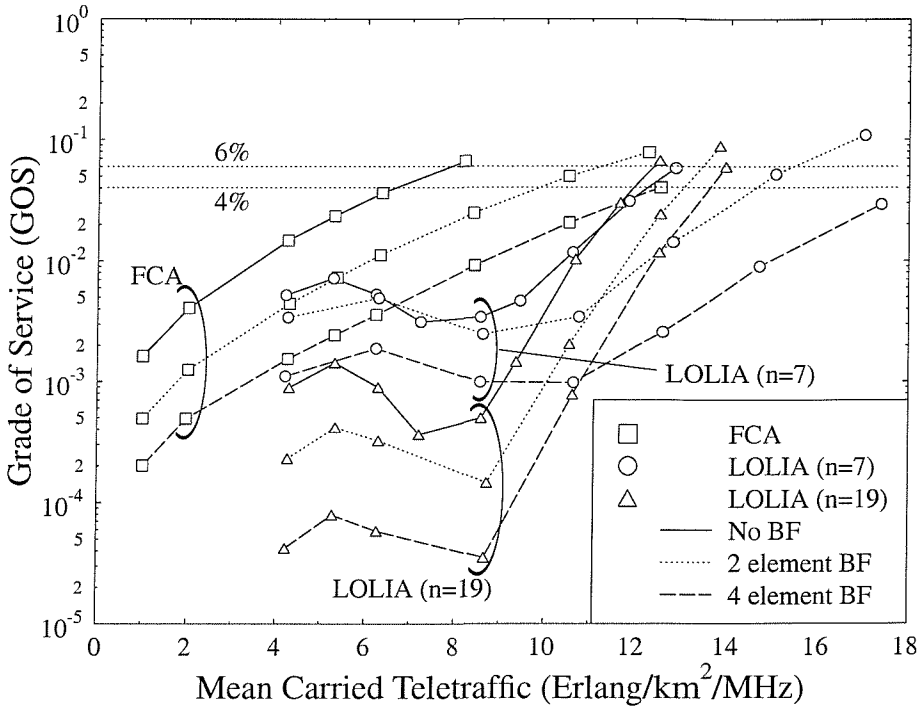

Figure 3.52: GOS performance versus mean carried traffic, for the LOLIA using 7 and 19 'local' base stations, and for FCA employing a 7-cell reuse cluster, under a uniform geographic traffic distribution, for a single antenna element, as well as for two and four element antenna arrays with beamforming in a **LOS environment** using wrap-around. See Figure 3.26 for the corresponding "desert-island" scenario.

LOLIA in conjunction with $n = 7$ due to using AAAs were more modest, than for the FCA system. Specifically, 44% more users were supported by the four element AAA-assisted LOLIA using $n = 7$, when compared to the single antenna element based results. The network capacity of the LOLIA along with a 19-cell exclusion zone was higher, than that of the LOLIA using $n = 7$, until the limited number of channels available in conjunction with such a large exclusion zone became significant. Up to this point, the AAAs reduced the levels of interference, thus improving the network capacity. However, when using a four-element AAA, the new call blocking probability became the dominant network performance limiting factor.

3.7.3.2 Performance Results over a Multipath Channel

Following our previous experiments, where a purely LOS environment existed between the mobiles and their base stations, this section presents results for a multipath environment

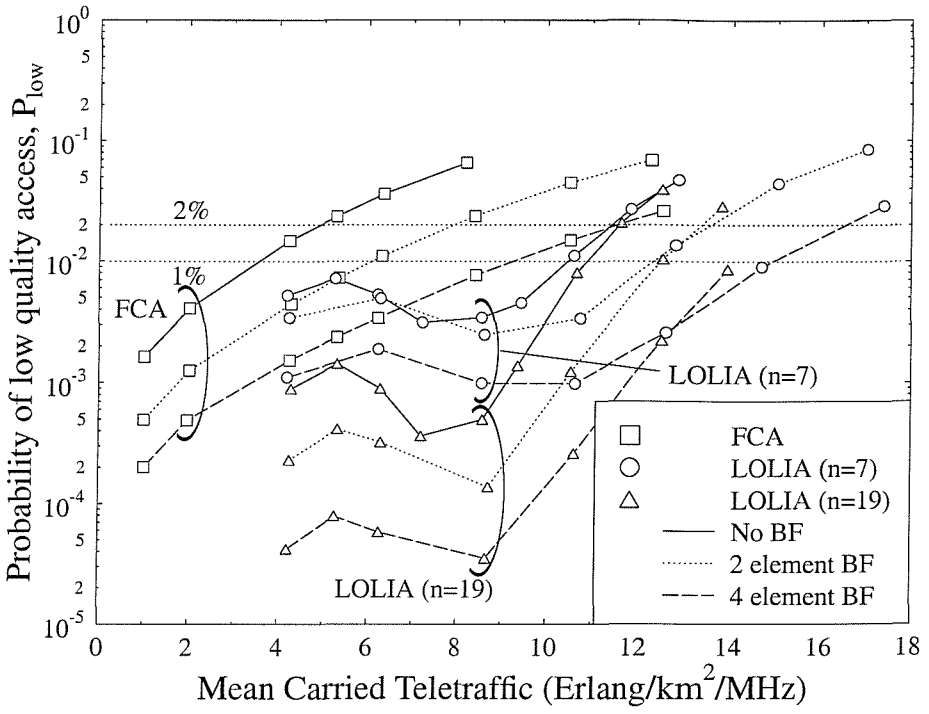

Figure 3.53: Probability of low quality access performance versus mean carried traffic, for the LOLIA using 7 and 19 'local' base stations, and for FCA employing a 7-cell reuse cluster, under a uniform geographic traffic distribution, for a single antenna element, as well as for two and four element antenna arrays with beamforming in a **LOS environment** using wrap-around. See Figure 3.25 for the corresponding "desert-island" scenario.

using two-, four- and eight-element AAAs.

Comparing the call blocking probabilities of the multipath environment, shown in Figure 3.55, with those of the LOS environment, shown in Figure 3.50, reveals that all of the channel allocation algorithms behave similarly for both radio environments. The FCA scheme actually behaved more unfavourably in terms of its new call blocking probability, as the number of AAA elements was increased. However, this is a consequence of the additional antenna elements improving the other performance measures, such as the call dropping rate. This enabled additional calls to be sustained at a given time, leading to a higher call blocking rate. In conjunction with an exclusion zone of 19 cells we found that the LOLIA's blocking performance was barely affected by the adaptive antenna arrays, whilst for $n = 7$ the blocked call rate was improved by a factor of 10 at a traffic load of 14-17 Erlang/km^2/MHz.

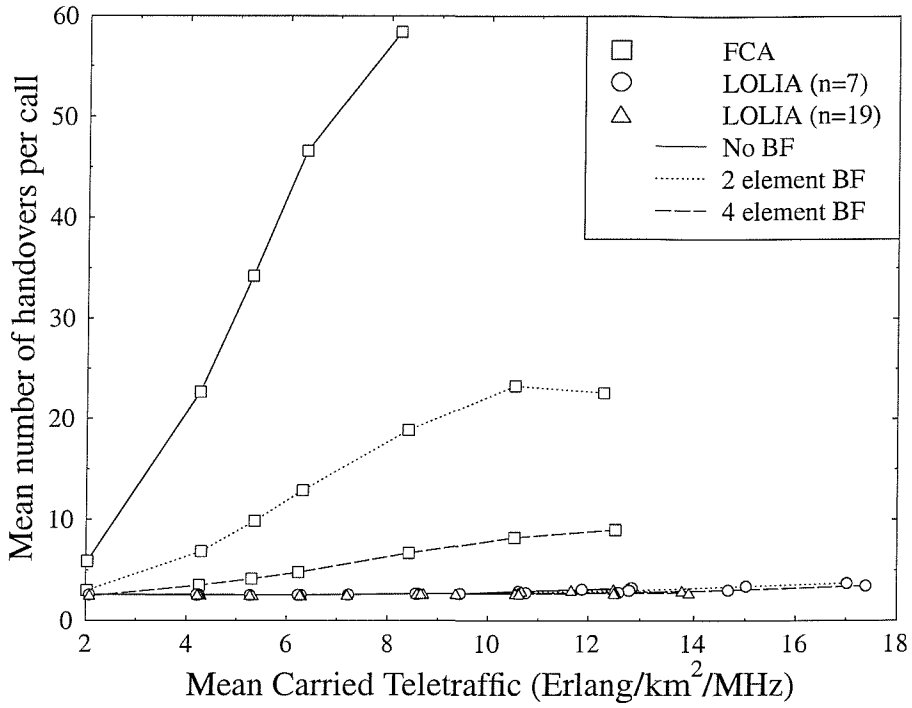

Figure 3.54: Mean number of successful handovers per call versus mean carried traffic, for comparison of the LOLIA using 7 and 19 'local' base stations, and for FCA employing a 7-cell reuse cluster, under a uniform geographic traffic distribution, for a single antenna element, as well as for two and four element antenna arrays with beamforming in a **LOS environment** using wrap-around. See Figure 3.27 for the corresponding "desert-island" scenario.

Figure 3.56 shows the probability of a dropped call in a multipath propagation environment, which was slightly higher than for the LOS scenario of Figure 3.51, when considered in the context of a given channel allocation algorithm and for a given antenna array size. The call dropping rate was improved with the aid of adaptive antenna arrays for all of the channel allocation algorithms, though the LOLIA using $n = 19$ did not benefft to the same extent as the other algorithms.

Again, as expected, the GOS curves in Figure 3.57 and the probability of low quality access curves of Figure 3.58 are similar in shape, with the differences resulting from the blocked call probability according to Equation 3.23. Hence, the GOS of the LOLIA having an exclusion zone of 19 base stations increases more rapidly, than its probability of low quality access. In addition, the gain in its low quality of access performance achieved by using the adaptive antenna arrays is reduced, in terms of the GOS, due to the limited blocking probability improvement offered by the adaptive antenna arrays. All three algorithms

Algorithm	Conservative $P_{FT} = 1\%$, $P_{low} = 1\%$ $P_B = 3\%$, $GOS = 4\%$			Lenient $P_{FT} = 1\%$, $P_{low} = 2\%$ $P_B = 5\%$, $GOS = 6\%$		
	Users	**Traffic**	**Limiting Factor**	**Users**	**Traffic**	**Limiting Factor**
FCA, 1 element	340	3.6	P_{low}	465	4.9	P_{low}
FCA, 2 elements	**575**	**6.1**	P_{low}	**755**	**7.9**	P_{low}
FCA, 4 elements	**885**	**9.3**	P_{low}	**1105**	**11.2**	P_{FT}
LOLIA (n=7), 1 element	990	10.5	P_{low}	1065	11.45	P_{low}
LOLIA (n=7), 2 elements	**1155**	**12.35**	P_{low}	**1260**	**13.5**	P_{low}
LOLIA (n=7), 4 elements	**1420**	**14.9**	P_{low}	**1535**	**16.5**	P_{low}
LOLIA (n=19), 1 element	1020	10.9	P_{low}	1090	11.6	P_{low}
LOLIA (n=19), 2 elements	**1200**	**12.5**	P_{low}	**1330**	**13.35**	P_{low}
LOLIA (n=19), 4 elements	**1335**	**13.45**	P_B	**1400**	**13.9**	P_B

Table 3.12: Maximum mean carried traffic, and maximum number of mobile users that can be supported by each configuration, whilst meeting the preset quality constraints defined in Section 3.6. The carried traffic is expressed in terms of normalised Erlangs (Erlang/km^2/MHz), for the network described in Table 3.3 in a **LOS environment** using wrap-around. See Table 3.5 for the corresponding "desert-island" results.

benefit significantly in terms of their low quality access performance from the employment of the adaptive antenna arrays. However, the significant blocking performance limitations of the LOLIA using $n = 19$ restricts its GOS performance gains.

Figure 3.59 demonstrates the significant impact that adaptive antenna arrays have on the mean number of handovers per call for the FCA algorithm in a multipath environment. Even in conjunction with adaptive antenna arrays more handovers per call were invoked, when using the FCA system, than for either of the LOLIAs using a single antenna element. Furthermore, a higher number of handovers was required in the multipath environment, than in the LOS scenario, for a given size of adaptive antenna array. The LOLIAs required significantly fewer handovers than the FCA, irrespective of the propagation environment, and did not benefit from the employment of adaptive antenna arrays in terms of the required handovers per call.

Table 3.13 presents results similar to those in Table 3.12, but for a multipath environment, with the bold values highlighting the adaptive antenna array sizes common to both sets of investigations. From this table it can be seen that the LOLIA using $n = 19$ carries approximately the same amount of traffic in the multipath scenario, which translates into a similar network capacity to that of the LOS scenario of Table 3.12. Again, the number of users supported by the network is limited by the probability of a low quality access and by

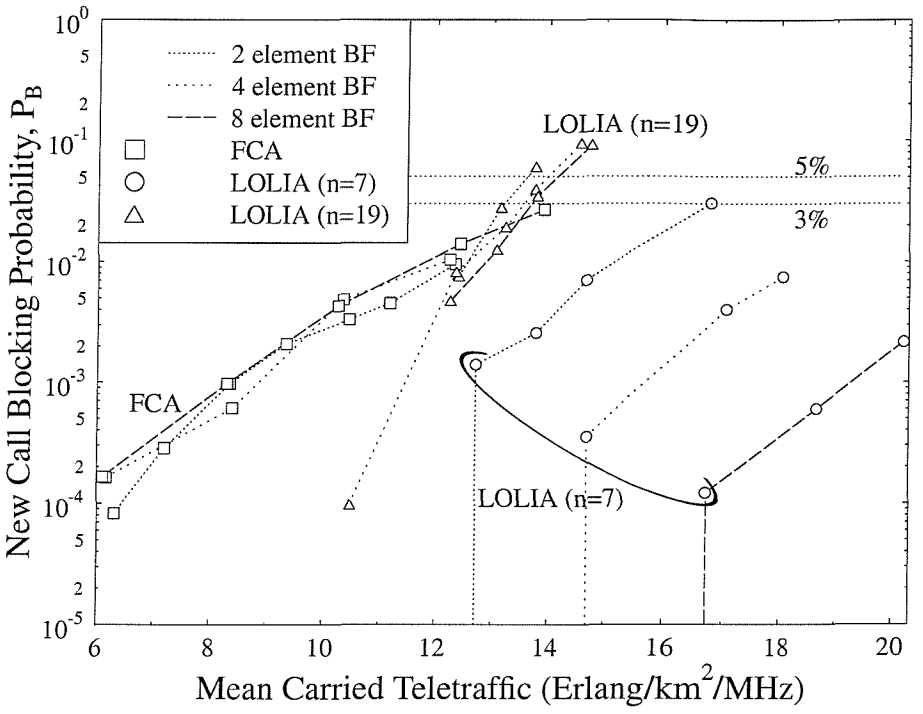

Figure 3.55: New call blocking probability performance versus mean carried traffic, for comparison of the LOLIA using 7 and 19 'local' base stations, and for FCA using a 7-cell reuse cluster, under a uniform geographic traffic distribution, for two, four and eight element antenna arrays with beamforming in a **multipath environment** using wrap-around. See Figure 3.29 for the corresponding "desert-island" scenario.

the new call blocking probability. The performance of the LOLIA using $n = 7$ was interference limited, where the smaller reuse distance or exclusion zone led to numerous sources of relatively strong interference, all requiring interference cancellation. Hence, as the number of adaptive antenna array elements increased, so did the number of users supported, with an average improvement of about 15% for each doubling of the number of array elements.

3.7.3.3 Performance over a Multipath Channel using Power Control

This section presents results obtained using the same wrap-around scenario of Section 3.7.1 over a multipath channel using power control. The power control algorithm was the same as that described in Section 3.7.2.3. The power control algorithm implemented attempted to independently adjust the mobile and base station transmit powers, such that the up- and down-link SINRs were within a given target SINR window. The use of a target SINR window allowed us to avoid constantly increasing and decreasing the transmission powers,

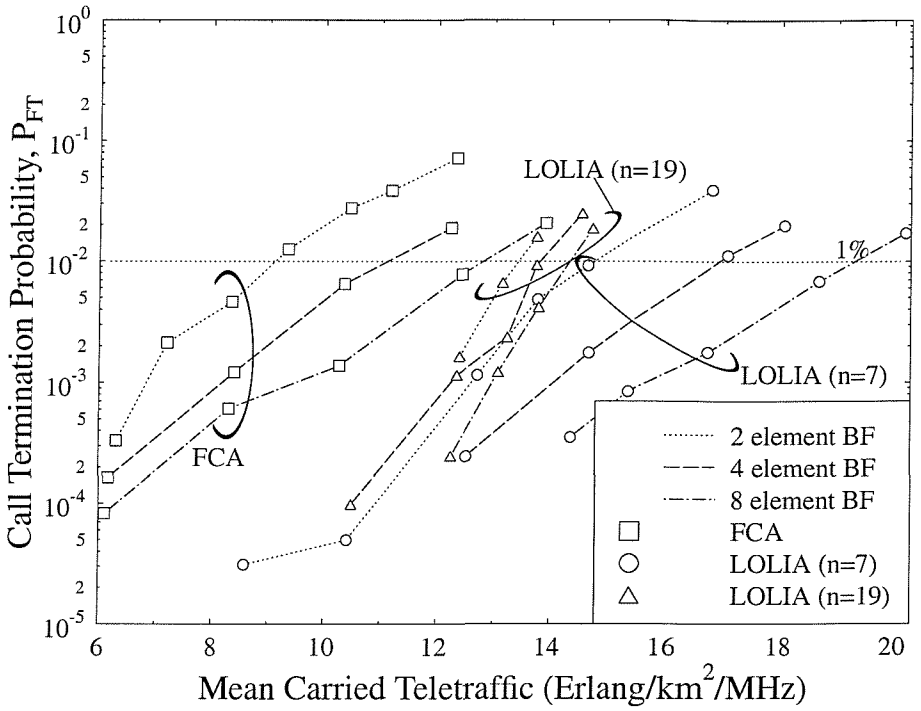

Figure 3.56: Call dropping probability performance versus mean carried traffic, for comparison of the LOLIA using 7 and 19 'local' base stations, and for FCA using a 7-cell reuse cluster, under a uniform geographic traffic distribution, for two, four and eight element antenna arrays with beamforming in a **multipath environment** using wrap-around. See Figure 3.30 for the corresponding "desert-island" scenario.

which could lead to potential power control instabilities within the network. Furthermore, the effect of employing a range of possible transmission powers is analogous to an inherent power control error plus slow fading phenomenon.

Figure 3.60 portrays the new call blocking probability versus the mean normalised carried traffic, expressed in terms of Erlangs/km^2/MHz. The figure shows that using power control in conjunction with the FCA algorithm resulted in a slight increase in the new call blocking probability as a direct consequence of the improved call dropping probability shown in Figure 3.61. In contrast, the blocking probability of the LOLIA improved significantly due to using power control, achieving a reduction by a factor of 4 to 34.

The new call blocking performance of the LOLIA was superior to that of the FCA algorithm both with and without power control, as seen in Figure 3.60, which is a result of the dynamic nature of the LOLIA. This enabled the LOLIA to allocate any of the available channels not used within the 7-cell exclusion zone (maximum of 7×8=56 channels in this

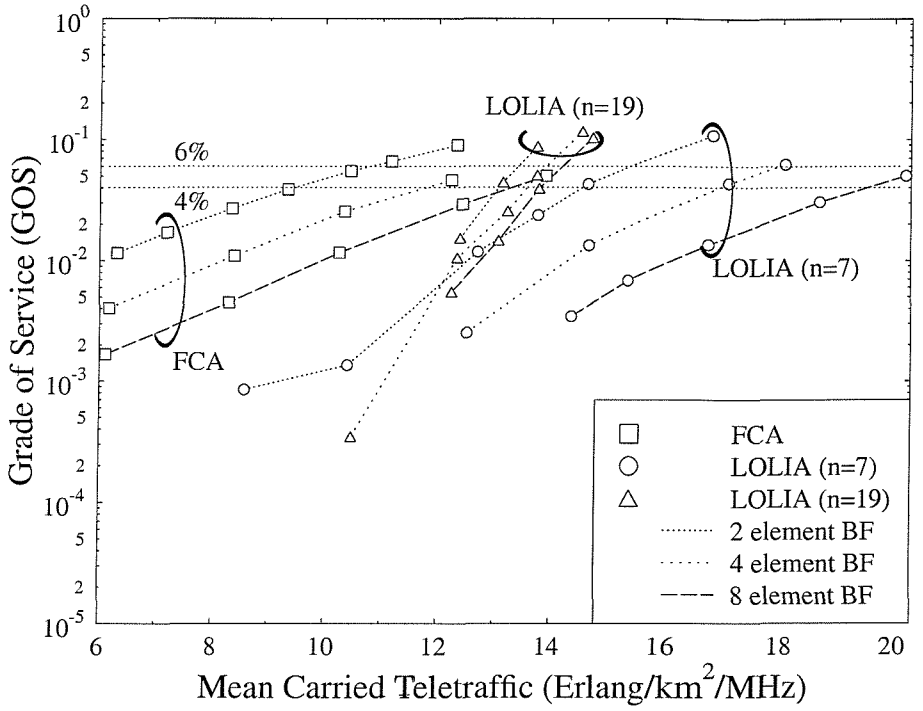

Figure 3.57: GOS performance versus mean carried traffic, for the comparison of the LOLIA with 7 and 19 'local' base stations, and for FCA using a 7-cell reuse cluster, under a uniform geographic traffic distribution, for two, four and eight element antenna arrays with beamforming in a **multipath environment** using wrap-around. See Figure 3.32 for the corresponding "desert-island" scenario.

scenario) to a new call request. However, the FCA algorithm only had one carrier frequency per base station, and therefore was less likely to be able to satisfy a new call request. The addition of power control to the LOLIA in conjunction with $n = 7$ led to a reduced new call blocking probability. Specifically, the new call blocking probability with power control was reduced to near that achieved using twice the number of antenna elements without power control. The higher new call blocking probability of the network using no power control can be attributed to the lower average SINR values, which prevent new call initiation, whereas the higher average SINR level of the network observed in Figure 3.35 in conjunction with power control enables additional calls to commence.

Figure 3.61 shows that the call dropping probability was significantly reduced for both the FCA algorithm and the LOLIA using $n = 7$, in conjunction with power control. The FCA algorithm in conjunction with power control offered a call dropping probability close to that of a similar network, without power control, and using twice the number of adaptive antenna elements. However, at traffic loads of below approximately 7 Erlangs/km^2/MHz the

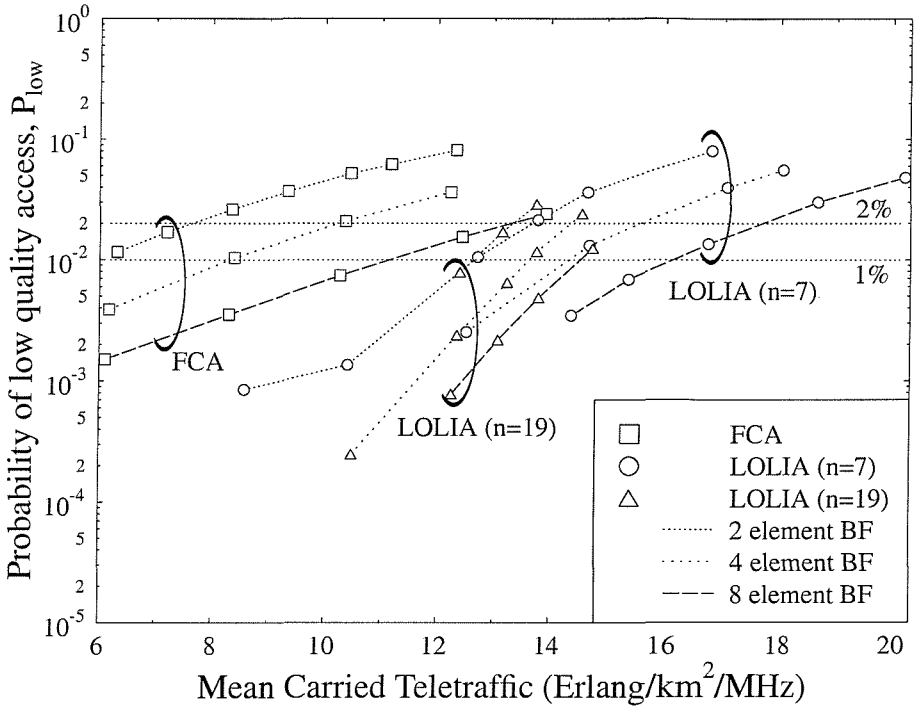

Figure 3.58: Probability of low quality access performance versus mean carried traffic, for the comparison of the LOLIA using 7 and 19 'local' base stations, and for FCA using a 7-cell reuse cluster, under a uniform geographic traffic distribution, for two, four and eight element antenna arrays with beamforming in a **multipath environment** using wrap-around. See Figure 3.31 for the corresponding "desert-island" scenario.

call dropping probability began to level off for the FCA algorithm. This phenomenon was also noticeable in the context of the LOLIA and resulted from the power control algorithm limiting the maximum SINR, leading to a flatter call dropping profile than that of the network without power control. Thus, at lower traffic loads the network without power control had a higher average SINR as was evidenced by Figure 3.35, leading to less dropped calls. However, at higher levels of teletraffic the power control algorithm offered a lower call dropping rate, as a consequence of the lower levels of interference present when using the power control scheme.

The FCA algorithm exhibited the greatest improvement in the probability of a low quality access due to the implementation of power control, as shown in Figure 3.62. Using a two element adaptive antenna array in conjunction with the power control algorithm resulted in a probability of low quality access approximately equal to that obtained using an eight element adaptive array without power control. The LOLIA also benefited from invoking the power control algorithm, but to a lesser extent, offering a performance close to that of

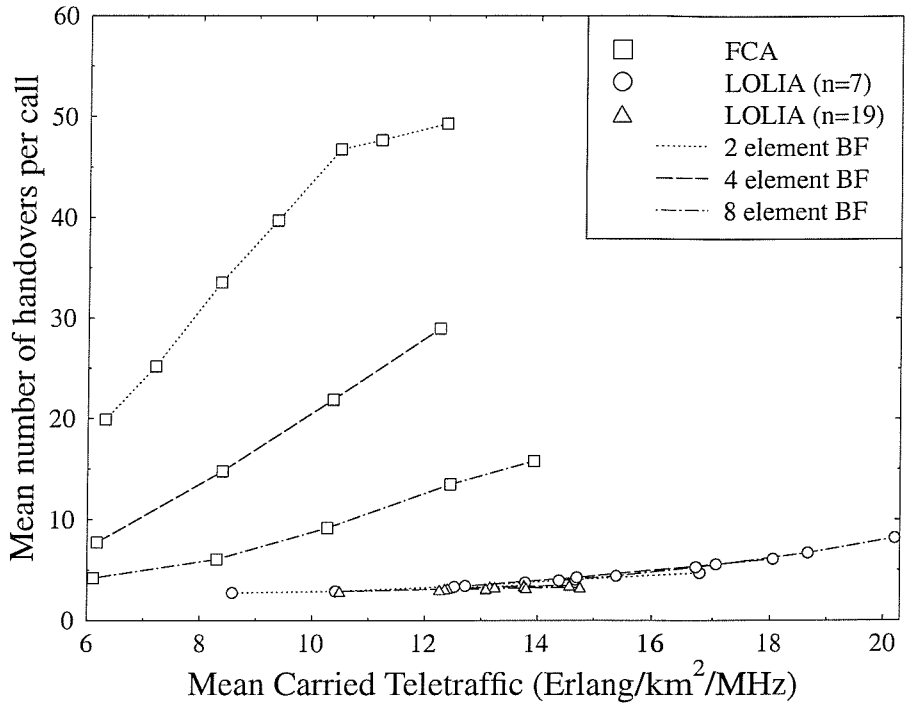

Figure 3.59: Mean number of successful handovers per call versus mean carried traffic, for comparison of the LOLIA using 7 and 19 'local' base stations, and for FCA using a 7-cell reuse cluster, under a uniform geographic traffic distribution, for two, four and eight element antenna arrays with beamforming in a **multipath environment** using wrap-around. See Figure 3.33 for the corresponding "desert-island" scenario.

an array with twice the number of elements without power control.

The GOS performance gains of the FCA algorithm using power control seen in Figure 3.63, were somewhat reduced compared to those of the probability of a low quality access in Figure 3.62, due to the similar blocking performances of the power-controlled and non-power-controlled scenarios seen in Figure 3.60. Nonetheless, the GOS gains remained quite high in Figure 3.63. The GOS gains of the LOLIA due to power control were also quite substantial, as seen in Figure 3.63.

The effect of power control on the mean number of handovers performed per call becomes explicit in Figure 3.64. From this figure it can be seen for the FCA algorithm that with respect to the number of handovers per call, the performance of the network employing power control significantly exceeded that of the network without power control using an adaptive antenna array of twice the number of antenna elements. The employment of power control in conjunction with the FCA algorithm led to a mean reduction by a factor

Algorithm	Conservative $P_{FT}=1\%$, $P_{low}=1\%$ $P_B=3\%$, $GOS=4\%$			Lenient $P_{FT}=1\%$, $P_{low}=2\%$ $P_B=5\%$, $GOS=6\%$		
	Users	**Traffic**	**Limiting Factor**	**Users**	**Traffic**	**Limiting Factor**
FCA, 2 element	**600**	**6.0**	P_{low}	**740**	**7.65**	P_{low}
FCA, 4 elements	**790**	**8.3**	P_{low}	**995**	**10.3**	P_{low}
FCA, 8 elements	1085	11.2	P_{low}	1250	12.8	P_{FT}
LOLIA (n=7), 2 element	**1195**	**12.65**	P_{low}	**1290**	**13.7**	P_{low}
LOLIA (n=7), 4 elements	**1370**	**14.35**	P_{low}	**1475**	**15.6**	P_{low}
LOLIA (n=7), 8 elements	1555	16.15	P_{low}	1700	17.7	P_{low}
LOLIA (n=19), 2 element	**1235**	**12.65**	P_{low}	**1325**	**13.3**	P_{low}
LOLIA (n=19), 4 elements	**1360**	**13.55**	P_B	**1410**	**13.8**	P_{FT}
LOLIA (n=19), 8 elements	1385	13.7	P_B	1475	14.15	P_B

Table 3.13: Maximum mean carried traffic, and maximum number of mobile users that can be supported by each configuration, whilst meeting the preset quality constraints defined in Section 3.6. The carried traffic is expressed in terms of normalised Erlangs (Erlang/km^2/MHz), for the network described in Table 3.3 in a **multipath environment** using wrap-around. See Table 3.6 for the corresponding "desert-island" results.

of 4.4 in the number of handovers. The inherently good performance of the LOLIA was also slightly improved on average.

A further advantage of using power control in a cellular mobile network is portrayed in Figure 3.65, which shows that the mean transmit power was reduced from the fixed transmit power of 10dBm due to power control. The mean transmit power of the FCA algorithm was reduced the most with reductions varying from 4.5dB to almost 9dB at the lowest traffic levels. Doubling the number of antenna elements comprising the base stations' adaptive antenna arrays from two to four, resulted in additional mean transmission power gains of almost 1dB at higher traffic loads, which is a consequence of the extra interference rejection capability of the four element array. The mean transmission powers of the LOLIAs were significantly higher due to the higher target SINRs required for maintaining an acceptable call dropping rate. This was a consequence of the dynamic nature of the LOLIA, leading to more rapidly changing interference levels, which required a relatively high target SINR of 31dB as seen in Table 3.7.

Table 3.14 presents similar results to Table 3.13, but using our power control algorithm, with the bold values highlighting the adaptive antenna array sizes common to both sets of investigations, for the sake of convenient comparison. The table shows the significant performance improvement obtained for both the LOLIA and the FCA algorithm in terms

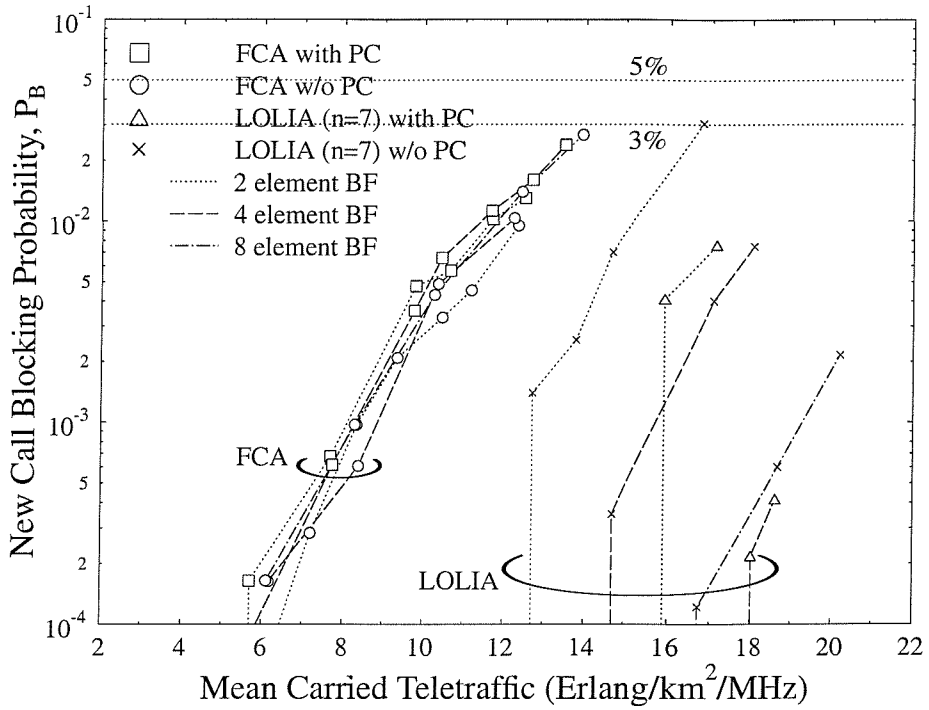

Figure 3.60: New call blocking probability versus mean carried traffic of the LOLIA using 7 'local' base stations, and for FCA employing a 7-cell reuse cluster, for two and four element antenna arrays, **with and without power control** using wrap-around. See Figure 3.36 for the corresponding "desert-island" scenario.

of the number of users supported with the advent of power control, whilst maintaining the desired network quality. In the conservative scenario, for example, the FCA algorithm using a two element adaptive antenna array and power control supported the same number of users as the network using an eight element adaptive antenna array without power control. The LOLIA-based network, however, did not benefit from the employment of the power control algorithm to the same extent, although still offered similar performance to that of a network without power control and using adaptive antenna arrays having twice the number of antenna elements.

3.7.3.4 Performance of an AQAM based Network using Power Control

This section presents our simulation results obtained for a network using burst-by-burst adaptive modulation [13, 101, 102, 103] invoked in order to improve the network's performance. Simulations were conducted for both a standard 7-cell FCA scheme and a 7-cell LOLIA assisted system. The results obtained for a 4-QAM based network using power

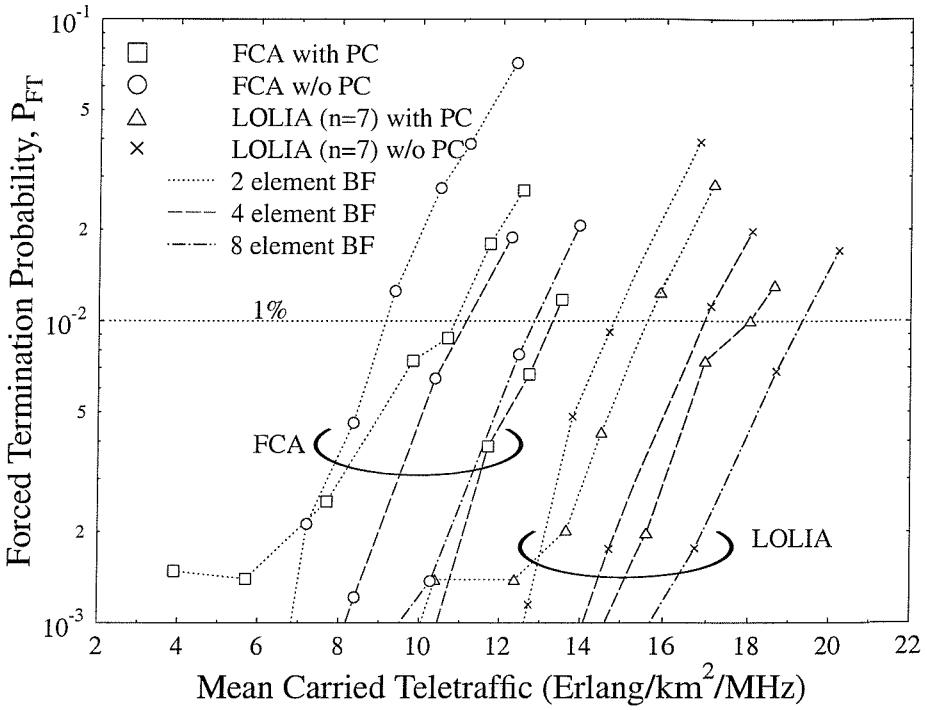

Figure 3.61: Call dropping probability versus mean carried traffic of the LOLIA using 7 'local' base stations, and for FCA employing a 7-cell reuse cluster, for two and four element antenna arrays, **with and without power control** using wrap-around. See Figure 3.37 for the corresponding "desert-island" scenario.

control were included for comparison purposes.

The new call blocking probability depicted in Figure 3.66 was essentially unchanged for the FCA algorithm using power control in conjunction with 4-QAM or AQAM, suggesting that the new call blocking performance of the FCA algorithm was limited by the lack of available frequency/timeslot combinations, rather than by inadequate signal quality. This hypothesis was confirmed by the improvement in the new call blocking performance of the LOLIA resulting from the superior signal quality of AQAM.

The corresponding call dropping probability is depicted in Figure 3.67. The AQAM LOLIA using $n = 7$ in conjunction with a two element adaptive antenna had, in general, a higher call dropping probability compared to that of power control assisted 4-QAM. However, the power control algorithm, when used in conjunction with AQAM, maintained the call dropping probability below the given threshold for a significantly higher traffic load. Similar performance trends were observed for both the two element and the four element adaptive array, although the higher interference rejection capability offered by

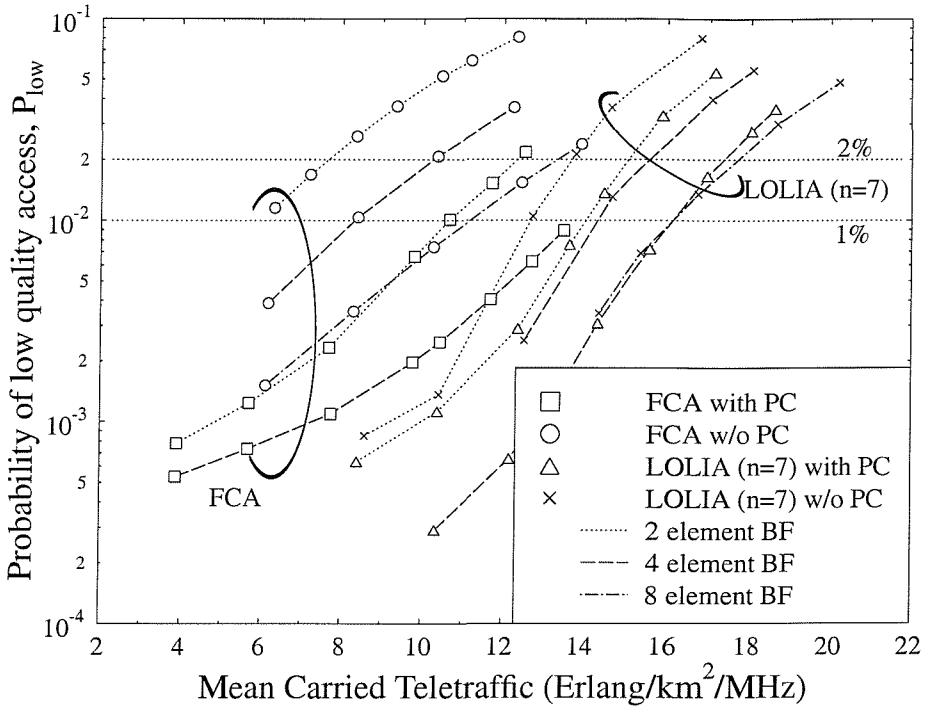

Figure 3.62: Probability of low quality outage versus mean carried traffic of the LOLIA using 7 'local' base stations, and for FCA employing a 7-cell reuse cluster, for two and four element antenna arrays, **with and without power control** using wrap-around. See Figure 3.38 for the corresponding "desert-island" scenario.

the four element array resulted in a substantially reduced call dropping probability. The dropped calls were caused almost exclusively by insufficient signal quality during the intra-cell handover process, thus increasing the number of adaptive antenna elements from two to four improved the call dropping performance. The high call dropping probability observed for traffic loads between 12 and 20 Erlangs/km^2/MHz when using the two element adaptive antenna array was due to the power control and AQAM attempting to trade-off modem throughput and transmit power against each other, whilst attempting to minimise the number of dropped calls. The extra interference suppression capability of the four-element adaptive antenna array led to a reduced call dropping probability. Hence, altering the AQAM mode selection algorithm of Figure 3.42, may improve its performance at these traffic loads, when used in conjunction with a two element antenna array.

The FCA algorithm dropped all of its calls during the inter-cell handover process due to the lack of available slots to handover to. However, since inter-cell handovers could be performed, if necessary, in order to improve the signal quality, the number of dropped

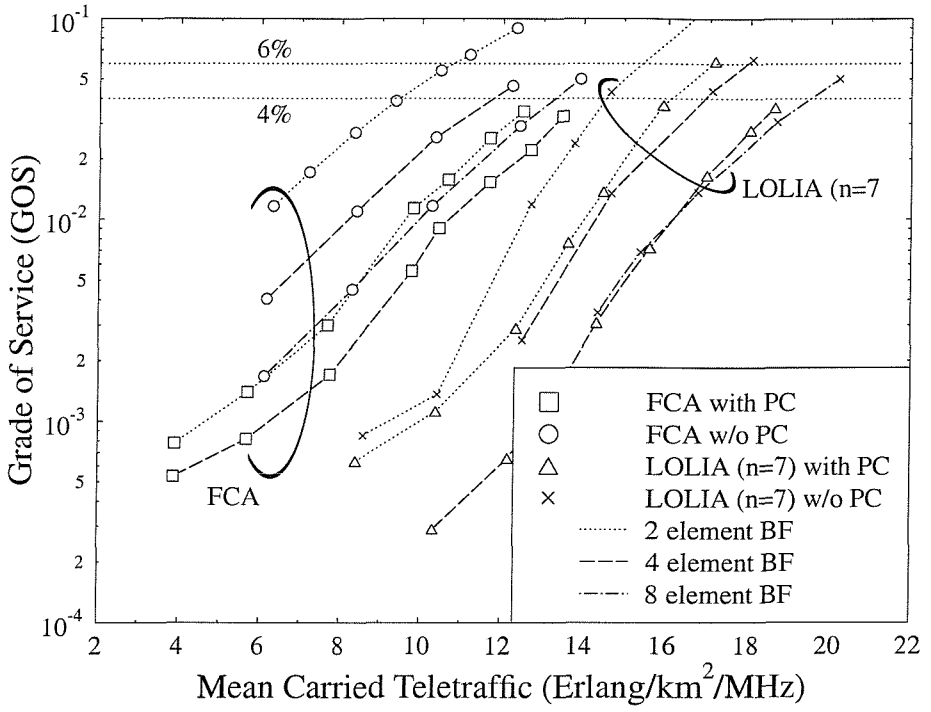

Figure 3.63: GOS performance versus mean carried traffic of the LOLIA using 7 'local' base stations, and for FCA employing a 7-cell reuse cluster, for two and four element antenna arrays, **with and without power control** using wrap-around. See Figure 3.39 for the corresponding "desert-island" scenario.

calls was reduced when using the four element adaptive array, due to its better interference rejection capability. All the calls were dropped during the inter-cell handover process, which means that no calls were dropped due to insufficient SINR or through the intra-cell handover process. This can be attributed to the AQAM scheme, which enabled users to drop to lower order modulation modes of the AQAM scheme, when the SINR became poor.

Figure 3.68 characterises the mean number of handovers per call for 4-QAM and AQAM, both using power control. The LOLIA using $n = 7$ performed a lower total number of handovers per call, when using AQAM, due its inherent resilience to poor signal quality conditions.

The breakdown of the handovers into inter-cell and intra-cell handovers is given in Figure 3.69. Observe that the improved interference rejection capability, and the associated superior SINR of the four-element array results in a lower number of intra-cell handovers for the LOLIA. Since the intra-cell handover process is the primary cause of dropped calls and less intra-cell handovers are performed when using a four-element antenna, more inter-cell

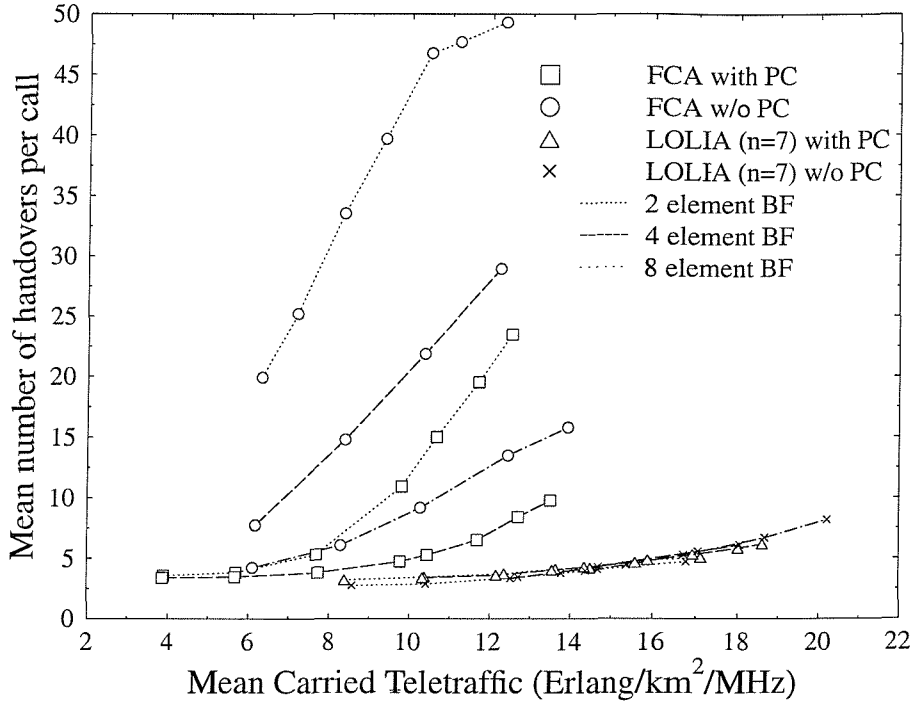

Figure 3.64: Mean number of successful handovers per call versus mean carried traffic of the LOLIA using 7 'local' base stations, and for FCA employing a 7-cell reuse cluster, for two and four element antenna arrays, **with and without power control** using wrap-around. See Figure 3.40 for the corresponding "desert-island" scenario.

handovers are necessitated in the network using four-element adaptive antenna arrays, as the users roam from cell to cell. In other words, since the LOLIA using a four element array drops less calls than when using a two element array, more users are in call at a given time, and hence these users cross more cell boundaries, thus necessitating more inter-cell handovers.

In contrast, the number of intra-cell handovers performed in conjunction with the FCA algorithm decreases, as the teletraffic rises, and as the number of antenna elements is increased from two to four. This is a consequence of the particular implementation of the modulation mode selection/power control algorithm and its interaction with the FCA handover process. The AQAM algorithm attempts to remain in the current modulation mode as long as possible, and hence as the SINR degrades, it will opt for performing an intra-cell handover in an attempt to maintain the SINR, rather than reconfiguring itself in order to use a lower-order modulation mode suitable for the reduced SINR level. Thus, when using a four-element adaptive antenna array, the average (and instantaneous) SINR is typically

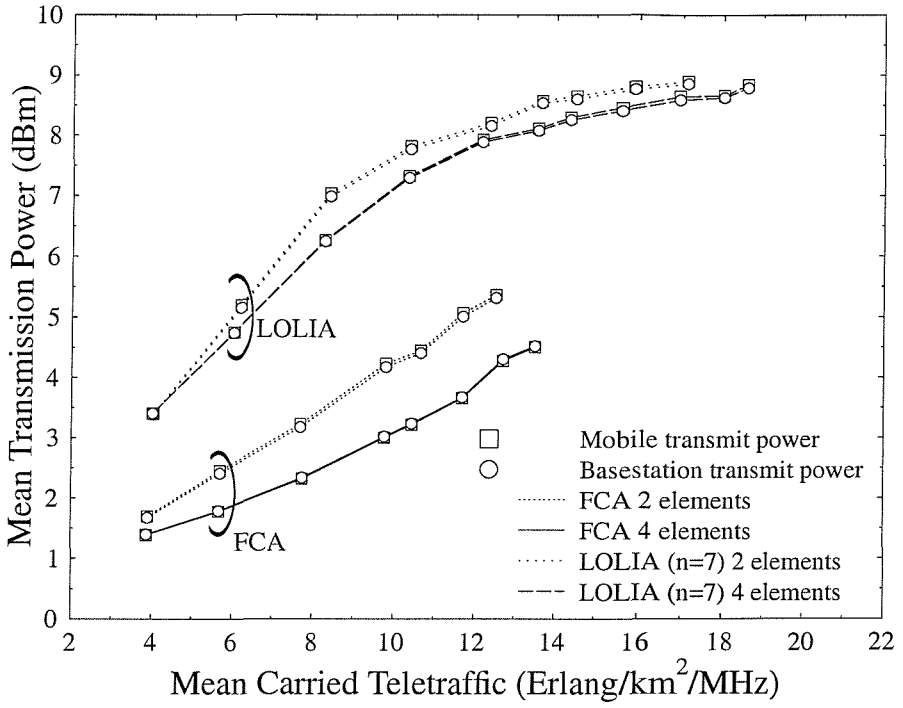

Figure 3.65: Mean transmit power versus mean carried traffic of the LOLIA using 7 'local' base stations, and for FCA employing a 7-cell reuse cluster, for two and four element antenna arrays, **with and without power control** using wrap-around. See Figure 3.41 for the corresponding "desert-island" scenario.

higher than that of a two-element array, leading to a more frequent employment of the less resilient higher-order modulation modes, which potentially requires additional intra-cell handovers. However, as the mean teletraffic increases, so does the level of interference in the network and a greater proportion of transmission time is spent in the lower-order modulation modes, thus requiring less intra-cell handovers, as illustrated in Figure 3.69.

The probability of a Low Quality (LQ) access is depicted in Figure 3.70, showing an interesting interaction between the FCA algorithm and the AQAM scheme. The probability of a LQ access occurring is reduced, as the traffic level increases and the number of antenna elements is decreased. This can be attributed to the less frequent usage of the higher-order modulation modes at the higher traffic loads. Hence the lower-order modulation modes are used more frequently and thus the chance of a LQ access taking place is reduced. The four-element adaptive antenna array leads to a higher probability of a low quality access, since its higher associated SINR levels activate a more frequent employment of the less robust, but higher-throughput, higher-order modulation modes. For example, let us consider the FCA

Algorithm	Conservative $P_{FT}=1\%$, $P_{low}=1\%$ $P_B=3\%$, $GOS=4\%$			Lenient $P_{FT}=1\%$, $P_{low}=2\%$ $P_B=5\%$, $GOS=6\%$		
	Users	**Traffic**	**Limiting Factor**	**Users**	**Traffic**	**Limiting Factor**
4-QAM without PC						
FCA, 2 element	**600**	**6.0**	P_{low}	**740**	**7.65**	P_{low}
FCA, 4 elements	**790**	**8.3**	P_{low}	**995**	**10.3**	P_{low}
FCA, 8 elements	1085	11.2	P_{low}	1250	12.8	P_{FT}
LOLIA (n=7), 2 element	**1195**	**12.65**	P_{low}	**1290**	**13.7**	P_{low}
LOLIA (n=7), 4 elements	**1370**	**14.35**	P_{low}	**1475**	**15.6**	P_{low}
LOLIA (n=7), 8 elements	1555	16.15	P_{low}	1700	17.7	P_{low}
4-QAM with PC						
FCA, 2 elements	**1090**	**10.6**	P_{low}	**1120**	**10.85**	P_{FT}
FCA, 4 elements	**1370**	**13.28**	P_{FT}	**1370**	**13.28**	P_{FT}
LOLIA (n=7), 2 elements	**1350**	**14.05**	P_{low}	**1445**	**15.1**	P_{low}
LOLIA (n=7), 4 elements	**1540**	**16.15**	P_{low}	**1640**	**17.35**	P_{low}

Table 3.14: Maximum mean carried traffic, and maximum number of mobile users that can be supported by each configuration, whilst meeting the preset quality constraints defined in Section 3.6. The carried traffic is expressed in terms of normalised Erlangs (Erlang/km^2/MHz), for the network described in Table 3.3 in a **multipath environment with and without power control** using wrap-around.

AQAM PC scenario supporting 400 users, which corresponded to a traffic load of about 4 Erlang/km^2/MHz. When using two antenna array elements, 85% of the LQ accesses occurred whilst in the 16-QAM mode, however, on increasing the number of antenna array elements to four this rose to 93%.

However, as the network loading rises, an increasing proportion of the LQ outages occur in the BPSK modulation mode. Coupled with the increase in the BPSK modulation mode's employment due to the low SINR constraints, the probability of a low quality outage is expected to increase at a certain traffic load. This can be seen in Figure 3.70, where the LQ outage probability is starting to rise for FCA in conjunction with both two and four elements, though the extra interference suppression capability of the four element array allows extra traffic to be carried, before this phenomenon commences. More specifically, although not explicit in Figure 3.70, we found that for a network supporting 1200 users, corresponding to a traffic load of about 12 Erlang/km^2/MHz, and employing two element adaptive antenna arrays, 43% of the LQ accesses occurred, whilst in the 16-QAM mode, versus 72% with four-element antenna arrays. Again, not explicitly shown in the figure, but increasing the number of users to 1400, or a traffic load of just less than 14 Erlang/km^2/MHz, reduced

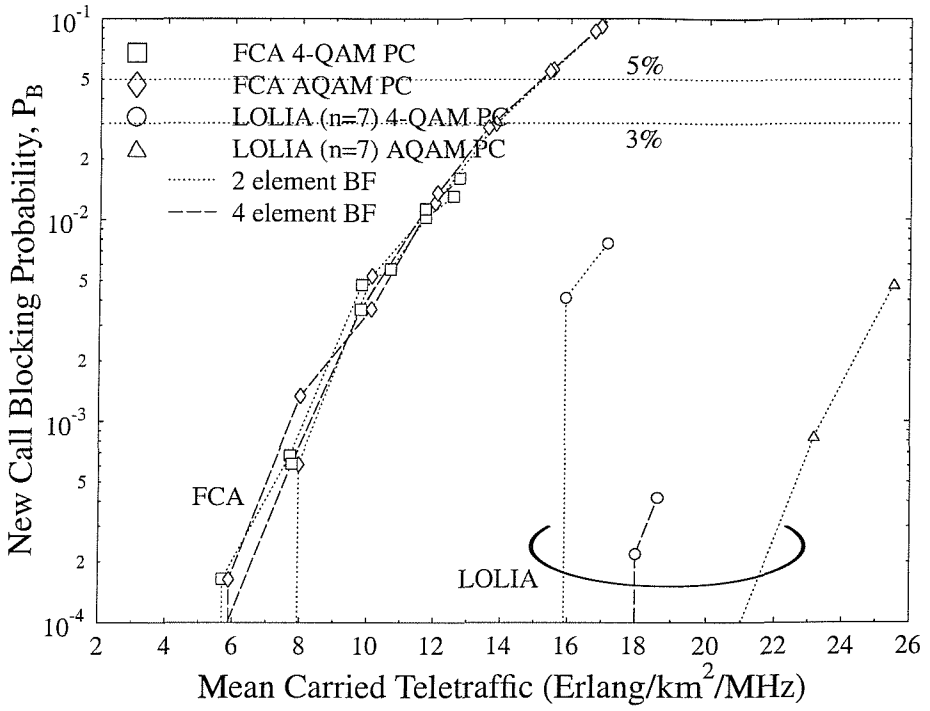

Figure 3.66: New call blocking probability versus mean carried traffic of the LOLIA using 7 'local' base stations, and for FCA employing a 7-cell reuse cluster, for two and four element antenna arrays, **with and without AQAM** using wrap-around. See Figure 3.43 for the corresponding "desert-island" scenario.

the number of 16-QAM LQ accesses, but increased the BPSK LQ outages to 69% and 31% for the two- and four-element arrays respectively, with reductions to 21% and 53% of the LQ outages in the 16-QAM mode.

From Figure 3.71 it can be seen that the GOS, as defined in Section 3.6, of the FCA algorithm did not benefit from invoking AQAM to the same extent as the LOLIA. This resulted from the fairly similar probability of low quality access performance of the two and four element antenna array assisted systems in Figure 3.70, and the limiting blocking performance observed in Figure 3.66. However, since the LOLIA did not suffer from these limiting factors, its GOS improved due to the employment of both adaptive antenna arrays and AQAM techniques.

The average modem throughput expressed in bits per symbol versus the mean carried teletraffic is shown in Figure 3.72, demonstrating that the mean number of bits per symbol throughput of the users decreased, as the number of users supported increased. The FCA algorithm offered the lowest throughput and its performance degraded near-linearly upon

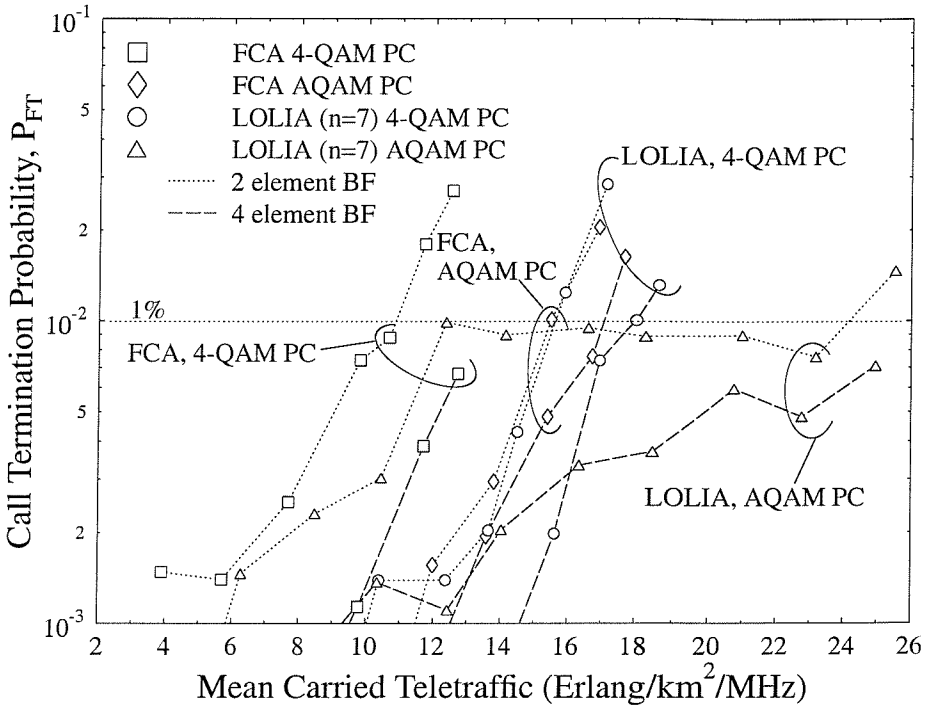

Figure 3.67: Call dropping, or forced termination, performance versus mean carried traffic of the LOLIA using 7 'local' base stations, and for FCA employing a 7-cell reuse cluster, for two and four element antenna arrays, **with and without AQAM** using wrap-around. See Figure 3.44 for the corresponding "desert-island" scenario.

increasing the number of users supported. At the user capacity limits of 1400 and 1565 users, the mean modem throughput was 2.45 BPS and 2.35 BPS for the conservative and lenient scenarios, respectively, using two element adaptive antenna arrays. Using four element adaptive antenna arrays the corresponding throughputs were 2.7 BPS and 2.6 BPS. The LOLIA, especially for lower levels of traffic, offered a higher modem throughput for a given level of teletraffic carried, with the BPS throughput performance gracefully decreasing, as the carried teletraffic continued to increase. The capacity limiting factor of the LOLIA was the throughput restriction of 2.0 BPS.

The mean transmission power results of Figure 3.73 demonstrate that the employment of AQAM is capable of reducing the power transmitted, both for the up- and the down-link. At low traffic levels the FCA algorithm performed noticeably worse in transmitted power terms, than the LOLIA. However, as the traffic load increased, the difference became negligible. The mean power reduction, when compared to a fixed transmission power of 10dBm, varied from approximately 1dB to more than 6dB. A 1dB reduction in transmission

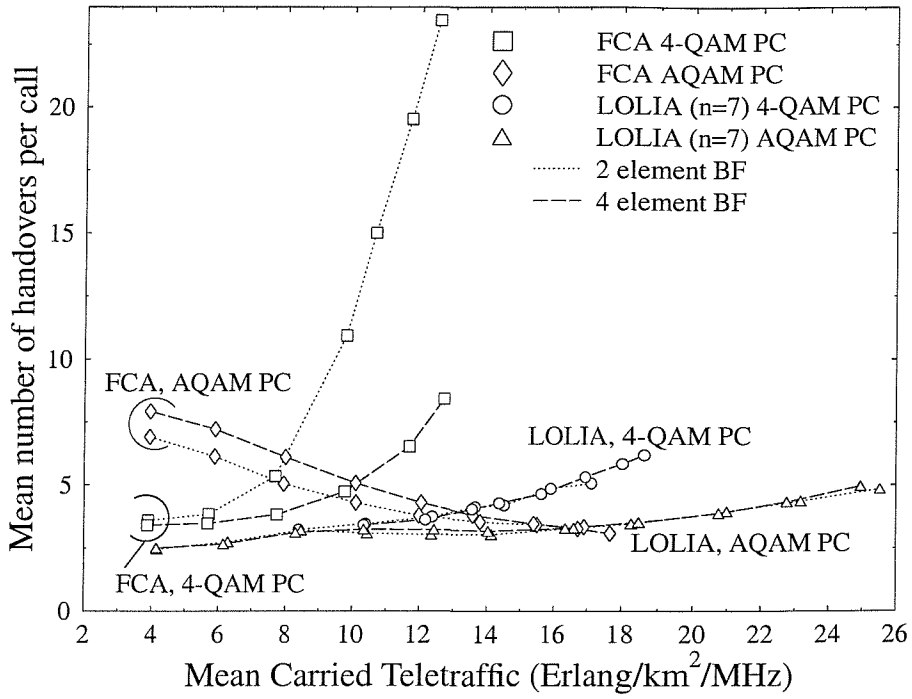

Figure 3.68: Mean number of successful handovers per call versus mean carried traffic of the LOLIA using 7 'local' base stations, and for FCA employing a 7-cell reuse cluster, for two and four element antenna arrays, **with and without AQAM** using wrap-around. See Figure 3.47 for the corresponding "desert-island" scenario.

power is not particularly significant for the mobile user, especially since at this network load a throughput of just 2 bits/symbol is possible. The difference between the network using AQAM and that without, though, is the overall improved call quality that can be achieved in the context of our performance metrics, and the significantly increased number of users that can be supported by the network.

Again, the constraint of a minimum throughput of 2 bits/symbol was invoked in order to ensure a fair comparison with the fixed 4-QAM based network.

Table 3.15 shows the performance of the various networks using AQAM with power control, as well as 4-QAM with and without power control, in terms of the number of users supported. A mean increase of 61% was achieved in terms of the number of users by the addition of power control to the FCA algorithm based 4-QAM network. Invoking AQAM and power control led to a further average user capacity increase of almost 22%, with any further gains limited by the lack of free frequency/timeslot combinations available for new calls to start. Therefore, since the network capacity of the FCA algorithm when using

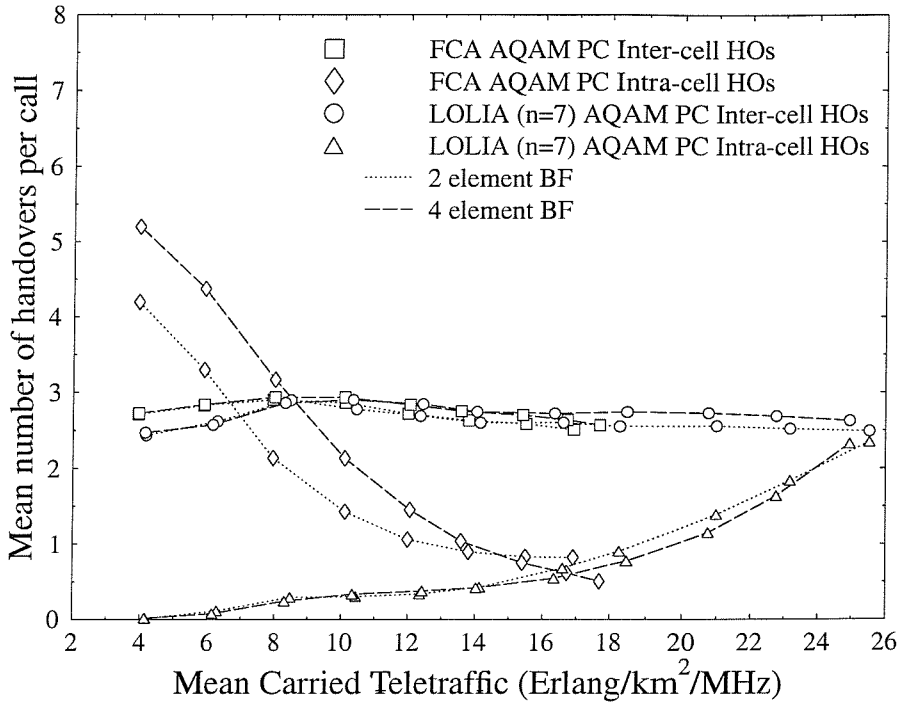

Figure 3.69: Mean number of successful inter-cell and intra-cell handovers per call versus mean carried traffic of the LOLIA using 7 'local' base stations, and for FCA employing a 7-cell reuse cluster, for two and four element antenna arrays, in conjunction **with AQAM** using wrap-around.

adaptive modulation was not limited by co-channel interference, it would be possible to reduce the frequency re-use distance to increase the network capacity.

The performance of the LOLIA was not limited in this sense, however, and the addition of power control to the 4-QAM network provided an mean increase of 12% extra users supported. In conjunction with AQAM techniques this user capacity was further extended by an average of 39%, thus supporting an additional 56% more users, when compared to the 4-QAM network using no power control.

3.8 Summary

In this chapter we have examined the network capacity and performance of the FCA algorithm and the LOLIA using an exclusion zone of seven or 19 base stations, in the context of LOS and multipath propagation environments. We have shown that the addition of power control results in a substantially increased number of supported users, additionally

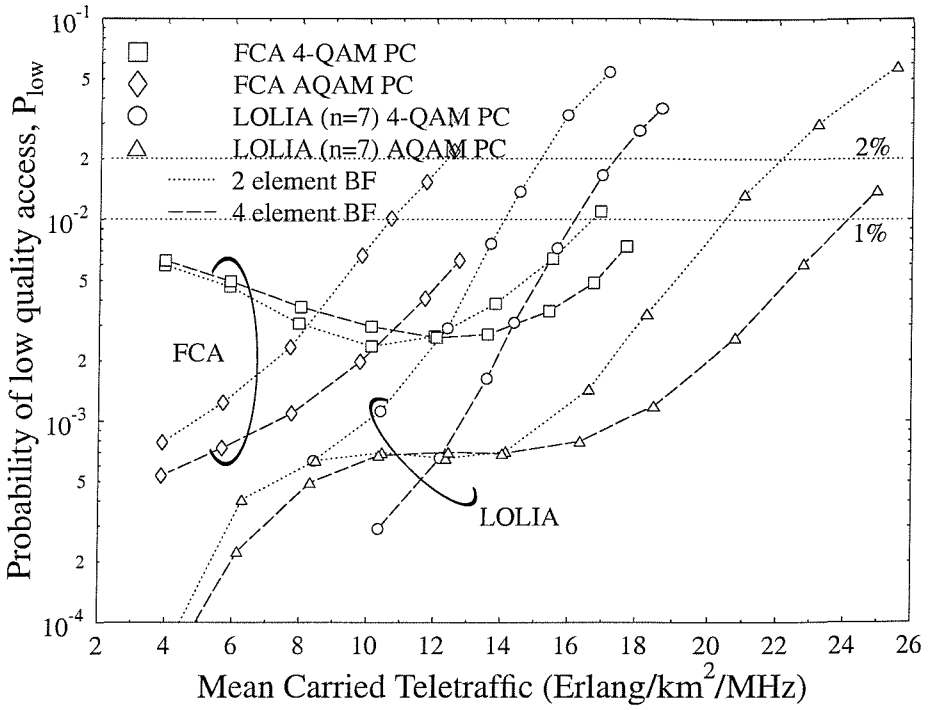

Figure 3.70: Probability of low quality access versus mean carried traffic of the LOLIA using 7 'local' base stations, and for FCA employing a 7-cell reuse cluster, for two and four element antenna arrays, **with and without AQAM** using wrap-around. See Figure 3.45 for the corresponding "desert-island" scenario.

benefiting from a superior call quality, and reduced transmission power for a given number of adaptive antenna array elements located at the base stations. The advantages of using AQAM within a mobile cellular network have also been illustrated, resulting in performance improvements in terms of the mean modem throughout, call quality, mean transmission power and the number of supported users. The next chapter involves the investigation of network capacity in the context of a CDMA-based UMTS-type FDD mode network.

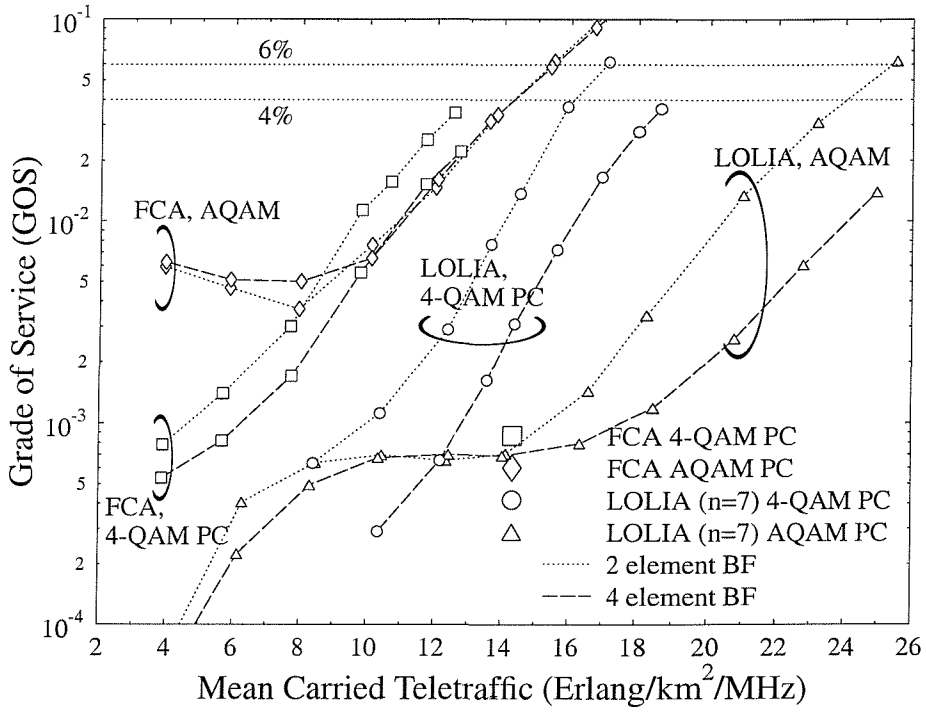

Figure 3.71: GOS performance versus mean carried traffic of the LOLIA using 7 'local' base stations, and for FCA employing a 7-cell reuse cluster, for two and four element antenna arrays, **with and without AQAM** using wrap-around. See Figure 3.46 for the corresponding "desert-island" scenario.

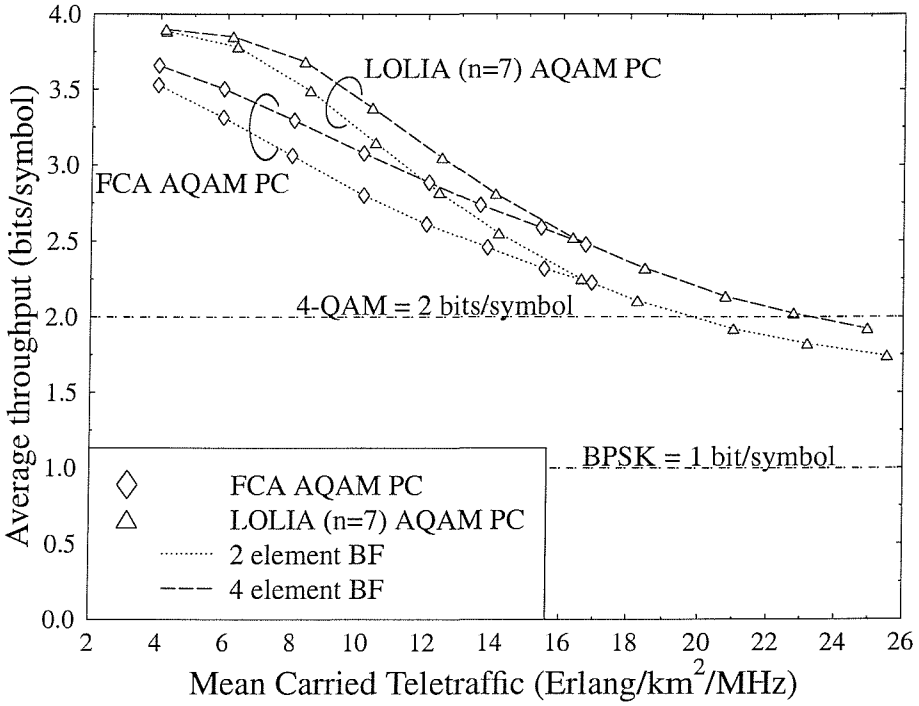

Figure 3.72: Mean throughput of users in terms of bits per symbol versus mean carried traffic of the LOLIA using 7 'local' base stations, and for FCA employing a 7-cell reuse cluster, for two and four element antenna arrays, **using AQAM** using wrap-around. See Figure 3.49 for the corresponding "desert-island" scenario.

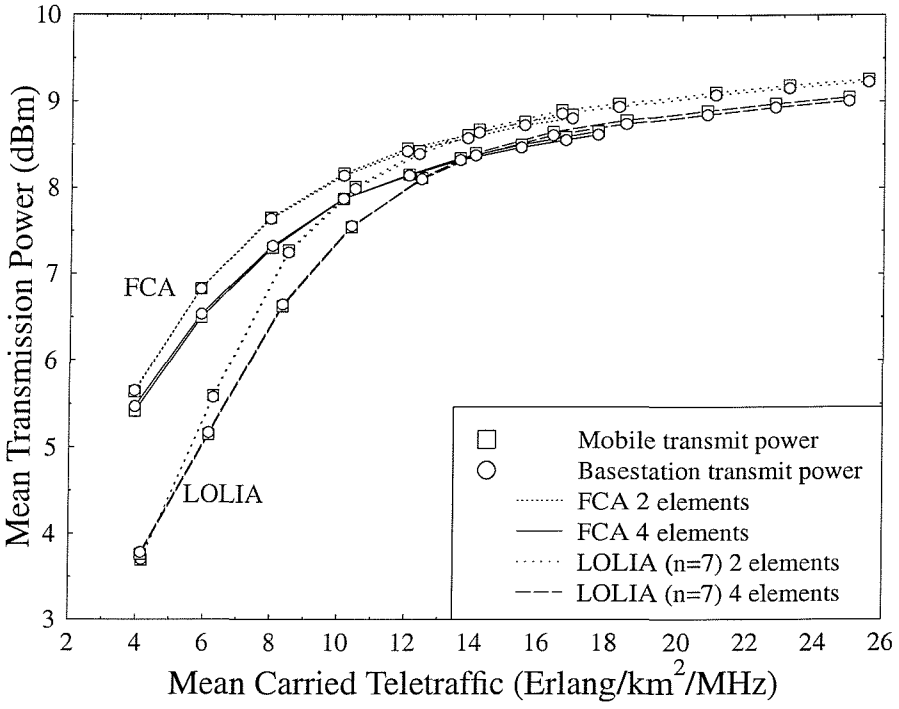

Figure 3.73: Mean transmit power versus mean carried traffic of the LOLIA using 7 'local' base stations, and for FCA employing a 7-cell reuse cluster, for two and four element antenna arrays, **using AQAM** using wrap-around. See Figure 3.45 for the corresponding "desert-island" scenario.

Algorithm	Conservative $P_{FT} = 1\%$, $P_{low} = 1\%$ $GOS = 4\%$, $P_B = 3\%$			Lenient $P_{FT} = 1\%$, $P_{low} = 2\%$ $GOS = 6\%$, $P_B = 5\%$		
	Users	**Traffic**	**Limiting Factor**	**Users**	**Traffic**	**Limiting Factor**
4-QAM without PC						
FCA, 2 elements	600	6.0	P_{low}	740	7.65	P_{low}
FCA, 4 elements	790	8.3	P_{low}	995	10.3	P_{low}
LOLIA (n=7), 2 elements	1195	12.65	P_{low}	1290	13.7	P_{low}
LOLIA (n=7), 4 elements	1370	14.35	P_{low}	1475	15.6	P_{low}
4-QAM with PC						
FCA, 2 elements	1090	10.6	P_{low}	1120	10.85	P_{FT}
FCA, 4 elements	1370	13.275	P_{FT}	1370	13.275	P_{FT}
LOLIA (n=7), 2 elements	1350	14.05	P_{low}	1445	15.1	P_{low}
LOLIA (n=7), 4 elements	1540	16.15	P_{low}	1640	17.35	P_{low}
AQAM with PC						
FCA, 2 elements	1400	13.8	P_B	1565	15.20	P_B
FCA, 4 elements	1415	13.7	P_B	1575	15.15	P_B
LOLIA (n=7), 2 elements	1910	19.75	BPS	1910	19.75	BPS
LOLIA (n=7), 4 elements	2245	23.25	BPS	2245	23.25	BPS

Table 3.15: Maximum mean carried traffic, and maximum number of mobile users that can be supported by each configuration, whilst meeting the preset quality constraints defined in Section 3.6. The carried traffic is expressed in terms of normalised Erlangs (Erlang/km^2/MHz), for the network described in Table 3.3 in a **multipath environment with and without power control and AQAM** using wrap-around.

Chapter 4

UTRA Network Performance

4.1 Introduction

In January 1998, the European standardisation body for third generation mobile radio systems, the European Telecommunications Standards Institute - Special Mobile Group (ETSI SMG), agreed upon a radio access scheme for third generation mobile radio systems, referred to as the Universal Mobile Telecommunication System (UMTS) [11, 104]. The UMTS Terrestrial Radio Access (UTRA) consists of two modes, a Frequency Division Duplex (FDD) mode, where the uplink and downlink are transmitted on different frequencies, and a Time Division Duplex (TDD) mode, where the uplink and the downlink are transmitted on the same carrier frequency, but multiplexed in time. The agreement recommends the employment of Wideband Code Division Multiple Access (W-CDMA) for UTRA FDD and Time Division - Code Division Multiple Access (TD-CDMA) for UTRA TDD. TD-CDMA is based on a combination of Time Division Multiple Access (TDMA) and CDMA, whereas W-CDMA is a purely CDMA-based system. The UTRA scheme can be used for operation within a minimum spectrum of 2 x 5 MHz for UTRA FDD and 5 MHz for UTRA TDD. Both duplex or paired and simplex or unpaired frequency bands have been identified in the region of 2 GHz to be used for the UTRA third generation mobile radio system. Both modes of UTRA have been harmonised with respect to the basic system parameters, such as carrier spacing, chip rate and frame length. Thereby, FDD/TDD dual mode operation is facilitated, which provides a basis for the development of low cost terminals. Furthermore, the interworking of UTRA with GSM [11] is ensured.

In UTRA, the different service needs are supported in a spectrally efficient way by a combination of FDD and TDD. The FDD mode is intended for applications in both macro- and micro-cellular environments, supporting data rates of up to 384kbps and high mobility.

The TDD mode, on the other hand, is more suited to micro and pico-cellular environments, as well as for licensed and unlicensed cordless, wireless local area networking and wireless local loop applications. It makes efficient use of the unpaired spectrum - for example in wireless Internet applications, where much of the teletraffic is in the downlink - and supports data rates of up to 2 Mbps. Therefore, the TDD mode is particularly well suited for environments generating a high traffic density (e.g. in city centres, business areas, airports etc.) and for indoor coverage, where the applications require high data rates and tend to have highly asymmetric traffic again, as in Internet access.

In parallel to the European activities, extensive work on third generation mobile radio has been carried out in Japan and in the USA. The Japanese standardisation body known as the Association of Radio Industry and Business (ARIB) also opted for W-CDMA, and the Japanese and European proposals for FDD have now converged. Similar concepts have also been developed by the North-American T1 standardisation body for the pan-American third generation (3G) system known as cdma2000 [11].

In order to work towards a truly global third generation mobile radio standard, the Third Generation Partnership Project (3GPP) was formed in December 1998. 3GPP consists of members of the standardisation bodies in Europe (ETSI), the US (T1), Japan (ARIB), Korea (TTA - Telecommunications Technologies Association), and China (CWTS - China Wireless Telecommunications Standard). 3GPP merged the already well harmonised proposals by the regional standardisation bodies and now works towards a single common third generation mobile radio standard under the terminology UTRA, retaining its two modes, and aiming to operate on the basis of the evolved GSM core network. The Third Generation Partnership Project 2 (3GPP2), on the other hand, works towards a third generation mobile radio standard, which is based on an evolved IS-95 type system which was originally referred to as cdma2000 [11]. In June 1999, major international operators in the Operator Harmonisation Group (OHG) proposed a harmonised G3G (Global Third Generation) concept, which has been accepted by 3GPP and 3GPP2. The harmonised G3G concept is a single standard with the following three modes of operation:

- CDMA direct spread (CDMA-DS), based on UTRA FDD as specified by 3GPP.
- CDMA multi-carrier (CDMA-MC), based on cdma2000 using FDD as specified by 3GPP2.
- TDD (CDMA TDD) based on UTRA TDD as specified by 3GPP.

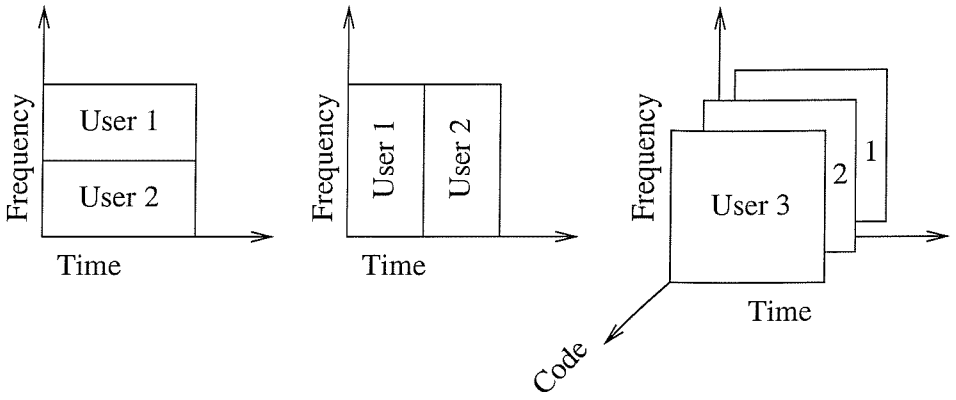

Figure 4.1: Multiple access schemes : FDMA (left), TDMA (middle) and CDMA (right)

4.2 Direct Sequence Code Division Multiple Access

Traditional ways of separating signals in time using TDMA and in frequency ensure that the signals are transmitted orthogonal in either time or frequency and hence they are non-interfering. In CDMA different users are separated employing a set of waveforms exhibiting good correlation properties, which are known as spreading codes. Figure 4.1 illustrates the principles of FDMA, TDMA and CDMA. More explicitly, FDMA uses a fraction of the total FDMA frequency band for each communications link for the whole duration of a conversation, while TDMA uses the entire bandwidth of a TDMA channel for a fraction of the TDMA frame, namely for the duration of a time slot. Finally, CDMA uses the entire available frequency band all the time and separates the users with the aid of unique, orthogonal user signature sequences.

In a CDMA digital communications system, such as that shown in Figure 4.2, the data stream is multiplied by the spreading code, which replaces each data bit with a sequence of code chips. A chip is defined as the basic element of the spreading code, which typically assumes binary values. Hence, the spreading process consists of replacing each bit in the original user's data sequence with the complete spreading code. The chip rate is significantly higher than the data rate, hence causing the bandwidth of the user's data to be spread, as shown in Figure 4.2.

At the receiver, the composite signal containing the spread data of multiple users is multiplied by a synchronised version of the spreading code of the wanted user. The specific auto-correlation properties of the codes allow the receiver to identify and recover each delayed, attenuated and phase-rotated replica of the transmitted signal, provided that the signals are separated by more than one chip period and the receiver has the capability of

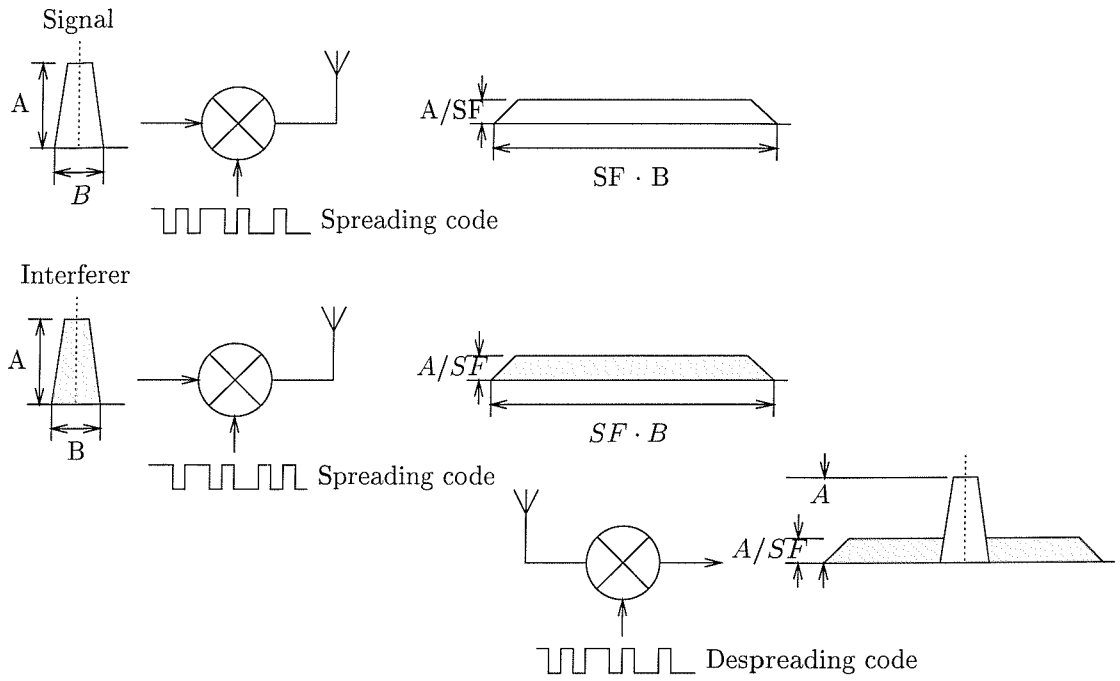

Figure 4.2: CDMA Spreading and Despreading Processes

tracking each significant path. This is achieved using a Rake receiver [5] that can process multiple delayed received signals. Coherent combination of these transmitted signal replicas allows the original signal to be recovered. The unwanted signals of the other simultaneous users remain wideband, having a bandwidth equal to that of the noise, and appear as additional noise with respect to the wanted signal. Since the bandwidth of the despread wanted signal is reduced relative to this noise, the signal-to-noise ratio of the wanted signal is enhanced by the despreading process in proportion to the ratio of the spread and despread bandwidths, since the noise power outside the useful despread signal's bandwidth can be removed by a low-pass filter. This bandwidth ratio is equal to the ratio of the chip rate to the data rate, which is known as the Processing Gain (PG). For this process to work efficiently, the signals of all of the users should be received at or near the same power at the receiver. This is achieved with the aid of power control, which is one of the critical elements of a CDMA system. The performance of the power control scheme directly affects the capacity of the CDMA network.

4.3 UMTS Terrestrial Radio Access

A bandwidth of 155 MHz in the region of 2.0 GHz has been allocated for UMTS services in Europe. The paired bands of 1920-1980 MHz (uplink) and 2110-2170 MHz (downlink) have been set aside for FDD W-CDMA systems, and the unpaired frequency bands of 1900-1920 MHz and 2010-2025 MHz for TDD CDMA systems.

A UTRA Network (UTRAN) consists of one or several Radio Network Sub-systems (RNSs), which in turn consist of base stations (referred to as Node Bs) and Radio Network Controllers (RNCs). A Node B may serve one or multiple cells. Mobile stations are known as User Equipment (UE), which are expected to support multi-mode operation in order to enable handovers between the FDD and TDD modes and, prior to complete UTRAN coverage, also to GSM. The key parameters of UTRA have been defined as in Table 4.1.

Duplex scheme	FDD	TDD
Multiple access scheme	W-CDMA	TD-CDMA
Chip rate	3.84 Mchip/s	3.84 Mchip/s
Spreading factor range	4-512	1-16
Frequency bands	1920-1980 MHz (UL)	1900-1920 MHz
	2110-2170 MHz (DL)	2010-2025 MHz
Modulation mode	4-QAM/QPSK	4-QAM/QPSK
Bandwidth	5 MHz	5 MHz
Nyquist pulse shaping	0.22	0.22
Frame length	10 ms	10 ms
Number of timeslots per frame	15	15

Table 4.1: Key UTRA Parameters

4.3.1 Spreading and Modulation

As usual, the uplink is defined as the transmission path from the mobile station to the base station, which receives the unsynchronised channel impaired signals from the network's mobiles. The base station has the task of extracting the wanted signal from the received signal contaminated by both intra- and inter-cell interference. However, as described in Section 4.2, some degree of isolation between interfering users is achieved due to employing unique orthogonal spreading codes, although their orthogonality is destroyed by the hostile mobile channel.

The spreading process consists of two operations. The first one is the channelisation operation, which transforms every data symbol into a number of chips, thus increasing the

bandwidth of the signal, as seen in Figure 4.2 of Section 4.2. The channelisation codes in UTRA are Orthogonal Variable Spreading Factor (OVSF) codes [11] that preserve the orthogonality between a given user's different physical channels, which are also capable of supporting multirate operation. These codes will be further discussed in the context of Figure 4.4. The second operation related to the spreading, namely the "scrambling" process then multiplies the resultant signals separately on the I- and Q-branches by a complex-valued scrambling code, as shown in Figure 4.3. The scrambling codes may be one of either 2^{24} different "long" codes or 2^{24} "short" uplink scrambling codes.

The Dedicated Physical Control CHannel (DPCCH) [11, 105] is spread to the chip rate by the channelisation code C_c, while the n^{th} Dedicated Physical Data CHannel (DPDCH), namely DPDCH$_n$, is spread to the chip rate by the channelisation code $C_{d,n}$. One DPCCH and up to six parallel DPDCHs can be transmitted simultaneously, i.e. $1 \leq n \leq 6$ as seen in Figure 4.3). However, it is beneficial to transmit with the aid of a single DPDCH, if the required bit-rate can be provided by a single DPDCH for reasons of terminal amplifier efficiency. This is because multi-code transmissions increase the peak-to-average ratio of the transmission, which reduces the efficiency of the terminal's power amplifier [104]. The maximum user data rate achievable with the aid of a single code is derived from the maximum channel bit rate, which is 960 kbps using a spreading factor of four without channel coding in the 1999 version of the UTRA standard. However, at the time of writing a spreading factor of one is being considered by the standardisation body. With channel coding the maximum practical user data rate for single code transmission is of the order of 400-500 kbps. For achieving higher data rates parallel multi-code channels are used. This allows up to six parallel codes to be used, three in the I channel and three in the Q channel, increasing the achievable channel bit rate to 5740 kbps, which can accommodate a 2 Mbps user data rate or even higher data rates, if the channel coding rate is 1/2.

The OVSF codes [106] can be defined using the code tree of Figure 4.4. In Figure 4.4, the channelisation codes are uniquely described by $C_{ch,SF,k}$, where SF is the spreading factor of the codes, and k is the code index where $1 \leq k \leq SF - 1$. Each level in the code tree defines spreading codes of length SF, corresponding to a particular spreading factor of SF. The number of codes available for a particular spreading factor is equal to the spreading factor itself. All the codes of the same level in the code tree constitute a set and they are orthogonal to each other. Any two codes of different levels are also orthogonal to each other, as long as one of them is not the mother of the other code. For example, the codes $c_{15}(2)$, $c_7(1)$ and $c_3(1)$ are all the mother codes of $c_{31}(3)$ and hence are not orthogonal to $c_{31}(3)$, where the number in the round bracket indicates the code index. Thus not all the codes within the code tree can be used simultaneously by a mobile station. Specifically, a

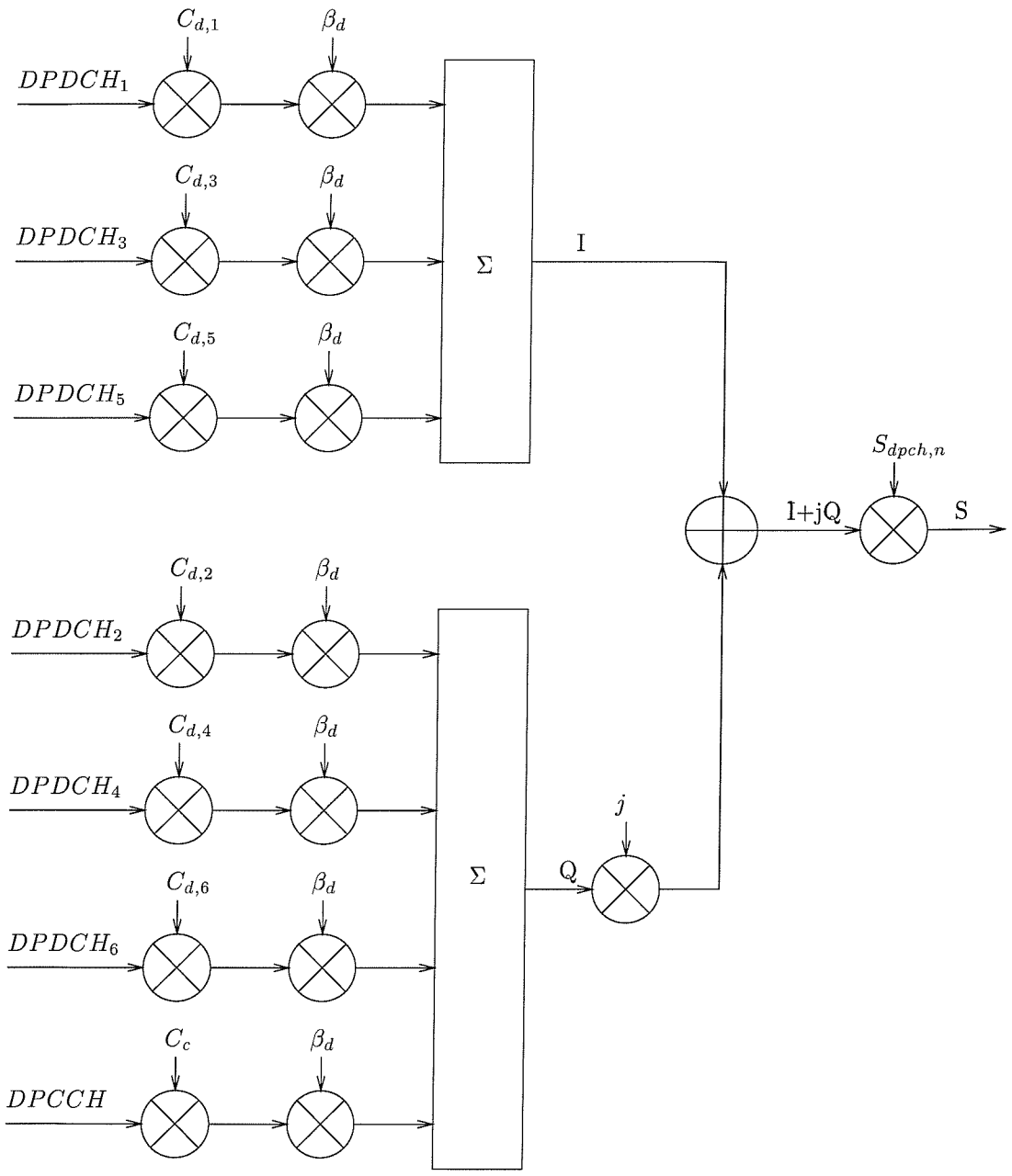

Figure 4.3: Spreading for uplink DPCCH and DPDCHs

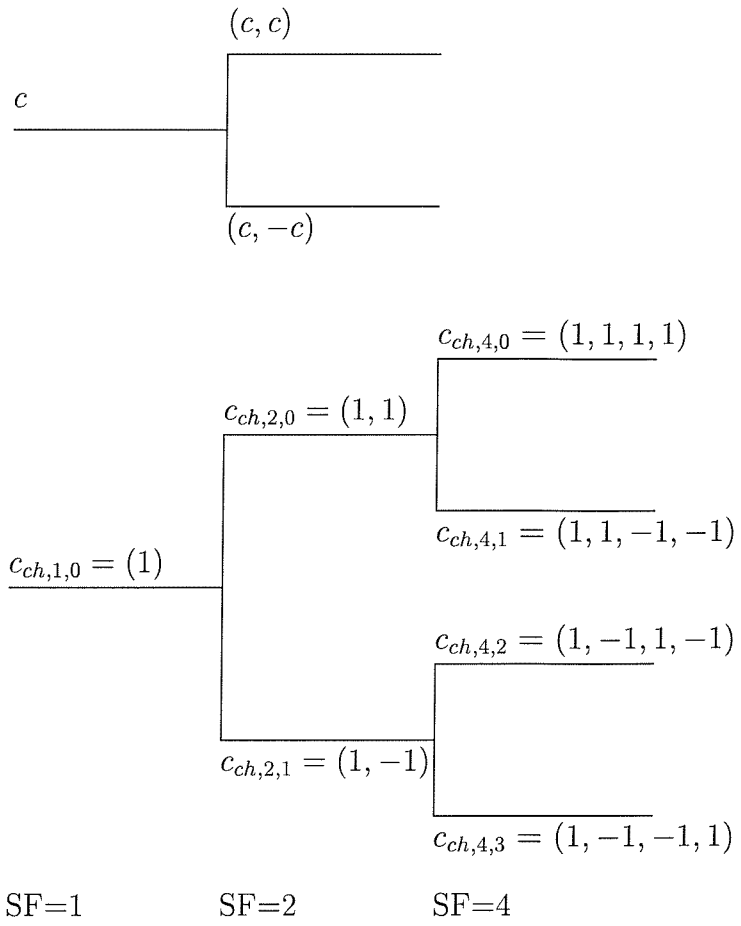

Figure 4.4: Code tree for the generation of Orthogonal Variable Spreading Factor (OVSF) codes

code can be used by an MS if and only if no other code on the path from the specific code to the root of the tree, or in the sub-tree below the specific node is used by the same MS.

For the DPCCH and DPDCHs the following applies :

- The PDCCH is always spread by code $C_c = C_{ch,256,0}$.
- When only one DPDCH is to be transmitted, DPDCH_1 is spread by the code $C_{d,1} = C_{ch,SF,k}$, where SF is the spreading factor of DPDCH_1 and $k = SF/4$.
- When more than one DPDCHs have to be transmitted, all DPDCHs have spreading factors equal to four. Furthermore, DPDCH_n is spread by the code $C_{d,n} = C_{ch,4,k}$, where $k = 1$ if $n \subset \{1,2\}$, $k = 3$ if $n \subset \{3,4\}$, and $k = 2$ if $n \subset \{5,6\}$.

A fundamental difference between the uplink and the downlink is that in the downlink

synchronisation is common to all users and channels of a given cell. This enables us to exploit the cross-correlation properties of the OVSF codes, which were originally proposed in [106]. These codes offer perfect cross-correlation in an ideal channel, but there is only a limited number of these codes available. The employment of OVSF codes allows the spreading factor to be changed and orthogonality between the spreading codes of different lengths to be maintained. The codes are selected from the code tree, which is illustrated in Figure 4.4. As illustrated above, there are certain restrictions as to which of the channelisation codes can be used for transmission from a single source. Another physical channel may invoke a certain code from the tree, if no other physical channel to be transmitted employing the same code tree is using a code on an underlying branch, since this would be equivalent to using a higher spreading factor code generated from the spreading code to be used, which are not orthogonal to each other on the same branch of the code tree. Neither can a smaller spreading factor code on the path to the root of the tree be used. Hence, the number of available codes depends on the required transmission rate and spreading factor of each physical channel.

In the UTRA downlink a part of the multi-user interference can be orthogonal - apart from the channel effects. The users within the same cell share the same scrambling code, but use different channelisation/OVSF codes. In a non-dispersive downlink channel, all intra-cell users are synchronised and therefore they are perfectly orthogonal. Unfortunately, in most cases the channel will be dispersive, implying that non-synchronised interference will be suppressed only by a factor corresponding to the processing gain, and thus they will interfere with the desired signal. The interference from other cells which is referred to as inter-cell interference, is non-orthogonal, due to employing different scrambling but possibly the same channelisation codes. Therefore inter-cell interference is also suppressed by a factor corresponding to the processing gain.

The channelisation code used for the the Primary Common PIlot CHannel (CPICH) is fixed to $C_{ch,256,0}$, while the channelisation code for the Primary Common Control Physical CHannel (CCPCH) is fixed to $C_{ch,256,1}$ [105]. The channelisation codes for all other physical channels are assigned by the UTRAN [105].

A total of $2^{18} - 1 = 262143$ scrambling codes, numbered as $0 \ldots 262142$ can be generated. However, not all of the scrambling codes are used. The scrambling codes are divided into 512 sets, each consisting of a primary scrambling code and 15 secondary scrambling codes [105].

More specifically, the primary scrambling codes consist of scrambling codes $n = 16 * i$, where $i = 0 \ldots 511$. The i^{th} set of secondary scrambling codes consists of scrambling codes $16*i+k$ where $k = 1 \ldots 15$. There is a one-to-one mapping between each primary scrambling

code and the associated 15 secondary scrambling codes in a set, such that the i^{th} primary scrambling code uniquely identifies the i^{th} set of secondary scrambling codes. Hence, according to the above statement, scrambling codes $k = 0 \ldots 8191$ are used. Each of these codes is associated with a left alternative scrambling code and a right alternative scrambling code, that may be used for the so-called compressed frames. Specifically, compressed frames are shortened duration frames transmitted right before a handover, in order to create an inactive period during which no useful data is transmitted. This allows the transceivers to carry out operations necessary for the handover to be successful. The left alternative scrambling code associated with scrambling code k is the scrambling code $k + 8192$, while the corresponding right alternative scrambling code is scrambling code $k + 16384$. In compressed frames, the left alternative scrambling code is used, if $n < SF/2$ and the right alternative scrambling code is used, if $n \geq SF/2$, where $C_{ch,SF,n}$ is the channelisation code used for non-compressed frames.

The set of 512 primary scrambling codes is further divided into 64 scrambling code groups, each consisting of 8 primary scrambling codes. The j^{th} scrambling code group consists of primary scrambling codes $16 * 8 * j + 16 * k$, where $j = 0 \ldots 63$ and $k = 0 \ldots 7$.

Each cell is allocated one and only one primary scrambling code. The primary CCPCH and primary CPICH are always transmitted using this primary scrambling code. The other downlink physical channels can be spread and transmitted with the aid of either the primary scrambling code or a secondary scrambling code from the set associated with the primary scrambling code of the cell.

4.3.2 Common Pilot Channel

The Common PIlot CHannel (CPICH) is an unmodulated downlink code channel, which is scrambled with the aid of the cell-specific primary scrambling code. The function of the downlink CPICH is to aid the Channel Impulse Response (CIR) estimation necessary for the detection of the dedicated channel at the mobile station and to provide the CIR estimation reference for the demodulation of the common channels, which are not associated with the dedicated channels.

UTRA has two types of common pilot channels, namely the primary and secondary CPICHs. Their difference is that the primary CPICH is always spread by the primary scrambling code defined in Section 4.3.1. More explicitly, the primary CPICH is associated with a fixed channelisation code allocation and there is only one such channel and channelisation code for a cell or sector. The secondary CPICH may use any channelisation code of length 256 and may use a secondary scrambling code as well. A typical application of

secondary CPICHs usage would be in conjunction with narrow antenna beams intended for service provision at specific teletraffic "hot spots" or places exhibiting a high traffic density [104].

An important application of the primary common pilot channel is during the collection of channel quality measurements for assisting during the handover and cell selection process. The measured CPICH reception level at the terminal can be used for handover decisions. Furthermore, by adjusting the CPICH power level the cell load can be balanced between different cells, since reducing the CPICH power level encourages some of the terminals to handover to other cells, while increasing it invites more terminals to handover to the cell, as well as to make their initial access to the network in that cell.

4.3.3 Power Control

Agile and accurate power control is perhaps the most important aspect in W-CDMA, in particular on the uplink, since a single high-powered rogue mobile can cause serious performance degradation to other users in the cell. The problem is referred to as the "near-far effect" and occurs when, for example, one mobile is near the cell edge, and another is near the cell centre. In this situation, the mobile at the cell edge is exposed to a significantly higher pathloss, say 70 dB higher, than that of the mobile near the cell centre. If there were no power control mechanisms in place, the mobile near the base station could easily "overpower" the mobile at the cell edge, and thus may block a large part of the cell. The optimum strategy in the sense of maximising the system's capacity is to equalise the received power per bit of all mobile stations at all times.

A so-called open-loop power control mechanism [104] attempts to make a rough estimate of the expected pathloss by means of a downlink beacon signal, but this method can be highly inaccurate. The prime reason for this is that the fast fading is essentially uncorrelated between the uplink and downlink, due to the large frequency separation of the uplink and downlink band of the W-CDMA FDD mode. Open-loop power control is however, used in W-CDMA, but only to provide a coarse initial power setting of the mobile station at the beginning of a connection.

A better solution is to employ fast closed-loop power control [104]. In closed-loop power control in the uplink, the base station performs frequent estimates of the received SIR and compares it to the target SIR. If the measured SIR is higher than the target SIR, the base station commands the mobile station to reduce the power, while if it is too low it will instruct the MS to increase its power. Since each 10 ms UTRA frame consists of 15 time slots, each corresponding to one power control power adjustment period, this procedure

takes place at a rate of 1500 Hz. This is far faster than any significant change of pathloss, including street corner effects, and indeed faster than the speed of Rayleigh fading for low to moderate mobile speeds. The street corner effect occurs, when a mobile turns a street corner and hence the received signal power drops markedly. Therefore, the mobile responds by rapidly increasing its transmit power, which may inflict severe interference upon other closely located base stations. In response, mobiles using these base stations increase their transmit powers in order to maintain their connection quality. This is undesirable, since it results in a high level of co-channel interference, leading to excessive transmission powers and reducing the achievable battery life. The same closed-loop power control technique is used on the downlink, although the rationale is different. More specifically, there is no near-far problem due to the one-to-many distributive scenario, i.e. all the signals originate from the single base station to all mobiles. It is, however, desirable to provide a marginal amount of additional power to mobile stations near the cell edge, since they suffer from increased inter-cell interference. Hence, the closed loop power control in CDMA systems ensures that each mobile transmits just sufficient power to satisfy the outer-loop power control scheme's SIR target. The SIR target is controlled by an outer-loop power control process that adjusts the required SIR in order to meet the Bit Error Ratio (BER) requirements of a particular service. At higher mobile speeds typically a higher SIR is necessary for attaining a given BER/FER.

4.3.3.1 Uplink Power Control

The uplink's inner-loop power control adjusts the mobile's transmit power in order to maintain the received uplink SIR at the given SIR target, namely at SIR_{target}. The base stations that are communicating with the mobile generate Transit Power Control (TPC) commands and transmit them, once per slot, to the mobile. The mobile then derives from the TPC commands of the various base stations, a single TPC command, TPC_cmd, for each slot, combining multiple received TPC commands if necessary. In [107] two algorithms were defined for the processing of TPC commands and hence for deriving TPC_cmd.

Algorithm 1 : [107]

When not in soft-handover, i.e. when the mobile communicates with a single base station, only one TPC command will be received in each slot. Hence, for each slot, if the TPC command is equal to 0 ($SIR > SIR_{target}$) then $TPC\_cmd = -1$, otherwise, if the TPC command is 1 ($SIR < SIR_{target}$) then $TPC\_cmd = 1$, which implies powering down or up, respectively.

When in soft handover, multiple TPC commands are received in each slot from the

different base stations in the active base station set. If all of the base station's TPC commands are identical, then they are combined to form a single TPC command, namely TPC_cmd. However, if the TPC commands of the different base stations differ, then a soft decision W_i is generated for each of the TPC commands, TPC_i, where $i = 1, 2, \ldots, N$, and N is the number of TPC commands. These N soft decisions are then used to form a combined TPC command TPC_cmd according to :

$$TPC\_cmd = \gamma(W_1, W_2, \ldots, W_N) \tag{4.1}$$

where TPC_cmd is either -1 or +1 and $\gamma()$ is the decision function combining the soft values, $W_1, \ldots, W_N$.

If the N TPC commands appear to be uncorrelated, and have a similar probability of being 0 or 1, then function $\gamma()$ should be defined such that the probability that the output of the function $\gamma()$ is equal to 1, is greater than or equal to $1/2^N$, and the probability that the output of $\gamma()$ is equal to -1, shall be greater than or equal to 0.5 [107]. Alternatively, the function $\gamma()$ should be defined such that $P(\gamma() = 1) \geq 1/2^N$ and $P(\gamma() = -1) \geq 0.5$.

Algorithm 2 : [107]

When not in soft handover, only one TPC command will be received in each slot, and the mobile will process the maximum 15 TPC commands in a five-slot cycle, where the sets of five slots are aligned with the frame boundaries and the sets do not overlap. Therefore, when not in soft handover, for the first four slots of a five-slot set $TPC\_cmd = 0$ is used for indicating that no power control adjustments are made. For the fifth slot of a set the mobile performs hard decisions on all five of the received TPC commands. If all five hard decisions result in a binary 1, then we set $TPC\_cmd = 1$. In contrast, if all five hard decisions yield a binary 0, then $TPC\_cmd = -1$ is set, else $TPC\_cmd = 0$.

When the mobile is in soft handover, multiple TPC commands will be received in each slot from each of the base stations in the set of active base stations. When the TPC commands of the active base stations are identical, then they can be combined into a single TPC command. However, when the received TPC commands are different, the mobile makes a hard decision concerning the value of each TPC command for three consecutive slots, resulting in N hard decisions for each of the three slots, where N is the number of base stations within the active set. The sets of three slots are aligned to the frame boundaries and do not overlap. Then $TPC\_cmd = 0$ is set for the first two slots of the three-slot set, and then TPC_cmd is determined for the third slot as follows.

The temporary command TPC_temp_i is determined for each of the N sets of three TPC commands of the consecutive slots by setting $TPC\_temp_i = 1$ if all three TPC hard decisions

are binary 1. In contrast, if all three TPC hard decisions are binary 0, $TPC\_temp_i = -1$ is set, otherwise we set $TPC\_temp_i = 0$. These temporary TPC commands are then used to determine the combined TPC command for the third slot invoking the decision function $\gamma(TPC\_temp_1, TPC\_temp_2, \ldots, TPC\_temp_N)$ defined as:

$$\begin{aligned} TPC\_cmd = 1 \quad & \text{if } \frac{1}{N}\sum_{i=1}^{N} TPC\_temp_i > 0.5 \\ TPC\_cmd = -1 \quad & \text{if } \frac{1}{N}\sum_{i=1}^{N} TPC\_temp_i < -0.5 \\ TPC\_cmd = 0 \quad & \text{otherwise.} \end{aligned} \tag{4.2}$$

4.3.3.2 Downlink Power Control

The downlink transmit power control procedure simultaneously controls the power of a DPCCH and its corresponding DPDCHs, both of which are adjusted by the same amount, and hence the relative power difference between the DPCCH and DPDCHs remains constant.

The mobile generates TPC commands for controlling the base station's transmit power and sends them in the TPC field of the uplink DPCCH. When the mobile is not in soft handover, the TPC command generated is transmitted in the first available TPC field using the uplink DPCCH. In contrast, when the mobile is in soft handover, it checks the downlink power control mode (DPC_MODE) before generating the TPC command. If $DPC\_MODE = 0$, the mobile sends a unique TPC command in the first available TPC field in the uplink DPCCH. If however, $DPC\_MODE = 1$, the mobile repeats the same TPC command over three consecutive slots of the same frame and the new TPC command is transmitted to the base station in an effort the control its power at the beginning of the next frame. The minimum required transmit power step size is 1dB, with a smaller step size of 0.5dB being optional. The power control step size can be increased from 1dB to 2dB, thus allowing a 30dB correction range during the 15 slots of a 10ms frame. The maximum transmit powers are +21dBm and +24dBm, although it is likely that in the first phase of network deployment most terminals will belong to the 21dBm power class [104].

4.3.4 Soft Handover

Theoretically, the ability of CDMA to despread the interfering signals, and thus adequately operate at low signal-to-noise ratios, allows a CDMA network to have a frequency reuse factor of one [104]. Traditionally, non-CDMA based networks have required adjacent cells to

have different carrier frequencies, in order to reduce the co-channel interference to acceptable levels. Therefore, when a mobile hands over from one cell to another, it has to re-tune its synthesizer to the new carrier frequency, i.e. it performs an inter-frequency handover. This process is a "break-before-make" procedure, known as a hard handover, and hence call disruption or interruption is possible. However, in a CDMA based network, having a frequency reuse factor of one so-called soft handovers may be performed, which is a "make-before-break" process, potentially allowing for a smoother handover between cells. During a soft handover a mobile is connected to two or more base stations simultaneously, thus utilising more network resources and transmitting more signals, which interfere with other users. Therefore, it is in the network operator's interests to minimise the number of users in soft handover, whilst maintaining a satisfactory quality of service. In soft handover, each connected base station receives and demodulates the user's data, and selection diversity is performed between the base stations, i.e. the best version of the uplink frame is selected. In the downlink, the mobile station performs maximal ratio combining [5] of the signal received from the multiple base stations. This diversity combining improves the coverage in regions of previously low-quality service provision, but at the expense of increased backhaul connections.

The set of base stations engaged in soft handover is known as the *active set.* The mobile station continuously monitors the received power level of the PIlot CHannels (PICHs) transmitted by its neighbouring base stations. The received pilot power levels of these base stations are then compared to two thresholds, the acceptance threshold, T_{acc} and the dropping threshold T_{drop}. Therefore, as a mobile moves away from base station 1, and towards base station 2, the pilot signal strength received from base station 2 increases. When the pilot strength exceeds the *acceptance threshold*, T_{acc}, the mobile station enters the soft handover state, as shown in Figure 4.5. As the mobile continues to move away from base station 1, its pilot strength decreases, until it falls below the *drop threshold.* After a given time interval, T_{drop}, during which the signal strength from base station 1 has not exceeded the drop threshold, base station 1 is removed from the active set.

4.3.5 Signal-to-Interference plus Noise Ratio Calculations

4.3.5.1 Downlink

The interference received at the mobile can be divided into interference due to the signals transmitted to other mobiles from the same base station, which is known as intra-cell interference, and that received due to the signals transmitted to other mobiles from other base stations, which is termed inter-cell interference. In an ideal case, the intra-cell interference

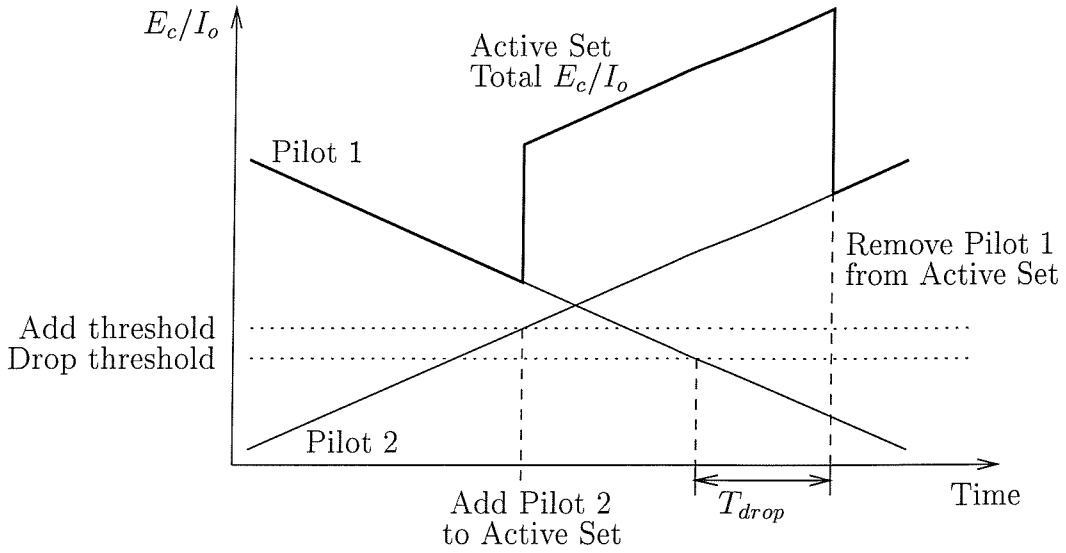

Figure 4.5: The soft handover process showing the process of adding and dropping base stations from the active set.

would be zero, since all the signals from the base station are subjected to the same channel conditions, and orthogonal channelisation codes are used for separating the users. However, after propagation through a dispersive multipath channel, this orthogonality is eroded. The intra-cell and inter-cell interference values are always non-zero when in a single-user scenario due to the inevitable interference inflicted by the common pilot channels.

The instantaneous SINR is obtained by dividing the received signal powers by the total interference plus thermal noise power, and then by multiplying this ratio by the spreading factor, SF, yielding

$$SINR_{DL} = \frac{SF \cdot S}{(1-\alpha)I_{Intra} + I_{Inter} + N_0}, \tag{4.3}$$

where $\alpha = 1$ corresponds to the ideal case of perfectly orthogonal intra-cell interference, and $\alpha = 0$ is for completely asynchronous intra-cell interference. Furthermore, N_0 is the thermal noise power, S is the received signal power, I_{Intra} is the intra-cell interference and I_{Inter} is the inter-cell interference. Again, the interference plus noise power is scaled by the spreading factor, SF, since after the low-pass filtering the noise bandwidth is reduced by a factor of SF during the despreading process.

When in soft handover, the maximum ratio combining is performed on the N received signals of the N active base stations. Therefore, provided that the active base stations' received signals are independent, the SINR in this situation is :

$$SINR_{DL} = SINR_{DL_1} + SINR_{DL_2} + \ldots + SINR_{DL_N}. \tag{4.4}$$

4.3.5.2 Uplink

The uplink differs from the downlink in that the multiple access interference is asynchronous in the uplink due to the un-coordinated transmissions of the mobile stations, whereas it may remain quasi-synchronous in the downlink. Therefore, the intra-cell uplink interference is not orthogonal. A possible solution for mitigating this problem is employing Multi-User Detectors (MUDs) [108] at the base stations.

Thus, we define β as the MUD's efficiency, which effectively gives the percentage of the intra-cell interference that is removed by the MUD. Setting $\beta = 0.0$ implies 0% efficiency, when the intra-cell interference is not reduced by the MUD, whereas $\beta = 1.0$ results in the perfect suppression of all the intra-cell interference. Therefore, the expression for the uplink SINR is :

$$SINR_{UL} = \frac{SF \cdot S}{(1-\beta)I_{Intra} + I_{Inter} + N_0}. \tag{4.5}$$

When in soft handover, selection diversity is performed on the N received signals at each of the active base stations. Therefore, the SINR in this situation becomes :

$$SINR_{UL} = \max(SINR_{UL_1}, SINR_{UL_2}, \ldots, SINR_{UL_N}). \tag{4.6}$$

4.3.6 Multi-User Detection

Multiple access communications using DS-CDMA is interference limited due to the Multiple Access Interference (MAI) generated by the users transmitting simultaneously within the same bandwidth. The signals received from the users are separated with the aid of the despreader using spreading sequences that are unique to each user. Again, these spreading sequences are usually non-orthogonal. Even if they are orthogonal, the asynchronous uplink transmissions of the users or the time-varying nature of the mobile radio channel may partially destroy this orthogonality. The non-orthogonal nature of the codes results in residual MAI, which degrades the performance of the system. The frequency selective mobile radio channel also gives rise to Inter-Symbol Interference (ISI) due to dispersive multipath propagation. This is exacerbated by the fact that the mobile radio channel is time-varying.

Conventional CDMA detectors - such as the matched filter [5, 109] and the RAKE combiner [110] - are optimised for detecting the signal of a single desired user. RAKE combiners exploit the inherent multi-path diversity in CDMA, since they essentially consist of matched filters combining each resolvable path of the multipath channel. The outputs of these matched filters are then coherently combined according to a diversity combining

technique, such as maximal ratio combining [72], equal gain combining or selective diversity combining . These conventional single-user detectors are inefficient, because the interference is treated as noise, and our knowledge concerning the CIR of the mobile channel, or that of the spreading sequences of the interferers is not exploited. The efficiency of these detectors is dependent on the cross-correlation (CCL) between the spreading codes of all the users. The higher the cross-correlation, the higher the MAI. This CCL-induced MAI is exacerbated by the effects of the dispersive multi-path channel and asynchronous transmissions. The utilisation of these conventional receivers results in an interference-limited system. Another weakness of the above-mentioned conventional CDMA detectors is the phenomenon known as the "near-far effect" [111, 112]. For conventional detectors to operate efficiently, the signals received from all the users have to arrive at the receiver with approximately the same power. A signal that has a significantly weaker signal strength compared to the other signals will be "swamped" by the relatively higher powers of the other signals and the quality of the weaker signal at the output of the conventional receiver will be severely degraded. Therefore, stringent power control algorithms are needed to ensure that the signals arrive at similar powers at the receiver, in order to achieve a similar quality of service for different users [112, 113]. Using conventional detectors to detect a signal corrupted by MAI, while encountering a hostile channel results in an irreducible BER, even if the E_s/N_0 ratio is increased. This is because at high E_s/N_0 values the probability of errors due to thermal noise is insignificant compared to the errors caused by the MAI and the channel. Therefore, detectors that can reduce or remove the effects of MAI and ISI are needed in order to achieve user capacity gains. These detectors also have to be "near-far resistant", in order to avoid the need for stringent power control requirements. In order to mitigate the problem of MAI, Verdú [108] proposed the optimum multi-user detector for asynchronous Gaussian multiple access channels. This optimum detector significantly outperforms the conventional detector and it is near-far resistant, but unfortunately its complexity increases exponentially according to the order of $O(2^{NK})$, where N is the number of overlapping asynchronous bits considered in the detector's window, and K is the number of interfering users. In order to reduce the complexity of the receiver and yet to provide an acceptable BER performance, significant research efforts have been invested in the field of sub-optimal CDMA multiuser receivers [108, 114].

In summary, multi-user detectors reduce the error floor due to MAI and this translates into user capacity gains for the system. These multi-user detectors are also near-far resistant to a certain extent and this results in less stringent power control requirements. However, multi-user detectors are more complex than conventional detectors. Coherent detectors require the explicit knowledge of the channel impulse response estimates, which implies

that a channel estimator is needed in the receiver and hence training sequences have to be included in the transmission frames. Training sequences are specified in the TDD mode of the UTRA standard and enable the channel impulse response of each simultaneously received user to be obtained, which is necessary in order for the multi-user detectors to be able to separate the data received for each user. These multi-user detectors also exhibit an inherent latency, which results in delayed reception. Multi-user detection is more suitable for the uplink receiver since the base station has to detect all users' signals anyway and it can tolerate a higher complexity. In contrast, a hand-held mobile receiver is required to be compact and lightweight, imposing restrictions on the available processing power. Recent research into blind MUDs has shown that data detection is possible for the desired user without invoking the knowledge of the spreading sequences and channel estimates of other users. Hence using these detectors for downlink receivers is becoming feasible.

4.4 Simulation Results

This section presents simulation results obtained for an FDD mode UMTS type CDMA cellular network, investigating the applicability of various soft handover metrics when subjected to different propagation conditions. This is followed by performance curves obtained using adaptive antenna arrays, when subjected to both non-shadowed as well as shadowed propagation conditions. The performance of adaptive modulation techniques used in conjunction with adaptive antenna arrays in a shadow faded environment is then characterised.

4.4.1 Simulation Parameters

Simulations of an FDD mode UMTS type CDMA based cellular network were conducted for various scenarios and algorithms in order to study the interactions of the processes involved in such a network. As in the standard, the frame length was set to 10 ms, containing 15 power control timeslots. The power control target SINR was chosen to give a Bit Error Ratio (BER) of 1×10^{-3}, with a low quality outage occurring at a BER of 5×10^{-3} and an outage taking place at a BER of 1×10^{-2}. The received SINRs at both the mobile and the base stations were required for each of the power control timeslots, and hence the outage and low quality outage statistics were gathered. If the received SINR was found to be below the outage SINR for 75 consecutive power control timeslots, corresponding to 5 consecutive transmission frames or 50 ms, the call was dropped. The post despreading SINRs necessary for obtaining the target BERs were determined with the aid of physical-layer simulations using a 4-QAM modulation scheme, in conjunction with 1/2 rate turbo coding and joint

detection over a COST 207 seven-path Bad Urban channel [115]. For a spreading factor of 16, the post-de-spreading SINR required to give a BER of 1×10^{-3} was 8.0 dB, for a BER of 5×10^{-3} it was 7.0 dB, and for a BER of 1×10^{-2} was about 6.6 dB. These values can be seen along with the other system parameters in Table 4.2. The-pre de-spreading SINR is related to E_b/N_o and to the spreading factor by :

$$SINR = (E_b/N_o)/SF, \tag{4.7}$$

where the spreading factor $SF = W/R$, with W being the chip rate and R the data rate. A receiver noise figure of 7 dB was assumed for both the mobile and the base stations [104]. Thus, in conjunction with a thermal noise density of -174 dBm/Hz and a noise bandwidth of 3.84 MHz, this resulted in a receiver noise power of -100 dBm. The power control algorithm used was relatively simple, and unrelated to the previously introduced schemes of Section 4.3.3. Furthermore, since it allowed a full transmission power change of 15 dB within a 15-slot UTRA data frame, the power control scheme advocated is unlikely to limit the network's capacity. Specifically, for each of the 15 timeslots per transmitted frame, both the mobile and base station transmit powers were adjusted such that the received SINR was greater than the target SINR, but less than the target SINR plus 1 dB of hysteresis. When in soft handover, a mobile's transmission power was only increased, if all of the base stations in the Active Base station Set (ABS) requested a power increase, but was it decreased if any of the base stations in the ABS had an excessive received SINR. In the downlink, if the received SINR at the mobile was insufficiently high then all of the active base stations were commanded to increase their transmission powers. Similarly, if the received SINR was unnecessarily high, then the active base stations would reduce their transmit powers. The downlink intra-cell interference orthogonality factor, α, as described in Section 4.3.5, was set to 0.5 [116, 117, 118]. Due to the frequency reuse factor of one, with its associated low frequency reuse distance, it was necessary for both the mobiles and the base stations, when initiating a new call or entering soft handover, to increase their transmitted power gradually. This was required to prevent sudden increases in the level of interference, particularly on links using the same base station. Hence, by gradually increasing the transmit power to the desired level, the other users of the network were capable of compensating for the increased interference by increasing their transmit powers, without encountering undesirable outages. In an FDMA/TDMA network this effect is less noticeable due to the significantly higher frequency reuse distance.

Since a dropped call is less desirable from a user's viewpoint than a blocked call, two resource allocation queues were invoked, one for new calls and the other - higher priority - queue, for handovers. By forming a queue of the handover requests, which have a higher priority during contention for network resources than new calls, it is possible to reduce the

Parameter	Value	Parameter	Value
Frame length	10 ms	Timeslots per frame	15
Target E_b/N_o	8.0 dB	Outage E_b/N_o	6.6 dB
Low Quality (LQ) Outage E_b/N_o	7.0 dB	BS Pilot Power	-5 dBm
BS/MS Minimum TX Power	-44 dBm	BS Antenna Gain	11 dBi
BS/MS Maximum TX Power	+21 dBm	MS Antenna Gain	0 dBi
Attenuation at 1 m reference point	39 dB	Pathloss exponent	-3.5
Power control SINR hysteresis	1 dB	Cell radius	150 m
Downlink scrambling codes per BS	1	Modulation scheme	4-QAM
Downlink OVSF codes per BS	Variable	Max new-call queue-time	5 s
Uplink scrambling codes per BS	Variable	Average inter-call time	300 s
Uplink OVSF codes per BS	Variable	Average call length	60 s
Spreading factor	Variable	Data/voice bit rate	Variable
Remove BS from ABS threshold	Variable	Add BS to ABS threshold	Variable
User speed	1.34 m/s	Noisefloor	-100 dBm
	(3 mph)	Size of ABS	2

Table 4.2: Simulation parameters of the UTRA-type CDMA based cellular network.

number of dropped calls at the expense of an increased blocked call probability. A further advantage of the Handover Queueing System (HQS) is that during the time a handover is in the queue, previously allocated resources may become available, hence increasing the probability of a successful handover. However, in a CDMA based network the capacity is not hard-limited by the number of frequency/timeslot combinations available, like in a FDMA/TDMA based network such as GSM. The main limiting factors are the number of available downlink spreading and OVSF codes, with the number of available OVSF codes restricted to the spreading factor minus one, since an OVSF code is used for the pilot channel. This is because although the pilot channel has a spreading factor of 256, it removes an entire branch of the OVSF code generation tree. Other limiting factors are the interference levels in conjunction with the restricted maximum transmit power, resulting in excessive call dropping rates. New call allocation requests were queued for up to 5s, if they could not be immediately satisfied, and were blocked if the request had not been completed successfully within the 5s.

Similarly to our TDMA-based investigations portrayed in Chapter 3, several network performance metrics were used in order to quantify the quality of service provided by the cellular network, namely the :

- New Call Blocking probability, P_B,
- Call Dropping or Forced Termination probability, P_{FT},

- Probability of low quality connection, P_{low},
- Probability of Outage, P_{out},
- Grade Of Service, GOS.

The new call blocking probability, P_B, is defined as the probability that a new call is denied access to the network. In an FDMA/TDMA based network, such as GSM, this may occur because there are no available physical channels at the desired base station or the available channels are subject to excessive interference. However, in a CDMA based network this does not occur, provided that no interference level based call admission control is performed and hence the new call blocking probability is typically very low.

The call dropping probability, P_{FT}, is the probability that a call is forced to terminate prematurely. In a GSM type network, an insufficiently high SINR, which inevitably leads to dropped calls, may be remedied by an intra- or inter-cell handover. However, in CDMA either the transmit power must be increased, or a soft handover must be performed in order to exploit the available diversity gain.

Again, the probability of a low quality connection is defined as :

$$\begin{aligned} P_{low} &= P\{SINR_{uplink} < SINR_{req} \text{ or } SINR_{downlink} < SINR_{req}\} \\ &= P\{min(SINR_{uplink}, SINR_{downlink}) < SINR_{req}\}. \end{aligned} \tag{4.8}$$

The GOS was defined in [80] as :

$$\begin{aligned} GOS &= P\{\text{unsuccessful or low-quality call access}\} \\ &= P\{\text{call is blocked}\} + P\{\text{call is admitted}\} \times \\ &\quad P\{\text{low signal quality and call is admitted}\} \\ &= P_B + (1 - P_B)P_{low}, \end{aligned} \tag{4.9}$$

and is interpreted as the probability of unsuccessful network access (blocking), or low quality access, when a call is admitted to the system.

In our forthcoming investigations, in order to compare the network capacities of different networks, similarly to our TDMA-based investigations in Chapter 3, it was decided to use two scenarios defined as :

- A *conservative scenario*, where the maximum acceptable value for the new call blocking probability, P_B, is 3%, the maximum call dropping probability, P_{FT}, is 1%, and P_{low} is 1%.

- A *lenient scenario*, where the maximum acceptable value for the new call blocking probability, P_B, is 5%, the maximum call dropping probability, P_{FT}, is 1%, and P_{low} is 2%.

In the next section we consider the network's performance considering both fixed and normalised soft handover thresholds using both received pilot power and received pilot power versus interference threshold metrics. A spreading factor of 16 was used, corresponding to a channel data rate of 3.84Mbps/16 = 240 kbps with no channel coding, or 120 kbps when using 1/2 rate channel coding. It must be noted at this stage that the results presented in the following sections are network capacities obtained using a spreading factor of 16. The network capacity results presented in the previous chapter, which were obtained for an FDMA/TDMA GSM-like system, were achieved for speech-rate users. Here we assumed that the channel coded speech-rate was 15 kbps, which is the lowest possible Dedicated Physical Data CHannel (DPDCH) rate. Speech users having a channel coded rate of 15 kbps may be supported by invoking a spreading factor of 256. Hence, subjecting the channel data rate of 15 kbps to 1/2 rate channel coding gives a speech-rate of 7.5 kbps, or if protected by a 2/3 rate code the speech-rate becomes 10 kbps, which are sufficiently high for employing the so-called Advanced MultiRate (AMR) speech codec [119, 120, 121] capable of operating at rates between 4.7 kbps and 12.2 kbps. Therefore, by multiplying the resultant network capacities according to a factor of 256/16=16, it is possible to estimate the number of speech users supported by a speech-rate network. However, with the aid of our exploratory simulations, conducted using a spreading factor of 256, which are not presented here, we achieved network capacities higher than 30 times the network capacity supported in conjunction with a spreading factor of 16. Therefore, it would appear that the system is likely to support more than 16 times the number of 240 kbps data users, when communicating at the approximately 16 times lower speech-rate, employing a high spreading factor of 256. Hence, using the above-mentioned scaling factor of 16 we arrive at the lower bound of network capacity. A mobile speed of 3 mph was used in conjunction with a cell size of 150m radius, which was necessarily small in order to be able to support the previously assumed 240 kbps high target data rate. The performance advantages of using both adaptive beamforming and adaptive modulation assisted networks are also investigated.

4.4.2 The Effect of Pilot Power on Soft Handover Results

In this section we consider the settings of the soft handover thresholds, for an IS-95 type handover algorithm [122], where the handover decisions are based on downlink pilot power measurements. Selecting inappropriate values for the soft handover thresholds, namely

for the *acceptance threshold* and the *drop threshold*, may result in an excessive number of new blocked and dropped calls in certain parts of the simulation area. For example, if the *acceptance threshold* for adding a base station to the active set is too high (Threshold B in Figure 4.6), then a user may be located within a cell, but it would be unable to add any base stations to its active base station set, and hence it is unable to initiate a call. Figure 4.6 illustrates this phenomenon and shows that the *acceptance thresholds* must be set sufficiently low for ensuring that at least one base station covers every part of the network.

Another consequence of setting the *acceptance threshold* to an excessively high value, is that soft handovers may not be completed. This may occur when a user leaving the coverage area of a cell, since the pilot signal from that cell drops below the *drop threshold*, before the signal from the adjacent cell becomes sufficiently strong for it to be added to the active base station set. However, if the *acceptance threshold*, in conjunction with the *drop threshold*, is set correctly, then new calls and soft handovers should take place as required, so long as the availability of network resources allows it. Care must be taken however, not to set the soft handover threshold too low, otherwise the mobiles occupy additional network resources and create extra interference, due to initiating unnecessary soft-handovers.

4.4.2.1 Fixed Received Pilot Power Thresholds without Shadowing

Figure 4.7 shows the new call blocking probability of a network using a spreading factor of 16, in conjunction with fixed received pilot signal strength based soft handover thresholds without imposing any shadowing effects. The figure illustrates that reducing both the acceptance and the dropping soft handover thresholds results in an improved new call blocking performance. Reducing the threshold at which further base stations may be added to the Active Base station Set (ABS) increases the probability that base stations exist within the ABS, when a new call request is made. Hence, as expected, the new call blocking probability is reduced, when the acceptance threshold is reduced. Similarly, dropping the threshold at which base stations are removed from the ABS also results in an improved new call blocking probability, since a base station is more likely to be retained in the ABS as a mobile moves away from it. Therefore, should a mobile attempt to initiate a call in this situation, there is a greater chance that the ABS will contain a suitable base station.

The associated call dropping probability is depicted in Figure 4.8, indicating that reducing the soft handover thresholds, and thus increasing the time spent in soft handover, improved the performance up to a certain point. However, above this point the additional interference inflicted by the soft handover process led to a degraded performance. For example, in this

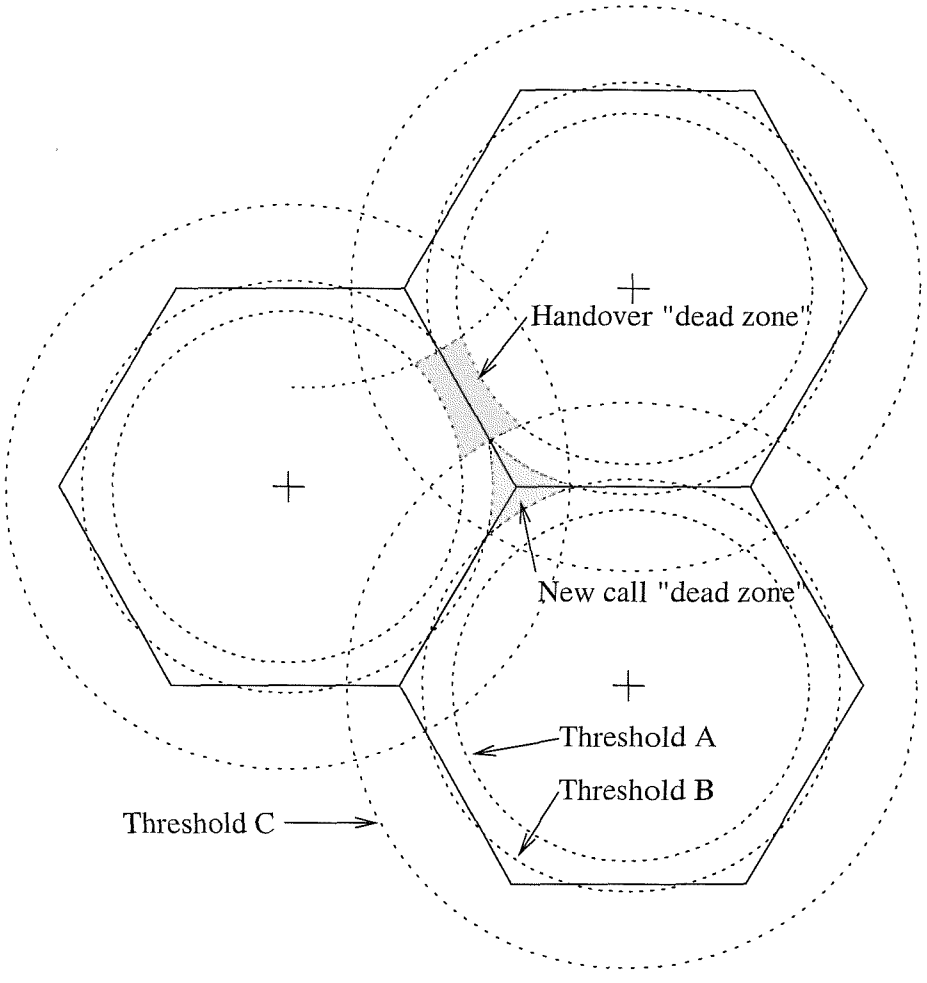

Figure 4.6: This figure indicates that using inappropriate soft handover thresholds may lead to blocked and dropped calls due to insufficient pilot coverage of the simulation area. Threshold A is the drop threshold, which when combined with the acceptance threshold C can fail to cover the simulation area sufficiently well, thus leading to soft handover failure. When combining threshold A with the acceptance threshold B, users located in the "new call dead zone" may become unable to initiate calls.

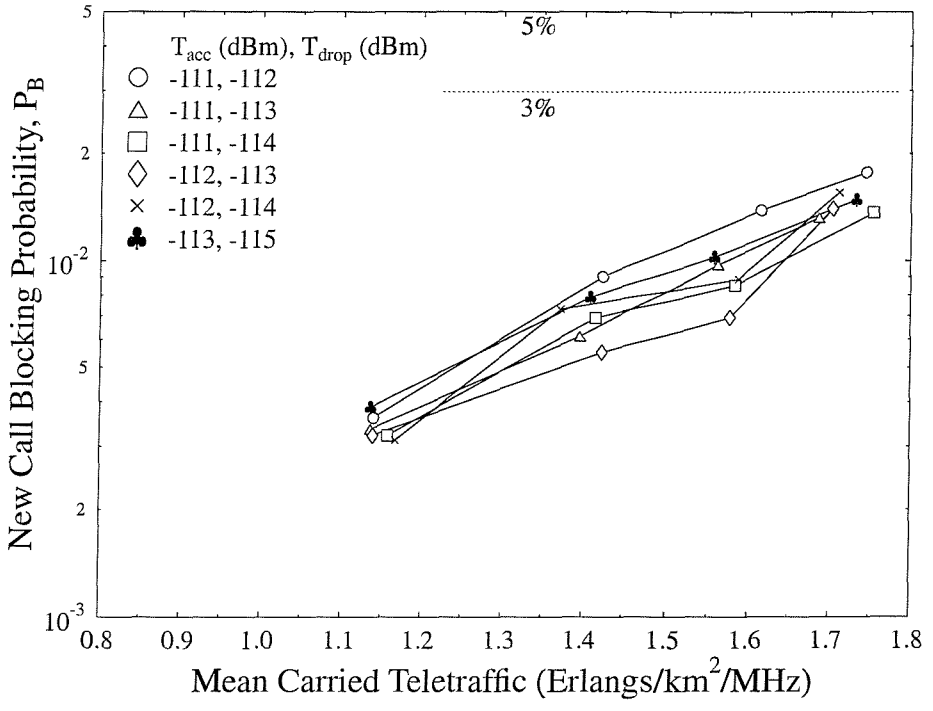

Figure 4.7: New call blocking probability versus mean carried traffic of a CDMA based cellular network using **fixed received pilot power** based soft handover thresholds **without shadowing** for SF=16.

figure the performance associated with T_{acc}=-111 dBm improved, when T_{drop} was decreased from -112 dBm to -113 dBm. However, at high traffic levels the performance degraded when T_{drop} was decreased further, to -114 dBm. The call dropping probability obtained using T_{acc}=-113 dBm and T_{drop}=-115 dBm was markedly lower for the lesser levels of traffic carried due to the extra diversity gain provided by the soft handover process. However, since these soft handover thresholds resulted in a greater proportion of time spent in soft handover, the levels of interference were increased, and thus at the higher traffic levels the performance degraded rapidly, as can be seen in Figure 4.8. Hence, the call dropping performance is based on a trade-off between the diversity gain provided by the soft handover process and the associated additional interference.

The probability of low quality access (not explicitly shown) was similar in terms of its character to the call dropping probability, since reducing T_{drop} improved the performance to a certain point, after which it degraded.

The mean number of base stations in the ABS is shown in Figure 4.9, illustrating that

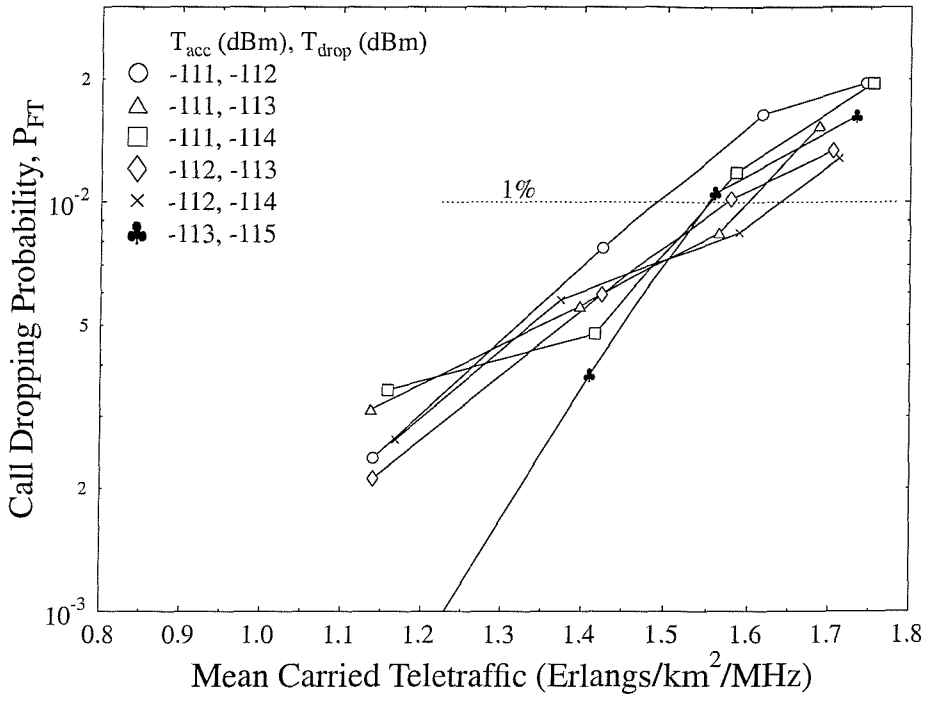

Figure 4.8: Call dropping probability versus mean carried traffic of a CDMA based cellular network using **fixed received pilot power** based soft handover thresholds **without shadowing** for SF=16.

reducing the soft handover thresholds leads, on average, to a higher number of base stations in the ABS. Therefore, a greater proportion of call time is spent in soft handover. The associated diversity gain improves the link quality of the reference user but additional co-channel interference is generated by the diversity links, thus ultimately reducing the call quality, as shown in Figure 4.8. Additionally, this extra co-channel interference required more transmission power for maintaining the target SINR as depicted in Figure 4.10. This figure shows that when lower soft handover thresholds are used, and thus a greater proportion of time is spent in soft handover, greater levels of co-channel interference are present, and thus the required mean transmission powers became higher. It is interesting to note that for the highest soft handover thresholds employed in Figure 4.10, the downlink transmission power required for maintaining the target SINR is lower than the uplink transmission power, whereas, for the lower soft handover thresholds, the required mean uplink transmission power is lower than the downlink transmission power. The required downlink transmission power was, in general, lower than the uplink transmission power due to the mobile stations' ability to perform maximal ratio combining when in soft handover. This

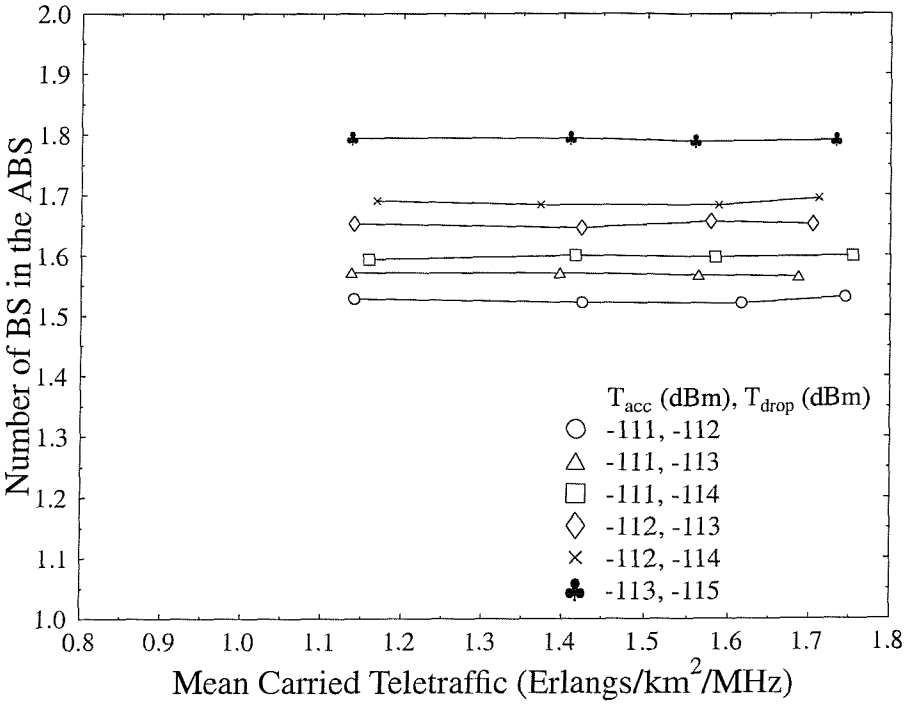

Figure 4.9: Mean number of base stations in the active base station set versus mean carried traffic of a CDMA based cellular network using **fixed received pilot power** based soft handover thresholds **without shadowing** for SF=16.

was observed despite the absence of the pilot interference in the uplink, and despite the base stations' ability to perform selective diversity which offers less diversity gain when compared to maximal ratio combining. However, reducing the soft handover thresholds to the lowest levels shown in Figure 4.10, led to increased co-channel interference on the downlink, thus requiring higher base station transmission powers, as clearly seen in the figure.

In summary, as seen by comparing Figures 4.7-4.10 the maximum capacity of the network using fixed received pilot power based soft handover thresholds was limited by the call dropping probability. The new call blocking probability remained below the 3% limit, thanks to the appropriate choice of thresholds used, whilst the probability of low quality access was constantly below the 1% mark. Therefore, the maximum normalised teletraffic load was 1.64 Erlangs/km^2/MHz, corresponding to a total network capacity of 290 users, while satisfying both quality of service constraints, was achieved with the aid of an acceptance threshold of -112 dBm and a dropping threshold of -114 dBm. A mean ABS size of 1.7 base stations was registered at this traffic level, and both the mobile and base stations exhibited a mean transmission power of 5.1 dBm.

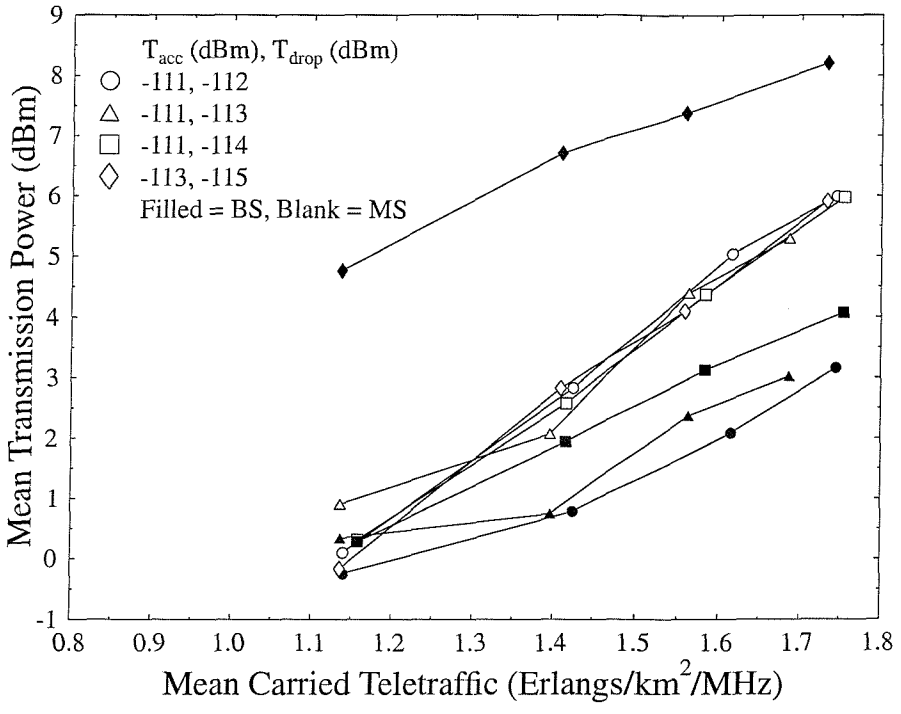

Figure 4.10: Mean transmission power versus mean carried traffic of a CDMA based cellular network using **fixed received pilot power** based soft handover thresholds **without shadowing** for SF=16.

4.4.2.2 Fixed Received Pilot Power Thresholds with 0.5 Hz Shadowing

In this section we examine the achievable performance, upon using fixed received pilot power based soft handover thresholds when subjected to log-normal shadow fading having a standard deviation of 3 dB and a maximum frequency of 0.5 Hz.

The call dropping results of Figure 4.11 suggested that the network's performance was poor when using fixed received pilot power soft handover thresholds in the above mentioned shadow fading environment. The root cause of the problem is that the fixed thresholds must be set such that the received pilot signals, even when subjected to shadow fading, are retained in the active set. Therefore, setting the thresholds too high results in the base stations being removed from the active set, thus leading to an excessive number of dropped calls. However, if the thresholds are set too low, in order to counteract this phenomenon, then the base stations can be in soft handover for too high a proportion of time, and thus an unacceptable level of low quality accesses is generated due to the additional co-channel interference inflicted by the high number of active base stations. Figure 4.11 shows that

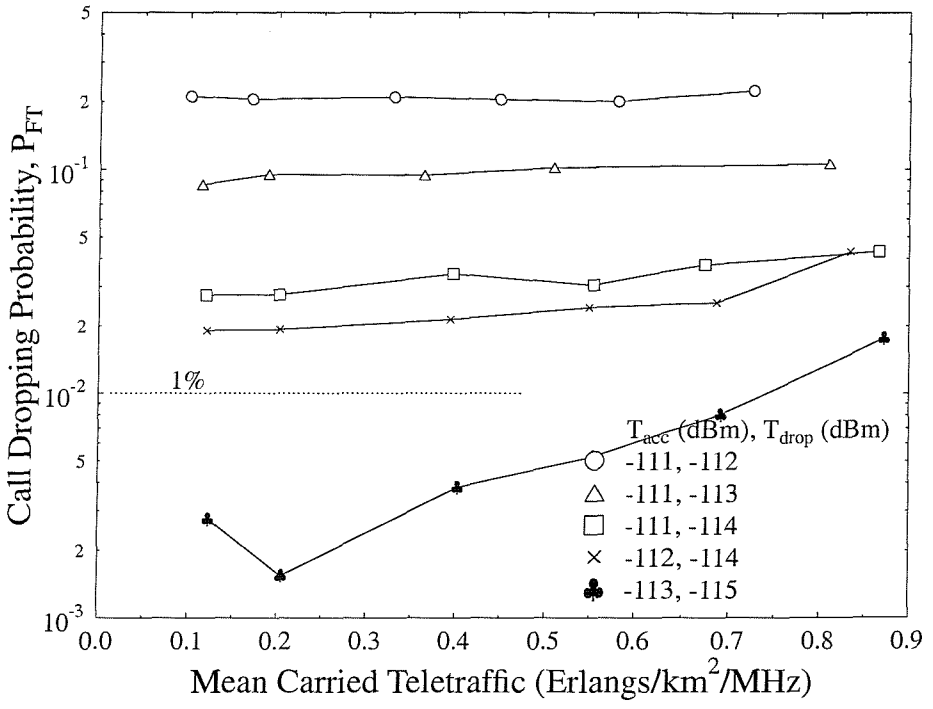

Figure 4.11: Call dropping probability versus mean carried traffic of a CDMA based cellular network using **fixed received pilot power** based soft handover thresholds in conjunction **with 0.5 Hz shadowing having a standard deviation of 3 dB** for SF=16.

reducing the soft handover thresholds improved the network's call dropping probability, but Figure 4.12 illustrates that reducing the soft handover thresholds engendered an increase in the probability of a low quality access.

The network cannot satisfy the quality requirements of the conservative scenario, namely that of maintaining a call dropping probability of 1% combined with a maximum probability of low quality access below 1%. However, the entire network supported 127 users, whilst meeting the lenient scenario's set of criteria, which consists of a maximum call dropping probability of 1% and a probability of low quality access of below 2%, using the thresholds of T_{acc}=-113 dBm and T_{drop}=-115 dBm.

4.4.2.3 Fixed Received Pilot Power Thresholds with 1.0 Hz Shadowing

This section presents results obtained using fixed receiver pilot power based soft handover thresholds in conjunction with log-normal shadow fading having a standard deviation of 3 dB and a maximum fading frequency of 1.0 Hz.

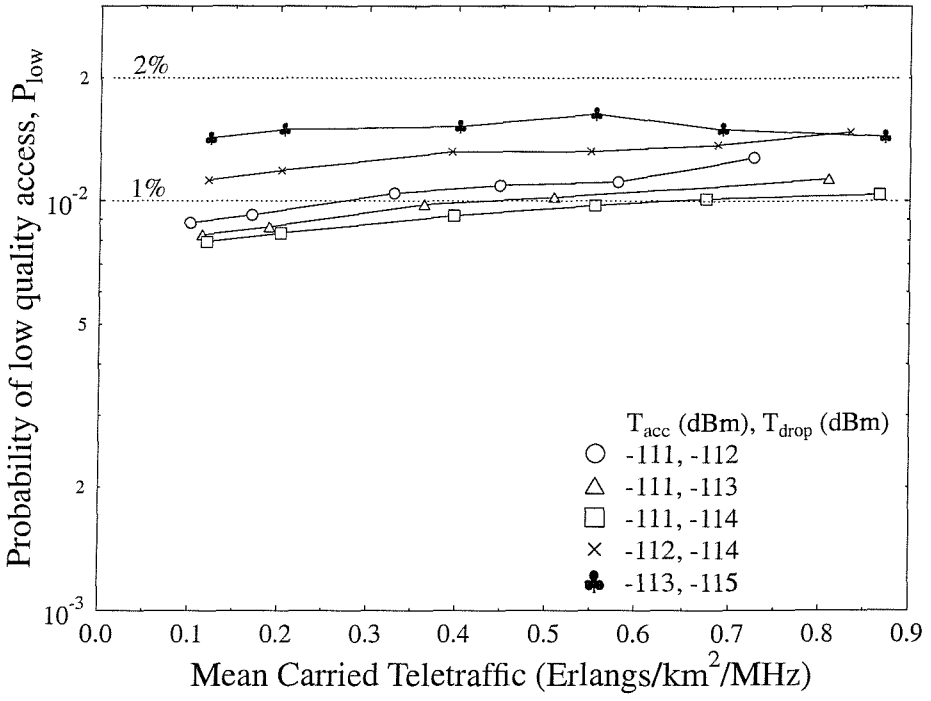

Figure 4.12: Probability of low quality access versus mean carried traffic of a CDMA based cellular network using **fixed received pilot power** based soft handover thresholds in conjunction **with 0.5 Hz shadowing having a standard deviation of 3 dB** for SF=16.

The corresponding call dropping probability is depicted in Figure 4.13, showing that using fixed thresholds in a propagation environment exposed to shadow fading resulted in a very poor performance. This was due to the shadow fading induced fluctuations of the received pilot signal power, which resulted in removing base stations from the ABS mid-call, which ultimately engendered dropped calls. Hence, lowering the fixed thresholds significantly reduced the call dropping probability. However, this led to a deterioration of the low quality access probability, as shown in Figure 4.14. The probability of low quality access was also very poor due to the rapidly fluctuating interference-limited environment. This was shown particularly explicitly in conjunction with T_{acc}=-113 dBm and T_{drop}=-115 dBm, where reducing the number of users resulted in a degradation of the low quality access performance due to the higher deviation of the reduced number of combined sources of interference. In contrast, adding more users led to a near-constant level of interference that varied less dramatically.

It was found that the network was unable to support any users at the required service quality, since using the thresholds that allowed the maximum 1% call dropping probability

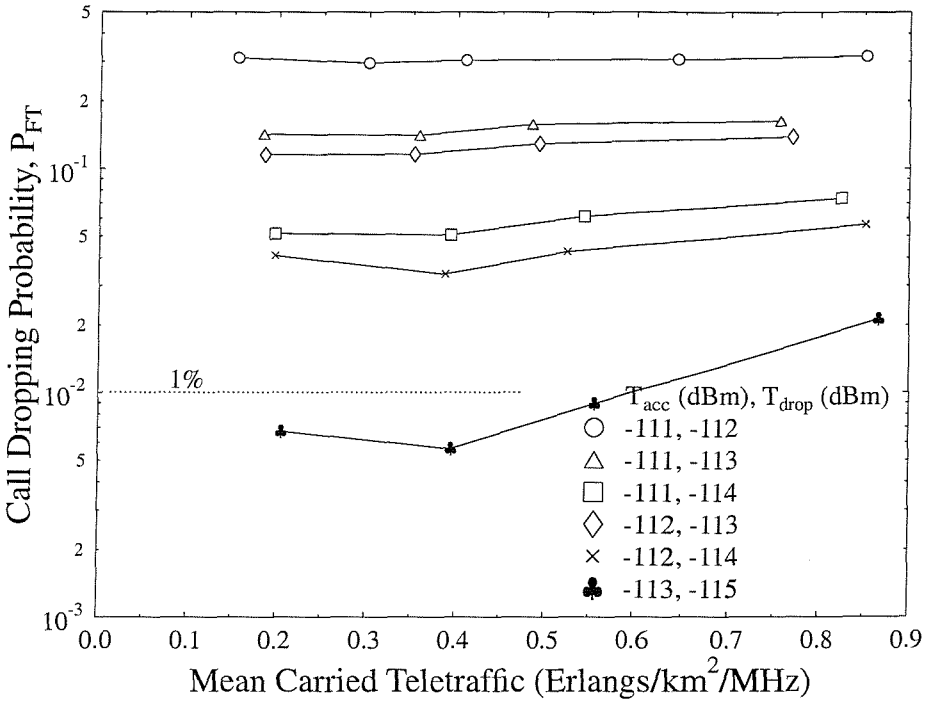

Figure 4.13: Call dropping probability versus mean carried traffic of a CDMA based cellular network using **fixed received pilot power** based soft handover thresholds in conjunction **with 1 Hz shadowing having a standard deviation of 3 dB** for SF=16.

restriction to be met, led to a greater than 2% probability of a low quality outage occurring.

4.4.2.4 Summary

In summary of our findings in the context of Figure 4.7-4.14, a disadvantage of using fixed soft handover thresholds is that in some locations all pilot signals may be weak, whereas in other locations, all of the pilot signals may be strong due to the localised propagation environment or terrain. Hence, using relative or normalised soft handover thresholds is expected to be advantageous in terms of overcoming this limitation. An additional benefit of using dynamic thresholds is confirmed within a fading environment, where the received pilot power may drop momentarily below a fixed threshold, thus causing unnecessary removals and additions to/from the ABS. However, these base stations may have been the only base stations in the ABS, thus ultimately resulting in a dropped call. When using dynamically controlled thresholds this scenario would not have occurred. Hence, in the next section we considered the performance of using relative received pilot power based soft handover thresholds under both non-shadowing and shadowing impaired propagation conditions.

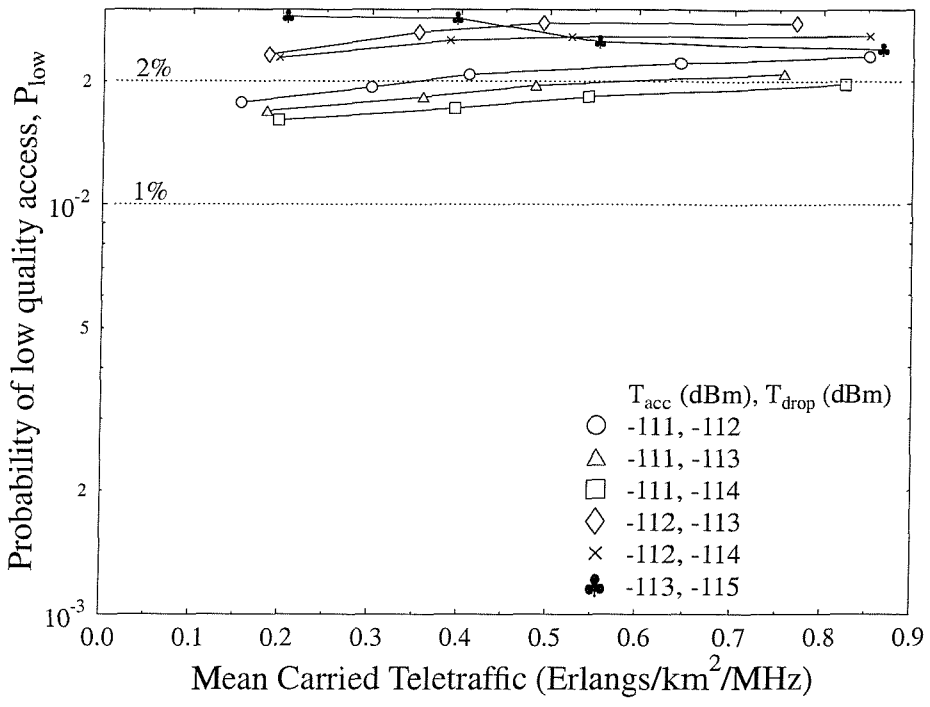

Figure 4.14: Probability of low quality access versus mean carried traffic of a CDMA based cellular network using **fixed received pilot power** based soft handover thresholds in conjunction **with 1 Hz shadowing having a standard deviation of 3 dB** for SF=16.

To summarise, using fixed received pilot power thresholds in a non-shadowing environment resulted in a total network capacity of 290 users for both quality of service scenarios, namely for both the conservative and lenient scenarios considered. However, this performance was severely degraded in a shadow fading impaired propagation environment, where a total network capacity of 127 users was supported in conjunction with a maximum shadow fading frequency of 0.5 Hz. Unfortunately, the network capacity could not be evaluated when using a maximum shadow fading frequency of 1.0 Hz due to the contrasting characteristics of the dropped call and low quality access probability results.

4.4.2.5 Relative Received Pilot Power Thresholds without Shadowing

Employing relative received pilot power thresholds is important in realistic propagation environments exposed to shadow fading. More explicitly, in contrast to the previously used thresholds, which were expressed in terms of dBm, i.e. with respect to 1 mW, in this section the thresholds T_{acc} and T_{drop} are expressed in terms of dB relative to the received pilot strength of the base stations in the ABS. Their employment also caters for situations, where the absolute pilot power may be too low for use in conjunction with fixed thresholds, but nonetheless sufficiently high for reliable communications. Hence, in this section we examine the performance of relative received pilot power based soft handover thresholds in a non-shadow faded environment.

The call dropping performance is depicted in Figure 4.15, which shows that reducing the soft handover thresholds, and thus increasing the time spent in soft handover, improved the call dropping performance. It was also found in the cases considered here, that simultaneously the probability of a low quality access decreased, as illustrated by Figure 4.16. However, it was also evident in both figures, that reducing the soft handover thresholds past a certain point resulted in degraded performance due to the extra interference incurred during the soft handover process.

Since the probability of low quality access was under the 1% threshold, the network capacity for both the lenient and conservative scenarios were the same, namely 1.65 Erlangs/km^2/ MHz or a total of 288 users over the entire simulation area of 2.86 km^2. The mean ABS size was 1.7 base stations, with a mean mobile transmission power of 4.1 dBm and an average base station transmit power of 4.7 dBm.

4.4.2.6 Relative Received Pilot Power Thresholds with 0.5 Hz Shadowing

In this section we present results obtained using relative received pilot power based soft handover thresholds in a shadowing-impaired propagation environment. The maximum shadow fading frequency was 0.5 Hz and the standard deviation of the log-normal shadowing was 3 dB.

Figure 4.17 depicts the call dropping probability for several relative thresholds and shows that by reducing both the thresholds, the call dropping performance is improved. This enables the mobile to add base stations to its ABS earlier on during the soft handover process, and to relinquish them at a much later stage than in the case of using higher handover thresholds. Therefore, using lower relative soft handover thresholds results in longer period of time spent in soft handover, as can be seen in Figure 4.18, which shows

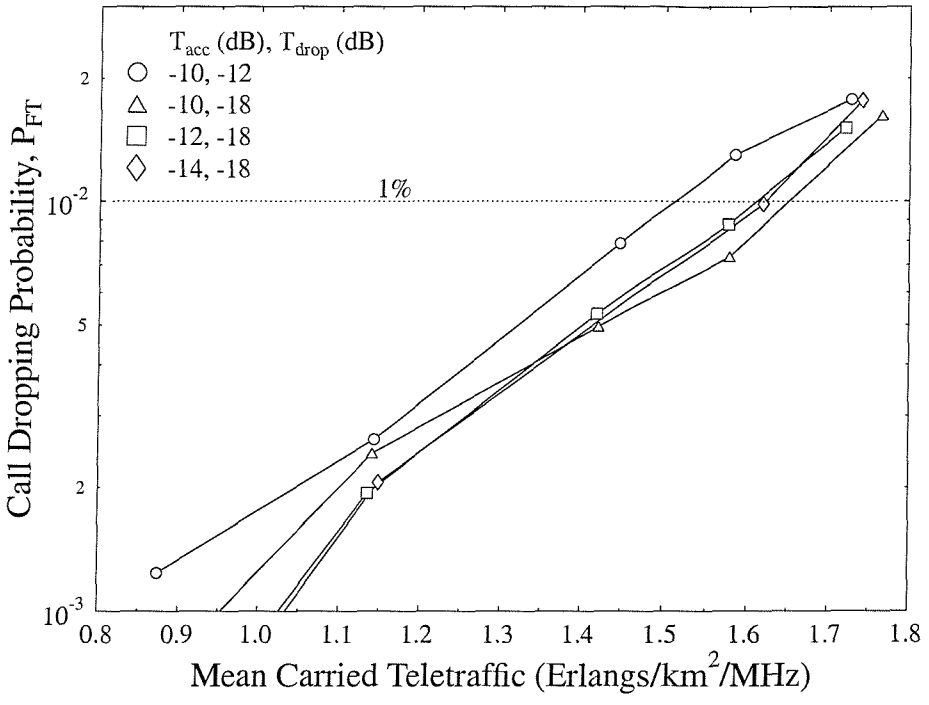

Figure 4.15: Call dropping probability versus mean carried traffic of a CDMA based cellular network using **relative received pilot power** based soft handover thresholds **without shadowing** for SF=16.

the mean number of base stations in the ABS.

The probability of low quality access is shown in Figure 4.19, illustrating that, in general, as the relative soft handover thresholds were reduced, the probability of low quality access increased. This demonstrated that spending more time in soft handover generated more co-channel interference and thus degraded the network's performance. However, the difference between the two thresholds must also be considered. For example, the probability of low quality access is higher in conjunction with T_{acc}=-16 dB and T_{drop}=-18 dB, than using T_{acc}=-16 dB and T_{drop}=-20 dB, since the latter scenario has a higher mean number of base stations in its ABS. Therefore, there is a point at which the soft handover gain experienced by the desired user outweighs the detrimental effects of the extra interference generated by base stations' transmissions to users engaged in the soft handover process.

Figure 4.20 shows the mean transmission powers of both the mobiles and the base stations. The mobiles are required to transmit at a lower power than the base stations, because the base stations are not subjected to downlink pilot power interference and to soft handover interference. Furthermore, the mobiles are not affected by the level of the soft handover

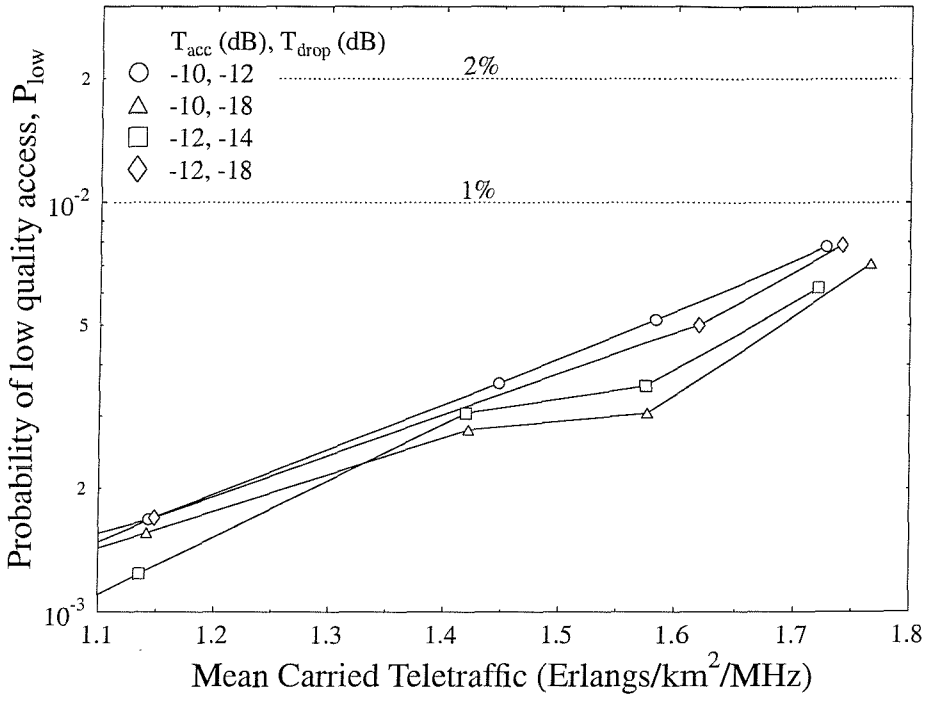

Figure 4.16: Probability of low quality access versus mean carried traffic of a CDMA based cellular network using **relative received pilot power** based soft handover thresholds **without shadowing** for SF=16.

thresholds, because only selective diversity is performed in the uplink, and hence the mobile transmits as if not in soft handover. As the soft handover thresholds were reduced, the time spent in soft handover increased and thus the mean base transmission power had to be increased in order to overcome the additional downlink interference.

The maximum network capacity of 0.835 Erlangs/km^2/MHz, or 144 users over the entire simulation area, was achieved using the soft handover thresholds of T_{acc}=-14 dB and T_{drop}=-18 dB for the conservative scenario. The mean ABS size was 1.77 base stations, while the mean mobile transmit power was -1.5 dBm and 0.6 dBm for the base stations. In the lenient scenario a maximum teletraffic load of 0.865 Erlangs/km^2/MHz, corresponding to a total network capacity of 146 users was maintained using soft handover thresholds of T_{acc}=-16 dB and T_{drop}=-18 dB. The mean number of base stations in the ABS was 1.78, with an average transmit power of -1.5 dBm for the mobile handset, and 1.3 dBm for the base station.

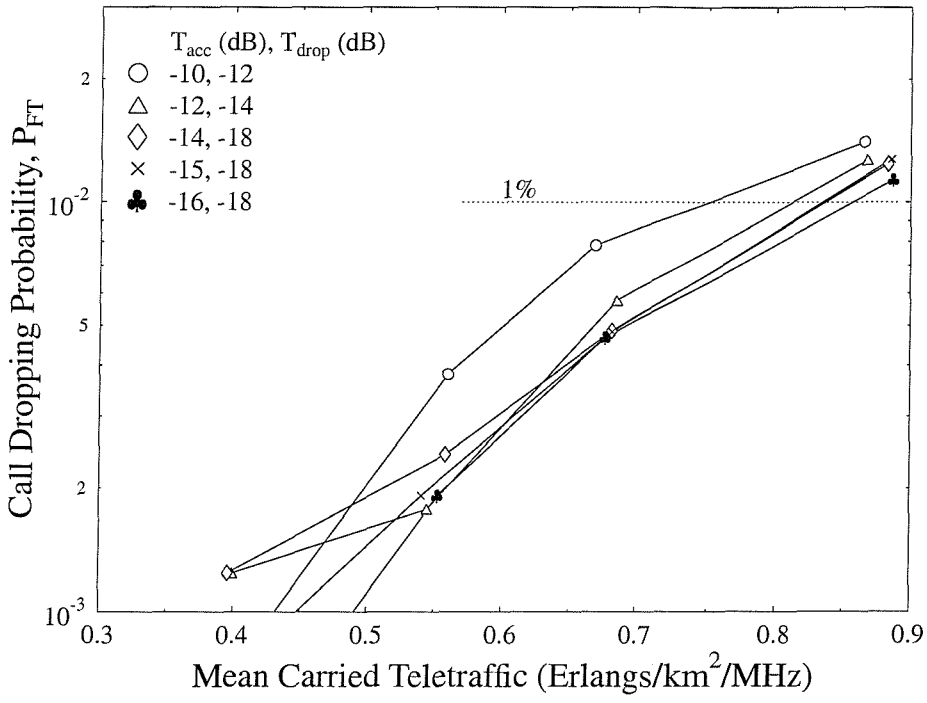

Figure 4.17: Call dropping probability versus mean carried traffic of a CDMA based cellular network using **relative received pilot power** based soft handover thresholds in conjunction **with 0.5 Hz shadowing and a standard deviation of 3 dB** for SF=16.

4.4.2.7 Relative Received Pilot Power Thresholds with 1.0 Hz Shadowing

In this section we present further performance results obtained using relative received pilot power based soft handover thresholds in a shadowing propagation environment. The maximum shadow fading frequency was 1.0 Hz and the standard deviation of the log-normal shadowing was 3 dB.

On comparing the call dropping probability curves seen in Figure 4.21 with the call dropping probability obtained for a maximum shadow fading frequency of 0.5 Hz in Figure 4.17 it was found that the performance of the 1.0 Hz frequency shadowing scenario was slightly worse. However, the greatest performance difference was observed in the probability of low quality access, as can be seen in Figure 4.22.

Using the soft handover thresholds which gave a good performance for a maximum shadow fading frequency of 0.5 Hz resulted in significantly poorer low quality access performance for a maximum shadowing frequency of 1.0 Hz. In order to obtain a probability of low quality access of below 1% it was necessary to use markedly different soft handover thresholds,

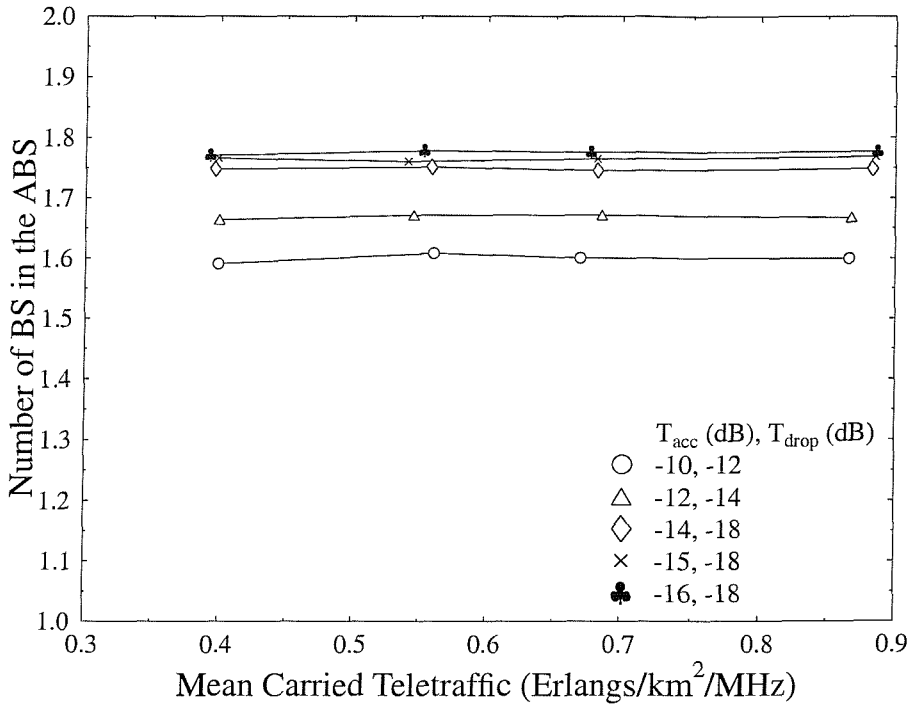

Figure 4.18: Mean number of base stations in the active base station set versus mean carried traffic of a CDMA based cellular network using **relative received pilot power** based soft handover thresholds in conjunction **with 0.5 Hz shadowing and a standard deviation of 3 dB** for SF=16.

which reduced the time spent in soft handover and hence also the size of the ABS, as illustrated in Figure 4.23.

For the conservative scenario, where the maximum probability of low quality access, P_{low}, was set to 1%, the maximum network capacity was found to be 0.69 Erlangs/km^2/MHz, equivalent to a total network capacity of 127 users, obtained using T_{drop}=-2 dB and T_{acc}=-16 dB. In contrast, in the lenient scenario, where the P_{low} limit was 2%, the maximum number of users supported was found to be 144, or 0.825 Erlangs/km^2/MHz, in conjunction with T_{acc}=-14 dB and T_{drop}=-18 dB.

4.4.2.8 Summary

In summary, using relative received pilot power as a soft handover metric has resulted in a significantly improved performance in comparison to that of the fixed received pilot power based results in a shadow fading environment. In the non-shadowed environment the network capacity was approximately the same as when using the fixed threshold algorithm,

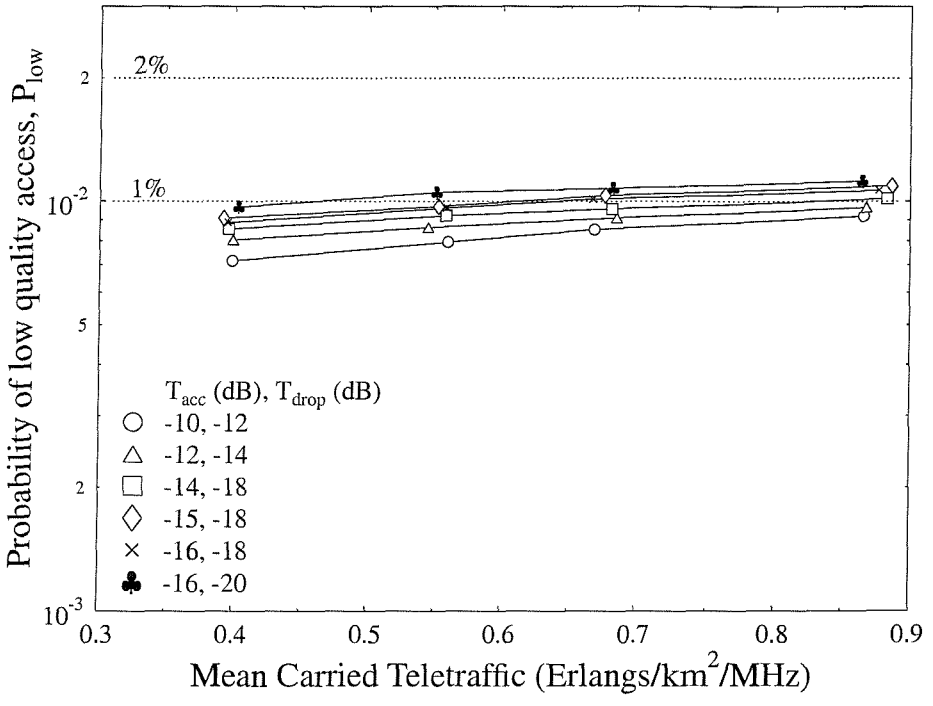

Figure 4.19: Probability of low quality access versus mean carried traffic of a CDMA based cellular network using **relative received pilot power** based soft handover thresholds in conjunction **with 0.5 Hz shadowing and a standard deviation of 3 dB** for SF=16.

albeit with a slightly improved mean transmission power. Due to the time varying nature of the received signals subjected to shadow fading, using relative thresholds has been found to be more amenable to employment in a realistic propagation environment, than using fixed thresholds. In conclusion, without shadow fading the network supported a total of 288 users, whilst with a maximum shadow fading frequency of 0.5 Hz, approximately 145 users were supported by the entire network, for both the conservative and lenient scenarios. However, different soft handover thresholds were required for each situation, for achieving these capacities. At a maximum shadowing frequency of 1.0 Hz, a total of 127 users were supported in the conservative scenario, and 144 in the lenient scenario. However, again, different soft handover thresholds were required in each scenario in order to maximise the network capacity.

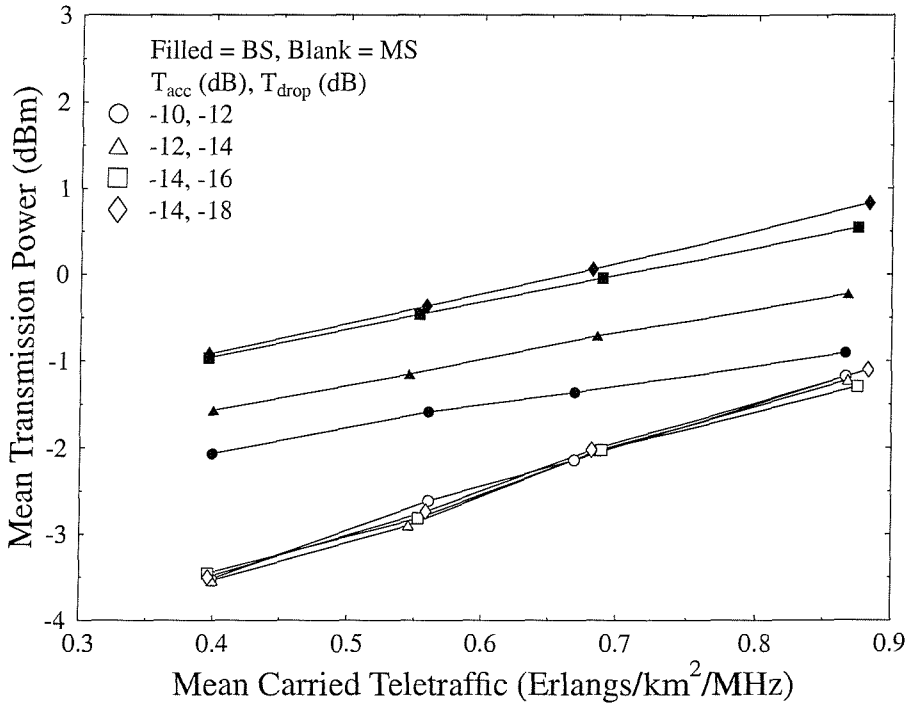

Figure 4.20: Mean transmission power versus mean carried traffic of a CDMA based cellular network using **relative received pilot power** based soft handover thresholds in conjunction **with 0.5 Hz shadowing and a standard deviation of 3 dB** for SF=16.

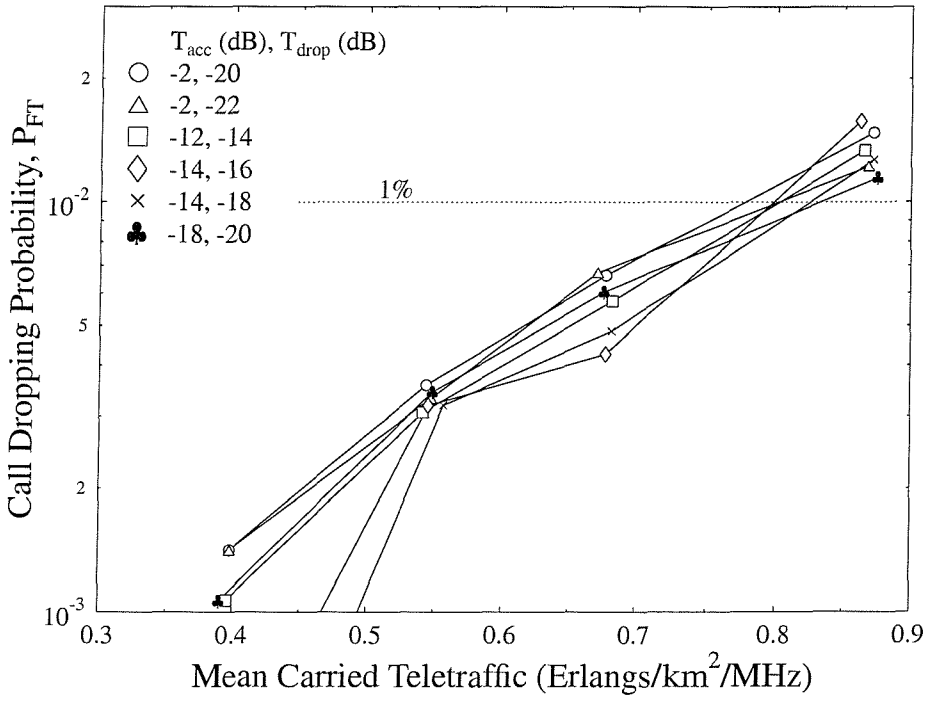

Figure 4.21: Call dropping probability versus mean carried traffic of a CDMA based cellular network using **relative received pilot power** based soft handover thresholds in conjunction **with 1 Hz shadowing and a standard deviation of 3 dB** for SF=16.

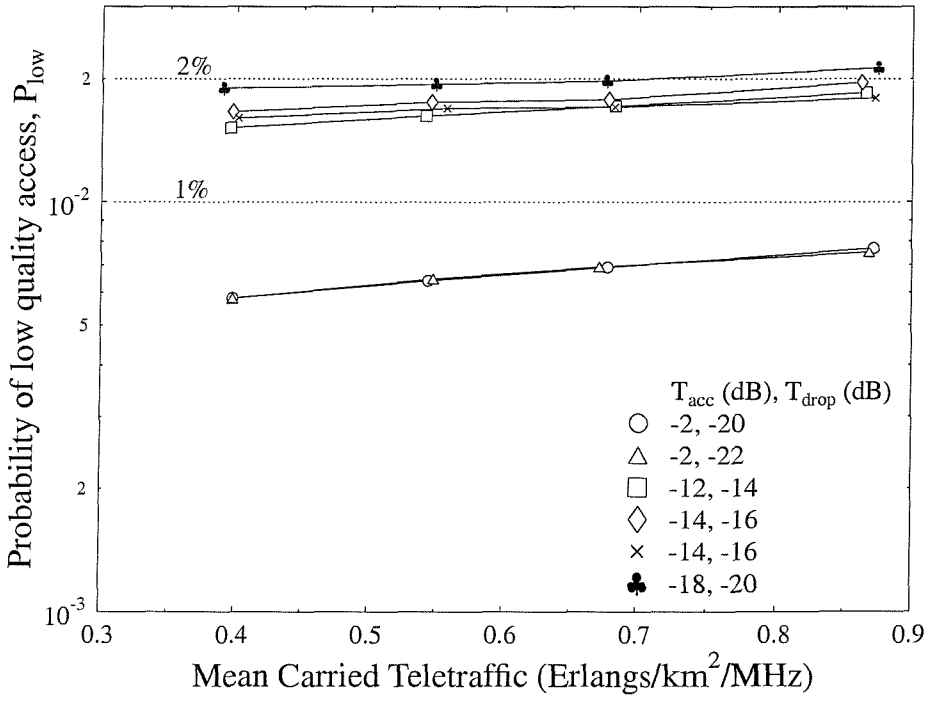

Figure 4.22: Probability of low quality access versus mean carried traffic of a CDMA based cellular network using **relative received pilot power** based soft handover thresholds in conjunction **with 1 Hz shadowing and a standard deviation of 3 dB** for SF=16.

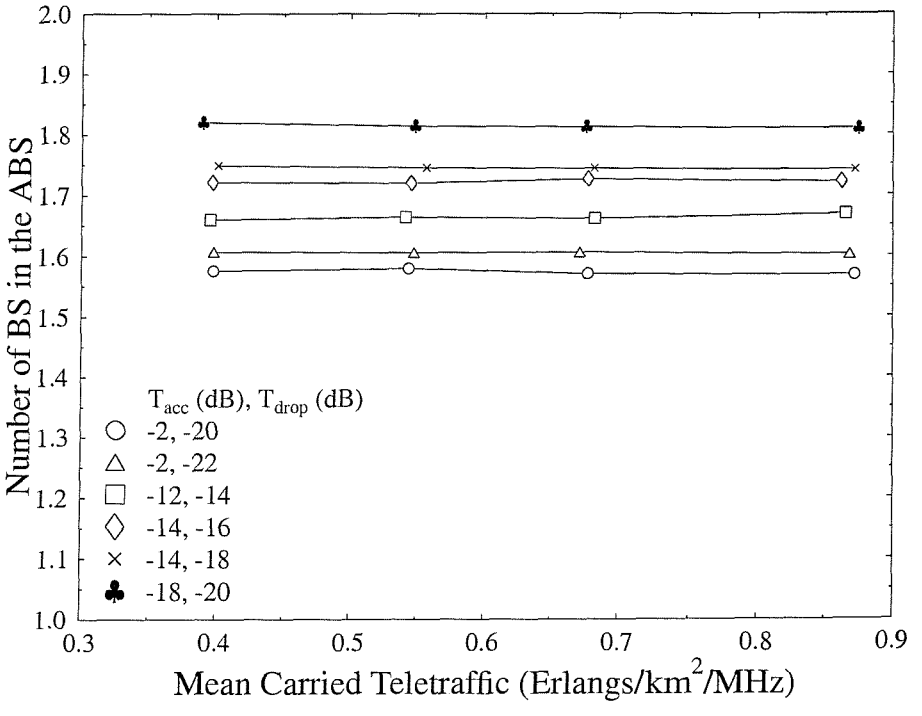

Figure 4.23: Mean number of base stations in the active base station set versus mean carried traffic of a CDMA based cellular network using **relative received pilot power** based soft handover thresholds in conjunction **with 1 Hz shadowing and a standard deviation of 3 dB** for SF=16.

4.4.3 E_c/I_o Power Based Soft Handover Results

An alternative soft handover metric used to determine "cell ownership" is the pilot to downlink interference ratio of a cell, which was proposed for employment in the 3rd generation systems [104]. The pilot to downlink interference ratio, or E_c/I_o, may be calculated thus as [123]:

$$\frac{E_c}{I_o} = \frac{P_{pilot}}{P_{pilot} + N_0 + \sum_{k=1}^{N_{cells}} P_k T_k}, \tag{4.10}$$

where P_k is the total transmit power of cell k, T_k is the transmission gain which includes antenna gain and pathloss as well as shadowing, N_0 is the thermal noise power and N_{cells} is the number of cells in the network. The advantage of using such a scheme is that it is not an absolute measurement that is used, but the ratio of the pilot power to the interference power. Thus, if fixed thresholds were used a form of admission control may be employed for new calls if the interference level became too high. A further advantage is that it takes into account the time-varying nature of the interference level in a shadowed environment.

4.4.3.1 Fixed E_c/I_o Thresholds without Shadowing

The new call blocking probability obtained when using fixed E_c/I_o soft handover thresholds without any form of shadow fading is shown in Figure 4.24, which suggests that in general, lowering the soft handover thresholds reduced the probability of a new call attempt being blocked. However, it was found that in conjunction with T_{drop}=-40 dB, dropping the threshold T_{acc} from -20 dB to -24 dB actually increased the new call blocking probability. This was attributed to the fact that the lower threshold precipitated a higher level of co-channel interference, since there was a higher mean number of base stations in the ABS, as evidenced by Figure 4.25. Therefore, since the mean level of interference present in the network is higher, when using a lower threshold, and the threshold determines the value of the pilot to downlink interference ratio at which base stations may be added to the ABS, a more frequent blocking of calls occurs. Alternatively, a lower threshold resulted in a higher level of downlink interference due to the additional interference inflicted by supporting the mobiles in soft handover, which prevented base stations from being included in the ABS due to insufficient pilot to interference "head-room". This then ultimately led to blocked calls due to the lack of base stations in the ABS.

Again, the mean number of base stations in the ABS is given in Figure 4.25, which illustrates that as expected, reducing the soft handover thresholds increased the proportion of time spent in soft handover, and thus reduced the mean number of base stations in the ABS. The average size of the ABS was found to decrease, as the network's traffic load

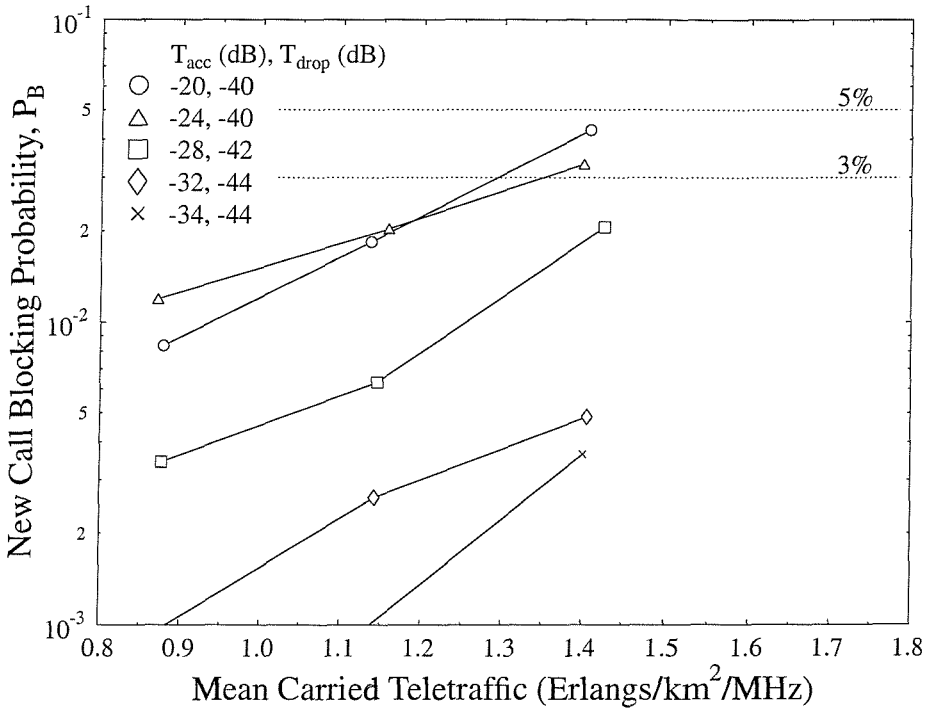

Figure 4.24: New call blocking probability versus mean carried traffic of a CDMA based cellular network using **fixed** E_c/I_o based soft handover thresholds **without shadowing** for SF=16.

increased. This was a consequence of the increased interference levels associated with the higher traffic loads, which therefore effectively reduced the pilot to interference ratio at a given point, and hence base stations were less likely to be in soft handover and in the ABS.

Figure 4.26 depicts the mean transmission powers for both the uplink and the downlink, for a range of different soft handover thresholds. These results show similar trends to the results presented in previous sections, with the required average downlink transmission power increasing, since a greater proportion of call time is spent in soft handover. Again, the mean uplink transmission power varied only slightly, since the selection diversity technique of the base stations only marginally affected the received interference power at the base stations.

Figure 4.27 shows the call dropping performance, indicating that lowering the soft handover thresholds generally improved the call dropping performance. However, reducing the soft handover thresholds too much resulted in a degradation of the call dropping probability due to the increased levels of co-channel interference inherent, when a higher proportion of the call time is spent in soft handover. This is explicitly illustrated by Figure 4.28, which

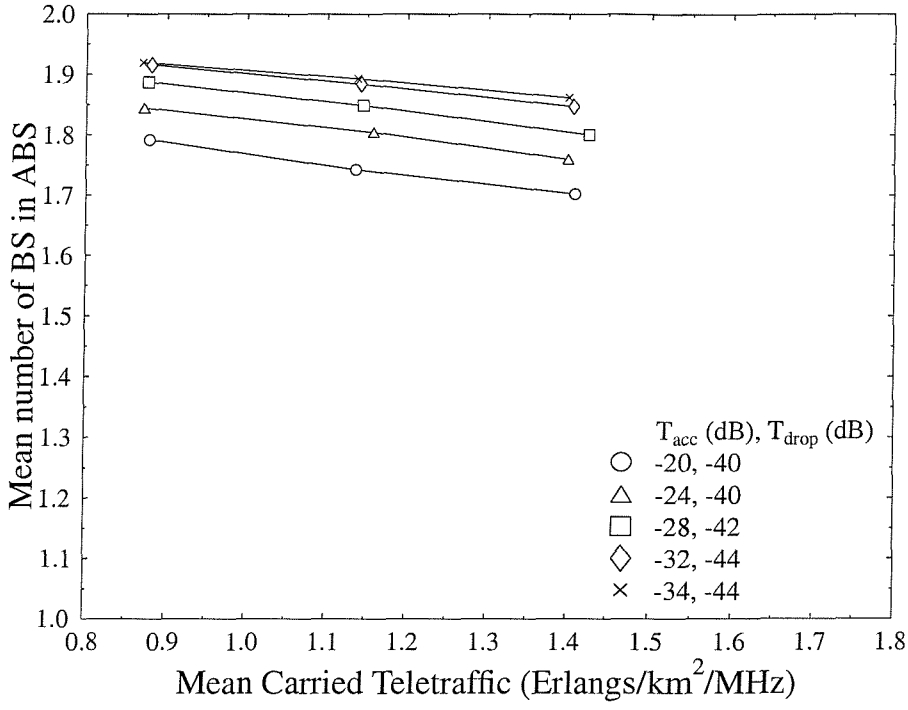

Figure 4.25: Mean number of base stations in the active base station set versus mean carried traffic of a CDMA based cellular network using **fixed** E_c/I_o based soft handover thresholds **without shadowing** for SF=16.

indicates that reducing the soft handover thresholds caused a significant degradation in the probability of low quality access. This was a consequence of the additional co-channel interference associated with the soft handover process. The figure also shows that there is a point, where the diversity gain of the mobiles obtained with the advent of the soft handover procedure outweighs the extra interference that it generates.

On the whole, the capacity of the network when using fixed E_c/I_o soft handover thresholds was lower than when using fixed received pilot power based soft handover thresholds. This can be attributed to the fact that the E_c/I_o thresholds are related to the interference level of the network, which changes with the network load and propagation conditions. Hence using a fixed threshold is sub-optimal. In the conservative scenario, the network capacity was 1.275 Erlangs/km^2/MHz, corresponding to a total network capacity of 223 users. In the lenient scenario, this increased to 1.305 Erlangs/km^2/MHz, or 231 users. In contrast, when using fixed received pilot power thresholds the entire network supported 290 users.

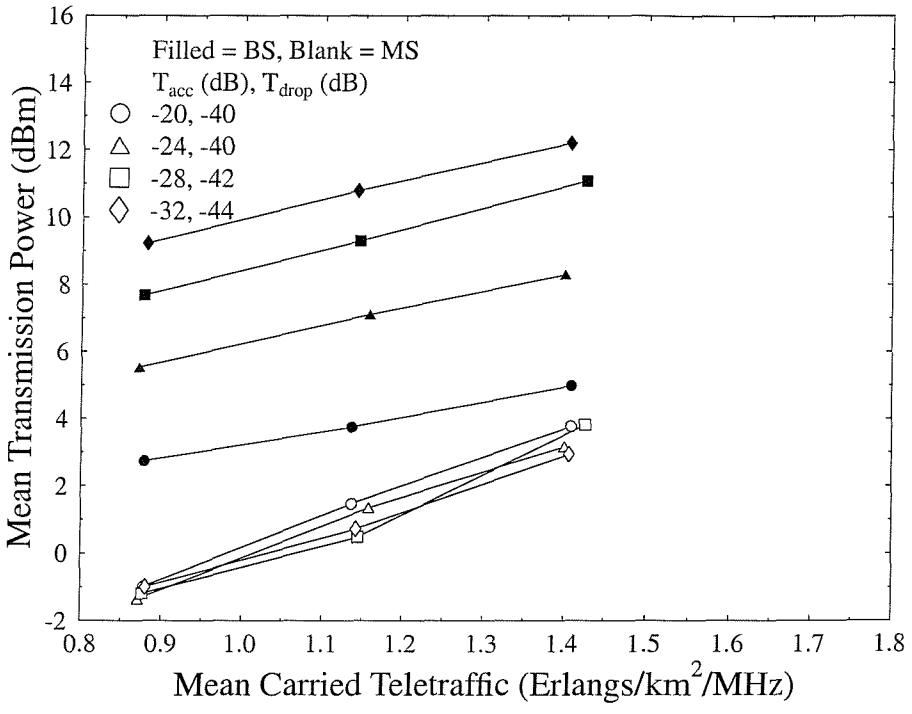

Figure 4.26: Mean transmission power versus mean carried traffic of a CDMA based cellular network using **fixed received** E_c/I_o based soft handover thresholds **without shadowing** for SF=16.

4.4.3.2 Fixed E_c/I_o Thresholds with 0.5 Hz Shadowing

In this section we consider fixed pilot to downlink interference ratio based soft handover thresholds in a propagation environment exhibiting shadow fading in conjunction with a maximum fading frequency of 0.5 Hz and a standard deviation of 3 dB.

Examining Figure 4.29, which shows the call dropping probability, we see, again, that reducing the soft handover thresholds typically resulted in a lower probability of a dropped call. However, since the handover thresholds are dependent upon the interference level, there was some interaction between the handover thresholds and the call dropping rate. For example, it can be seen in the figure that when T_{drop}=-40 dB, the call dropping probability fell as T_{acc} was reduced from -20 dB to -24 dB. However, on lowering T_{acc} further, to -26 dB, the call dropping rate at low traffic loads became markedly higher. A similar phenomenon was observed in Figure 4.30, which shows the probability of low quality outage.

It is explicitly seen from Figures 4.29 and 4.30 that the performance of the fixed E_c/I_o soft handover threshold based scheme clearly exceeded that of the fixed received pilot power

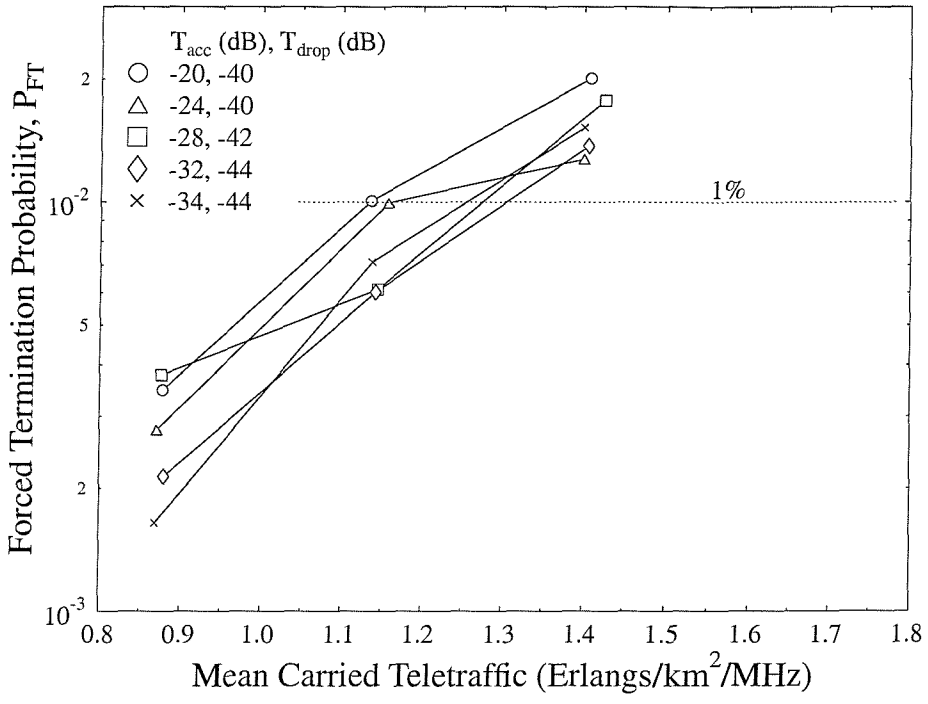

Figure 4.27: Call dropping probability versus mean carried traffic of a CDMA based cellular network using **fixed received** E_c/I_o based soft handover thresholds **without shadowing** for SF=16.

threshold based system in a shadow fading environment. The network supported a teletraffic load of 0.7 Erlangs/km^2/MHz or a total of 129 users in the conservative scenario, which rose to 0.78 Erlangs/km^2/MHz, or 140 users, in the lenient scenario. These network capacities were achieved with the aid of a mean number of active base stations in the ABS, which were 1.88 and 1.91, respectively. In order to achieve the total network capacity of 129 users in the conservative scenario, a mean mobile transmit power of -2.4 dBm was required, while the mean base station transmission power was 7 dBm. For the lenient scenario, these figures were -2.4 dBm and 8.7 dBm, respectively.

4.4.3.3 Fixed E_c/I_o Thresholds with 1.0 Hz Shadowing

Increasing the maximum shadow fading frequency from 0.5 Hz to 1.0 Hz resulted in an increased call dropping probability and a greater probability of low quality access, for a given level of carried teletraffic. This is clearly seen by comparing Figures 4.31 and 4.32 with Figures 4.29 and 4.30. Explicitly, Figure 4.31 and 4.32 show that reducing the soft handover threshold, T_{acc} from -20 dB to -24 dB led to both an increased call dropping

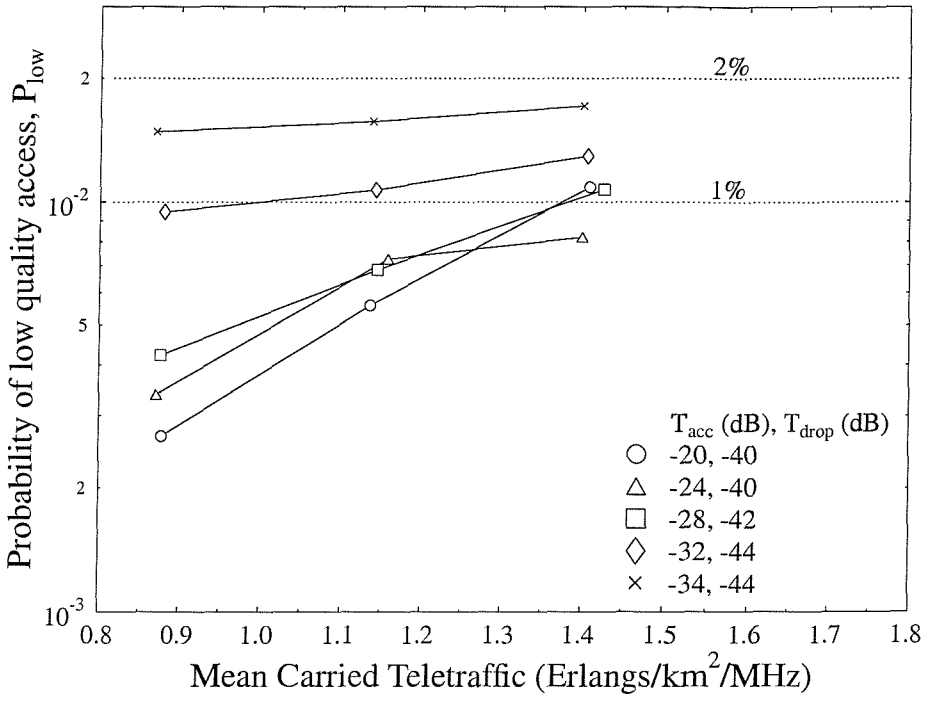

Figure 4.28: Probability of low quality access versus mean carried traffic of a CDMA based cellular network using **fixed received** E_c/I_o based soft handover thresholds **without shadowing** for SF=16.

probability and an increased probability of low quality access. This can be attributed to the extra co-channel interference generated by the greater proportion of call time being spent in soft handover. This is also confirmed by the increased probability of low quality access observed in Figure 4.32 for lower soft handover thresholds T_{acc} and T_{drop}.

The network capacity of the conservative scenario was 0.583 Erlangs/km^2/MHz, giving an entire network capacity of 107 users. In the lenient scenario the network supported a total of 128 users or a traffic load of 0.675 Erlangs/km^2/MHz was carried. The 107 users were serviced in conjunction with a mean ABS size of 1.86, a mean mobile transmit power of -3 dBm and a mean base station transmit power of 4.5 dBm. The 128 users supported in the lenient scenario necessitated an average mobile transmit power of -3 dBm and an average base station transmit power of 9.5 dBm. The mean number of base stations in the ABS was 1.91.

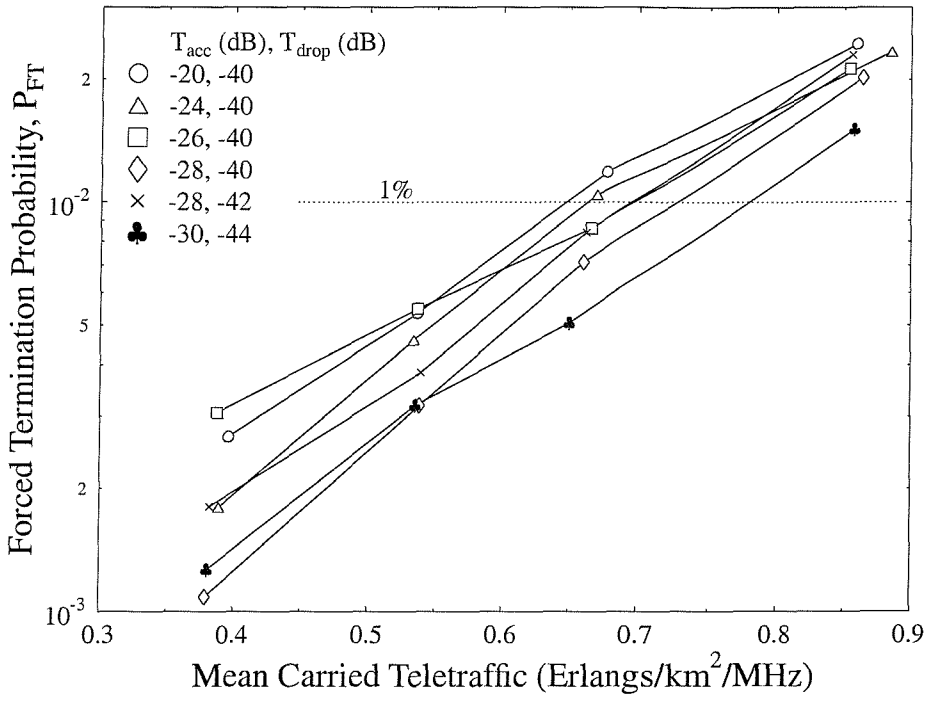

Figure 4.29: Call dropping probability versus mean carried traffic of a CDMA based cellular network using **fixed received** E_c/I_o based soft handover thresholds in conjunction **with 0.5 Hz shadowing and a standard deviation of 3 dB** for SF=16.

4.4.3.4 Summary

In summary, a maximum network capacity of 290 users was obtained when employing the fixed E_c/I_o soft handover thresholds. This capacity was equal to that when using fixed received pilot power thresholds in the lenient scenario without shadow fading. However, in the conservative scenario the network capacity was reduced from 290 to 231 users. Nevertheless, when a realistic shadowed propagation environment was considered, using the pilot power to interference ratio based soft handover metric improved the network capacity significantly. This was particularly evident in conjunction with the maximum shadow fading frequency of 1.0 Hz, when using the fixed received pilot power thresholds no users could be supported whilst maintaining the desired call quality. In contrast, using the fixed E_c/I_o soft handover thresholds led to a total network capacity of between 107 and 128 users, for the conservative and lenient scenarios, respectively. This capacity increase was the benefit of the more efficient soft handover mechanism, which was capable of taking into account the interference level experienced, leading to a more intelligent selection of base station supporting the call. At a maximum shadow fading frequency of 0.5 Hz the network

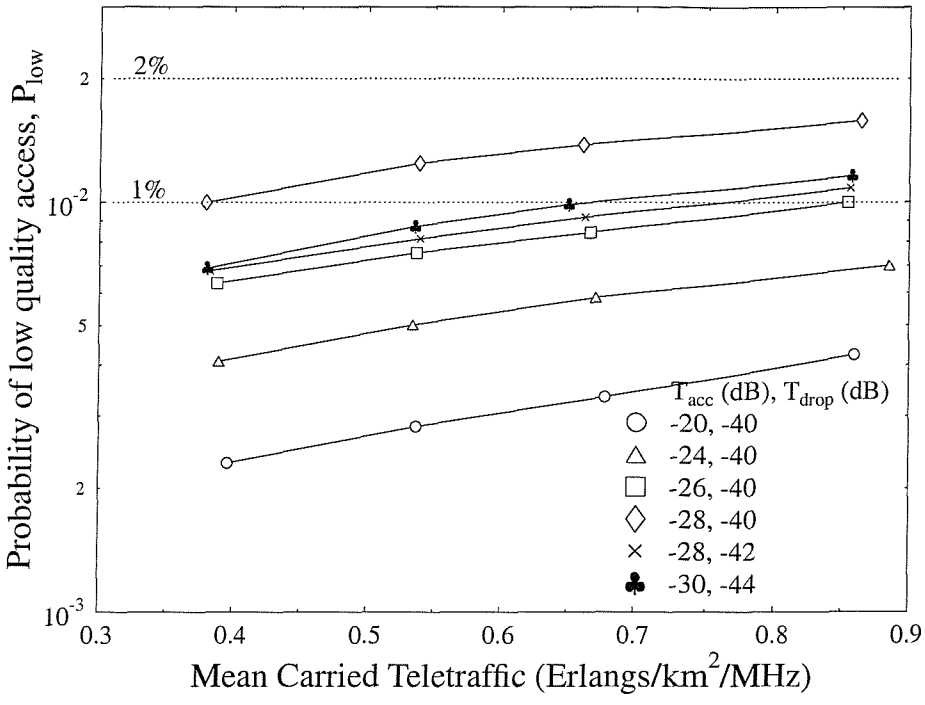

Figure 4.30: Probability of low quality access versus mean carried traffic of a CDMA based cellular network using **fixed received** E_c/I_o based soft handover thresholds in conjunction **with 0.5 Hz shadowing and a standard deviation of 3 dB** for SF=16.

had a maximum capacity of 129 and 140 users, for the conservative and lenient scenario, respectively, when using the fixed E_c/I_o soft handover thresholds.

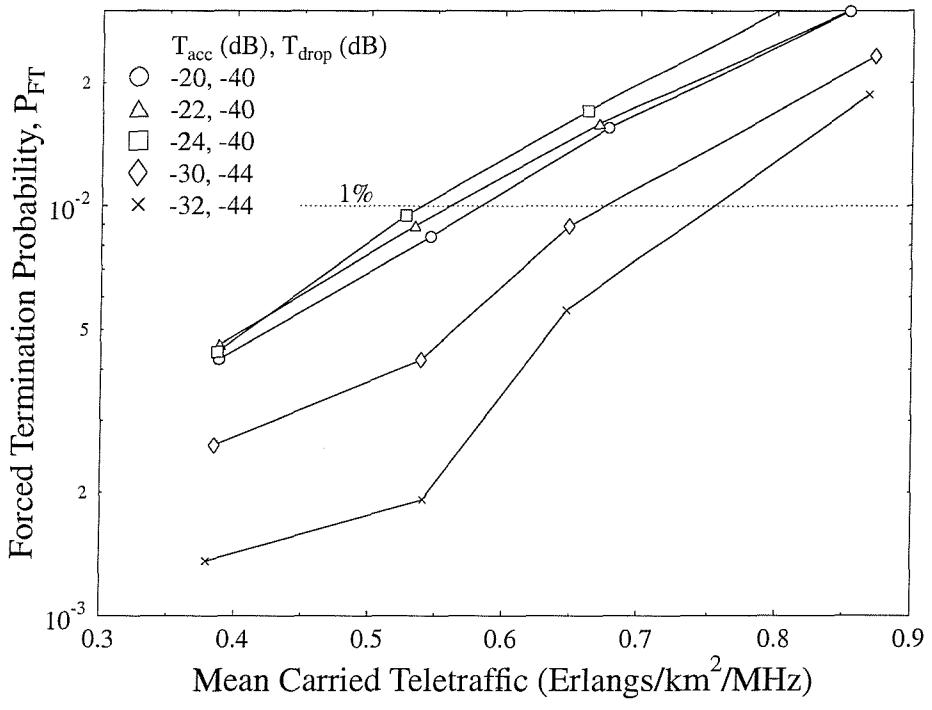

Figure 4.31: Call dropping probability versus mean carried traffic of a CDMA based cellular network using **fixed received** E_c/I_o based soft handover thresholds in conjunction **with 1.0 Hz shadowing and a standard deviation of 3 dB** for SF=16.

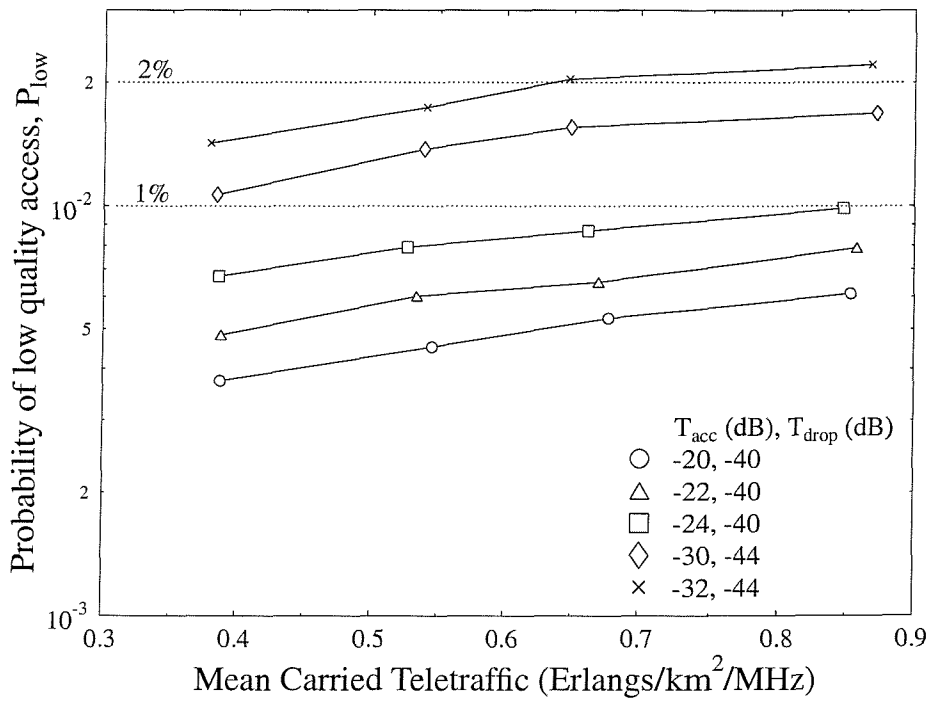

Figure 4.32: Probability of low quality access versus mean carried traffic of a CDMA based cellular network using **fixed received** E_c/I_o based soft handover thresholds in conjunction **with 1.0 Hz shadowing and a standard deviation of 3 dB** for SF=16.

4.4.3.5 Relative E_c/I_o Thresholds without Shadowing

In this section we combined the benefits of using the received E_c/I_o ratio and relative soft handover thresholds, thus ensuring that variations in both the received pilot signal strength and interference levels were monitored in the soft handover process.

The call dropping performance is shown in Figure 4.33, illustrating that reducing the soft handover thresholds improved the probability of dropped calls, in particular at higher traffic loads. This phenomenon is also evident in Figure 4.34, which shows the probability of a low quality outage. However, in some cases it was evident that excessive reduction of the thresholds led to increasing the co-channel interference, and hence to a greater probability of outage associated with low quality. Again, this was the consequence of supporting an excessive number of users in soft handover, which provided a beneficial diversity gain for the mobiles but also increased the amount of downlink interference inflicted by the base stations supporting the soft handovers.

The entire network supported a total of 256 users employing soft handover thresholds of T_{acc}=-12 dB and T_{drop}=-16 dB. The mean number of base stations in the active set was 1.68, and the mean mobile transmit power was 3.1 dBm. The average base station transmit power was 2.7 dBm.

4.4.3.6 Relative E_c/I_o Thresholds with 0.5 Hz Shadowing

Examining the call dropping probability graphs in Figure 4.35 shows that the probability of a dropped call was significantly lower than that of the other soft handover algorithms considered for the same propagation environment. This was because the handover algorithm was capable of taking the current interference levels into account, when deciding whether to initiate a handover, additionally, the employment of the relative thresholds minimised the chances of making an inappropriate soft handover decision concerning the most suitable base station to use. The superiority of this soft handover algorithm was further emphasised by the associated low probability of a low quality access, as illustrated in Figure 4.36, which was an order of magnitude lower than that achieved using the alternative soft handover algorithms.

When T_{acc} was set to -10 dB the ultimate capacity of the network was only marginally affected by changing T_{drop}, although some variation could be observed in the call dropping probability. Furthermore, the probability of low quality access increased for the lowest values of T_{drop}. This degradation of the probability of low quality access was due to the higher proportion of time spent in soft handover, as indicated by the correspondingly increased

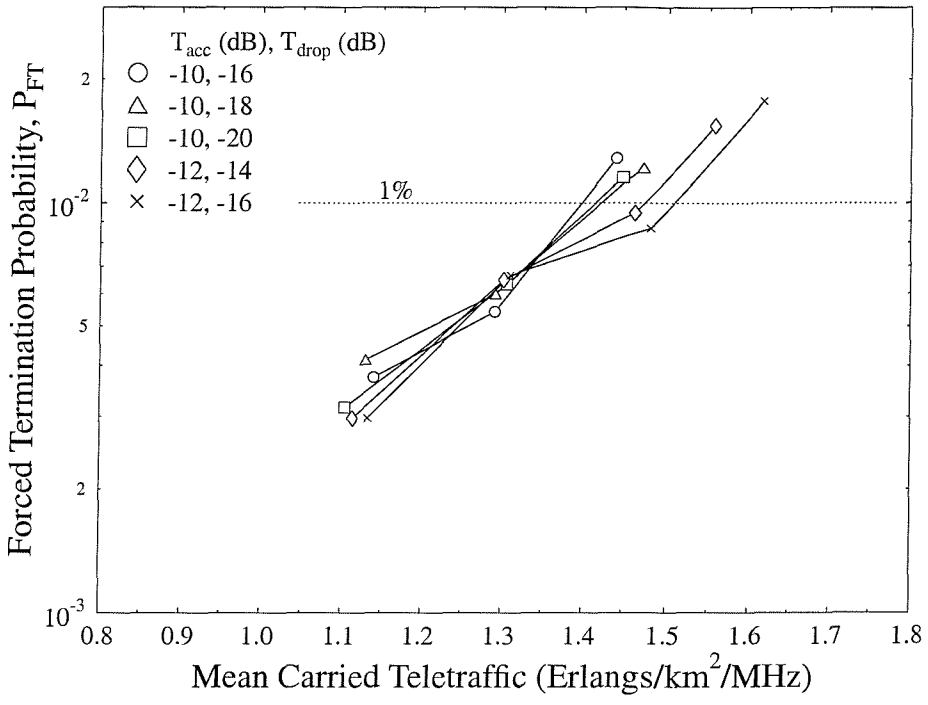

Figure 4.33: Call dropping probability versus mean carried traffic of a CDMA based cellular network using **relative received** E_c/I_o based soft handover thresholds **without shadowing** for SF=16.

ABS size in Figure 4.37, which was a consequence of the associated increased co-channel interference levels.

The mean transmit power curves of Figure 4.38 exhibited a different characteristic in comparison to that observed for the other soft handover algorithms. Specifically, at low traffic loads the mean mobile transmit power was less than that of the base stations, whereas at the higher traffic loads, the mobile transmit power was greater than that of the base stations. Although, comparing this graph with Figure 4.20 revealed that the spread and the rate of change of the mobile transmit power versus the traffic load was similar in both scenarios, the mean base station transmission power was lower in Figure 4.38. This reduced base station transmission power, again demonstrated the superiority of this soft handover algorithm, which manifested itself in its more efficient use of resources.

Since the probability of low quality access fell well below the 1% threshold, both the conservative and lenient scenarios exhibited the same total network capacity, which was slightly above 150 users for the entire network. This was achieved on average with the aid of 1.65 base stations, at a mean mobile transmit power of -1.2 dBm and at a mean base

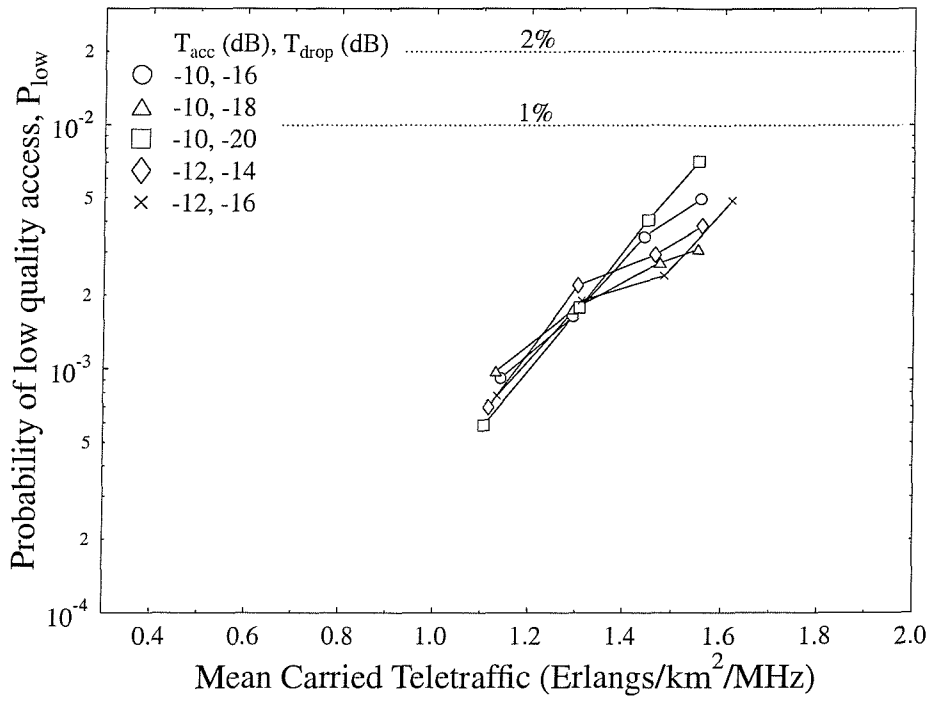

Figure 4.34: Probability of low quality access versus mean carried traffic of a CDMA based cellular network using **relative received** E_c/I_o based soft handover thresholds **without shadowing** for SF=16.

station transmit power of -1.7 dBm.

4.4.3.7 Relative E_c/I_o Thresholds with 1.0 Hz Shadowing

The call dropping probability shown in Figure 4.39 is slightly worse than that obtained in Figure 4.35 for a maximum shadow fading frequency of 0.5 Hz, with a greater performance difference achieved by altering T_{drop}. A similar performance degradation was observed for the probability of low quality access in Figure 4.40, with an associated relatively low impact due to varying the soft handover thresholds. Although not explicitly shown, we found that the mean transmission powers were similar to those required for a maximum shadow fading frequency of 0.5 Hz.

4.4.3.8 Summary

In summary, the employment of relative E_c/I_o soft handover thresholds resulted in a superior network performance and capacity under all the propagation conditions investigated.

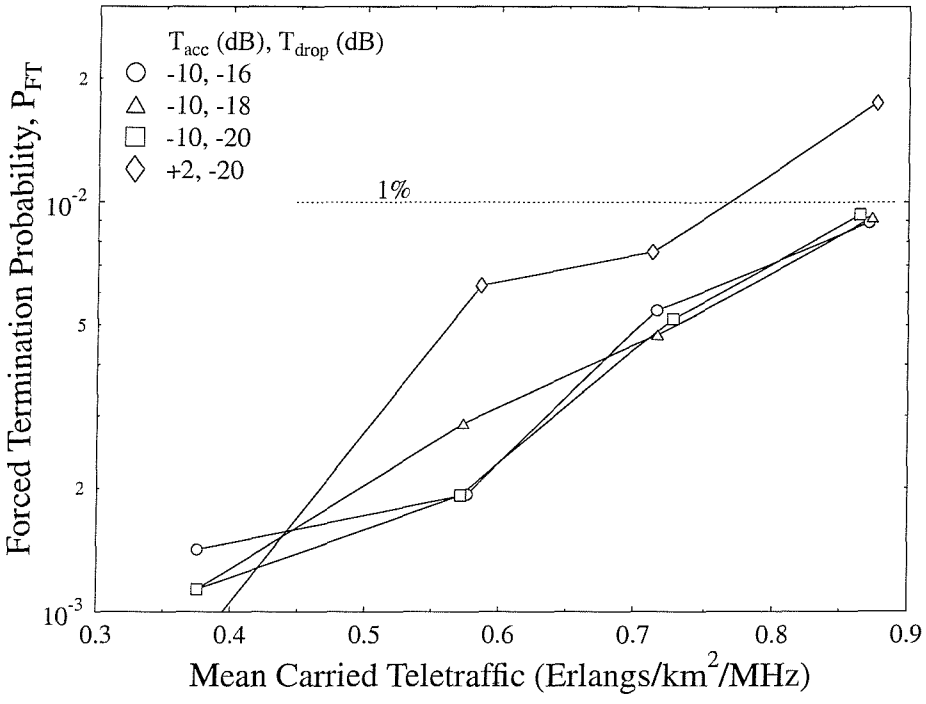

Figure 4.35: Call dropping probability versus mean carried traffic of a CDMA based cellular network using **relative received** E_c/I_o based soft handover thresholds in conjunction **with 0.5 Hz shadowing and a standard deviation of 3 dB** for SF=16.

This was achieved whilst invoking the lowest average number of base stations and the minimum mean base station transmit power. A further advantage of this handover scheme is that the same soft handover thresholds excelled in all of the propagation environments studied, unlike the previously considered algorithms, which obtained their best results at different thresholds for different conditions. The entire network capacity was 256 users without shadow fading, with a mean ABS size of 1.68. At a maximum shadowing frequency of 0.5 Hz the network supported just over a total of 150 users, whilst 144 users were served by the entire network, when a maximum shadow fading frequency of 1.0 Hz was encountered.

4.4.4 Overview of Results

Table 4.3 summarises the results obtained for the various soft handover algorithms over the three different propagation environments considered. The fixed receiver pilot power based algorithm performed the least impressively overall, as expected due to its inherent inability to cope with shadow fading. However, it did offer a high network capacity in a

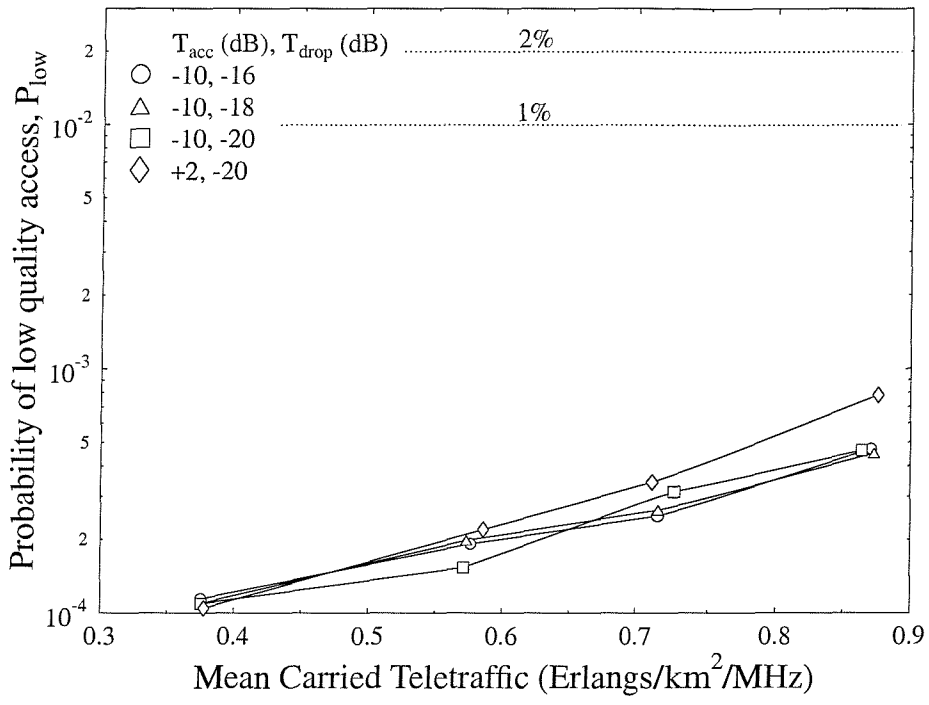

Figure 4.36: Probability of low quality access versus mean carried traffic of a CDMA based cellular network using **relative received** E_c/I_o based soft handover thresholds in conjunction **with 0.5 Hz shadowing and a standard deviation of 3 dB** for SF=16.

non-shadowed environment. Using the relative received pilot power based soft handover algorithm improved the performance under shadow fading, but different fading rates required different thresholds to meet the conservative and lenient quality criteria. The performance of the fixed E_c/I_o based soft handover algorithm also varied significantly, when using the same thresholds for the two different fading rates considered. However, the maximum network capacity achieved under the different shadow fading conditions was significantly higher, than that of the fixed received pilot power based algorithm. This benefit resulted from the inclusion of the interference levels in the handover process, which thus took into account the fading of both the signal and the co-channel interference. Combining the relative threshold based scheme with using E_c/I_o thresholds allowed us to support the highest number of users under the shadow fading conditions investigated. Whilst its performance was not the highest in the non-shadowed environment, this propagation environment is often unrealistic, and hence the relative received E_c/I_o based soft handover algorithm was chosen as the basis for our future investigations, while using the soft handover thresholds of T_{acc}=-10 dB and T_{drop}=-18 dB. The advantages of this handover algorithm were its reduced

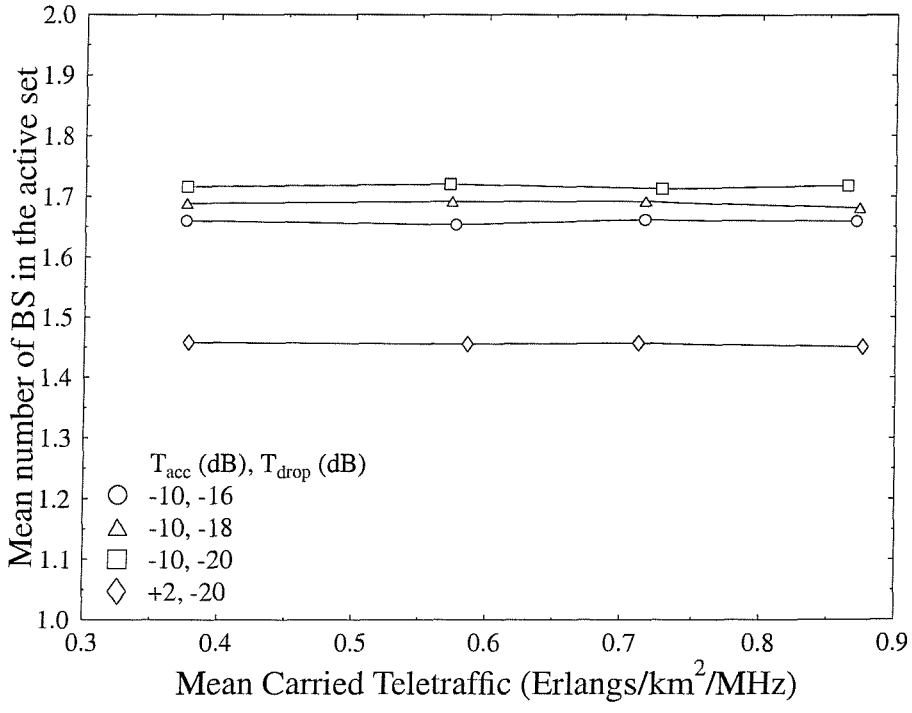

Figure 4.37: Mean number of base stations in the active base station set versus mean carried traffic of a CDMA based cellular network using **relative received** E_c/I_o based soft handover thresholds in conjunction **with 0.5 Hz shadowing and a standard deviation of 3 dB** for SF=16.

fraction of time spent in soft handover, and its ability to perform well under both shadow fading conditions evaluated, whilst utilising the same soft handover thresholds. Since the constraining factor of these network capacity results was the probability of a dropped call, P_{FT}, which was the same for both scenarios, further network capacity results were only shown for the conservative scenario.

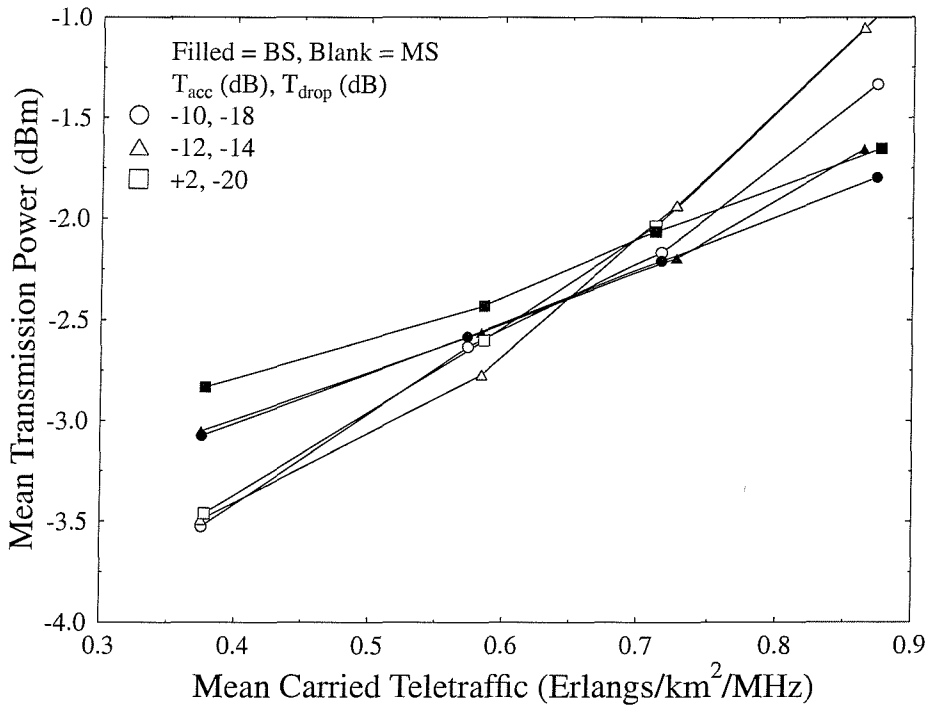

Figure 4.38: Mean transmission power versus mean carried traffic of a CDMA based cellular network using **relative received** E_c/I_o based soft handover thresholds in conjunction **with 0.5 Hz shadowing and a standard deviation of 3 dB** for SF=16.

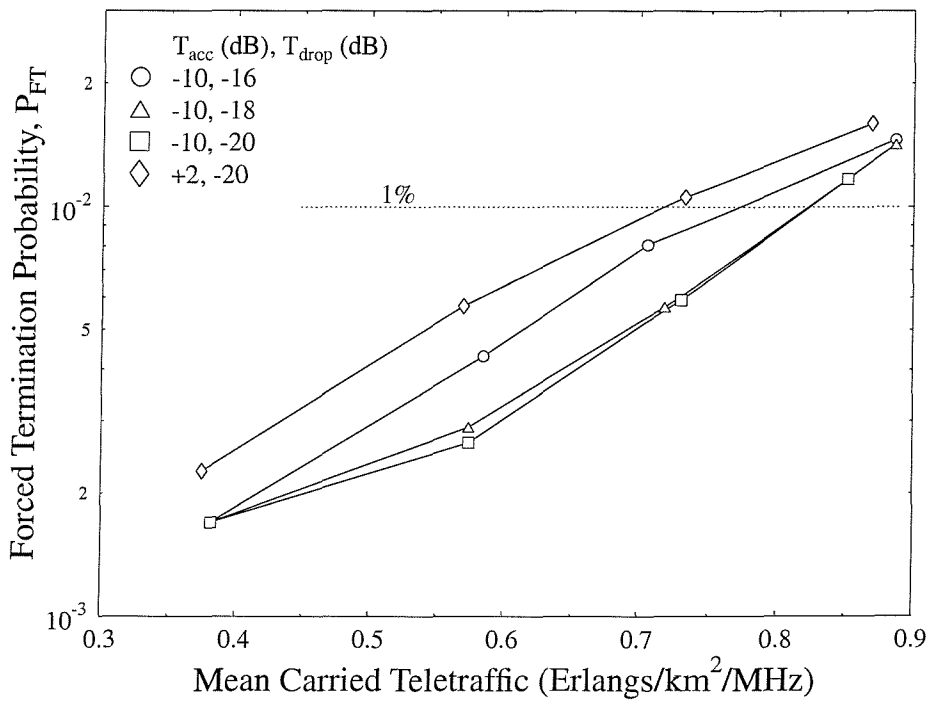

Figure 4.39: Call dropping probability versus mean carried traffic of a CDMA based cellular network using **relative received** E_c/I_o based soft handover thresholds in conjunction **with 1.0 Hz shadowing and a standard deviation of 3 dB** for SF=16.

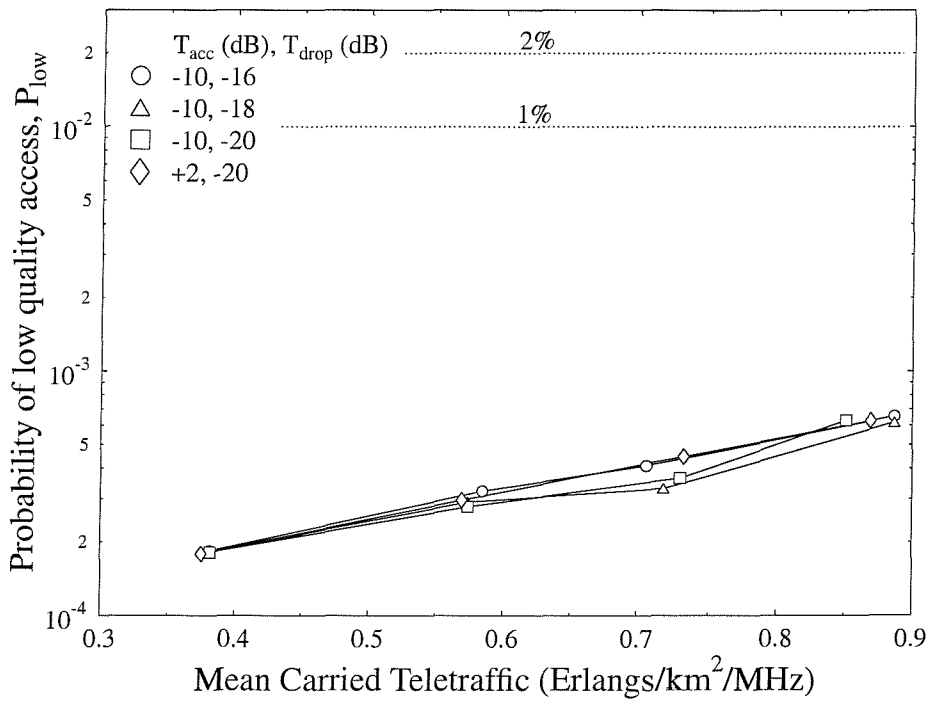

Figure 4.40: Probability of low quality access versus mean carried traffic of a CDMA based cellular network using **relative received** E_c/I_o based soft handover thresholds in conjunction **with 1.0 Hz shadowing and a standard deviation of 3 dB** for SF=16.

Soft handover algorithm	Shadowing	Conservative scenario P_{FT}=1%, P_{low}=1%				Lenient scenario P_{FT}=1%, P_{low}=2%			
				Power (dBm)				Power (dBm)	
		Users	ABS	MS	BS	Users	ABS	MS	BS
Fixed pilot pwr.	No	290	1.7	5.1	5.1	290	1.7	5.1	5.1
Fixed pilot pwr.	0.5 Hz, 3dB	-	-	-	-	127	1.83	-2.0	6.5
Fixed pilot pwr.	1.0 Hz, 3dB	-	-	-	-	-	-	-	-
Delta pilot pwr.	No	288	1.7	4.1	4.7	288	1.7	4.1	4.1
Delta pilot pwr.	0.5 Hz, 3dB	144	1.77	-1.5	0.6	146	1.78	-1.5	1.3
Delta pilot pwr.	1.0 Hz, 3dB	127	1.5	-2.4	-1.9	144	1.72	-1.5	0.8
Fixed E_c/I_o	No	223	1.83	2.0	10.0	231	1.86	2.0	10.3
Fixed E_c/I_o	0.5 Hz, 3dB	129	1.88	-2.4	7.0	140	1.91	-2.4	8.7
Fixed E_c/I_o	1.0 Hz, 3dB	107	1.86	-3.0	4.5	128	1.91	-3.0	9.5
Delta E_c/I_o	No	256	1.68	3.1	2.7	256	1.68	3.1	2.7
Delta E_c/I_o	0.5 Hz, 3dB	$\approx$150	1.65	-1.2	-1.7	$\approx$150	1.65	-1.2	-1.7
Delta E_c/I_o	1.0 Hz, 3dB	144	1.65	-1.1	-1.6	144	1.65	-1.1	-1.6

Table 4.3: Maximum number of mobile users that can be supported by the network, for different soft handover metrics/algorithms whilst meeting the preset quality constraints. The mean number of base stations in the Active Base station Set (ABS) is also presented, along with the mean mobile and mean base station transmit powers.

4.4.5 Performance of Adaptive Antenna Arrays in a High Data Rate Pedestrian Environment

In our previous investigations we endeavoured to identify the soft handover algorithm, which supports the greatest number of users, at the best call quality, regardless of the propagation conditions. In the section we study the impact of adaptive antenna arrays on the network's performance. The investigations were conducted using the relative E_c/I_o based soft handover algorithm in conjunction with T_{acc}=-10 dB and T_{drop}=-18 dB, using a spreading factor of 16. Given that the chip rate of UTRA is 3.84 Mchips/sec, this spreading factor corresponds to a channel data rate of $3.84\times10^6/16$=240 kbps. Applying 1/2 rate error correction coding would result in an effective data throughput of 120 kbps, whereas utilising a 2/3 rate error correction code would provide a useful throughput of 160 kps. As in the previous simulations a cell radius of 150 m was assumed and a pedestrian walking velocity of 3 mph was used. In our previous investigations employing adaptive antenna arrays at the base station and using a FDMA/TDMA based network, as in Chapter 3, we observed quite significant performance gains as a direct result of the interference rejection capabilities of the adaptive antenna arrays invoked. Since the CDMA based network considered here has a frequency reuse of 1, the levels of co-channel interference are significantly higher, and hence the adaptive antennas may be able to null the interference more effectively. However, the greater number of interference sources may limit the achievable interference rejection.

Network performance results were obtained using two and four element adaptive antenna arrays, both in the absence of shadow fading, and in the presence of 0.5 Hz and 1.0 Hz frequency shadow fading exhibiting a standard deviation of 3 dB. The adaptive beamforming algorithm used was the Sample Matrix Inversion (SMI) algorithm, as described in Chapter 2 and used in the FDMA/TDMA network simulations of Chapter 3. The specific adaptive beamforming implementation used in the CDMA based network was identical to that used in the FDMA/TDMA network simulations. Briefly, one of the eight possible 8-bit BPSK reference signals was used to identify the desired user, and the remaining interfering users were assigned the other seven 8-bit reference signals. The received signal's autocorrelation matrix was then calculated, and from the knowledge of the desired user's reference signal, the receiver's optimal antenna array weights were determined with the aid of the SMI algorithm. The reader is referred to Section 3.7.1 for further details. Since this implementation of the algorithm only calculated the receiver's antenna array weights, i.e. the antenna arrays weights used by the base station in the uplink, these weights may not be suitable for use in the downlink, when independent up/downlink shadow fading is experienced. Hence, further investigations were conducted, where the uplink and downlink interference scenarios were identical, in order to determine the potential performance gain that may be achieved by

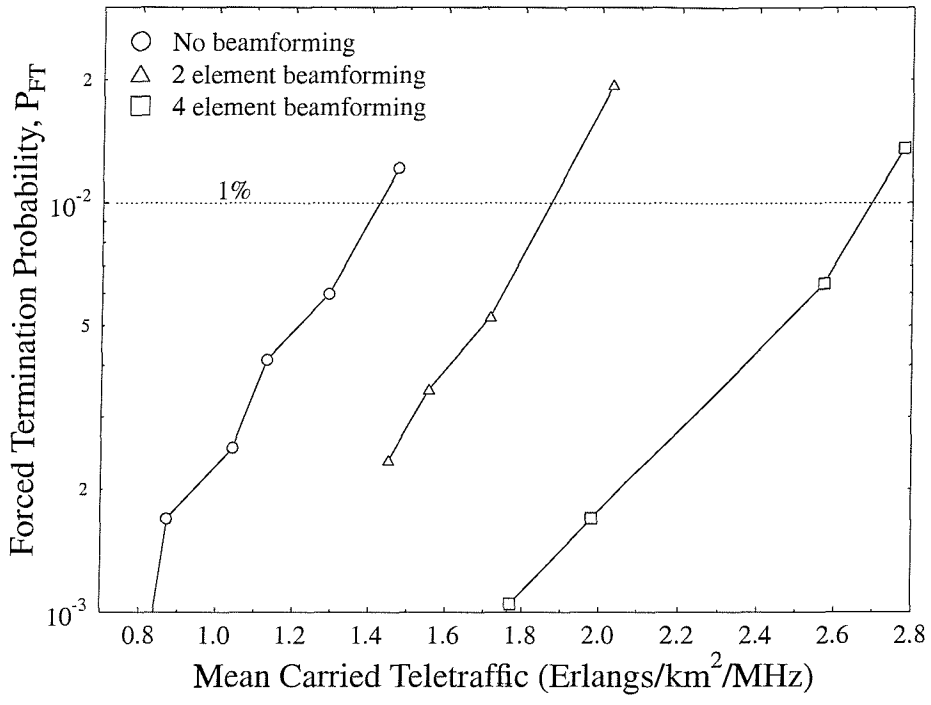

Figure 4.41: Call dropping probability versus mean carried traffic of a CDMA based cellular network using **relative received** E_c/I_o based soft handover thresholds **with and without beamforming and without shadowing** for SF=16.

separately calculating the antenna array weights to be used in the downlink. The antenna array weights were re-calculated for every power control step, i.e. 15 times per UTRA data frame, due to the potential significant changes in terms of the desired signal and interference powers that may occur during one UTRA frame as a result of the possible 15 dB change in power transmitted by each user.

Figure 4.41 shows the significant reduction in the probability of a dropped call, or probability of a forced termination, P_{FT}, achieved by employing adaptive antenna arrays in a non-shadowed propagation environment. The figure has demonstrated that, even with only two antenna elements, the adaptive antenna arrays have considerably reduced the levels of co-channel interference, leading to a reduced call dropping probability. This has been achieved in spite of the numerous sources of co-channel interference resulting from the frequency reuse factor of one, which was remarkable in the light of the limited number of degrees of freedom of the two element array. Without employing antenna arrays at the base stations the network capacity was limited to 256 users, or to a teletraffic load of approximately 1.4 Erlangs/km^2/MHz. However, with the advent of two element adaptive antenna

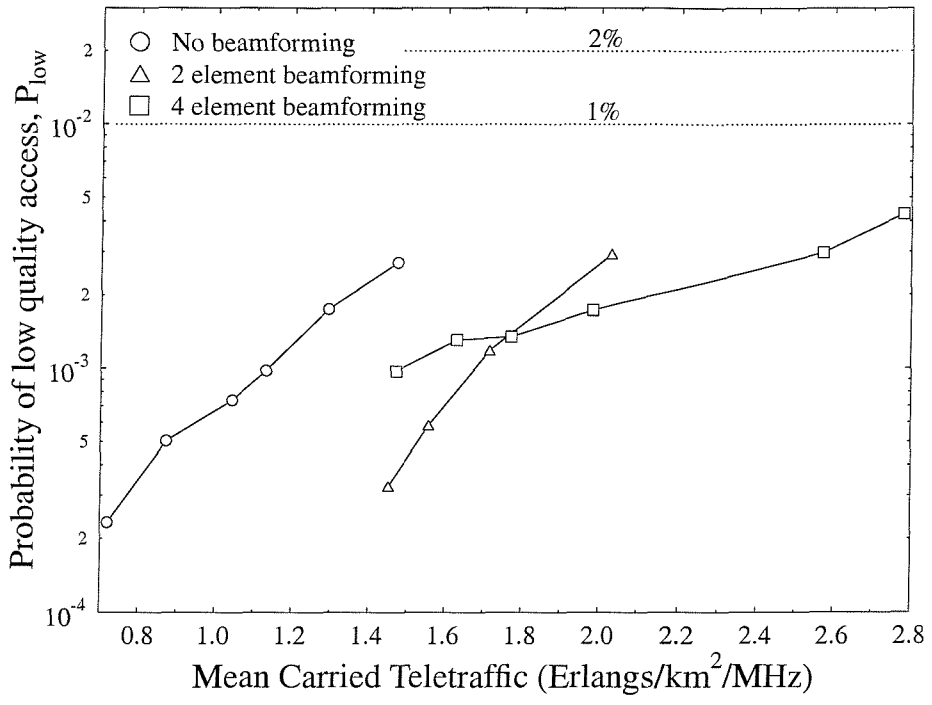

Figure 4.42: Probability of low quality access versus mean carried traffic of a CDMA based cellular network using **relative received** E_c/I_o based soft handover thresholds **with and without beamforming and without shadowing** for SF=16.

arrays at the base stations the number of users supported by the network rose by 27% to 325 users, or almost 1.9 Erlangs/km^2/MHz. Replacing the two element adaptive antenna arrays with four element arrays led to a further rise of 48%, or 88% with respect to the capacity of the network using no antenna arrays. This is associated with a network capacity of 480 users, or 2.75 Erlangs/km^2/MHz. A summary of the network capacities achieved under different conditions is given in Table 4.4.

The probability of low quality outage, presented in Figure 4.42 also exhibited a substantial improvement with the advent of two element adaptive antenna arrays. However, the performance gains obtained when invoking four element adaptive antenna arrays were more involved. It can be seen from the figure that higher traffic loads were carried with a sufficiently low probability of a low quality occurring, and at higher traffic loads the probability of a low quality access was lower than that achieved using a two element array. However, at lower traffic loads the performance was worse than that obtained when using two element arrays, and the gradient of the performance curve was significantly lower. Further in-depth

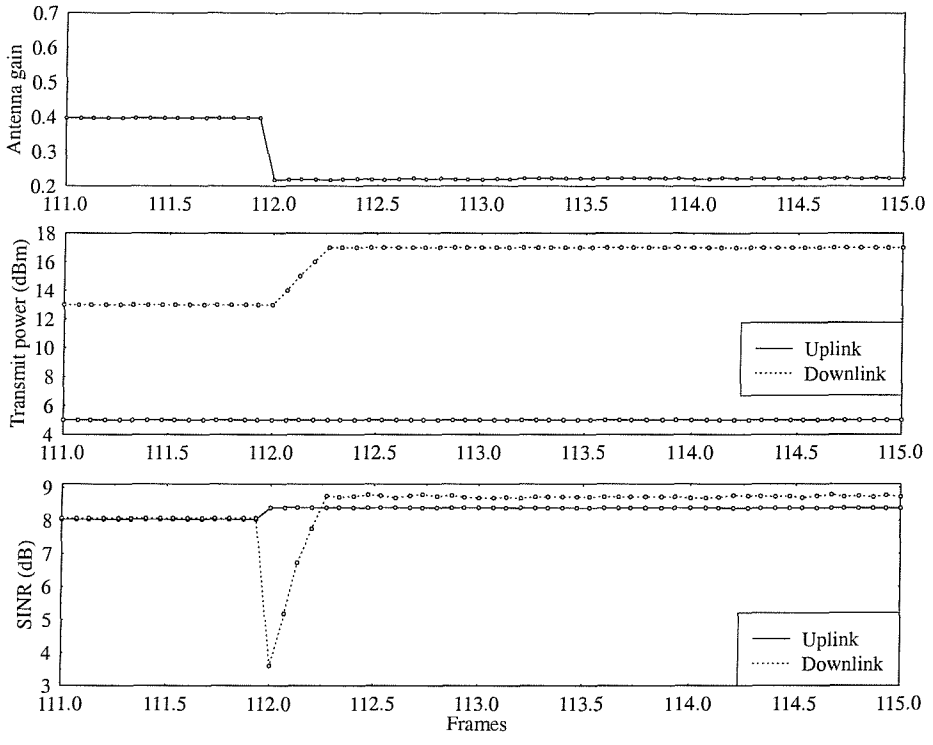

Figure 4.43: The changes in the antenna array gain, versus time, in the direction of the desired user, the up- and down-link transmission powers, and the up- and down-link received SINRs, when a new call starts using four element adaptive antenna arrays without shadowing in conjunction with the **original power ramping** algorithm and SF=16.

analysis of the results suggested that the vast majority of the low quality outages were occurring when new calls started. When a user decided to commence communications with the base station, the current interference level was measured, and the target transmission power was determined in order to reach the target SINR necessary for reliable communications. However, in order to avoid disrupting existing calls the transmission power was ramped up slowly, until the target SINR was reached. A network using no adaptive antenna arrays, i.e. employing omnidirectional antennas, can be viewed as offering equal gain to all users of the network, which we assumed to be 1.0, or 0 dB. Thus, when a new call is initiated, the level of interference rises gradually, and the power control algorithm ensures that the existing users compensate for the increased level of co-channel interference by increasing their transmission power. In a network using adaptive antenna arrays, the adaptive antenna arrays are used to null the sources of interference, and in doing so the array may reduce the antenna gain in the direction of the desired user, in order to maximise the SINR. Hence a user starting a new call, even if it has low transmission power, can alter the antenna array's response, and thus the antenna gain experienced by the existing users. This phenomenon

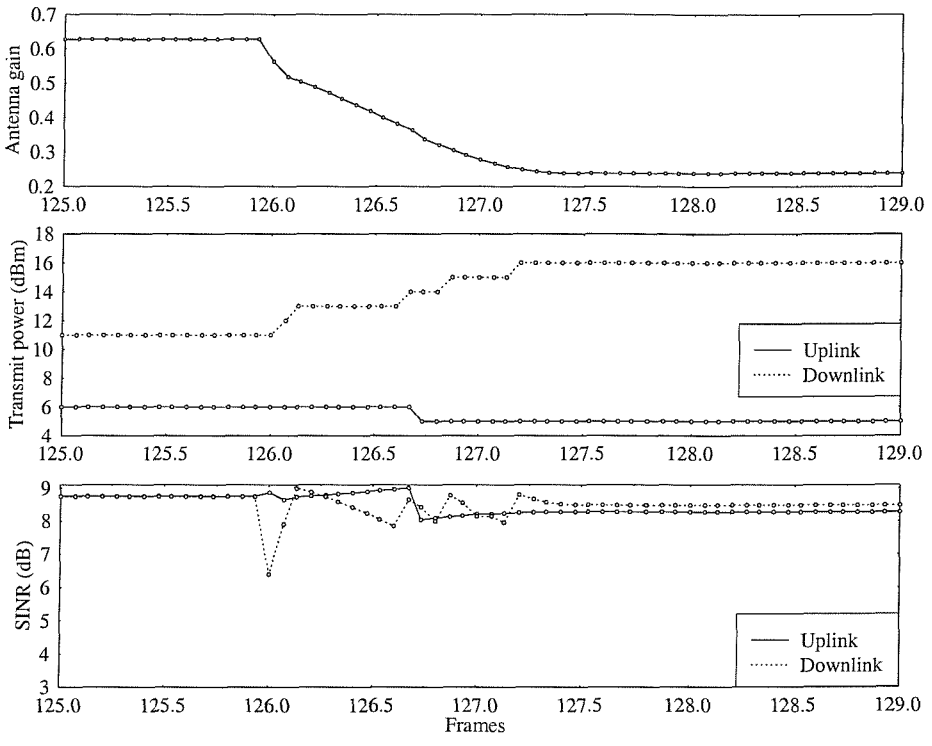

Figure 4.44: The changes in the antenna array gain, versus time, in the direction of the desired user, the up- and down-link transmission powers, and the up- and down-link received SINRs, when a new call starts using four element adaptive antenna arrays without shadowing in conjunction with a **slower power ramping** algorithm and SF=16.

is more marked, when using four element arrays since their directivity, and thus sensitivity to interfering signals, is greater.

Figure 4.43 illustrates this phenomenon, where another user starts a new call at frame 112 suddenly reducing the antenna gain in the direction of the desired user from 0.4 to just above 0.2, a drop of 3 dB. As can be seen from the figure, the downlink SINR falls sharply below the low quality outage threshold of 7.0 dB, resulting in several consecutive outages, until the downlink transmission power is increased sufficiently. The impact of reducing the initial transmission power, in order to ensure that the power ramping takes place more gently, is depicted in Figure 4.44. In this figure it can be seen that the antenna gain falls much more gently, over a prolonged period of time, thus reducing the number of low quality outages, as the downlink transmission power is increased in an effort to compensate for the lower antenna gain. It is of interest to note how the received SINR varies as the antenna gain and the power control algorithm interact, in order to maintain the target SINR.

Even though the employment of adaptive antenna arrays can result in the attenuation of

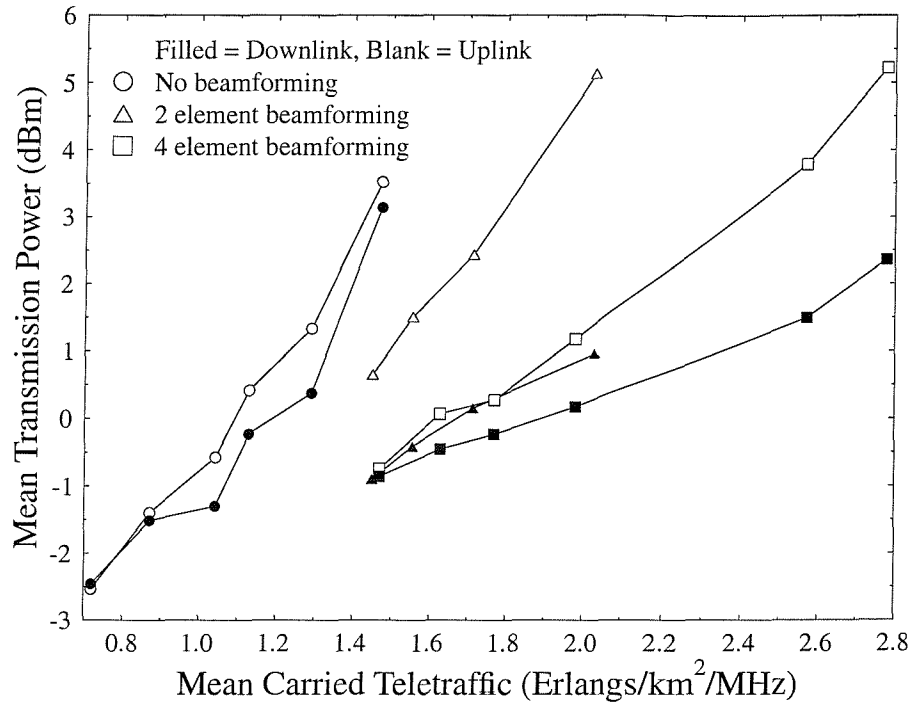

Figure 4.45: Mean transmission power versus mean carried traffic of a CDMA based cellular network using **relative received** E_c/I_o based soft handover thresholds **with and without beamforming and without shadowing** for SF=16.

the desired signal, this is performed in order to maximise the received SINR, and thus the levels of interference are attenuated more strongly, ultimately leading to the reduction of the mean transmission power, as emphasised by Figure 4.45. This figure clearly shows the lower levels of transmission power, required in order to maintain an acceptable performance, whilst using adaptive antenna arrays at the base stations. A reduction of 3 dB in the mean mobile transmission power was achieved by invoking two element antenna arrays, and a further reduction of 1.5 dB resulted from using four element arrays. These power budget savings were obtained in conjunction with reduced levels of co-channel interference, leading to superior call quality, as illustrated in Figures 4.41 and 4.42. A greater performance advantage was evident in the uplink scenario, suggesting that the selective base station diversity techniques employed in the uplink are amenable to amalgamation with adaptive antenna arrays. In contrast, the maximum ratio combining performed at the mobile inherently reduces the impact of co-channel interference, and hence benefits to a lesser extent from the employment of adaptive antenna arrays.

The impact of adaptive antenna arrays in a propagation environment subjected to shadow

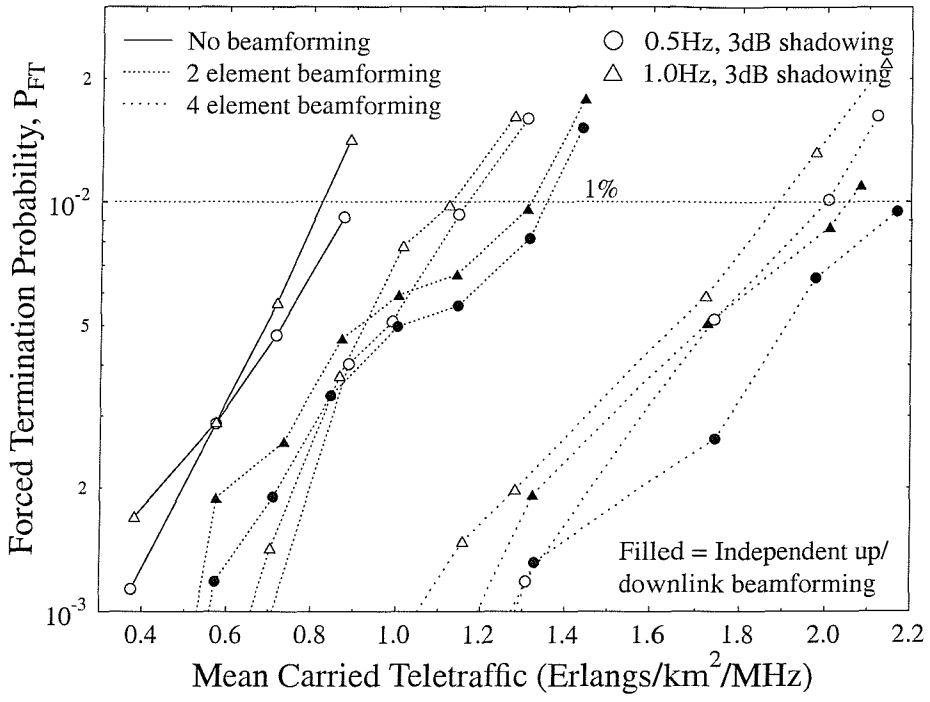

Figure 4.46: Call dropping probability versus mean carried traffic of a CDMA based cellular network using **relative received** E_c/I_o based soft handover thresholds **with and without beamforming and with shadowing having a standard deviation of 3 dB** for SF=16.

fading was then investigated. The associated call dropping performance is shown in Figure 4.46. This figure illustrates the substantial network capacity gains achieved with the aid of both two and four element adaptive antenna arrays under shadow fading propagation conditions. Simulations were conducted in conjunction with log-normal shadow fading having a standard deviation of 3 dB, and maximum shadowing frequencies of both 0.5 Hz and 1.0 Hz. As expected the network capacity was reduced at the faster fading frequency. The effect of performing independent up- and down-link beamforming, as opposed to using the base station's receive antenna array weights in the downlink was also studied, and a small, but not insignificant call dropping probability reduction can be seen in the Figure 4.46. The network supported just over 150 users, and 144 users, when subjected to 0.5 Hz and 1.0 Hz frequency shadow fading, respectively. With the application of two element adaptive antenna arrays, re-using the base station's uplink receiver weights on the downlink, these capacities increased by 35% and 40%, to 203 users and 201 users. Performing independent up- and down-link beamforming resulted in a mean further increase of 13% in the network capacity. The implementation of four element adaptive antenna arrays led to a network

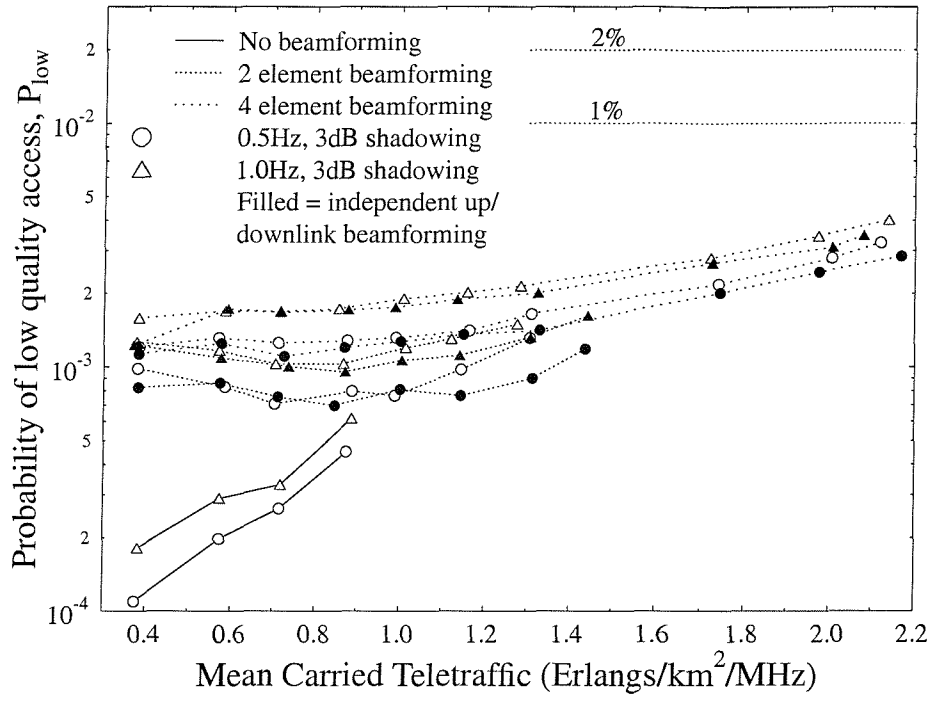

Figure 4.47: Probability of low quality access versus mean carried traffic of a CDMA based cellular network using **relative received** E_c/I_o based soft handover thresholds **with and without beamforming and with shadowing having a standard deviation of 3 dB** for SF=16.

capacity of 349 users at a 0.5 Hz shadowing frequency, and 333 users at a 1.0 Hz shadowing frequency. This corresponded to relative gains of 133% and 131% over the capacity provided without beamforming. Invoking independent up- and down-link beamforming gave another boost of 7% and 10% to network capacity for 0.5 Hz and 1.0 Hz frequency shadowing environments, respectively, giving final network capacities of just over 375 users and 365 users.

Similar trends were observed regarding the probability of low quality outage to those found in the non-shadowing scenarios. However, the trend was much more prevalent under shadowing, due to greater variation of the received signal strengths, as a result of the shadow fading, as shown in Figure 4.47. The figure indicates that the trend is also evident, when using two element adaptive antenna arrays in conjunction with shadow fading. As expected, the performance deteriorated as the number of antenna elements increased, and when the maximum shadow fading frequency was increased from 0.5 Hz to 1.0 Hz. It should be noted, however that the probability of low quality access always remained below the 1% constraint

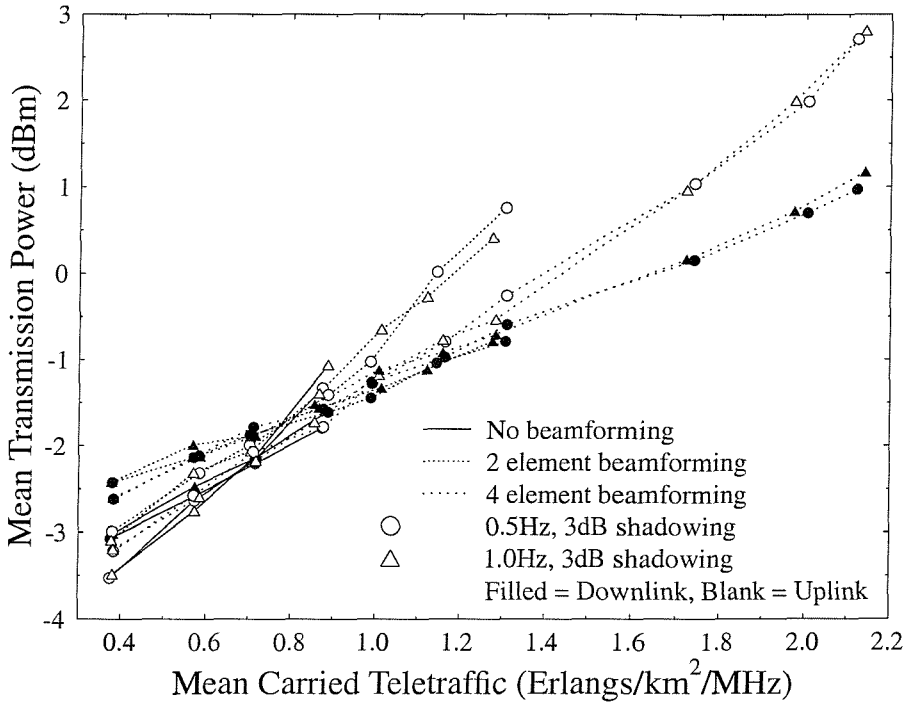

Figure 4.48: Mean transmission power versus mean carried traffic of a CDMA based cellular network using **relative received** E_c/I_o based soft handover thresholds **with and without beamforming and shadowing having a standard deviation of 3 dB** for SF=16.

of the conservative scenario, and the call dropping probability was considerably reduced by the adaptive antenna arrays.

The mean transmission power performance is depicted in Figure 4.48, suggesting that as for the non-shadowing scenario of Figure 4.45, the number of antenna elements had only a limited impact on the base stations' transmission power, although there was some reduction in the mobile stations' mean transmission power. The mean transmission powers required when using independent up- and down-link beamforming are not explicitly shown, but were slightly less than those presented here, with a mean reduction of about 0.4 dB.

A summary of the maximum network capacities of the networks considered in this section both with and without shadowing, employing beamforming using two and four element arrays is given in Table 4.4, along with the teletraffic carried and the mean mobile and base station transmission powers required.

The lower bounds of the maximum network capacities obtained under identical scenarios in conjunction with a spreading factor of 256, are also presented in Table 4.5, leading to a bit rate of 15 kbps, which is suitable for use by speech-rate users. The network capacity

calculations were performed by scaling the number of users supported, as presented in Table 4.4, by the ratio of their spreading factors, i.e. 256/16=16. Further interesting user capacity figures can be inferred for a variety of target bit rates by comparing Tables 4.4, 4.5, 4.7 and 4.8 and applying the appropriate spreading factor related scaling mentioned in the context of estimating the number of 15 kbps speech users supported.

Shadowing	Beamforming:	independent up/down-link	Conservative scenario, P_{FT}=1%, P_{low}=1% Users	Traffic (Erlangs /km^2/MHz)	Power (dBm) MS	BS
No	No	-	256	1.42	3.1	2.7
No	2 elements	-	325	1.87	3.75	0.55
No	4 elements	-	480	2.75	4.55	1.85
0.5 Hz, 3 dB	No	-	≈150	0.87	-1.2	-1.7
0.5 Hz, 3 dB	2 elements	No	203	1.16	0.1	-1.1
0.5 Hz, 3 dB	4 elements	No	349	2.0	2.0	0.65
0.5 Hz, 3 dB	2 elements	Yes	233	1.35	0.2	-0.8
0.5 Hz, 3 dB	4 elements	Yes	≈375	2.2	2.15	0.85
1.0 Hz, 3 dB	No	-	144	0.82	-1.1	-1.6
1.0 Hz, 3 dB	2 elements	No	201	1.12	-0.3	-1.1
1.0 Hz, 3 dB	4 elements	No	333	1.88	1.6	0.5
1.0 Hz, 3 dB	2 elements	Yes	225	1.31	0.1	-0.9
1.0 Hz, 3 dB	4 elements	Yes	365	2.05	1.65	0.6

Table 4.4: Maximum mean carried traffic and maximum number of mobile users that can be supported by the network, whilst meeting the conservative quality constraints. The carried traffic is expressed in terms of normalised Erlangs (Erlang/km^2/MHz) for the network described in Table 4.2 both **with and without beamforming (as well as with and without independent up/down-link beamforming), and also with and without shadow fading having a standard deviation of 3 dB** for SF=16.

Shadowing	Beamforming:	independent up/down-link	Users when SF=256	Traffic (Erlangs /km^2/MHz)
No	No	-	4096	22.7
No	2 elements	-	5200	29.9
No	4 elements	-	7680	44.0
0.5 Hz, 3 dB	No	-	2400	13.9
0.5 Hz, 3 dB	2 elements	No	3248	18.6
0.5 Hz, 3 dB	4 elements	No	5584	32.0
0.5 Hz, 3 dB	2 elements	Yes	3728	21.6
0.5 Hz, 3 dB	4 elements	Yes	6000	35.2
1.0 Hz, 3 dB	No	-	2304	13.1
1.0 Hz, 3 dB	2 elements	No	3216	17.9
1.0 Hz, 3 dB	4 elements	No	5328	30.1
1.0 Hz, 3 dB	2 elements	Yes	3600	21.0
1.0 Hz, 3 dB	4 elements	Yes	5840	32.8

Table 4.5: A lower bound estimate of the maximum mean traffic and the maximum number of mobile **speech-rate** users that can be supported by the network, whilst meeting the **conservative quality constraints**. The carried traffic is expressed in terms of normalised Erlangs (Erlang/km^2/MHz) for the network described in Table 4.2 both **with and without beamforming (as well as with and without independent up/down-link beamforming), and also with and without shadow fading having a standard deviation of 3 dB** for SF=256. The number of users supported in conjunction with a spreading factor of 256 was calculated by multiplying the capacities obtained in Table 4.4 by 256/16=16.

4.4.6 Performance of Adaptive Antenna Arrays and Adaptive Modulation in a High Data Rate Pedestrian Environment

In this section we build upon the results presented in the previous section by applying Adaptive Quadrature Amplitude Modulation (AQAM) techniques. The various scenarios and channel conditions investigated were identical to those of the previous section, except for the application of AQAM. Since in the previous section an increased network capacity was achieved due to using independent up- and down-link beamforming, this procedure was invoked in these simulations. AQAM involves the selection of the appropriate modulation mode in order to maximise the achievable data throughput over a channel, whilst minimising the Bit Error Ratio (BER). More explicitly, the philosophy behind adaptive modulation is the most appropriate selection of a modulation mode according to the instantaneous radio channel quality experienced [12, 13]. Therefore, if the SINR of the channel is high, then a high-order modulation mode may be employed, thus exploiting the temporal fluctuation of the radio channel's quality. Similarly, if the channel is of low quality, exhibiting a low SINR, a high-order modulation mode would result in an unacceptably high BER or FER, and hence a more robust, but lower throughput modulation mode would be employed. Therefore, adaptive modulation combats the effects of time-variant channel quality, while also attempting to maximise the achieved data throughput, and maintaining a given BER or FER. In the investigations conducted, the modulation modes of the up and downlink were determined independently, thus taking advantage of the lower levels of co-channel interference on the uplink, or of the potentially greater transmit power of the base stations.

The particular implementation of AQAM used in these investigations is illustrated in Figure 4.49. This figure describes the algorithm in the context of the downlink, but the same implementation was used also in the uplink. The first step in the process was to establish the current modulation mode. If the user was invoking 16-QAM and the SINR was found to be below the Low Quality (LQ) outage SINR threshold after the completion of the power control iterations, then the modulation mode for the next data frame was 4-QAM. Alternatively, if the SINR was above the LQ outage SINR threshold, but any of the base stations in the ABS were using a transmit power within 15 dB (the maximum possible power change during a 15-slot UTRA data frame) of the maximum transmit power, then the 4-QAM modulation mode was selected. This "headroom" was introduced in order to provide a measure of protection, since if the interference conditions degrade, then at least 15 dB of increased transmit power would be available in order to mitigate the consequences of the SINR reduction experienced.

A similar procedure was invoked, when switching to other legitimate AQAM modes from

the 4-QAM mode. If the SINR was below the 4-QAM target SINR and any one of the base stations in the ABS was within 15 dB of the maximum transmit power, then the BPSK modulation mode was employed for the next data frame. However, if the SINR exceeded the 4-QAM target SINR and there would be 15 dB of headroom in the transmit power budget in excess of the extra transmit power required for switching from 4-QAM to 16-QAM, then the 16-QAM modulation mode was invoked.

And finally, when in the BPSK mode, the 4-QAM modulation mode was selected if the SINR exceeded the BPSK target SINR, and the transmit power of any of the base stations in the ABS was less than the power required to transmit reliably using 4-QAM, while being at least 15 dB below the maximum transmit power. The algorithm was activated at the end of each 15-slot UTRA data frame, after the power control algorithm had performed its 15 iterations per data frame, and thus the AQAM mode selection was performed on a UTRA transmission frame-by-frame basis. When changing from a lower-order modulation to a higher-order modulation mode, the lower-order mode was retained for an extra frame in order to ramp up the transmit power to the required level, as shown in Figure 4.50(a). Conversely, when changing from a higher-order modulation mode to a lower-order modulation mode, the lower-order modulation mode was employed whilst ramping the power down, in order to avoid excessive outages in the higher-order modulation mode due to the reduction of the transmit power, as illustrated in Figure 4.50(b).

Table 4.6 gives the BPSK, 4-QAM and 16-QAM SINR thresholds used in the simulations. The BPSK SINR thresholds were 4 dB lower than those necessary when using 4-QAM, while the 16-QAM SINR thresholds were 5.5 dB higher [115]. In other words, in moving from the BPSK modulation mode to the 4-QAM modulation mode, the target SINR, low quality outage SINR and outage SINR all increased by 4 dB. When switching to the 16-QAM mode from the 4-QAM mode, the SINR thresholds increased by 5.5 dB. However, setting the BPSK to 4-QAM and the 4-QAM to 16-QAM mode switching thresholds to a value 7 dB higher than the SINR required for maintaining the target BER/FER was necessary in order to prevent excessive outages due to sudden dramatic channel-induced variations in the SINR levels.

SINR Threshold	BPSK	4-QAM	16-QAM
Outage SINR	2.6 dB	6.6 dB	12.1 dB
Low Quality Outage SINR	3.0 dB	7.0 dB	12.5 dB
Target SINR	4.0 dB	8.0 dB	13.5 dB

Table 4.6: The target SINR, low quality outage SINR and outage SINR thresholds used for the BPSK, 4-QAM and 16-QAM modulation modes of the adaptive modem.

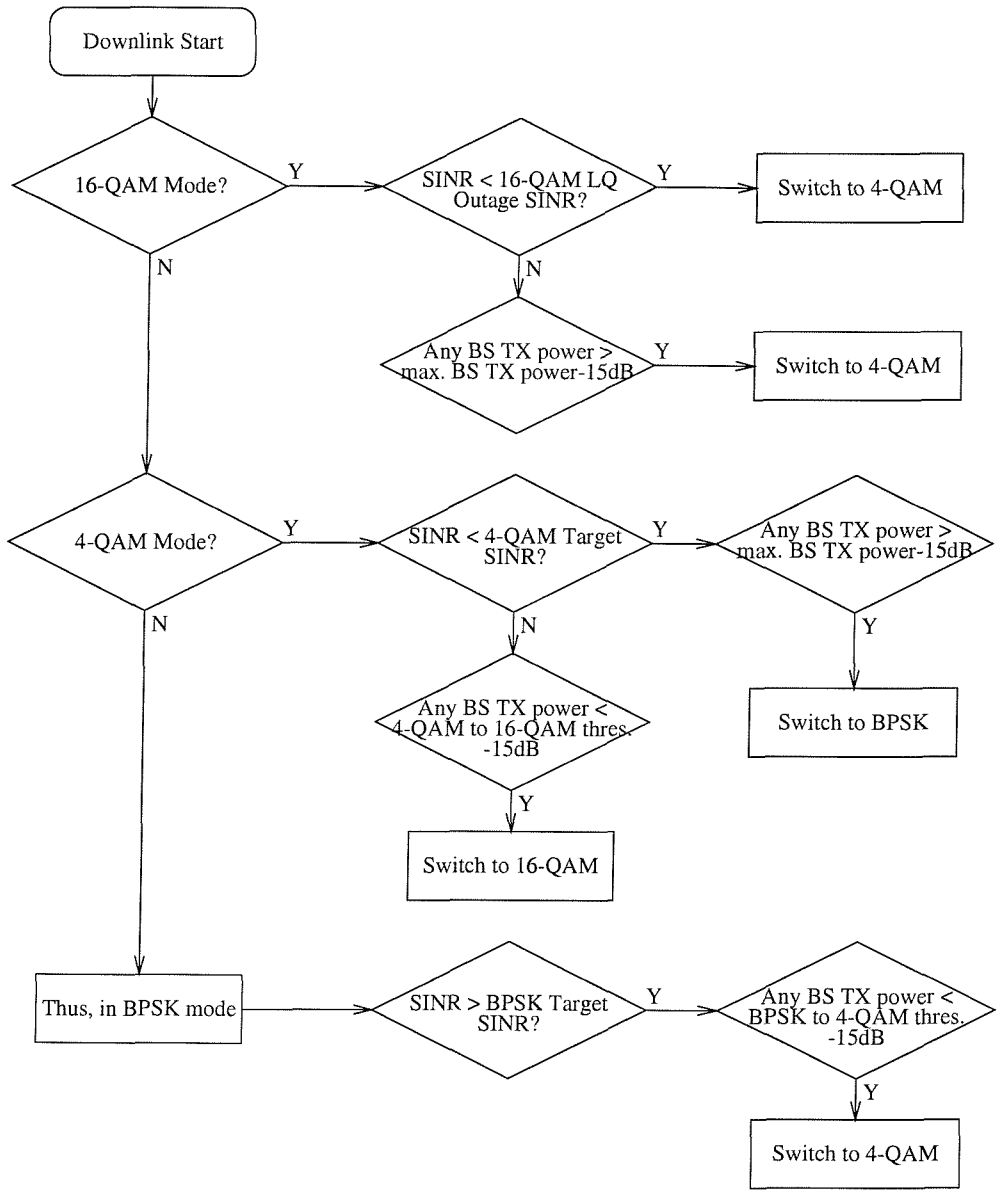

Figure 4.49: The AQAM mode switching algorithm used in the downlink of the CDMA based cellular network.

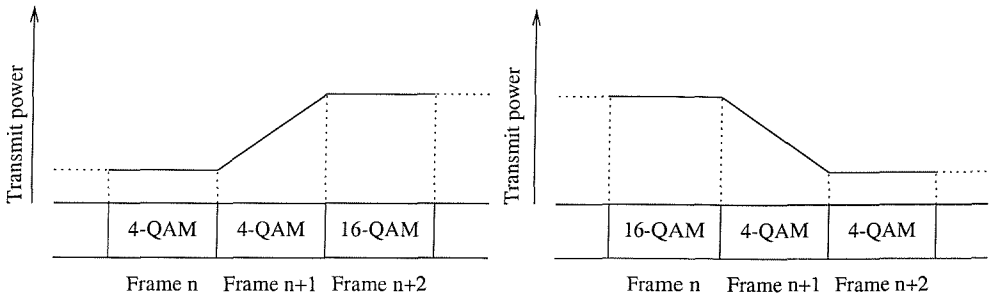

(a) Ramping up the transmit power whilst remaining in the lower order modulation mode.

(b) Ramping down the transmit power whilst switching to the lower order modulation mode.

Figure 4.50: Power rampimg requirements whilst switching modulation modes.

Performance results were obtained both with and without beamforming in a log-normal shadow fading environment, at maximum fading frequencies of 0.5 Hz and 1.0 Hz, and a standard deviation of 3 dB. A pedestrian velocity of 3 mph, a cell radius of 150 m and a spreading factor of 16 were used, as in our previous investigations.

Figure 4.51 shows the significant reduction in the probability of a dropped call, achieved by employing adaptive antenna arrays in conjunction with adaptive modulation in a log-normal shadow faded environment. The figure demonstrates that, even with the aid of a two element adaptive antenna array and its limited degrees of freedom, a substantial call dropping probability reduction was achieved. The performance benefit of increasing the array's degrees of freedom, achieved by increasing the number of antenna elements, becomes explicit from the figure, resulting in a further call dropping probability reduction. Simulations were conducted in conjunction with log-normal shadow fading having a standard deviation of 3 dB, and maximum shadowing frequencies of 0.5 Hz and 1.0 Hz. As expected, the call dropping probability was generally higher at the faster fading frequency, as demonstrated by Figure 4.51. The network was found to support 223 users, corresponding to a traffic load of 1.27 Erlang/km^2/MHz, when subjected to 0.5 Hz frequency shadow fading. The capacity of the network was reduced to 218 users, or 1.24 Erlang/km^2/MHz, upon increasing the maximum shadow fading frequency to 1.0 Hz. On employing two element adaptive antenna arrays, the network capacity increased by 64% to 366 users, or to an equivalent traffic load of 2.11 Erlang/km^2/MHz when subjected to 0.5 Hz frequency shadow fading. When the maximum shadow fading frequency was raised to 1.0 Hz, the number of users supported by the network was 341 users, or 1.98 Erlang/km^2/MHz, representing an increase of 56% in comparison to the network without adaptive antenna arrays. Increasing the number of antenna elements to four, whilst imposing shadow fading with a maximum frequency of

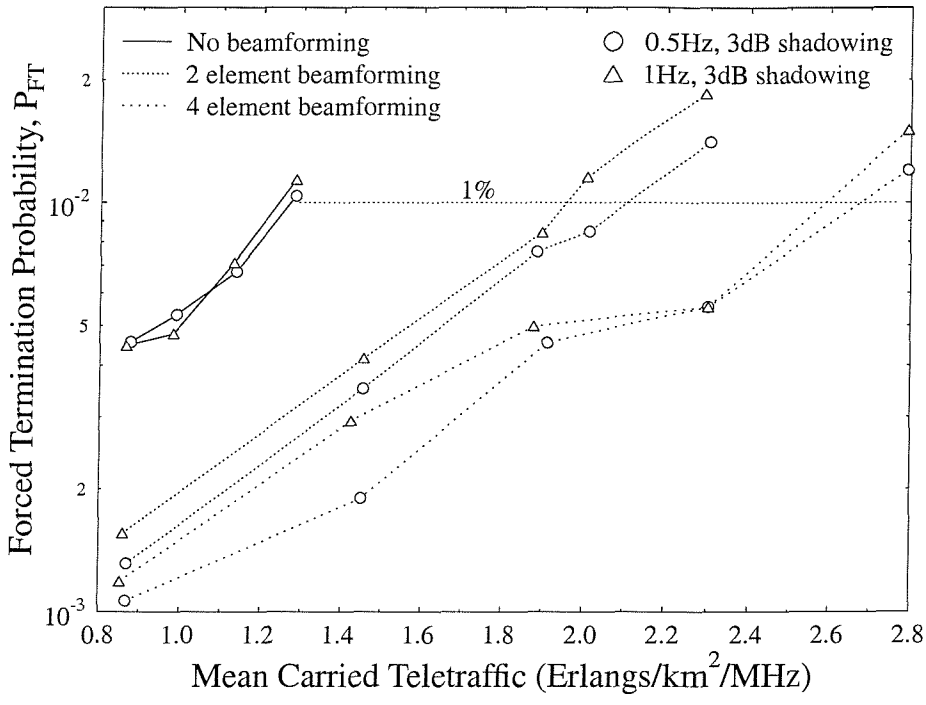

Figure 4.51: Call dropping probability versus mean carried traffic of a CDMA based cellular network using **relative received** E_c/I_o based soft handover thresholds both **with and without beamforming in conjunction with AQAM as well as with shadowing having a standard deviation of 3 dB** for SF=16. See Figure 4.46 for corresponding results without adaptive modulation.

0.5 Hz, resulted in a network capacity of 2.68 Erlang/km^2/MHz or 476 users, corresponding to a gain of an extra 30% with respect to the network employing two element arrays, and of 113% in comparison to the network employing no adaptive antenna arrays. In conjunction with a maximum shadow fading frequency of 1.0 Hz the network capacity was 460 users or 2.59 Erlang/km^2/MHz, which represented an increase of 35% with respect to the network invoking two element antenna arrays, or 111% relative to the identical network without adaptive antenna arrays.

The probability of low quality outage, presented in Figure 4.52, did not benefit from the application of adaptive antenna arrays, or from the employment of adaptive modulation. Figure 4.47 depicts the probability of low quality outage without adaptive modulation, and upon comparing these results to those obtained in conjunction with adaptive modulation shown in Figure 4.52, the performance degradation due to adaptive modulation can be explicitly seen. However, the increase in the probability of low quality access can be attributed to the employment of less robust, but higher throughput, higher-order modulation modes

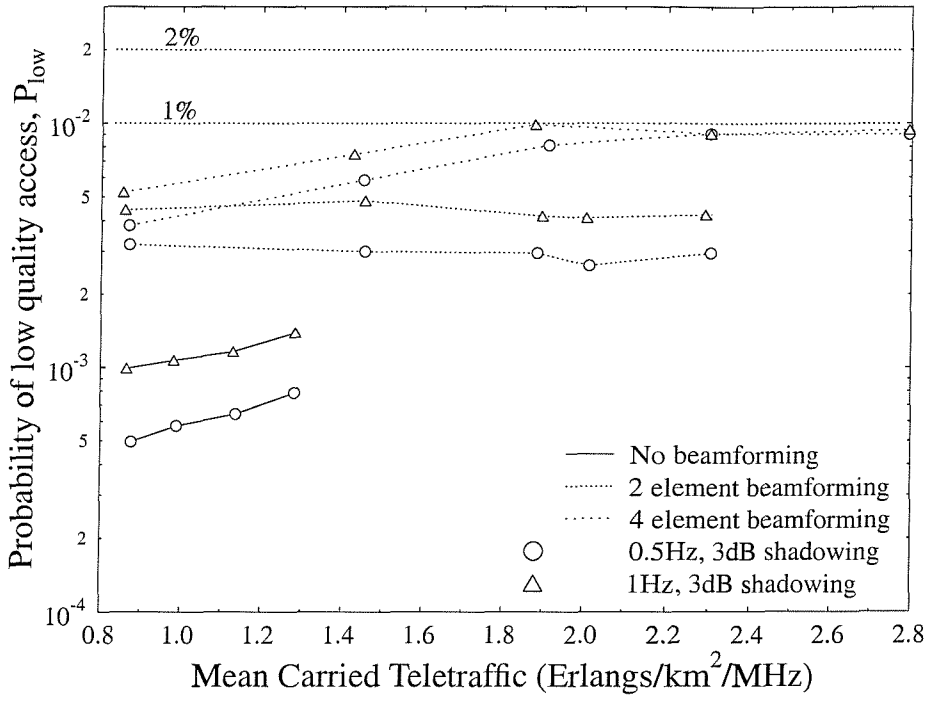

Figure 4.52: Probability of low quality access versus mean carried traffic of a CDMA based cellular network using **relative received** E_c/I_o based soft handover thresholds both **with and without beamforming in conjunction with AQAM as well as with shadowing having a standard deviation of 3 dB** for SF=16. See Figure 4.47 for corresponding results without adaptive modulation.

invoked by the adaptive modulation scheme. Hence, under given propagation conditions and using the fixed 4-QAM modulation mode a low quality outage may not occur, yet when using adaptive modulation and a higher order modulation mode, the same propagation conditions may inflict a low quality outage. This phenomenon is further exacerbated by the adaptive antenna arrays, as described in Section 4.4.5, where the addition of a new source of interference, constituted by a user initiating a new call, results in an abrupt change in the gain of the antenna in the direction of the desired user. This in turn leads to low quality outages, which are more likely to occur for prolonged periods of time, when using a higher order modulation mode. Again, increasing the number of antenna elements from two to four results in an increased probability of a low quality outage due to the sharper antenna directivity. This results in a higher sensitivity to changes in the interference incident upon it.

The mean transmission power versus teletraffic performance is depicted in Figure 4.53, suggesting that the mean uplink transmission power was always significantly below the

mean downlink transmission power, which can be attributed to the pilot power interference encountered by the mobiles in the downlink. This explanation can be confirmed by examining Figure 4.54, which demonstrates that the mean modem throughput in the downlink, without adaptive antenna arrays, was lower than that in the uplink even in conjunction with increased downlink transmission power. Invoking adaptive antenna arrays at the base stations reduced the mean uplink transmission power required in order to meet the service quality targets of the network. The attainable downlink power reduction increased as the number of antenna array elements increased, as a result of the superior interference rejection achieved with the aid of a higher number of array elements. A further advantage of employing a larger number of antenna array elements was the associated increase in the mean uplink modem throughput, which became more significant at higher traffic loads. In the downlink scenario, however, increasing the number of adaptive antenna array elements led to an increased mean downlink transmission power, albeit with a substantially improved mean downlink modem throughput. This suggests that there was some interaction between the adaptive antenna arrays, the adaptive modulation mode switching algorithm and the maximal ratio combining performed at the mobiles. In contrast, simple switched diversity was performed by the base stations on the uplink, thus avoiding such a situation. However, the increase in the mean downlink transmission power resulted in a much more substantial increase in the mean downlink modem throughput, especially with the advent of the four element antenna arrays, which exhibited an approximately 0.5 BPS throughput gain over the two element arrays for identical high traffic loads which can be seen in Figure 4.54.

A summary of the maximum user capacities of the networks considered in this section in conjunction with log-normal shadowing having a standard deviation of 3 dB, with and without employing beamforming using two and four element arrays is given in Table 4.7. The teletraffic carried, the mean mobile and base station transmission powers required, and the mean up- and down-link modem data throughputs achieved are also shown in Table 4.7. Similarly, the lower bounds of the maximum network capacities obtained under identical scenarios in conjunction with a spreading factor of 256, leading to a bit rate of 15 kbps, suitable for speech-rate users are presented in Table 4.8. The network capacity calculations were performed by scaling the number of users supported, as presented in Table 4.7, by the ratio of their spreading factors, i.e. by 256/16=16.

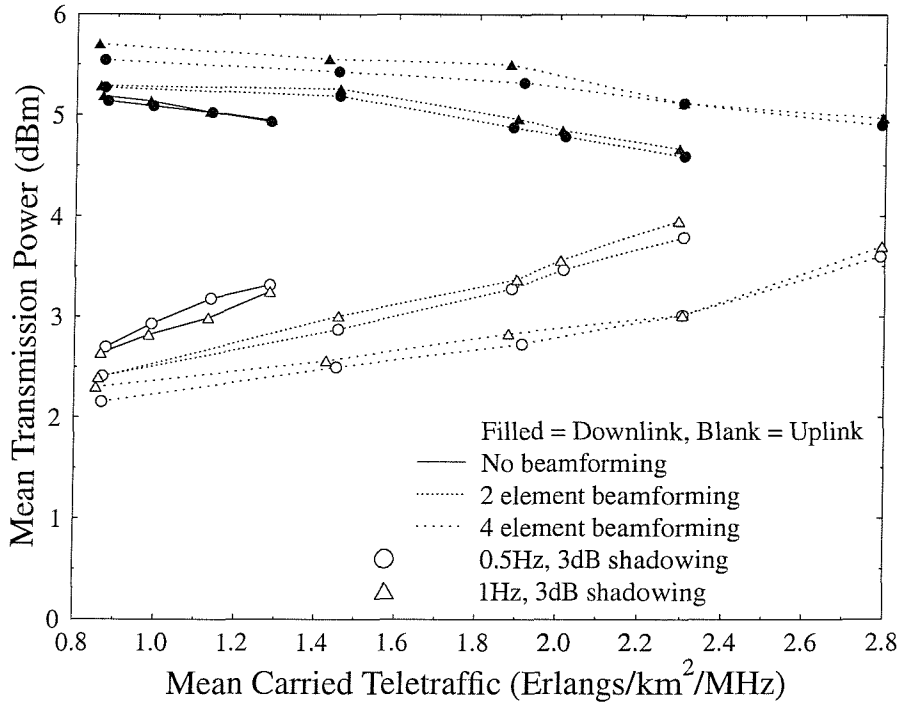

Figure 4.53: Mean transmission power versus mean carried traffic of a CDMA based cellular network using **relative received** E_c/I_o based soft handover thresholds both **with and without beamforming in conjunction with AQAM as well as with shadowing having a standard deviation of 3 dB** for SF=16. See Figure 4.48 for corresponding results without adaptive modulation.

		Conservative scenario					
			Traffic (Erlangs	Power (dBm)		Throughput (BPS)	
Shadowing	Beamforming	Users	/km^2/MHz)	MS	BS	Uplink	Downlink
0.5 Hz, 3 dB	No	223	1.27	3.25	4.95	2.86	2.95
0.5 Hz, 3 dB	2 elements	366	2.11	3.55	4.7	2.56	2.66
0.5 Hz, 3 dB	4 elements	476	2.68	3.4	5.0	2.35	2.72
1.0 Hz, 3 dB	No	218	1.24	3.3	4.95	2.87	2.96
1.0 Hz, 3 dB	2 elements	341	1.98	3.5	4.9	2.62	2.73
1.0 Hz, 3 dB	4 elements	460	2.59	3.5	4.95	2.4	2.8

Table 4.7: Maximum mean carried traffic and maximum number of mobile users that can be supported by the network, whilst meeting the conservative quality constraints. The carried traffic is expressed in terms of normalised Erlangs (Erlang/km^2/MHz), for the network described in Table 4.2 both **with and without beamforming (using independent up/down-link beamforming), in conjunction with shadow fading having a standard deviation of 3 dB, whilst employing adaptive modulation techniques** for SF=16.

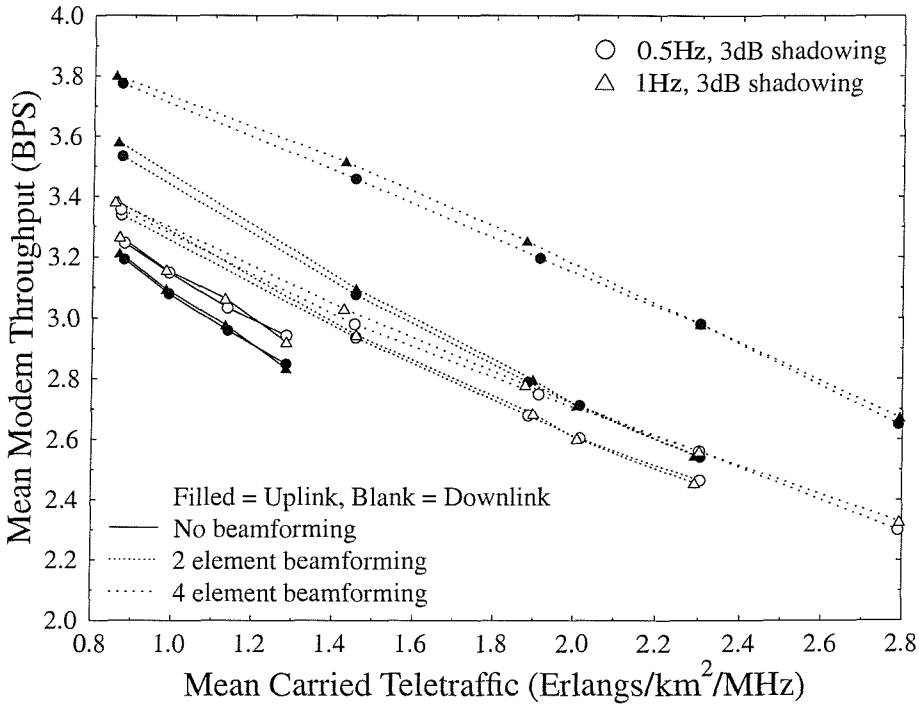

Figure 4.54: Mean modem throughput versus mean carried traffic of a CDMA based cellular network using **relative received** E_c/I_o based soft handover thresholds both **with and without beamforming in conjunction with AQAM as well as with shadowing having a standard deviation of 3 dB** for SF=16.

Shadowing	Beamforming	Conservative scenario Users	Traffic (Erlangs /km^2/MHz)
0.5 Hz, 3 dB	No	3568	20.3
0.5 Hz, 3 dB	2 elements	5856	33.8
0.5 Hz, 3 dB	4 elements	7616	42.9
1.0 Hz, 3 dB	No	3488	19.8
1.0 Hz, 3 dB	2 elements	5456	31.7
1.0 Hz, 3 dB	4 elements	7360	41.4

Table 4.8: A lower bound estimate of the maximum mean carried traffic and maximum number of mobile **speech-rate** users that can be supported by the network, whilst meeting the conservative quality constraints. The carried traffic is expressed in terms of normalised Erlangs (Erlang/km^2/MHz), for the network described in Table 4.2 both **with and without beamforming (using independent up/down-link beamforming), in conjunction with shadow fading having a standard deviation of 3 dB, whilst employing adaptive modulation techniques** for SF=256. The number of users supported in conjunction with a spreading factor of 256 was calculated by multiplying the capacities obtained in Table 4.7 by 256/16=16.

4.5 Summary

We commenced this chapter with a brief overview of the background behind the 3G UTRA standard. This was followed in Sections 4.2 and 4.3 by an introduction to CDMA and the techniques invoked in the UTRA standard.

Network capacity studies were then conducted in Section 4.4, which evaluated the performance of four different soft handover algorithms in the context of both non-shadowed and log-normal shadow faded propagation environments. The algorithm using relative received pilot-to-interference ratio measurements at the mobile, in order to determine the most suitable base stations for soft handover, was found to offer the highest network capacity when subjected to shadow fading propagation conditions. Hence, this algorithm and its associated parameters, were selected for use in our further investigations. The impact of adaptive antenna arrays upon the network capacity was then considered in Section 4.4.5 in both non-shadowed and log-normal shadow faded propagation environments. Considerable network capacity gains were achieved, employing both two and four element adaptive antenna arrays. This work was then extended in Section 4.4.6 by the application of adaptive modulation techniques in conjunction with the previously studied adaptive antenna arrays in a log-normal shadow faded propagation environment, which elicited further significant network capacity gains.

Chapter 5

Conclusions and Further Work

5.1 Summary and Conclusions

In this thesis we have discussed the performance implications of adaptive antenna arrays and adaptive modulation techniques in both FDMA/TDMA and CDMA cellular mobile communications networks.

In Chapter 2 we investigated antenna arrays and adaptive beamforming algorithms. We commenced, in Section 2.2.2, by considering the possible applications of antenna arrays and their related benefits. The signal model used was then described in Section 2.2.3 and a rudimentary example of how beamforming operates was presented. Section 2.3 highlighted the process of adaptive beamforming using several different temporal reference techniques, along with the approaches used in spatial reference techniques. The challenges that must be overcome before beamforming for the downlink becomes feasible were also discussed in Section 2.3.5. Results were presented showing how the SMI, ULMS and NLMS beamforming algorithms behaved for a two element adaptive antenna in conjunction with varying eigenvalue spread and reference signal length. The SMI algorithm was shown to converge rapidly, irrespective of the eigenvalue spread. The performance of the ULMS beamformer was shown to be highly dependent upon the input signal power presented to the antenna, rendering it impractical. However, the NLMS algorithm was found to be far superior in this respect and it was later shown to approach the performance of the SMI beamformer for a three element adaptive array. A low SNR gives a poor estimate of the received signal's cross-correlation matrix, resulting in similar performance for all three algorithms. However, as the SNR improves, the SMI technique guarantees a stronger interference rejection. The SMI algorithm is more complex for a large number of antenna elements, but for a realistic number of elements, such as four, its complexity is below that of the LMS routines.

In Chapter 3 the performance gains achieved using adaptive antenna arrays at the base stations in a cellular network were investigated for both LOS and multipath environments. A exposure to modelling an adaptive array was provided in Section 3.2, before an overview of fixed and dynamic channel allocation schemes was conducted in Section 3.3. Section 3.5 then reviewed some of the different models available for simulating multipath environments, followed by a more detailed portrayal of the Geometrically Based Single-Bounce Elliptical Model (GBSBEM). The metrics used for characterising the performance of mobile cellular networks were presented under both LOS and multipath propagation conditions, with and without adaptive antenna arrays. The network capacity was found to increase, when using adaptive antenna arrays, with further increases achieved due to the adoption of power control. An adaptive modulation mode switching algorithm with combined power control was developed and network capacity investigations were conducted. Employing adaptive modulation using adaptive antenna arrays was found to increase the network's capacity significantly, whilst providing a superior call quality and a higher mean modem throughput.

Our investigations in Chapter 3 initially focused on the non-wraparound or "desert island" type networks, where the outer cells of the simulation area are subjected to lower levels of co-channel interference, a scenario that may be encountered in the suburbs of large conurbations. Simulations were carried out for the FCA algorithm, and the LOLIA using nearest base station constraints of 7 and 19, when exposed to LOS propagation conditions. The FCA algorithm offered the lowest network capacity, but benefited the most from employing adaptive antenna arrays. Specifically, the network capacity of FCA increased by 67%, when employing two element antenna arrays at the base stations, and 144%, when using four element arrays. The LOLIA using a nearest base station constraint of 7 cells supported a higher number of users, but the adaptive antenna arrays did not result in such dramatic improvements in network capacity. Explicitly, a 22% increase was observed for the two element case, and a 58% when using four elements. However, the network capacity supported by the LOLIA in conjunction with $n = 7$ always exceeded that of the FCA algorithm. When using a 19 base station constraint, the LOLIA resulted in the highest network capacity without employing adaptive antenna arrays, although the large frequency reuse distance of this algorithm led to a negligible increase in network capacity through.

We then conducted further simulations in Section 3.7.2.2 using a more realistic 3-ray multipath propagation environment. Again, the FCA algorithm supported the lowest number of users, and gained the most from invoking adaptive antenna arrays. Using a four element array instead of a two element array led to a network capacity increase of 35%, and replacing the four element array with one employing eight elements resulted in a 24-34% increase in the number of users supported. The LOLIA employing $n = 7$ supported the

greatest number of users, but did not benefit from the same capacity increases as the FCA algorithm with the advent of adaptive antenna arrays. The number of users supported increased by 18% upon upgrading the system from two to four element adaptive antenna arrays, and by between 5% and 15% upon using eight element arrays in place of the four element arrays. Using a frequency reuse constraint of 19 in conjunction with the LOLIA resulted in a network whose capacity was restricted by the high new call blocking probability associated with its large frequency reuse distance. This large frequency reuse distance led to low levels of co-channel interference, which could not be nulled effectively by the adaptive antenna arrays, and hence the network capacity did not increase by more than 5% upon doubling the number of antenna elements comprising the array. Hence, our future studies only considered the FCA algorithm and the LOLIA in conjunction with $n = 7$.

The network capacity gains accruing from the implementation of power control over the same 3-ray multipath channel, as in the previous section, were then investigated for the FCA algorithm and the LOLIA using $n = 7$. Significant network capacity increases were observed for all of the scenarios considered. Specifically, the network capacity without power control and using a given number of antenna elements, was frequently exceeded by that of an identical scenario using power control and half the number of antenna elements. On comparing otherwise identical scenarios, an increase in the network capacity of between 28% and 72% was attributed to the implementation of power control, whilst using the FCA algorithm. When employing the LOLIA and power control, the number of users supported increased by between 8.5% and 15%. The network capacity gains resulting from increasing the number of elements in the adaptive antenna arrays were reduced however, to 11% and 17% for the FCA algorithm. In contrast, the adaptive nature of the LOLIA enabled it to maintain the network capacity increases of 12-17%, achieved due to increasing the number of elements comprising the adaptive arrays.

The implementation of adaptive modulation techniques was then investigated in Section 3.7.2.4, since they allow the exploitation of good near-instantaneous channel conditions, whilst providing resilience when subjected to poor quality channels. The network capacity of the FCA algorithm was found to increase by 6-12%, when invoking adaptive modulation in conjunction with two element adaptive antenna arrays. However, when using four element adaptive antenna arrays the network capacity was reduced upon invoking adaptive modulation. This was due to the improved call dropping probability accruing from employing adaptive modulation, leading in turn to a lower number of frequency/timeslot combinations available for new calls. Since the new call blocking probability was the factor limiting the network's capacity, the capacity was reduced. This phenomenon was not observed, when employing the LOLIA, which supported 43% more users on average upon

invoking adaptive modulation techniques. Doubling the number of antenna elements led to an extra 20% supported users.

In summary, the network using the FCA algorithm supported 2400 users, or 14 Erlangs/km^2/MHz, in the conservative scenario, and approximately 2735 users, or 15.6 Erlangs/km^2/MHz, in the lenient scenario. When using the LOLIA 7 channel allocation algorithm and two element adaptive antenna arrays, 3675 users (23.1 Erlangs/km^2/MHz) were carried under the conservative conditions, and 4115 users (25.4 Erlangs/km^2/MHz) under the lenient specifications. When invoking four element adaptive antenna arrays, 4460 users (27.4 Erlangs/km^2/MHz) and 4940 users (29.6 Erlangs/km^2/MHz) were supported under the conservative and lenient scenarios, respectively.

In Section 3.7.3 our investigations then led us to consider results obtained for an infinite network using the so-called "wraparound" technique, which allows a cellular network to be simulated as if part of a much larger network, thus inflicting similar levels of co-channel interference upon all cells within the network. The FCA algorithm again supported the lowest number of users, but benefited the most from the employment of adaptive antenna arrays, resulting in network capacity increases of between 46 and 70%, when employing adaptive antenna arrays, or when using four rather than two elements. The LOLIA using a nearest base station constraint of 7, supported an extra 17-23% of users due to the application of adaptive antenna arrays at the base stations. As in the "desert island" scenarios, the LOLIA in conjunction with a frequency reuse constraint of 19 base stations, offered the greatest network capacity without adaptive antenna arrays. However, when using two element arrays, the network capacity grew by almost 20%, since the limiting factor was the co-channel interference, not the new call blocking probability. The extra interference rejection potential offered by the four element arrays was also exploited, but was also somewhat limited, since the new call blocking probability became the capacity limiting constraint once again.

Under 3-ray multipath propagation conditions the network capacities of both the FCA algorithm and the LOLIAs were limited by the probability of low quality access, and hence invoking adaptive beamforming techniques increased the number of users supported. For an adaptive antenna array consisting of a given number of elements, the FCA algorithm supported the least number of users, and although exhibiting the greatest capacity gains due to the adaptive antenna arrays, the LOLIA 7 employing two element arrays exceeded the capacity of the FCA algorithm using eight element arrays. The LOLIA in conjunction with a frequency reuse of 19 base stations benefited from doubling the number of antenna elements from two, to four, and from four, to eight, but the network capacity was then limited by the new call blocking probability, and hence further increases in the number of

antenna array elements would have had no impact on the network's capacity.

The addition of power control in the "infinite" network was then considered under the above 3-ray multipath conditions. The capacity gains were significant for both the FCA algorithm and the LOLIA 7, when compared to our identical investigations conducted without power control. Again, the network capacity when using the FCA algorithm benefited the most, with the number of users supported increasing by between 38 and 82%, exhibiting a mean increase of 61%. However, the LOLIA 7 based network still supported the greatest number of users, although the capacity gains of the power control were limited to around 12%.

The employment of adaptive modulation techniques led to the saturation of network resources for the FCA algorithm, with the network capacity limited by the number of frequency/timeslot combinations available for new calls. Hence, increasing the number of antenna elements from two to four resulted in an increase in the mean modem throughput from 2.4 BPS to 2.7 BPS, and a small reduction in the mean transmission power. The adaptive nature of the LOLIA allowed it to fully exploit the potential of adaptive modulation and supported more than 32% extra users. The limiting factor of the LOLIA's network capacity was the requirement of a minimum mean modem throughput of 2.0 BPS.

Therefore, the FCA algorithm supported 1400 users, and carried a teletraffic load of 13.8 Erlangs/km^2/MHz in the conservative scenario and 1570 users, or 15.2 Erlangs/km^2/MHz of traffic under the lenient conditions. The LOLIA however supported an extra 35% of users, giving a network capacity of 1910 users, or 19.75 Erlangs/km^2/MHz, when using two element adaptive antenna arrays for both the conservative and lenient scenarios. Utilising four element antenna arrays at the base stations allowed 2245 users, or 23.25 Erlangs/km^2/MHz of network traffic to be supported at the required quality levels of the conservative and lenient scenarios.

Thus, the network capacity was found to substantially increase, when using adaptive antenna arrays, with further increases achieved through the adoption of power control. An adaptive modulation mode switching algorithm combined with power control was developed and network simulations were conducted. Employing adaptive modulation in conjunction with adaptive antenna arrays was found to increase the network capacity significantly, whilst providing superior call quality and a greater mean modem throughput.

Chapter 4 examined the performance of a CDMA based cellular mobile network, very similar in its nature to the FDD-mode of the proposed UTRA standard. A comparison of various soft handover algorithms was conducted in both non-shadowed and shadowed propagation environments. The algorithm that was found to offer the highest network

capacity, i.e. the highest number of users supported at a given quality of service, used the relative received E_c/I_o for determining cell ownership. The impact of using adaptive antenna arrays at the base stations was then investigated, in both non-shadowed and shadowed environments for high data rate users. This work was then extended by the application of adaptive modulation techniques, in conjunction with adaptive antenna arrays.

The network capacity in terms of the number of users supported, was 256 when experiencing no log-normal shadow fading and using no adaptive antenna arrays. However, with the application of two element adaptive antenna arrays the network capacity increased by 27% to 325 users, and when upgrading the system to four element arrays, the capacity of the network increased by a further 47% to 480 users. When subjected to log-normal shadow fading having a standard deviation of 3 dB in conjunction with a maximum fading frequency of 0.5 Hz, the network capacity without adaptive antennas was reduced to about 150 users. Again, invoking adaptive antenna arrays at the base stations increased the network capacity to 203 users, and 349 users, when employing two and four array elements, respectively.

We then applied independent up- and down-link beamforming. This implied determining separately the optimum weights for both the up- and the down-link, rather than re-using the antenna array weights calculated for the uplink scenario in the downlink. This measure led to further network capacity gains. Specifically, employing independent up- and down-link beamforming resulted in 15% and 7% network capacity increases, for the two and four element arrays, respectively, giving total network capacities of 349 and 375 users. Increasing the maximum shadow fading frequency from 0.5 Hz to 1.0 Hz slightly reduced the maximum number of users supported by the network, resulting in a network capacity of 144 users without beamforming, and capacities of 201 and 333 users, when invoking two and four element arrays, respectively. These absolute network capacity increases corresponded to relative network capacity gains of 40% and 131%, respectively. Again, performing independent up- and down-link beamforming increased the network capacities, with 225 and 365 users supported by the two and four element adaptive antenna arrays, respectively. Hence, these results show that applying both two and four element adaptive antenna arrays have led to significant network capacity increases both with and without log-normal shadow fading. Furthermore, the capacity of the network was found to be reduced by approximately 40%, when subjected to log-normal shadow fading having a standard deviation of 3 dB. However, increasing the maximum log-normal fading frequency from 0.5 Hz to 1.0 Hz had little impact on the total network capacity.

These results were then extended by applying adaptive modulation techniques, both with and without adaptive antenna arrays, which were performing independent up- and down-link beamforming in conjunction with log-normal shadow fading having a standard deviation

of 3 dB as well as maximum fading frequencies of 0.5 Hz and 1.0 Hz. Without adaptive antenna arrays the network supported 223 users, at a mean uplink modem throughput of 2.86 BPS. The mean throughput of the downlink was 2.95 BPS. Upon increasing the maximum shadowing frequency from 0.5 Hz to 1.0 Hz the network capacity fell slightly to 218 users, whilst the mean modem throughputs remained essentially unchanged. However, invoking two element adaptive antenna arrays enhanced the network capacities by 64% upon encountering 0.5 Hz shadow fading, and by 56% when subjected to 1.0 Hz shadowing. In both cases the mean modem throughput dropped by approximately 0.3 BPS. A further 0.2 BPS reduction of the mean modem throughput occurred, when applying four element adaptive antenna arrays. However, this allowed an extra 30% of users to be supported, when subjected to shadow fading fluctuating at a maximum frequency of 0.5 Hz and 35% in conjunction with 1.0 Hz frequency shadowing. Therefore, these results have shown the significant network capacity increases achieved by invoking adaptive modulation techniques. These network capacity improvements have been achieved in conjunction with a higher mean modem throughput, albeit at a slightly higher mean transmission power.

The performance results obtained for the UTRA-type network of Chapter 4 were obtained for high data rate users communicating at a raw data rate of 240 kbps, using a spreading factor of 16. However, as described in Section 4.4, some exploratory investigations not presented in this thesis demonstrated that the increase in the number of users supported by the network, was up to a factor of two higher than expected on the basis of simple spreading factor proportionate scaling. Specifically, the expected increase in switching from a spreading factor of 16 to 256 was a factor of 256/16=16, and hence Tables 4.5 and 4.8 were presented showing the potential worst-case network capacities achieved by multiplying the high data rate results by 16. Even when considering these user capacities, the teletraffic carried by the network normalised with respect to both the occupied bandwidth and the network's area, was found to be higher than that achieved by the FDMA/TDMA based networks considered in Chapter 3.

5.2 Further work

Future work that builds upon the investigations considered here includes applying beamforming techniques to the pilot signals, or developing a method by which the pilot signals received at the mobile may be cancelled. In future systems the carrier frequency may be sufficiently high so that two antenna elements may be incorporated into the mobile handset, thus enabling beamforming to be performed at both ends of the data link. Further

research is required for optimising the AQAM mode switching criteria, which could amalgamate the power control and beamforming algorithms. This could be further developed to a joint optimisation of the adaptive modulation mode switching, power control and beamforming, and potentially could also be incorporated into multi-user detection algorithms. Additionally, the performance of multi-rate networks is worthy of investigation, especially when combined with adaptive modulation and adaptive beamforming techniques, which are particularly suitable for mitigating the significant levels of interference inflicted by the high data rate users. Since the high speed users inflict the majority of the interference as a result of their spreading factor and hence also receive a high level of interference from the numerous lower speed users, interference reduction techniques are of vital importance. This thesis has only considered uniform linear antenna arrays having an antenna element spacing of $\lambda/2$. However, other antenna array geometries, not exhibiting symmetry and possibly in conjunction with non-omnidirectional antenna elements may yield greater improvements in network capacity. More sophisticated propagation channel models tailored for different physical environments, such as macro- and pico-cells must also be considered, as should the TDD mode and the associated time slot allocation algorithms required for maximising the achievable network capacity, whilst maintaining the advantages of the asymmetric uplink/downlink data rate nature of the TDD mode.

Glossary

ABS	Active Base station Set is the set of base stations in use at any given time by a mobile station during soft handover.
AWGN	Additive White Gaussian Noise
BS	A common abbreviation for Base Station
CDMA	Code Division Multiple Access
CMA	Constant Modulus Algorithm
DCS1800	A digital mobile radio system standard, based on GSM, but operates at 1.8GHz at a lower power.
DOA	Direction Of Arrival
FDD	Frequency Division Duplex
GSM	A Pan-European digital mobile radio standard, operating at 900MHz.
HIPERLAN	High Performance Radio Local Area Network
IF	Intermediate Frequency
LMS	Least Mean Square, a stochastic gradient algorithm used in adapting coefficients of a system
MS	A common abbreviation for Mobile Station
MSE	Mean Square Error, a criterion used to optimised the coefficients of a system such that the noise contained in the received signal is minimised.
PDF	Probability Density Function
RF	Radio Frequency

RLS	Recursive Least Square
SDMA	Spatial Division Multiple Access
SINR	Signal to Interference plus Noise ratio, same as signal to noise ratio (SNR) when there is no interference.
SIR	Signal to Interference ratio
SNR	Signal to Noise Ratio, noise energy compared to the signal energy
TDD	Time Division Duplex
TDMA	Time Division Multiple Access
UMTS	Universal Mobile Telecommunication System

Bibliography

[1] M. Barrett and R. Arnott, "Adaptive antennas for mobile communications," *IEE Electronics & Communications Engineering Journal*, pp. 203–214, August 1994.

[2] S. C. Swales, M. A. Beach, D. J. Edwards, and J. P. McGeehan, "The Performance Enhancement of Multibeam Adaptive Base-Station Antennas for Cellular Land Mobile Radio Systems," *IEEE Transactions on Vehicular Technology*, vol. 39, pp. 56–67, February 1990.

[3] J. Litva and T. Lo, *Digital Beamforming in Wireless Communications.* Artech House, London, 1996.

[4] A. B. Carlson, *Communication Systems.* McGraw-Hill, 1986.

[5] J. G. Proakis, *Digital Communications.* Mc-Graw Hill International Editions, 3 ed., 1995.

[6] L. C. Godara, "Applications of Antenna Arrays to Mobile Communications, Part I: Performance Improvement, Feasibility, and System Considerations," *Proceedings of the IEEE*, vol. 85, pp. 1029–1060, July 1997.

[7] G. V. Tsoulos and M. A. Beach, "Calibration and Linearity issues for an Adaptive Antenna System," in *IEEE Proceedings of Vehicular Technology Conference*, pp. 1597–1600, 1997.

[8] B. D. V. Veen and K. M. Buckley, "Beamforming: A Versatile Approach to Spatial Filtering," *IEEE ASSP Magazine*, pp. 4–24, April 1988.

[9] A. J. Paulraj and B. C. Ng, "Space-Time Modems for Wireless Personal Communications," *IEEE Personal Communications*, pp. 36–48, February 1998.

[10] A. J. Paulraj and E. Lindskog, "Taxonomy of space-time processing for wireless networks," *IEEE Proceedings on Radar, Sonar and Navigation*, vol. 145, pp. 25–31, February 1998.

[11] R. Steele and L. Hanzo, *Mobile Radio Communications.* IEEE Press - John Wiley, 2nd ed., 1999.

[12] W. T. Webb and L. Hanzo, *Modern Quadrature Amplitude Modulation: Principles and Applications for Wireless Communications.* IEEE Press-Pentech Press, 1994. ISBN 0-7273-1701-6.

[13] L. Hanzo, W. T. Webb, and T. Keller, *Single- and Multi-Carrier Quadrature Amplitude Modulation.* John-Wiley, IEEE Press, 2000.

[14] J. S. Blogh, P. J. Cherriman, and L. Hanzo, "Adaptive Beamforming Assisted Dynamic Channel Allocation," in *Proceedings of VTC*, (Houston, USA), pp. 199–203, May 1999.

[15] J. S. Blogh, P. J. Cherriman, and L. Hanzo, "Comparative Study of Dynamic Channel Allocation Algorithms," *IEEE Transactions on Vehicular Technology*, 2001.

[16] J. S. Blogh, P. J. Cherriman, and L. Hanzo, "Dynamic Channel Allocation Using Adaptive Antennas and Power Control," in *Proceedings of ACTS Mobile Communications Summit*, (Sorrento), pp. 943–948, June 1999.

[17] J. S. Blogh, P. J. Cherriman, and L. Hanzo, "Dynamic Channel Allocation Techniques using Adaptive Modulation and Adaptive Antennas," *Accepted for publication in IEEE Journal on Selected Areas in Communications*, 2001.

[18] J. S. Blogh, P. J. Cherriman, and L. Hanzo, "Dynamic Channel Allocation Techniques using Adaptive Modulation and Adaptive Antennas," in *Proceedings of VTC Fall*, (Amsterdam, The Netherlands), pp. 2348–2352, September 1999.

[19] S. P. Applebaum, "Adaptive Arrays," tech. rep., Syracuse University Research Corporation, 1965. Reprinted in IEEE Transactions on Antennas and Propagation, September 1976.

[20] B. Widrow, P. E. Mantey, L. J. Griffiths, and B. B. Goode, "Adaptive Antenna Systems," *Proceedings of the IEEE*, vol. 55, pp. 2143–2159, December 1967.

[21] O. L. Frost III, "An Algorithm for Linearly Constrained Adaptive Array Processing," *Proceedings of the IEEE*, vol. 60, pp. 926–935, August 1972.

[22] L. J. Griffiths, "A Simple Adaptive Algorithm for Real-Time Processing in Antenna Arrays," *Proceedings of the IEEE*, vol. 57, pp. 1696–1704, October 1969.

[23] L. C. Godara, "Applications of Antenna Arrays to Mobile Communications, Part II: Beam-Forming and Direction-of-Arrival Considerations," *Proceedings of the IEEE*, vol. 85, pp. 1193–1245, August 1997.

[24] J. Capon, "High-resolution frequency-wavenumber spectrum analysis," *Proceedings of the IEEE*, vol. 57, pp. 1408–1418, August 1969.

[25] I. S. Reed, J. D. Mallett, and L. E. Brennan, "Rapid Convergence Rate in Adaptive Arrays," *IEEE Transactions on Aerospace and Electronic Systems*, vol. AES-10, pp. 853–863, November 1974.

[26] A. Paulraj and C. B. Papadias, "Space-Time Processing for Wireless Communications," *IEEE Signal Processing Magazine*, pp. 49–83, November 1997.

[27] J. E. Hudson, *Adaptive Array Principles.* Peregrinus, London, 1981.

[28] S. Haykin, *Adaptive Filter Theory.* Prentice-Hall International, 1991.

[29] B. Widrow and S. Steams, *Adaptive Signal Processing.* Prentice-Hall, 1985.

[30] R. A. Monzingo and T. W. Miller, *Introduction to Adaptive Arrays.* John Wiley & Sons, Inc., 1980.

[31] J. H. Winters, "Smart Antennas for Wireless Systems," *IEEE Personal Communications*, vol. 5, pp. 23–27, February 1998.

[32] U. Martin and I. Gaspard, "Capacity Enhancement of Narrowband CDMA by Intelligent Antennas," in *Proceedings of PIMRC*, pp. 90–94, 1997.

[33] A. R. Lopez, "Performance Predictions for Cellular Switched-Beam Intelligent Antenna Systems," *IEEE Communications Magazine*, pp. 152–154, October 1996.

[34] G. V. Tsoulos, M. A. Beach, and S. C. Swales, "On the Sensitivity of the Capacity Enhancement of a TDMA system with Adaptive Multibeam Antennas," in *IEEE VTC Proceedings*, pp. 165–169, 1997.

[35] C. M. Simmonds and M. A. Beach, "Active Calibration of Adaptive Antenna Arrays for Third Generation Systems," in *Proceedings of ACTS Summit*, 1997.

[36] P. Leth-Espensen, P. E. Mogensen, F. Frederiksen, K. Olesen, and S. L. Larsen, "Performance of Different Combining Algorithms for a GSM System applying Antenna Arrays," in *Proceedings of ACTS Summit*, 1997.

[37] M. Mizuno and T. Ohgane, "Application of Adaptive Array Antennas to Radio Communications," *Electronics and Communications in Japan, Part 1*, vol. 77, no. 2, pp. 48–56, 1994.

[38] H. Steyskal, "Digital Beamforming Antennas: An Introduction," *Microwave Journal*, pp. 107–124, January 1987.

[39] R. Kohno, *Wireless Communications: TDMA versus CDMA*, ch. 1. Spatial and Temporal Communication Theory using Software Antennas for Wireless Communications, pp. 293–321. Kluwer Academic Publishers, 1997.

[40] A. Mammela, *Diversity receivers in a fast fading multipath channel.* VTT Publications, 1995.

[41] W. Hollemans, "Performance Analysis of Cellular Digital Mobile Radio Systems including Diversity Techniques," in *Proceedings of PIMRC*, pp. 266–270, 1997.

[42] W. Jakes, ed., *Microwave Mobile Communications*. Wiley-Interscience, 1974.

[43] W. H. Tuttlebee, ed., *Cordless telecommunications in Europe : the evolution of personal communications*. London: Springer-Verlag, 1990. ISBN 3540196331.

[44] H. Ochsner, "The digital european cordless telecommunications specification, DECT," in Tuttlebee [43], pp. 273–285. ISBN 3540196331.

[45] Y. Ogawa and T. Ohgane, "Adaptive Antennas for Future Mobile Radio," *IEICE Trans. Fundamentals*, vol. E79-A, pp. 961–967, July 1996.

[46] P. Petrus, J. H. Reed, and T. S. Rappaport, "Effects of Directional Antennas at the Base Station on the Doppler Spectrum," *IEEE Communications Letters*, vol. 1, pp. 40–42, March 1997.

[47] N. Anderson and P. Howard, "Technology and Transceiver Architecture Considerations for Adaptive Antenna Systems," in *Proceedings of ACTS Summit*, pp. 965–970, 1997.

[48] J. Strandell, M. Wennstrom, A. Rydberg, T. Oberg, O. Gladh, L. Rexberg, E. Sandberg, B. V. Andersson, and M. Appelgren, "Experimental Evaluation of an Adaptive Antenna for a TDMA Mobile Telephony System," in *Proceedings of PIMRC*, pp. 79–84, 1997.

[49] J. J. Monot, J. Thibault, P. Chevalier, F. Pipon, S. Mayrargue, and A. Levy, "A fully programmable prototype for the experimentation of the SDMA concept and and use of smart antennas for UMTS and GSM/DCS1800 networks," in *Proceedings of PIMRC*, (Helsinki, Finland), pp. 534–538, September 1997.

[50] H. Krim and M. Viberg, "Two Decades of Array Signal Processing Research," *IEEE Signal Processing Magazine*, pp. 67–94, July 1996.

[51] S. Ponnekanti, A. Pollard, C. Taylor, and M. G. Kyeong, "Flexibility for the deployment of adaptive antennas in the IMT-2000 framework and enhanced interference cancellation," in *Proceedings of ACTS Summit*, 1997.

[52] J. H. Winters, J. Salz, and R. D. Gitlin, "The Impact of Antenna Diversity on the Capacity of Wireless Communication Systems," *IEEE Transactions on Communications*, vol. 42, pp. 1740–1751, February/March/April 1994.

[53] M. Barnard and S. McLaughlin, "Reconfigurable terminals for mobile communication systems," *IEE Electronics and Communication Engineering Journal*, vol. 12, pp. 281–292, December 2000.

[54] S. M. Leach, A. A. Agius, and S. R. Saunders, "The intelligent quadrifilar helix antenna," *IEE Proceedings of Microwave Antennas Propagation*, pp. 219–223, June 2000.

[55] P. Petrus, R. B. Ertel, and J. H. Reed, "Capacity Enhancement Using Adaptive Arrays in an AMPS System," *IEEE Transactions on Vehicular Technology*, vol. 47, pp. 717–727, August 1998.

[56] J. Laurila and E. Bonek, "SDMA Using Blind Adapation," in *Proceedings of ACTS Summit*, 1997.

[57] M. C. Wells, "Increasing the capacity of GSM cellular radio using adaptive antennas," *IEE Proceedings on Communications*, vol. 143, pp. 304–310, October 1996.

[58] J. H. Winters, "Signal Acquisition and Tracking with Adaptive Arrays in the Digital Mobile Radio System IS-54 with Flat Fading," *IEEE Transactions on Vehicular Technology*, vol. 42, November 1993.

[59] B. Widrow and E. Walach, "On the statistical efficiency of the LMS algorithm with nonstationary inputs," *IEEE Trans. Information Theory - Special Issue on Adaptive Filtering*, vol. 30, pp. 211–221, March 1984.

[60] Z. Raida, "Steering an Adaptive Antenna Array by the Simplified Kalman Filter," *IEEE Trans. on Antennas and Propagation*, vol. 43, pp. 627–629, June 1995.

[61] M. W. Ganz, R. L. Moses, and S. L. Wilson, "Convergence of the SMI Algorithms with Weak Interference," *IEE Trans. Antenna Propagation*, vol. 38, pp. 394–399, March 1990.

[62] H. Steyskal, "Array Error Effects in Adaptive Beamforming," *Microwave Journal*, September 1991.

[63] M. C. Vanderveen, C. B. Papadias, and A. Paulraj, "Joint Angle and Delay Estimation (JADE) for Multipath Signals Arriving at an Antenna Array," *IEEE Communications Letters*, vol. 1, pp. 12–14, January 1997.

[64] C. Passman and T. Wixforth, "A Calibrated Phased Array Antenna with Polarization Flexibility for the Tsunami (II) SDMA Field Trial," in *Proceedings of ACTS Summit*, 1997.

[65] D. N. Godard, "Self-Recovering Equalization and Carrier Tracking in Two-Dimensional Data Communication Systems," *IEEE Transactions on Communications*, vol. COM-28, pp. 1876–1875, November 1980.

[66] Z. Ding, R. A. Kennedy, B. D. O. Anderson, and C. R. Johnson Jr, "Ill-Convergence of Godard Blind Equalizers in Data Communication Systems," *IEEE Transactions on Communications*, vol. 39, pp. 1313–1327, September 1991.

[67] J. E. Mazo, "Analysis of decision-directed equalizer convergence," *Bell Systems Technical Journal*, 1980.

[68] D. Gerlach and A. Paulraj, "Adaptive Transmitting Antenna Arrays with Feedback," *IEEE Signal Processing Letters*, vol. 1, pp. 150–152, October 1994.

[69] D. Gerlach and A. Paulraj, "Base station transmitting antenna arrays for multipath environments," *Signal Processing*, pp. 59–73, 1996.

[70] T. Kanai, "Autonomous Reuse Partitioning in Cellular Systems," in *IEEE Proceedings of Vehicular Technology Conference*, vol. 2, pp. 782–785, 1992.

[71] I. Katzela and M. Naghshineh, "Channel Assignment Schemes for Cellular Mobile Telecommunication Systems: A Comprehensive Survey," *IEEE Personal Communications Magazine*, vol. 3, pp. 10–31, June 1996.

[72] M. Dell'Anna and A. H. Aghvami, "Performance of optimum and sub-optimum combining at the antenna array of a W-CDMA system," *IEEE Journal on Selected Areas in Communications*, pp. 2123–2137, December 1999.

[73] I. Howitt and Y. M. Hawwar, "Evaluation of Outage Probability Due to Cochannel Interference in Fading for a TDMA System with a Beamformer," in *Proceedings of VTC*, pp. 520–524, 1998.

[74] L. Ortigoza-Guerrero and A. H. Aghvami, "A self-adaptive prioritised hand-off DCA strategy for a microcellular environment," in *Proceedings of PIMRC*, (Helsinki, Finland), pp. 401–405, September 1997.

[75] L. Ortigoza-Guerrero and A. H. Aghvami, "A prioritised hand-off dynamic channel allocation strategy for PCS," *IEEE Transactions on Vehicular Technology*, pp. 1203–1215, July 1999.

[76] T. H. Le and H. Aghvami, "Fast channel access and DCA scheme for connection and connectionless-oriented services in UMTS," *Electronics Letters*, pp. 1048–1049, June 1999.

[77] L. G. Anderson, "A simulation study of some dynamic channel assignment algorithms in a high capacity mobile telecommunications system," *IEEE Trans. on Communication*, vol. 21, pp. 1294–1301, November 1973.

[78] J. C. I. Chuang, "Performance issues and algorithms for dynamic channel assignment," *IEEE JSAC*, vol. 11, pp. 955–963, August 1993.

[79] J. C. I. Chuang and N. R. Sollenberger, "Performance of autonomous dynamic channel assignment and power control for TDMA/FDMA wireless access," *IEEE JSAC*, vol. 12, pp. 1314–1323, October 1994.

[80] M. M. L. Cheng and J. C. I. Chuang, "Performance evaluation of distributed measurement-based dynamic channel assignment in local wireless communications," *IEEE JSAC*, vol. 14, pp. 698–710, May 1996.

[81] I. ChihLin and C. PiHui, "Local packing - distributed dynamic channel allocation at cellular base station," in *Proceedings of IEEE Globecom '93*, vol. 1, (Houston, TX, USA), pp. 293–301, Nov 29–Dec 2 1993.

[82] G. L. Stüber, *Principles of Mobile Communcation.* Kluwer Academic Publishers, 1996.

[83] A. Baiocchi, F. D. Priscoli, F. Grilli, and F. Sestini, "The geometric dynamic channel allocation as a practical strategy in mobile networks with bursty user mobility," *IEEE Trans. on Vech. Tech.*, vol. 44, pp. 14–23, Feb 1995.

[84] F. D. Priscoli, N. P. Magnani, V. Palestini, and F. Sestini, "Application of dynamic channel allocation strategies to the GSM cellular network," *IEEE Journal on Selected Areas in Comms.*, vol. 15, pp. 1558–1567, Oct 1997.

[85] P. J. Cherriman, F. Romiti, and L. Hanzo, "Channel Allocation for Third-generation Mobile Radio Systems," in *ACTS '98, Rhodes, Greece*, pp. 255–260, June 1998.

[86] R. B. Ertel, P. Cardieri, K. W. Sowerby, T. S. Rappaport, and J. H. Reed, "Overview of Spatial Channel Models for Antenna Array Communications Systems," *IEEE Personal Communications*, pp. 10–22, February 1998.

[87] J. C. Liberti and T. S. Rappaport, "A Geometrically Based Model for Line-Of-Sight Multipath Radio Channels," in *VTC Proceedings*, pp. 844–848, 1996.

[88] P. J. Cherriman, *Mobile Video Communications.* PhD thesis, University of Southampton, 1998.

[89] S. Tekinay and B. Jabbari, "Handover and Channel Assignment in Mobile Cellular Networks," *IEEE Communications Magazine*, pp. 42–46, November 1991.

[90] R. C. French, "The Effect of Fading and Shadowing on Channel Reuse in Mobile Radio," *IEEE Transactions on Vehicular Technology*, vol. 28, pp. 171–181, August 1979.

[91] W. Gosling, "A simple mathematical model of co-channel and adjacent channel interference in land mobile radio," *The Radio and Electronic Engineer*, vol. 48, pp. 619–622, December 1978.

[92] R. Muammar and S. C. Gupta, "Cochannel Interference in High-Capacity Mobile Radio Systems," *IEEE Transactions on Communications*, vol. 30, pp. 1973–1978, August 1982.

[93] P. Cherriman and L. Hanzo, "Programmable H.263-based wireless video transceivers for interference-limited environments," *IEEE Trans. on Circuits and Systems for Video Technology*, vol. 8, pp. 275–286, June 1998.

[94] L. Hanzo and J. Stefanov, "The Pan-European Digital Cellular Mobile Radio System – known as GSM," in *Mobile Radio Communications* (R. Steele, ed.), ch. 8, pp. 677–765, IEEE Press-Pentech Press, 1992.

[95] A. S. Tanenbaum, "Introduction to queueing theory," in *Computer Networks*, pp. 631–641, Prentice-Hall, 2nd ed., 1989. ISBN 0131668366.

[96] S. Tekinay and B. Jabbari, "Handover and channel assignment in mobile cellular networks," *IEEE Comms. Mag.*, pp. 42–46, November 1991.

[97] I. Katzela and M. Naghshineh, "Channel assignment schemes for cellular mobile telecommunication systems: A comprehensive survey," *IEEE Personal Comms.*, pp. 10–31, June 1996.

[98] P. J. Cherriman and L. Hanzo, "Error-rate-based power-controlled multimode H.263-assisted video telephony," *IEEE Transactions on Vehicular Technology*, vol. 48, pp. 1726–1738, September 1999.

[99] G. J. Foschini and Z. Miljanic, "Distributed Autonomous Wireless Channel Assignment Algorithm with Power Control," *IEEE Transactions on Vehicular Technology*, vol. 44, pp. 420–429, August 1995.

[100] J. C.-I. Chuang and N. R. Sollenberger, "Spectrum Resource Allocation for Wireless Packet Access with Application to Advanced Cellular Internet Service," *IEEE Journal On Selected Areas in Communications*, vol. 16, pp. 820–829, August 1998.

[101] J. M. Torrance, L. Hanzo, and T. Keller, "Interference Aspects of Adaptive Modems over Slow Rayleigh Fading Channels," *IEEE Transactions on Vehicular Technology*, vol. 48, pp. 1527–1545, September 1999.

[102] J. M. Torrance and L. Hanzo, "Latency and Networking Aspects of Adaptive Modems over Slow Indoors Rayleigh Fading Channels," *IEEE Transactions on Vehicular Technology*, vol. 48, pp. 1237–1251, July 1999.

[103] C. H. Wong and L. Hanzo, "Upper-bound performance of a wideband burst-by-burst adaptive mode," *IEEE Transactions on Communications*, March 2000.

[104] H. Holma and A. Toskala, eds., *WCDMA for UMTS : Radio Access for Third Generation Mobile Communications.* John Wiley & Sons, Ltd., 2000.

[105] "3rd Generation Partnership Project; Technical Specification Group Radio Access Network; Spreading and modulation (FDD)." 3G TS 25.213 V3.2.0 (2000-03).

[106] F. Adachi, M. Sawahashi, and K. Okawa, "Tree-structured Generation of Orthogonal Spreading Codes with Different Lengths for Forward Link of DS-CDMA Mobile," *Electronics Letters*, vol. 33, no. 1, pp. 27–28, 1997.

[107] "3rd Generation Partnership Project; Technical Specification Group Radio Access Network; Physical layer procedures (FDD)." 3G TS 25.214 V3.2.0 (2000-03).

[108] S. Verdú, *Multiuser Detection.* Cambridge University Press, 1998.

[109] A. D. Whalen, *Detection of signals in noise.* Academic Press, 1971.

[110] W. T. Webb and L. Hanzo, *Modern Quadrature Amplitude Modulation : Principles and Applications for Fixed and Wireless Channels.* John Wiley and IEEE Press, 1994.

[111] R. L. Pickholtz, L. B. Milstein, and D. L. Schilling, "Spread spectrum for mobile communications," *IEEE Transactions on Vehicular Technology*, vol. 40, pp. 313–322, May 1991.

[112] K. S. Gilhousen, I. M. Jacobs, R. Padovani, A. J. Viterbi, L. A. Weaver, and C. E. Wheatley, "On the capacity of a cellular CDMA system design," *IEEE Transactions on Vehicular Technology*, vol. 40, pp. 303–312, May 1991.

[113] L. Wang and A. H. Aghvami, "Optimal power allocation based on QoS balance for a multi-rate packet CDMA system with multi-media traffic," in *Proceedings of Globecom*, (Rio de Janeiro, Brazil), pp. 2778–2782, December 1999.

[114] D. Koulakiotis and A. H. Aghvami, "Data detection techniques for DS/CDMA mobile systems: A review," *IEEE Personal Communications*, pp. 24–34, June 2000.

[115] P. J. Cherriman, E. L. Kuan, and L. Hanzo, "Burst-by-burst adaptive joint-detection CDMA/H.263 based video telephony," in *Proceedings of the ACTS Mobile Communications Summit, Sorrento, Italy*, pp. 715–720, June 1999.

[116] J. Laiho-Steffens, A. Wacker, and P. Aikio, "The Impact of the Radio Network Planning and Site Configuration on the WCDMA Network Capacity and Quality of Service," in *IEEE Proceedings of Vehicular Technology Conference*, (Tokyo, Japan), pp. 1006–1010, 2000.

[117] R. D. Kimmo Hiltunen, "WCDMA Downlink Capacity Estimation," in *IEEE Proceedings of Vehicular Technology Conference*, (Tokyo, Japan), pp. 992–996, 2000.

[118] K. Sipilä, Z.-C. Honkasalo, J. Laiho-Steffens, and A. Wacker, "Estimation of Capacity and Required Transmission Power of WCDMA Downlink Based on a Downlink Pole Equation," in *IEEE Proceedings of Vehicular Technology Conference*, (Tokyo, Japan), pp. 1002–1005, 2000.

[119] "GSM 06.90: Digital cellular telecommunications system (Phase 2+)." Adaptive Multi-Rate (AMR) speech transcoding, version 7.0.0, Release 1998.

[120] S. Bruhn, E. Ekudden, and K. Hellwig, "Adaptive Multi-Rate: A new speech service for GSM and beyond," in *Proceedings of 3rd ITG Conference on Source and Channel Coding*, (Technical Univ. Munich, Germany), pp. 319–324, 17th-19th, January 2000.

[121] S. Bruhn, P. Blocher, K. Hellwig, and J. Sjoberg, "Concepts and Solutions for Link Adaptation and Inband Signalling for the GSM AMR Speech Coding Standard," in *Proceedings of VTC*, (Houston, Texas, USA), 16-20 May 1999.

[122] T. Ojanperä and R. Prasad, ed., *Wideband CDMA for 3rd Generation Mobile Communications*. Artech House Publishers, 1998.

[123] R. Owen, P. Jones, S. Dehgan, and D. Lister, "Uplink WCDMA capacity and range as a function of inter-to-intra cell interference: theory and practice," in *IEEE Proceedings of Vehicular Technology Conference*, vol. 1, (Tokyo, Japan), pp. 298–303, 2000.

[124] B. G. Evans and K. Baughan, "Visions of 4G," *IEE Electronics and Communication Engineering Journal*, vol. 12, pp. 293–303, December 2000.

Author Index

L

M

N

O

P

Index

R

S

T

U